Oxidative Medicine and Cellular Longevity

Antioxidants and Prooxidants: Effects on Health and Aging 2018

Lead Guest Editor: Márcio Carocho
Guest Editors: Isabel C. F. R. Ferreira, Patricia Morales, and Marina Sokovic

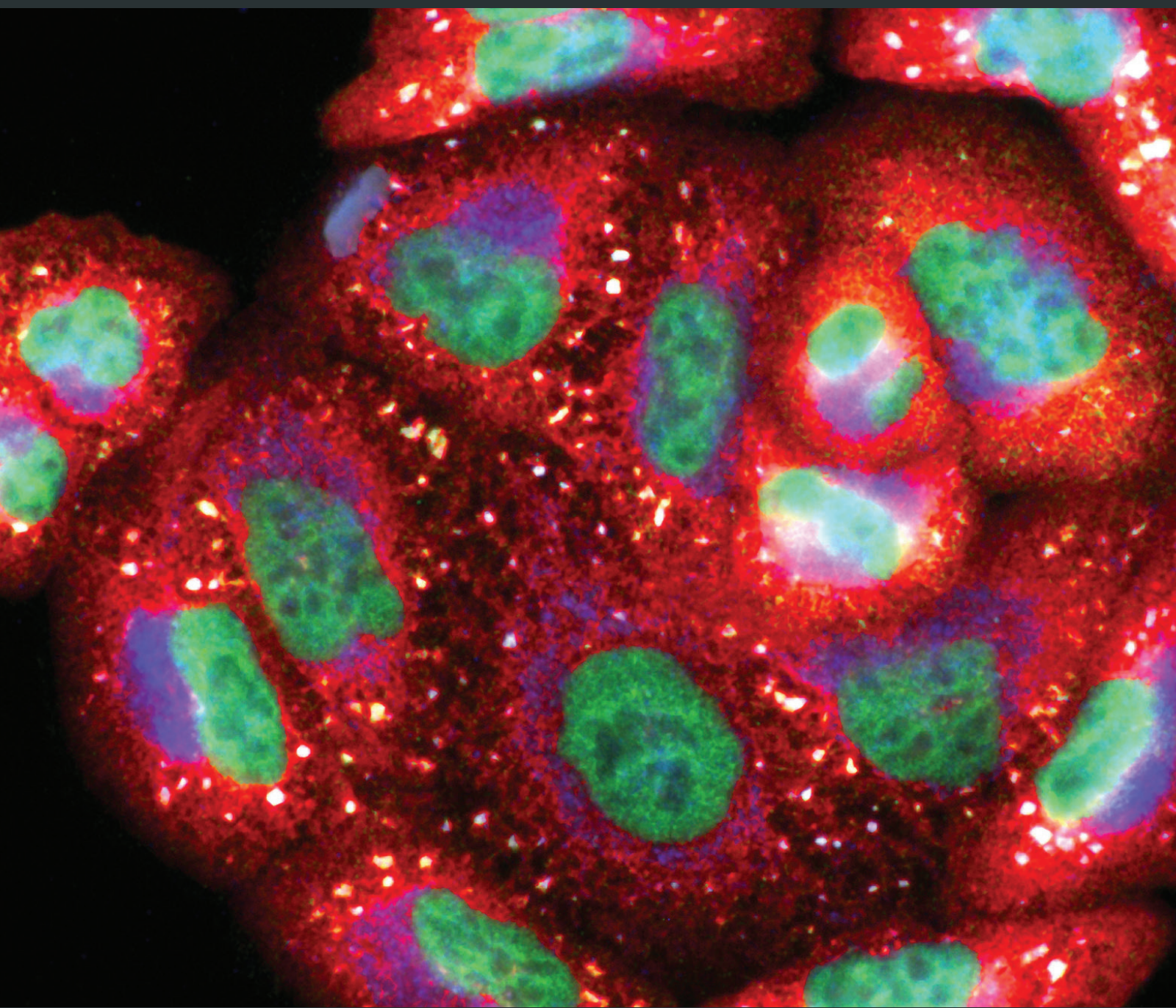

Antioxidants and Prooxidants: Effects on Health and Aging 2018

Oxidative Medicine and Cellular Longevity

Antioxidants and Prooxidants: Effects on Health and Aging 2018

Lead Guest Editor: Márcio Carocho
Guest Editors: Isabel C. F. R. Ferreira, Patricia Morales, and Marina Sokovic

Editorial Board

Contents

Hindawi
Oxidative Medicine and Cellular Longevity
Volume 2019, Article ID 7971613, 2 pages
https://doi.org/10.1155/2019/7971613

Editorial

Antioxidants and Prooxidants: Effects on Health and Aging 2018

Márcio Carocho,[1] **Isabel C. F. R. Ferreira**,[1] **Patricia Morales**,[2] **and Marina Soković**[3]

[1]*Centro de Investigação de Montanha (CIMO), Instituto Politécnico de Bragança, Portugal*
[2]*Faculty of Pharmacy, Complutense University of Madrid, Spain*
[3]*Institute of Biological Research, University of Belgrade, Serbia*

Correspondence should be addressed to Márcio Carocho; mcarocho@ipb.pt

Received 17 December 2018; Accepted 17 December 2018; Published 28 February 2019

In the mid 50's, a ground-breaking theory was proposed by Denham Harman, which revolutionized the understanding of biology and aging and to an extent helped shape the research that was put forward to understanding the mechanisms of growing old and the underlying workings at a cellular level [1]. This theory, known as the "Free Radical Theory of Aging," is the cornerstone of this special issue; health is the most important feature that a human being wishes for, although conscient of the demise of the body, conscient of growing old. Over the years, the theory has seen some tough arguments against it and others that back its overall postulations.

By 1992, after nearly 40 years of scientific advancements, Denham Harman wrote that "the data supporting this theory indicates that average life expectancy at birth may be increased by 5 or more years, by nutritious low-calorie diets supplemented with one or more free radical reaction inhibitors," paving the way for the increased incidence of research on plants, fruits, and vegetables, as possible "radical reaction inhibitors" when consumed regularly in the diet could help increase the 5 years of life expectancy. Still, D. Harman at the time understood that aging could be explained by many theories, namely, molecular cross linking, changes in immunological function, and the senescence genes in the DNA [2]. 40 years after its appearance, Beckman and Ames [3] wrote that the theory had matured and systematically revised the findings that had been brought forward in terms of the implications of free radicals, prooxidants, and aging. During the early 2000's, the theory was supported by many evidences that free radicals could explain recently discovered phenomena, although definitive proof that oxidised molecules were the primary cause of aging was lacking confirmation [4]. These revelations reduced the momentum the theory had been gaining in the previous decades. By 2014, Vadim Gladyshev had "killed" the theory, arguing that although Reactive Oxygen Species (ROS) were by-products responsible for cellular damage, their contribution to aging was governed by cellular metabolic organization, protective systems, and the individual's genotype. Furthermore, oxidative damage, individually or in combination, could not represent the cause of aging [5].

Even though its death had been predicted in 2014, the truth is that even though its name has been changed and its basic premises altered, the theory continues to inspire many researchers across the globe to find the mechanisms of health and aging. By 2018, "A Free Radical Theory of Frailty" was published, stating that oxidative damage correlates not with chronological age but with the human frailty state [6]. Still, even if researchers digress from the original theory and improve its reasonings, free radicals, oxidative stress, anti- and prooxidants, aging, and health are linked and are still as important to research today as they were 60 years ago.

Roughly a year ago, in our first editorial (2017) of the special issue "Antioxidants and Prooxidants: Effects on Health and Aging" [7], we wrote that the issue intended to shed some light on the dichotomy of antioxidants and prooxidants, given the important role that either have on the maintenance of health and their contribution to how aging unfolds. One year after, this 2018 edition aims at exactly the same outcome, to dwell deeper in the

understanding of this inevitable happening that is called aging. Today, even though mankind is closer, it still is not clear why we age, albeit the theories that have been postulated though the years. So, this quest for the answers should be the driving force to increase research on human health and aging, to reach the ultimate goal of knowing why we gradually lose our health and ultimately meet our demise.

This year's edition, comprised of 15 articles, focuses on many aspects of antioxidant and prooxidant activities, with authors from 9 distinct countries, namely, Russia, China, Czech Republic, Austria, Pakistan, Mexico, Greece, Italy, and Poland. The study types are quite diverse, with focus on *in vitro cell* lines both from human tumours and various mice cell lines, studies on rabbits, mice, rats, and two with humans, namely, athletes and professional football players. In this edition, there are some interesting articles; two of them report the antioxidant activity of natural compounds, namely, curcumin and ellagic acid. Fullerene derivatives are studied for their effectiveness against human lung fibroblasts while pyrrolidine dithiocarbamate is used to inhibit deoxynivalenol damage to the mitochondria. This same organelle is also targeted by isoliquiritigenin in another study. Antioxidant enzymes are also an important part of the special edition, with two articles devoted to their study. One focuses on the alleviation of intervertebral disc degeneration by modulating antioxidant enzymes with estradiol, while the other focuses on the consequences of impairment of aldehyde dehydrogenase. The effect of food in the redox status of elite football players is also researched, in this case, through the consumption of dark chocolate. Another study involving human studies, namely, athletes, in which the effect of exercise induced reductive stress is assessed as a protective mechanism against oxidative stress in blood mononuclear cells. Finally, the supply of zinc in a chronic cadmium environment is viewed in the sublingual gland structure. We hope that these articles are of interest to the readers of this special edition and may help the progress of science.

Conflicts of Interest

The editors declare that they have no conflicts of interest regarding the publication of this special issue.

Acknowledgments

We would like to thank the invaluable reviewers that anonymously contributed their time to review and improve the articles herein. A word of appreciation to the authors that chose the journal to publish their studies and specifically the ones that submitted their work in this special issue. We finally acknowledge the readers that are reading this edition and hope the contents in the edition is suitable to their needs, for it was carried out for them.

Márcio Carocho
Isabel C. F. R. Ferreira
Patricia Morales
Marina Soković

References

[1] D. Harman, "Aging: a theory based on free radical and radiation chemistry," *Journal of Gerontology*, vol. 11, no. 3, pp. 298–300, 1956.

[2] D. Harman, "Free radical theory of aging," *Mutation Research*, vol. 275, no. 3-6, pp. 257–266, 1992.

[3] K. B. Beckman and B. N. Ames, "The free radical theory of aging matures," *Physiological Reviews*, vol. 78, no. 2, pp. 547–581, 1998.

[4] A. P. Wickens, "Ageing and the free radical theory," *Respiration Physiology*, vol. 128, no. 3, pp. 379–391, 2001.

[5] V. N. Gladyshev, "The free radical theory of aging is dead. Long live the damage theory!," *Antioxidants & Redox Signaling*, vol. 20, pp. 727–731, 2014.

[6] J. Viña, C. Borras, and M. C. Gomez-Cabrera, "A free radical theory of frailty," *Free Radical Biology and Medicine*, vol. 124, pp. 358–363, 2018.

[7] M. Carocho, I. C. F. R. Ferreira, P. Morales, and M. Soković, "Antioxidants and prooxidants: effects on health and aging," *Oxidative Medicine and Cellular Longevity*, vol. 2018, Article ID 1472708, 2 pages, 2018.

Hindawi
Oxidative Medicine and Cellular Longevity
Volume 2019, Article ID 9817576, 12 pages
https://doi.org/10.1155/2019/9817576

Research Article

Isoliquiritigenin Induces Mitochondrial Dysfunction and Apoptosis by Inhibiting mitoNEET in a Reactive Oxygen Species-Dependent Manner in A375 Human Melanoma Cells

Xiao-Yu Chen,[1] **Huan-Huan Ren**,[2] **Dan Wang**,[1] **Ying Chen**,[1] **Chuan-Jun Qu**,[1] **Zhao-Hai Pan**,[1] **Xiao-Na Liu**,[1] **Wen-Jin Hao**,[1] **Wen-Juan Xu**,[1] **Ke-Jun Wang**,[1] **De-Fang Li**,[1] **and Qiu-Sheng Zheng**[1,2]

[1]*School of Integrated Traditional Chinese and Western Medicine, Binzhou Medical University, Yantai, 264003 Shandong, China*
[2]*Key Laboratory of Xinjiang Endemic Phytomedicine Resources of Ministry of Education, School of Pharmacy, Shihezi University, Shihezi, 832002 Xinjiang, China*

Correspondence should be addressed to De-Fang Li; lidefang@163.com and Qiu-Sheng Zheng; zqsyt@sohu.com

Received 5 July 2018; Revised 22 September 2018; Accepted 4 November 2018; Published 21 January 2019

Academic Editor: Márcio Carocho

The mitochondrial protein mitoNEET is a type of iron-sulfur protein localized to the outer membrane of mitochondria and is involved in a variety of human pathologies including cystic fibrosis, diabetes, muscle atrophy, and neurodegeneration. In the current study, we found that isoliquiritigenin (ISL), one of the components of the root of *Glycyrrhiza glabra L.*, could decrease the expression of mitoNEET in A375 melanoma cells. We also demonstrated that mitoNEET could regulate the content of reactive oxygen species (ROS), by showing that the ISL-mediated increase in the cellular ROS content could be mitigated by the mitoNEET overexpression. We also confirmed the important role of ROS in ISL-treated A375 cells. The increased apoptosis rate and the decreased mitochondrial membrane potential were mitigated by the overexpression of mitoNEET in A375 cells. These findings indicated that ISL could decrease the expression of mitoNEET, which regulated ROS content and subsequently induced mitochondrial dysfunction and apoptosis in A375 cells. Our findings also highlight mitoNEET as a promising mitochondrial target for cancer therapy.

1. Introduction

Melanoma is a malignancy of pigment-producing melanocytes that is diagnosed in approximately 132,000 individuals globally every year [1]. The diagnosis of melanoma is associated with a health burden and economic loss due to age-dependent incidence, primarily affecting individuals between the ages of 30 and 50. Indications for radiotherapy as a therapeutic approach are limited because melanoma is considered to be radioresistant traditionally [2]. In preclinical studies, a solid rationale could explain poor clinical outcomes of traditional radiotherapy. Sensitivity to conventional fractionation (1.8–3 Gy) is low in vitro in melanoma cells [3]. Current treatments for stage IV melanoma patients are limited and have shown little improvement. Therefore, alternative and effective therapies are sorely needed for a potential cure of this aggressive cancer.

Apoptosis, as one of the most clearly characterized processes of cell death, plays an important role in eliminating damaged cells. Cell apoptosis has obvious morphological and biochemical changes, such as DNA division into 180–200 base pairs, cellular fragmentation into apoptotic bodies, and phosphatidylserine externalization [4]. Caspase-3 activation in apoptotic cells cleaves poly (ADP-ribose) polymerase (PARP) into two fragments sized 31 and 85 kD; the resultant PARP inactivation leads to nucleosomal DNA fragmentation. There are two main apoptotic pathways: intrinsic (mitochondrial) and extrinsic (death receptor) [5]. The pivotal role of the mitochondria in apoptosis has been widely demonstrated [6, 7]. During apoptosis, mitochondria release soluble

proteins, including cytochrome c and Smac/DIABLO, from the intermembrane space to initiate the activation of caspases in the cytosol [8, 9]; the release of these proteins is a consequence of the compromised integrity of the mitochondrial outer membrane through its permeabilization. The dynamic events occurring within the mitochondria ultimately determine the initiation of apoptosis, emphasizing the close relationship between mitochondrial dysfunction and cell death.

Reactive oxygen species (ROS) are typically small, short-lived, highly active molecules [10, 11]. The first ROS-producing mitochondrial site is complex III located in the mitochondrial inner membrane [12]. Mitochondrial ROS production occurs mainly on the electron transport chain (ETC) [13, 14]. At physiological levels, ROS acts as a redox messenger in intracellular signal transduction and regulation, whereas excess cell death was induced by ROS via the intrinsic apoptotic pathway. Mitochondrial DNA (mtDNA) damage is a common event in the mitochondrial apoptotic pathway. Mitochondrial DNA damage impairs the transcription of mitochondrial proteins involved in ETC, leading to the rupture of respiratory chain, further increasing ROS production, and ultimately the loss of mitochondrial membrane potential (MMP) and damage to ATP synthesis [15]. ROS can oxidize phospholipid cardiolipin which binds cytochrome c to the outer lobe of the inner mitochondrial membrane [16]. Normally, cytochrome c shuttles electrons between the mitochondrial complexes III and IV. ROS-oxidized cardiolipin reduces the binding of cytochrome c and increases the level of free cytochrome c, which is likely to be released into the cytoplasm through the mitochondrial outer membrane and initiates apoptotic cascade (Circu et al., 2010). Thus, ROS can trigger mitochondrial dysfunction and apoptosis.

The mitochondrial protein mitoNEET (also known as CDGSH iron-sulfur domain 1 (CISD1)) is a member of iron-sulfur protein and is involved in a variety of human pathologies including diabetes, Wolfram syndrome 2, cystic fibrosis, muscle atrophy, and neurodegeneration. [17–19]. Early studies have shown that mitoNEET plays a key role in regulating cellular energy use and lipid metabolism. [20]. mitoNEET-null mice appeared to have a mitochondrial dysfunction [21], whereas mice overexpressing mitoNEET gained weight by increasing fat tissue [22]. Sohn and colleagues found that mitoNEET played a vital role in breast cancer cell proliferation and the formation of tumor [23]. Furthermore, the overexpression of mitoNEET in the MDA-MB-231 breast cancer cell line led to an increase in mitochondrial ETC complexes and tumor growth [23]. Collectively, mitoNEET may not only regulate energy consumption but also function as a novel antitumor therapeutic target. Recent studies on the effects of redox regulation by mitoNEET demonstrated that mice overexpressing mitoNEET exhibited decreased ROS generation from the mitochondria; however, oxidative phosphorylation and electron transport were significantly upregulated in the absence of mitoNEET [21, 23], suggesting that mitoNEET may also regulate the generation of ROS.

Isoliquiritigenin (ISL), one of the flavonoids of the root of *Glycyrrhiza glabra L.*, was previously shown to have antioxidant, anti-inflammatory, and tumor-suppressive effects [24–26]. Previously, we demonstrated that ISL could induce apoptosis in HeLa cells by inducing intracellular ROS levels [27]. ISL inhibited proliferation and induced apoptosis by alleviating hypoxia and reducing glycolysis in B16F10 mouse melanoma cells [28]. In this first study to provide novel insights into the therapeutic targets of ISL and elucidate the mechanism of ISL-induced mitochondrial dysfunction and apoptosis in melanoma cells, we hypothesized that mitoNEET might influence the proliferation and ROS regulation in ISL-treated A375 melanoma cells. We therefore examined the role of mitoNEET in ISL-induced mitochondrial dysfunction and apoptosis in A375 cells.

2. Material and Methods

2.1. Cell Culture. The A375 melanoma cell line was purchased from Shanghai Biological Institute (Shanghai, China), and cultures were maintained in Dulbecco's modified Eagle medium supplemented with 10% fetal bovine serum, penicillin/streptomycin (1 : 100), and 4 mM L-glutamine in a CO_2 incubator at 37°C.

2.2. Reagents. ISL (purity ≥ 98%) was purchased from Jiangxi Herb Tiangong Technology (Jiangxi, China). 2,7-Dichlorodihydro-fluorescein diacetate (DCFH-DA), dimethyl sulfoxide (DMSO), 3-(4,5-dimethylthiazol-2-yl)-2,5-diphenyl tetrazolium bromide (MTT), N-acetylcysteine (NAC), and L-buthionine sulfoximine (BSO) were purchased from Sigma. MitoSOX Red was purchased from Invitrogen (Carlsbad, CA, USA). 2,7-Dichlorodihydro-fluorescein diacetate (DCFH-DA), MitoTracker Green, JC-1, and apoptosis detection kits were purchased from Kaiji Biotech (Nanjing, China). Hoechst 33258, RIPA buffer, and GSH/GSSG detection kit were purchased from Beyotime Biotech (Shanghai, China). RNA isolation, cDNA synthesis, and SYBR Premix kits were purchased from Takara Biomedical Technology (Beijing, China). Membrane Protein Isolation Kit was purchased from Invent Biotechnologies (USA). All antibodies were obtained from Cell Signaling Technology (Cell Signaling, USA).

2.3. Overexpression of mitoNEET. mitoNEET cDNA was amplified by reverse transcription- (RT-) polymerase chain reaction (PCR) from the total RNA of A375 cells with primers and cloned into a pLVX-CMV-MCS-T2A-Zsgreen plasmid (details of cloning provided in Supplemental Data (available here)). A375 cells were transfected with the empty vector or the mitoNEET vector using Lipofectamine 2000 (Invitrogen), according to the manufacturer's instructions. The cells were collected 48 h after transfection, and cell lysates were immunoblotted for the indicated proteins.

2.4. Cell Proliferation Inhibition Assay. The effect of ISL on A375 cell proliferation was determined by measuring the absorbance of MTT. Cells (5×10^4 per well) were seeded in 96-well microtiter plates and treated with indicated ISL doses for 24 h. Next, 20 μL MTT solution (5 mg/mL in phosphate-buffered saline) was added to each well for an additional 4 h at 37°C. The MTT solution with the medium was discarded, and 200 μL dimethyl sulfoxide was added to each well to

dissolve the formazan crystals. Absorbance was measured at 570 nm using a Tecan Infinite M200 microplate reader (Tecan, USA).

2.5. Hoechst 33258 Staining. Hoechst 33258 staining was used to detect apoptotic morphological changes in nuclear chromatin. A375 cells were seeded in six-well plates and treated with ISL after 24 h. After pretreatment, the medium was removed and cells were fixed with 4% paraformaldehyde for 10 min at room temperature. After two washes with PBS, the cells were incubated with 0.5 mL Hoechst 33258 staining solution for 5 min. The morphological shape of the nucleus was viewed under an Olympus IX-70 fluorescence microscope (Olympus, Tokyo, Japan).

2.6. Flow Cytometry. Flow cytometric determination of apoptosis, number of mitochondria, MMP, and mitochondrial superoxide, and total ROS levels was performed using a FACSCalibur flow cytometer (BD Biosciences, Mountain View, CA, USA) and analyzed using the CellQuest software (BD Biosciences). The rate of apoptosis was determined using the annexin V/propidium iodide (PI) double staining method. The mitochondrial number, MMP, mitochondrial superoxide level, and intracellular ROS level were determined by incubating the cells with 100 nM MitoTracker Green for 15 min, 1 mM JC-1 for 30 min, 5 μM MitoSox Red for 20 min, and 10 mM DCF-DA for 20 min at 37°C before flow cytometric analyses, before analysis by flow cytometry.

2.7. Assessment of Cellular Morphology by Confocal Laser Scanning Microscopy. The previously described method by Quoilin et al. [29] was used to observe the morphological changes in A375 cells. A phase-contrast microscope equipped with a digital camera (Axio Observer, Zeiss, Germany) was used to observe and record the morphological changes of A375 cells after 24 h incubation with different concentrations of ISL. Specific fluorescent probes were used to detect mitochondrial activity and cellular oxidative stress including MitoTracker Green (100 nM for 20 min) for the mitochondrial number (Cottet-Rousselle et al., 2011), the potentiometric fluorescent dye JC-1 (1 mM for 10 min) for MMP, and MitoSOX Red (5 μM for 20 min) and DCF (10 mM for 10 min) for mitochondrial and total cellular ROS in living cells, respectively (Cottet-Rousselle et al., 2011; Mukhopadhyay et al., 2007). A375 cells were cultured on glass coverslips in 6-well plates and incubated at 37°C with the specific dyes before image capturing.

2.8. Measurement of Cytochrome c Release. A double antibody sandwich enzyme-linked immunosorbent assay kit (Enzo Life Sciences, Belgium) was used to detect cytosolic and mitochondrial cytochrome c concentrations, as described previously by Quoilin et al. [29]. Briefly, A375 cells were treated with different concentrations of ISL for 6 h. Cells were digested and suspended in PBS at a final concentration of 10^7 cells/mL. Next, the cell suspension was centrifuged at 500 g for 5 min. After remove supernatant, digitonin cell permeabilization buffer was added. The pellet was incubated with digitonin cell permeabilization buffer for 5 min on ice, then centrifuged at 100 g at 4°C for 10 min. The supernatant which contains the cytosolic fraction with cytochrome c (fraction I) was collected and kept on ice. RIPA cell lysis buffer was used to dissolve the pellet. After 15 min incubation on ice, the lysate was centrifuged at 5000 g at 4°C for 10 min. The supernatant which contains the mitochondrial fraction with cytochrome c (fraction II) was collected and kept on ice. According to the ELISA kit protocol, aliquots from fractions I and II were pipetted into wells of the 96-well plate, followed by the addition of appropriate antibodies, conjugates, and substrates into each well. The absorbance was detected at 405 nm by a Tecan Infinite M200 microplate reader.

2.9. Measurement of Complex I, II, III, and IV Activity Levels. Complex I and IV activity levels were measured by a commercial kit (Genmed, USA) following the manufacturer's instructions. Complex II and III activity levels were measured by a commercial kit from Cayman (USA).

2.10. GSH/GSSG Ratio. Ultrasonication was used to prepare cell extracts. Cell extracts in ice-cold 5% metaphosphoric acid was centrifuged at 10,000 g for 20 min, and the supernatants were collected. The GSH content and T-GSH/GSSG of the supernatants were, respectively, determined by commercial kits (NJBC, Nanjing, China). The absorbance at 420 nm was measured using a spectrophotometer. Reduced GSH levels were determined by subtracting the $2 \times$ GSSG values from the T-GSH values, and the GSH/GSSG ratio was calculated.

2.11. RNA Isolation and Relative Quantitative Real-Time RT-PCR. Total RNA was extracted from A375 cells using RNAiso Plus (Takara) and stored at −80°C until further use. cDNA was synthesized from total RNA with a PrimeScript RT reagent kit (Takara). PCR reaction was performed using the SYBR Premix Ex Taq II (Takara) in a Lightcycler 480 (Roche). The results were normalized based on glyceraldehyde 3-phosphate dehydrogenase (GAPDH) expression, and the $2^{-\Delta\Delta CT}$ method was used to analyze the relative levels of mRNA (Schmittgen et al., 2008). The primer sequences were as follows (5′-3′): mitoNEET, forward CGA GTT GAA TGG ATC GCA GC, reverse ACA ACG GCA GTA CAC AGC TT; β-actin, forward AGA AAA TCT GGC ACC ACA CC, reverse TAG CAC AGC CTG GAT AGC AA.

2.12. Western Blotting. A375 cells were lysed with RIPA buffer (Beyotime) supplemented with protease inhibitors (Beyotime). Mitochondrial membrane proteins were extracted using the mitochondrial membrane protein isolation kit (Invent Biotechnologies). The lysates were centrifuged at 12,000 g for 10 min at 4°C, and the protein concentrations were determined by a BCA Protein Assay Kit. Then the protein samples were denatured at 100°C for 10 min. Equal amounts of protein were loaded in each well of 10% sodium dodecyl sulfate polyacrylamide gels and transferred to polyvinylidene fluoride membranes (Millipore, Billerica, MA, USA), blocked with 5% nonfat milk for 1 h at room temperature, and then incubated with antibodies specific for mitoNEET, cleaved PARP, cleaved caspase-3, and tubulin (Cell Signaling, USA) at 4°C overnight. Signals were detected with horseradish

peroxidase-conjugated secondary antibodies using a chemiluminescence process (Millipore) as per the manufacturer's instructions. Protein bands were detected on a bioimaging system (Bio-Rad, Berkeley, CA, United States).

2.13. Statistical Analysis. Data were expressed as the means ± standard deviation (SD). Statistical differences were analyzed by one-way analysis of variance followed by multiple comparisons performed with the Bonferroni post hoc test (SPSS version 18.0). P values < 0.05 were considered statistically significant.

3. Results

3.1. ISL Inhibits A375 Cell Proliferation and Induces Apoptosis. ISL inhibited the proliferation of A375 cells in a dose-dependent manner (Figure 1(a)). Specifically, treatment with ISL at 40 and 60 μg/mL led to 69.86% and 92.22% reduction in the proliferation of A375 cells, respectively. As shown in Figure 1(b), staining with Hoechst 33258 revealed the presence of nuclear pyknosis in ISL-treated A375 cells. Additionally, the control cells exhibited a fusiform shape and higher transmittance. However, the cells treated by 40 μg/mL ISL showed a shrunken cellular profile and lower transmittance compared with the control cells (Figure 1(c)). To quantify the rate of apoptosis, the cells were stained with FITC-conjugated annexin V and PI. Whereas the percentage of apoptotic cells was negligible in the control cultures, the 24 h ISL exposure led to a dose-dependent increase in both early and late apoptotic cells (Figure 1(d)). Furthermore, the protein levels of cleaved PARP and cleaved caspase-3 cells were significantly elevated after the ISL treatment (Figures 1(e) and 1(f)).

3.2. ISL Induces Mitochondrial Dysfunction in A375 Cells. MitoTracker Green staining showed that the mitochondria of the A375 cells treated by ISL formed an ovoid and multibranch-structured network (Figure 2(a)). Additionally, the JC-1 staining revealed that the MMP decreased following ISL treatment (Figures 2(b) and 2(c)). In parallel, the activity levels of complexes I–IV were reduced with ISL treatment (Figures 2(d)–2(f)). We also determined the levels of cytosol cytochrome c and mitochondria cytochrome c in A375 cells by ELISA, which revealed that the cytosolic cytochrome c levels were significantly increased after 24 h of ISL treatment; however, no significant changes were observed in the mitochondrial cytochrome c content (Figure 2(g)).

3.3. ISL Triggers ROS Generation, Which Contributes to ISL-Induced Apoptosis and Mitochondrial Dysfunction in A375 Cells. To assess the effect of ISL on mitochondrial ROS generation, we loaded A375 cells with MitoSOX Red which is a fluorescent probe which specifically targets mitochondria ROS in viable cells. We found that MitoSOX Red exhibited a near-complete colocalization with the MitoTracker Green probe (yellow areas) and that the fluorescence intensity of MitoSOX Red was significantly increased in cultures treated with 40 μg/mL ISL compared with the control cultures (Figure 3(a)). As shown in Figure 3(b), the fluorescence intensity of MitoSOX Red, as detected by flow cytometry, was increased 2.4-fold in cultures treated with 40 μg/mL ISL for 6 h compared with the control cells (Figure 3(b)).

We next utilized DCFH-DA to fluorescently detect total cellular ROS levels. As shown in Figure 2(c), the untreated cells showed a slight green DCFH-DA fluorescence, indicating the presence of low-level ROS in the cells. In contrast, the ISL-treated cells showed an apparent green fluorescence, indicating that ISL could induce additional ROS production in A375 cells. The histogram showed that the intracellular ROS levels were increased 3.2-fold in cultures that were treated with ISL for 6 h compared with the control cultures (Figure 2(c)). Cotreatment of the cultures with NAC and ISL led to a significant reduction in the total ROS levels; however, the levels of total ROS were significantly increased in cultures cotreated with ISL and BSO (Figure 2(c)).

The GSH/GSSG ratio was significantly decreased in A375 cells treated with ISL and significantly increased in cultures cotreated with ISL and NAC. Additionally, the reduction in the GSH/GSSG ratio was worse in cultures cotreated with ISL and BSO than in cultures treated with ISL alone (Figure 3(d)). Furthermore, the inhibition rate was lower in cultures cotreated with ISL and NAC than those treated with 40 μg/mL ISL group, indicating a protective effect. The inhibition rate was significantly higher compared with the cultures cotreated with ISL and BSO (Figure 3(e)).

As shown in the representative images in Figure 3(f), we also evaluated the changes in a cell shape in response to ISL treatment. The control cells exhibited a fusiform shape, whereas the ISL-treated cells were smaller in size with lower transmittance, indicating that the overall state of the ISL-treated cells was worse with compromised attachment. In contrast, stable attachment to the culture dish surface was observed in cultures treated with NAC, whereas cotreatment with ISL and BSO led to the reduction in the size of cells which exhibited compromised attachment ability (Figure 3(f)).

Both the early and late apoptosis rates were decreased by NAC and ISL cotreatment of the A375 cells. As seen in Figure 3(g), 19.3% of the cells were annexin V-negative and PI-positive, indicating that ISL cotreatment with BSO might cause necrosis in A375 cells (Figure 3(g)). The MMP was also higher in cells cotreated with ISL and NAC compared with ISL-treated cells, which was reduced in cells cotreated with ISL and BSO (Figures 3(h) and 3(i)). The cytosolic cytochrome c levels were also significantly decreased by ISL cotreatment with NAC, which were increased in cells cotreated with ISL and BSO. However, no significant changes in mitochondrial cytochrome c content were observed (Figure 3(j)).

3.4. ISL Inhibits the Expression of mitoNEET, Which Regulates ROS. To determine whether ISL impacted the expression of mitoNEET, we first determined the protein expression levels of mitoNEET by western blotting in A375 cells. As shown in Figure 4(a) and quantified in Figure 4(b), a significant decrease in mitoNEET expression was observed after ISL treatment. To confirm the effect of mitoNEET in ISL-treated A375 cells, we engineered an A375 cell line that overexpressed mitoNEET and confirmed that they exhibited

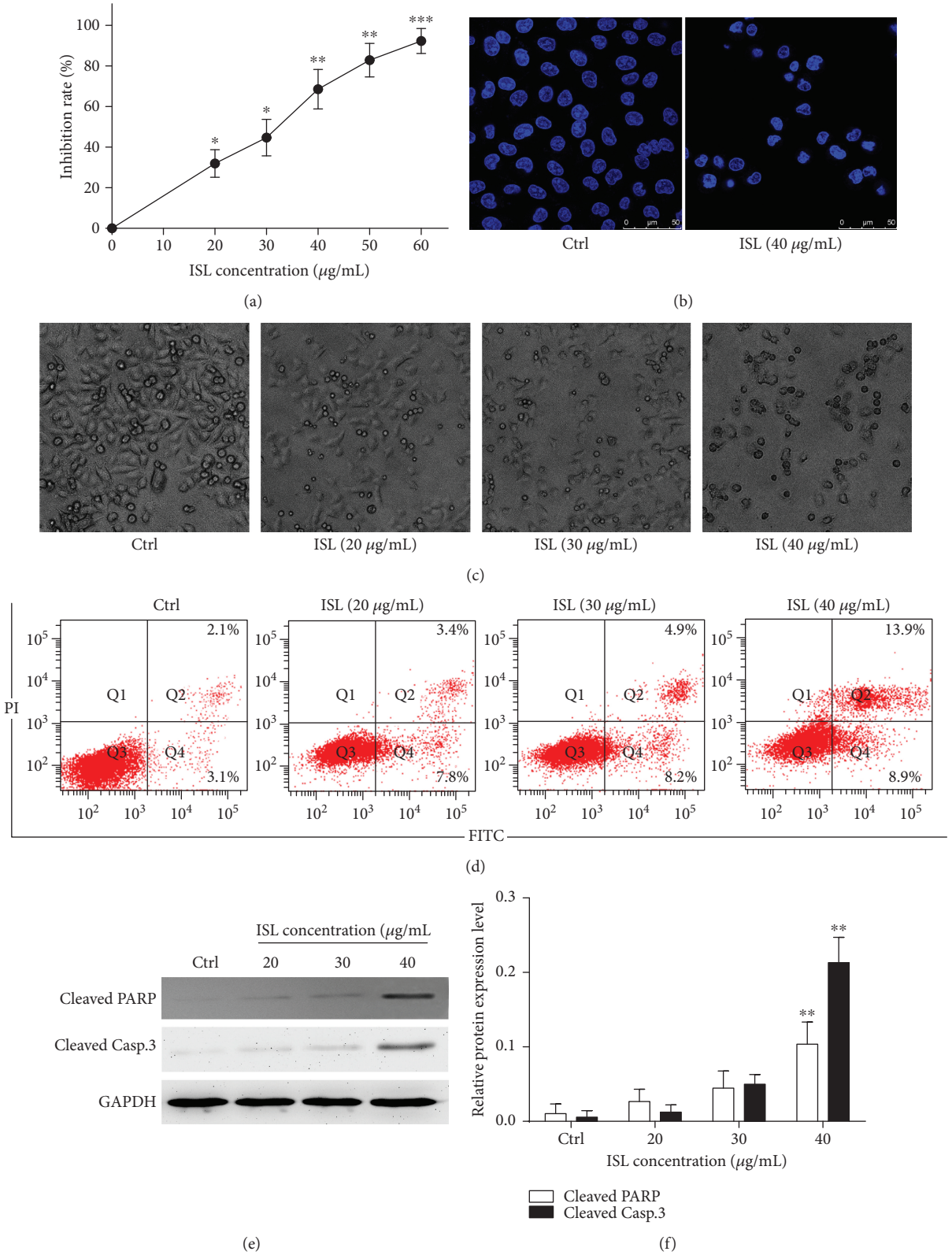

Figure 1: Isoliquiritigenin induces apoptosis in A375 melanoma cells. (a) Cell proliferation rate was detected by the MTT assay. (b) Hoechst 33258 staining showing nuclear shrinkage in A375 cells. (c) Phase-contrast micrographs (200x) showing morphological changes in isoliquiritigenin- (ISL-) treated A375 cells. (d) Apoptosis was measured by flow cytometry using double stain with annexin V and propidium iodide in A375 cells treated with ISL. (e) Western blotting analysis for cleaved PARP and cleaved caspase-3. (f) Analysis grayscale of band for western blotting. Data are expressed as band intensities of target protein/band intensity of the housekeeping protein. $^{*}P < 0.05$ and $^{**}P < 0.01$ versus control.

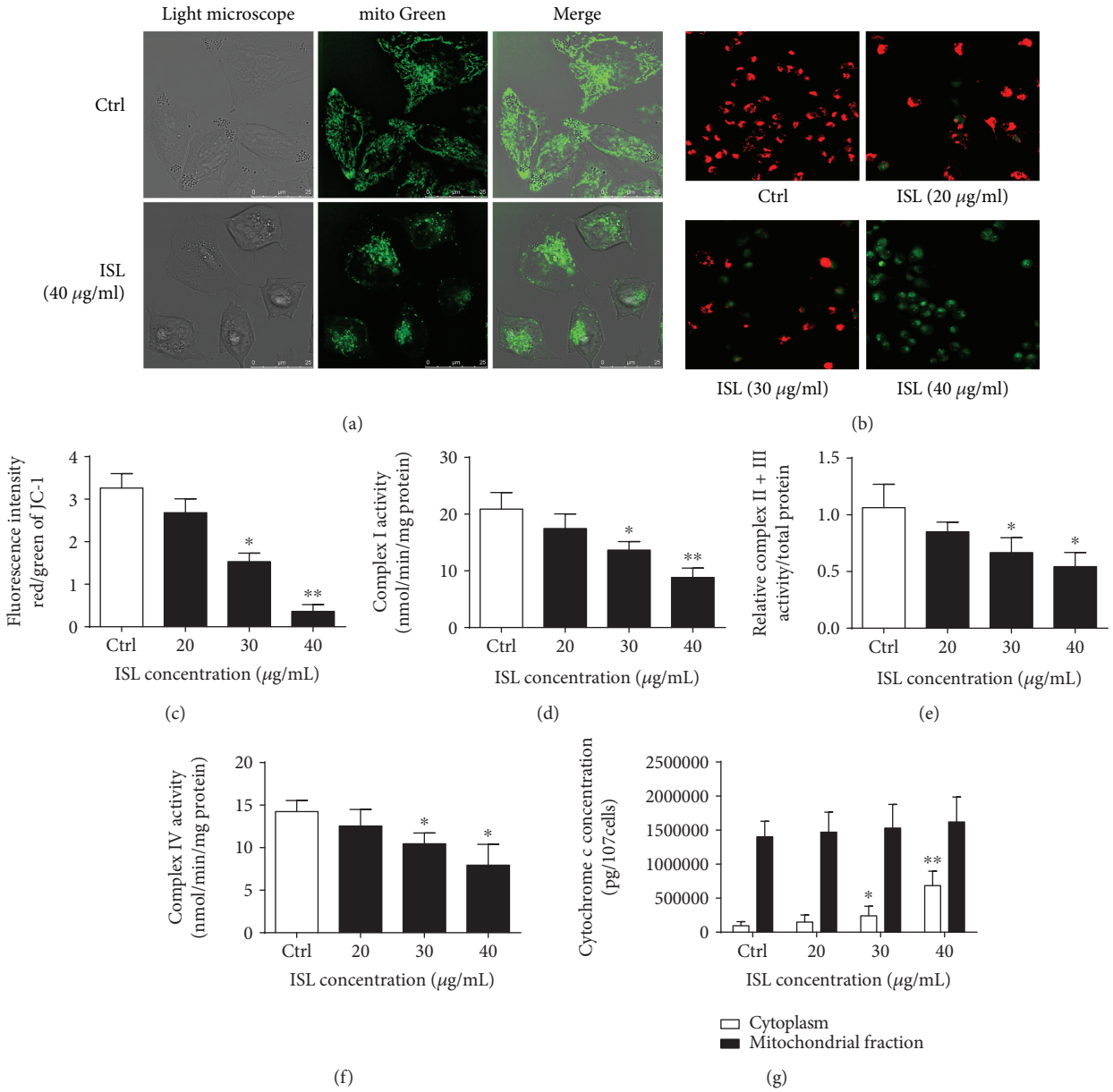

Figure 2: ISL induces mitochondrial dysfunction in A375 melanoma cells. (a) Representative confocal images showing the fluorescent distribution of MitoTracker Green (excitation, 495 nm; emission, 535 nm) in A375 cells with or without ISL treatment. (b) Representative confocal images showing the fluorescent JC-1 probe in A375 cells treated with different concentrations of ISL. (c) Quantification of the JC-1 fluorescence intensity detected by flow cytometry. (d–f) Complex I–IV activity analysis in ISL-treated A375 cells. (g) Cytosolic and mitochondrial cytochrome c concentrations determined by enzyme-linked immunosorbent assay. $^{*}P < 0.05$ and $^{**}P < 0.01$ versus control.

a significant increase in the mitoNEET expression compared with the control cells that expressed the empty vector (vector-Ctrl cells). Intriguingly, ISL treatment of the mitoNEET-overexpressing cells led to a reduction in mitoNEET expression compared with the untreated mitoNEET-overexpressing cells (Figures 4(a) and 4(b)).

We next examined the consequence of mitoNEET overexpression on cellular ROS generation. The mitoNEET-overexpressing cells showed a significantly lower levels of cellular ROS compared with the vector-Ctrl cells. In addition, ISL treatment resulted in a significant increase in the level of ROS in the mitoNEET-overexpressing cells (Figure 4(c)). The proliferation rate of the mitoNEET-overexpressing cells was significantly higher than that of the vector-Ctrl cells, and ISL treatment of the mitoNEET-overexpressing cells led to the proliferation rate significant decrease (Figure 4(d)). Furthermore, the mitoNEET-overexpressing cells exhibited a significantly higher MMP compared with the vector-Ctrl cells. However, ISL treatment led to a significant decrease of MMP in the mitoNEET-overexpressing A375 cells (Figure 4(e)). The levels of cleaved PARP and cleaved caspase-3, which were significantly higher in the ISL-

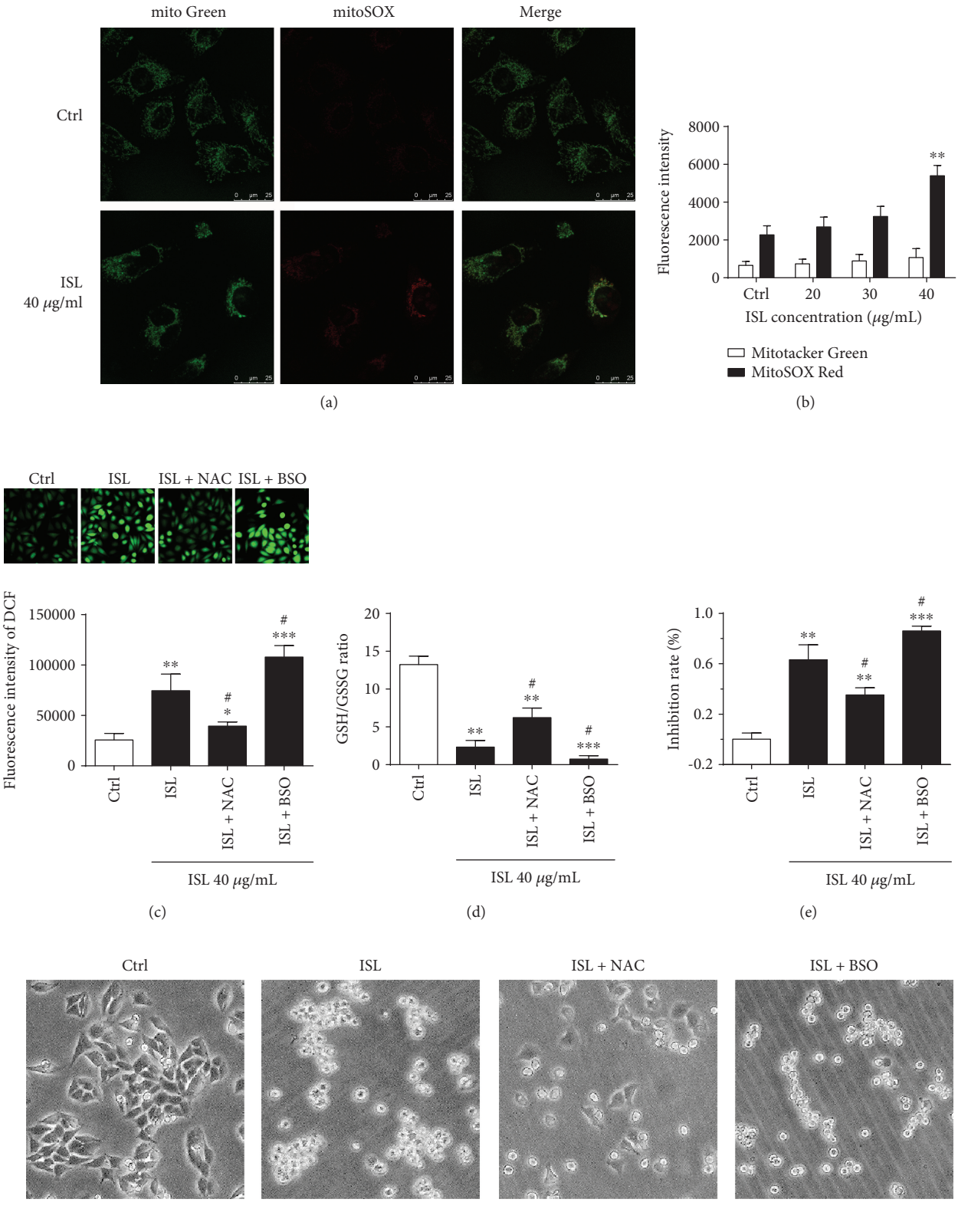

Figure 3: Continued.

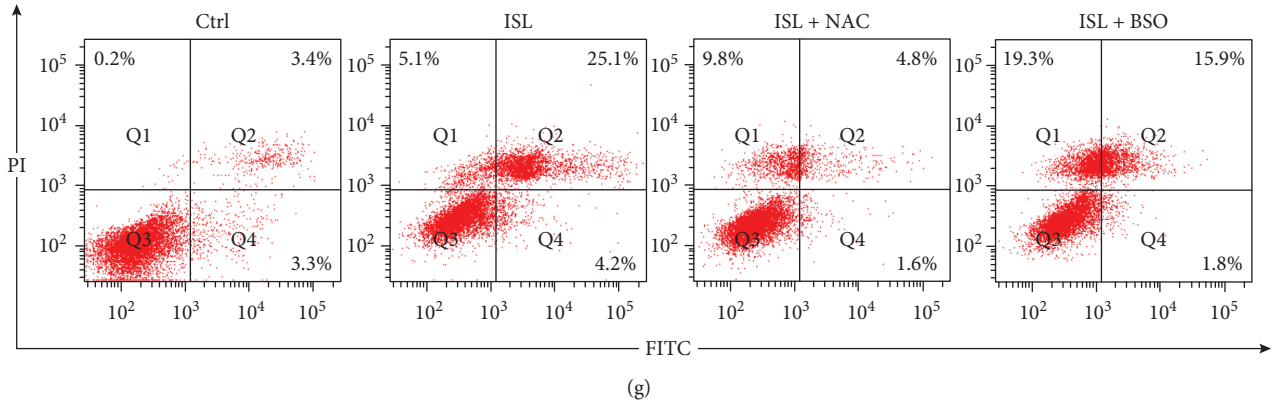

(g)

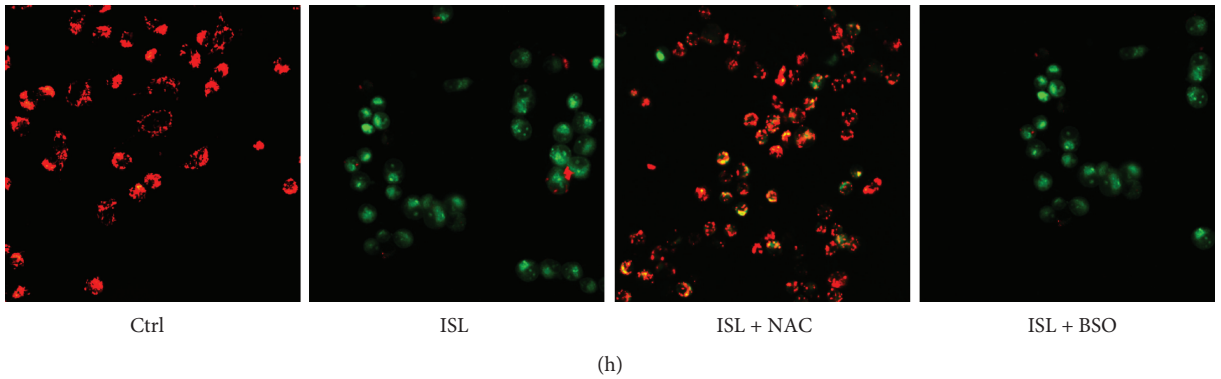

(h)

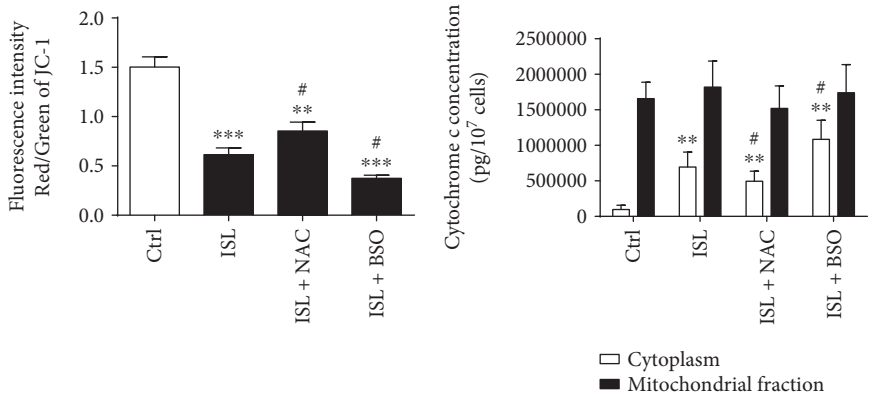

(i) (j)

Figure 3: ISL triggers the production of reactive oxygen species, which contributes to ISL-induced apoptosis and mitochondrial dysfunction in A375 cells. (a) Representative confocal microscopy images of mitochondrial network in A375 cells treated with or without ISL. (b) Quantification of the MitoSOX Red and MitoTracker Green fluorescence intensity detected by flow cytometry. (c) Representative confocal microscopy images of DCFH-DA and quantification of the DCFH-DA fluorescence intensity by flow cytometry. (d) Analysis of the GSSH/GSH ratio. (e) The inhibition rates of A375 cells treated by ISL alone or ISL cotreated with NAC or BSO. (f) Phase-contrast micrographs (200x) showing morphological changes in A375 cells treated with ISL alone or ISL cotreated with NAC or BSO. (g) Apoptosis rates of A375 cells determined by annexin V/PI double staining in response to indicated treatments. (h) Representative confocal microscopy images of the JC-1 probe in A375 cells treated by ISL alone or ISL cotreated with NAC or BSO. (i) Quantification of the JC-1 fluorescence intensity in A375 cells by flow cytometry. (j) Cytosolic and mitochondrial cytochrome c concentrations in A375 cells treated by ISL alone or ISL cotreated with NAC or BSO. $^{*}P < 0.05$, $^{**}P < 0.01$, and $^{***}P < 0.001$ versus control; $^{\#}P < 0.05$ versus ISL.

treated A375 cells compared with the control cells, were significantly lower in the ISL-treated mitoNEET-overexpressed cells (Figures 4(f)–4(h)). The expressions of cleaved PARP and cleaved caspase-3 were lower in the ISL-treated vector-mitoNEET cells compared with those in the ISL-treated cells, suggesting that mitoNEET might act as an antiapoptotic factor (Figures 4(f)–4(h)).

4. Discussion

Melanoma is the most aggressive form of skin cancer, and its poor prognosis is largely due to resistance to conventional chemotherapy with cytotoxic drugs. Compounds used in traditional Chinese medicine represent the characteristics of small molecules with weak receptor binding [30, 31],

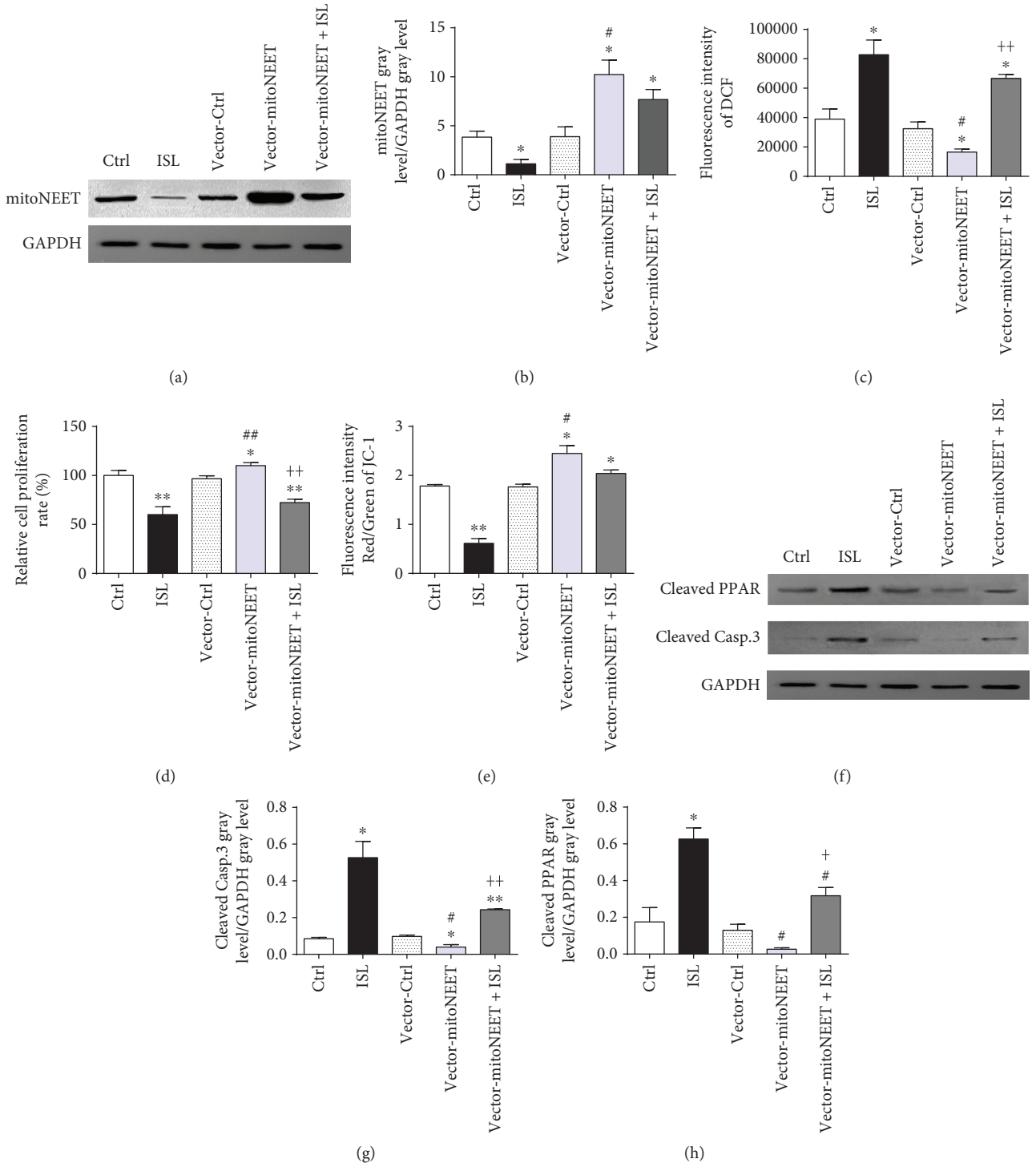

Figure 4: ISL inhibits the expression of mitoNEET, which regulates ROS, and subsequently induces apoptosis and mitochondrial dysfunction in A375 cells. (a) ISL inhibits the protein expression of mitoNEET in A375 cells detected by western blotting. (b) Relative band intensities of mitoNEET in empty vector- or mitoNEET-overexpressing cells with or without ISL treatment. (c) ISL regulates cellular ROS levels by controlling the mitoNEET expression. (d) ISL induces proliferation inhibition of A375 cells by inhibiting the expression of mitoNEET. (e) ISL decreases mitochondrial membrane potential by inhibiting the expression of mitoNEET in A375 cells. (f) ISL increases the expression of cleaved PARP and cleaved caspase-3 by inhibiting the expression of mitoNEET. (g–h) Relative band intensities of cleaved PARP and cleaved caspase-3 in empty vector- or mitoNEET-overexpressing cells with or without ISL treatment. $^{*}P < 0.05$ and $^{**}P < 0.01$ versus control; $^{\#}P < 0.05$ and $^{\#\#}P < 0.01$ versus ISL; and $^{+}P < 0.05$ and $^{++}P < 0.01$ versus vector-Ctrl.

implying that they can bind not just one target receptor but many, exerting various effects. In contrast, the potential for severe toxicity and serious side effects is higher with chemical drugs that bind a single target with a strong affinity. In general, compounds used in traditional Chinese medicine have better effects compared with chemotherapeutic drugs in melanoma therapy.

ISL is an important medicinal derived from licorice [32] that was demonstrated to induce apoptosis through distinct molecular mechanisms in several cell lines [33–35]. However, ISL as an inducer of mitochondrial dysfunction was rarely reported. In this study, we found that ISL-induced apoptosis and mitochondrial dysfunction were associated with the decrease of mitoNEET expression, which regulates cellular ROS levels. We found that the rate of apoptosis was increased, with cytochrome c release from the mitochondria after ISL treatment in A375 cells. Apoptotic morphological changes including clear nuclear pyknosis were also observed. Moreover, the levels of cleaved PARP and cleaved caspase-3 were significantly increased by ISL treatment. Caspase-3 activation leads to the DNA repair enzyme PARP cleavage. Cleaved PARP, which occurs early during the execution phase of apoptosis, is considered a general hallmark of apoptosis [36]. So the increase of cleaved PARP and cleaved caspase-3 indicated ISL could induce A375 cell apoptosis. The mitochondrion is involved in several levels of the fate of a cell, whether it will survive or not, and plays a key role in cell apoptosis signaling by controlling cellular energy metabolism and contributing to the control of ROS levels [37]. We found that the mitochondrial distribution was organized, with an ovoid-shaped and a multibranch structure, in A375 cells treated by ISL. We also found that there was a sharp decline in the MMP following the ISL treatment. Mitochondrial respiratory chain complex I-IV activity was also simultaneously decreased by the ISL treatment. Finally, we determined that the cytosolic cytochrome c levels were significantly increased after the ISL treatment, in the absence of a significant change in the mitochondrial cytochrome c content.

Previous studies demonstrated that ISL could induce ROS generation [25, 27, 38]. We indeed observed that the mitochondrial ROS levels were increased in response to ISL in A375 cells. Additionally, we also showed that the levels of total cellular ROS were also increased by the ISL treatment. We utilized the ROS scavenger NAC and the ROS agonist BSO to further elucidate the effect of ROS on ISL-induced apoptosis and mitochondrial dysfunction in A375 cells and found that NAC was protective against ISL-induced apoptosis and mitochondrial dysfunction. We further found that NAC cotreatment with ISL led to the inhibition and reduction in the apoptosis rate in A375 cells. The cellular morphology also exhibited an obvious improvement compared with that observed in the ISL-treated cells. The cotreatment with NAC also led to an increase in the MMP and a decrease in the cytosolic cytochrome c levels. In contrast, cotreatment of the cells with ISL and BSO led to increased inhibition and apoptosis rates, and the necrosis of A375 cells could be clearly observed by annexin V/PI double staining. The decrease in MMP and the increase in cytosolic cytochrome c levels were also observed in A375 cells cotreated with ISL and BSO. Overall, these findings demonstrate that ROS play an important role in ISL-induced apoptosis and mitochondrial dysfunction in A375 cells.

Several studies have showed the effects of mitoNEET on disease associated with oxidative stress such as cancer, obesity, and Parkinson's disease [22, 23]. Human NEET family members, including CISD1, CISD2 (also known as NAF1), and CISD3 (also known as Miner2), are important stress response proteins involved in the regulation of iron and ROS accumulation in the mitochondria [39]. Previous studies showed that the overexpression of mitoNEET in MDA-MB-231 breast cancer cells led to an increase in the expression of mitochondrial ETC complexes as well as the proliferation of tumor [23]. L929 fibrosarcoma cells constitutively express high levels of mitoNEET, which is required for tumor necrosis factor alpha- (TNF-α-) induced necroptosis in the presence of caspase inhibition [40]. Furthermore, mitoNEET serves as a mitochondrial binding site for the TNF-α-induced translocation of the Stat3-Grim-19 complex. Suppression of the mitoNEET expression prevented the TNF-α-induced translocation of the Stat3-Grim-19 complex to the mitochondria, with suppression of Grim-19 or Stat3 expression preserving cell viability in hepatocytes exposed to ethanol and fructose and treated with TNF-α [39]. We found that the expression of mitoNEET was decreased by ISL treatment in A375 cells. We also found that the cellular ROS levels could be regulated by mitoNEET, as observed by the significant increase in ROS levels by the inhibition of mitoNEET expression by ISL. However, mitoNEET overexpression led to a reduction in the cellular ROS levels. Further analysis revealed that the mitoNEET overexpression led to increases in the proliferation rate and the MMP of A375 cells, highlighting the relevance of mitoNEET as a regulator of the oxidative capacity of melanoma cells.

In summary, ISL induced apoptosis and mitochondrial dysfunction in A375 melanoma cells by inhibiting the expression of mitoNEET. The data provide evidence for a novel pathway in ISL-induced apoptosis of melanoma cells and highlight the unique role of mitoNEET as an essential molecule in mitochondrial injury and apoptosis.

Abbreviations

ISL: Isliquiritigenin
IMM: Mitochondrial inner membrane
OMM: Mitochondrial outer membrane
MOMP: Mitochondrial outer membrane permeabilization
ROS: Reactive oxygen species
CISD1: CDGSH iron sulfur domain 1
Casp.3: Caspase-3
NBT: Nitroblue tetrazolium
H_2O_2: Hydrogen peroxide
ROS: Reactive oxygen species
GSH: Reducted glutathione
GSSG: Oxidated glutathione
MTT: Methyl thiazolyl tetrazolium
ATP: Adenosine triphosphate
NAC: N-Acetyl-L-cysteine

BSO: Buthionine sulfoximine.

Data Availability

The data used to support the findings of this study are included in the article.

Conflicts of Interest

The authors declare that they have no conflicts of interest.

Authors' Contributions

The conception and design of the study were by X-Y. C., D-F. L., and Q-S. Z. The experiment was performed by X-Y. C., X-N. L., H-H. R., and D. W. The statistical analysis was calculated by X-Y. C. and X-N. L. under the supervision of D-F. L. and Q-S. Z. All authors contributed to the analysis and interpretation of the data. X-Y. C. wrote the manuscript. The preparation of the figures and the online supplementary figure was done by X-Y. C.

Acknowledgments

This study was funded by the National Natural Science Foundation of China (Grant nos. 81872162 and 81602556 to De-Fang Li, Grant no. 31870338 to Qiu-Sheng Zheng), the Natural Science Foundation of Shandong Province (Grant No. ZR2017JL030 to De-Fang Li), the Taishan Scholars Construction Engineering of Shandong Province (to De-Fang Li), Yantai High-End Talent Introduction Plan "Double Hundred" (to De-Fang Li), the Scientific Research Foundation of Binzhou Medical University (Grant no. BY2016KYQD01 to De-Fang Li), and the Dominant Disciplines' Talent Team Development Scheme of Higher Education of Shandong Province (to De-Fang Li).

Supplementary Materials

Figure S1: pLVX-CMV-MCS-T2A-Zsgreenn vector map. Figure S2: mitoNEET overexpression vector sequencing and matching result. Table S1: primers designed for mitoNEET and 3*flag. *(Supplementary Materials)*

References

[1] A. Norain and E. Dadachova, "Targeted radionuclide therapy of melanoma," *Seminars in Nuclear Medicine*, vol. 46, no. 3, pp. 250–259, 2016.

[2] A. Mahadevan, V. L. Patel, and N. Dagoglu, "Radiation therapy in the management of malignant melanoma," *Oncology*, vol. 29, no. 10, pp. 743–751, 2015.

[3] P. Gorayski, B. Burmeister, and M. Foote, "Radiotherapy for cutaneous melanoma: current and future applications," *Future Oncology*, vol. 11, no. 3, pp. 525–534, 2015.

[4] M. Schwarz, M. A. Andrade-Navarro, and A. Gross, "Mitochondrial carriers and pores: key regulators of the mitochondrial apoptotic program?," *Apoptosis*, vol. 12, no. 5, pp. 869–876, 2007.

[5] C. Liu, K. Gong, X. Mao, and W. Li, "Tetrandrine induces apoptosis by activating reactive oxygen species and repressing Akt activity in human hepatocellular carcinoma," *International Journal of Cancer*, vol. 129, no. 6, pp. 1519–1531, 2011.

[6] N. Lane and W. Martin, "The energetics of genome complexity," *Nature*, vol. 467, no. 7318, pp. 929–934, 2010.

[7] C. Wang and R. J. Youle, "The role of mitochondria in apoptosis," *Annual Review of Genetics*, vol. 43, no. 1, pp. 95–118, 2009.

[8] G. Kroemer, L. Galluzzi, and C. Brenner, "Mitochondrial membrane permeabilization in cell death," *Physiological Reviews*, vol. 87, no. 1, pp. 99–163, 2007.

[9] D. L. Vaux, "Apoptogenic factors released from mitochondria," *Biochimica et Biophysica Acta*, vol. 1813, no. 4, pp. 546–550, 2011.

[10] B. Halliwell, "Free radicals and antioxidants-quo vadis?," *Trends in Pharmacological Sciences*, vol. 32, no. 3, pp. 125–130, 2011.

[11] C. C. Winterbourn, "Are free radicals involved in thiol-based redox signaling?," *Free Radical Biology & Medicine*, vol. 80, pp. 164–170, 2015.

[12] Q. Chen, E. J. Vazquez, S. Moghaddas, C. L. Hoppel, and E. J. Lesnefsky, "Production of reactive oxygen species by mitochondria: central role of complex III," *The Journal of Biological Chemistry*, vol. 278, no. 38, pp. 36027–36031, 2003.

[13] Y. Liu, G. Fiskum, and D. Schubert, "Generation of reactive oxygen species by the mitochondrial electron transport chain," *Journal of Neurochemistry*, vol. 80, no. 5, pp. 780–787, 2002.

[14] J. F. Turrens, "Mitochondrial formation of reactive oxygen species," *The Journal of Physiology*, vol. 552, no. 2, pp. 335–344, 2003.

[15] S. Orrenius, V. Gogvadze, and B. Zhivotovsky, "Calcium and mitochondria in the regulation of cell death," *Biochemical and Biophysical Research Communications*, vol. 460, no. 1, pp. 72–81, 2015.

[16] M. L. Circu and T. Y. Aw, "Reactive oxygen species, cellular redox systems, and apoptosis," *Free Radical Biology & Medicine*, vol. 48, no. 6, pp. 749–762, 2010.

[17] G. L. Taminelli, V. Sotomayor, A. G. Valdivieso, M. L. Teiber, M. C. Marín, and T. A. Santa-Coloma, "CISD1 codifies a mitochondrial protein upregulated by the CFTR channel," *Biochemical and Biophysical Research Communications*, vol. 365, no. 4, pp. 856–862, 2008.

[18] S. E. Wiley, A. Y. Andreyev, A. S. Divakaruni et al., "Wolfram syndrome protein, Miner1, regulates sulphydryl redox status, the unfolded protein response, and Ca^{2+} homeostasis," *EMBO Molecular Medicine*, vol. 5, no. 6, pp. 904–918, 2013.

[19] J. A. Zuris, Y. Harir, A. R. Conlan et al., "Facile transfer of [2Fe-2S] clusters from the diabetes drug target mitoNEET to an apo-acceptor protein," *Proceedings of the National Academy of Sciences of the United States of America*, vol. 108, no. 32, pp. 13047–13052, 2011.

[20] J. A. Simoneau, J. H. Veerkamp, L. P. Turcotte, and D. E. Kelley, "Markers of capacity to utilize fatty acids in human skeletal muscle: relation to insulin resistance and obesity and effects of weight loss," *The FASEB Journal*, vol. 13, no. 14, pp. 2051–2060, 1999.

[21] S. E. Wiley, A. N. Murphy, S. A. Ross, P. van der Geer, and J. E. Dixon, "MitoNEET is an iron-containing outer mitochondrial membrane protein that regulates oxidative capacity,"

Proceedings of the National Academy of Sciences of the United States of America, vol. 104, no. 13, pp. 5318–5323, 2007.

[22] C. M. Kusminski, W. L. Holland, K. Sun et al., "MitoNEET-driven alterations in adipocyte mitochondrial activity reveal a crucial adaptive process that preserves insulin sensitivity in obesity," *Nature Medicine*, vol. 18, no. 10, pp. 1539–1549, 2012.

[23] Y. S. Sohn, S. Tamir, L. Song et al., "NAF-1 and mitoNEET are central to human breast cancer proliferation by maintaining mitochondrial homeostasis and promoting tumor growth," *Proceedings of the National Academy of Sciences of the United States of America*, vol. 110, no. 36, pp. 14676–14681, 2013.

[24] X. Chen, M. Yang, W. Hao et al., "Differentiation-inducing and anti-proliferative activities of isoliquiritigenin and all-trans-retinoic acid on B16F0 melanoma cells: mechanisms profiling by RNA-seq," *Gene*, vol. 592, no. 1, pp. 86–98, 2016.

[25] X. Chen, B. Zhang, X. Yuan et al., "Isoliquiritigenin-induced differentiation in mouse melanoma B16F0 cell line," *Oxidative Medicine and Cellular Longevity*, vol. 2012, Article ID 534934, 11 pages, 2012.

[26] D. Li, Z. Wang, H. Chen et al., "Isoliquiritigenin induces monocytic differentiation of HL-60 cells," *Free Radical Biology & Medicine*, vol. 46, no. 6, pp. 731–736, 2009.

[27] X. Yuan, B. Zhang, N. Chen et al., "Isoliquiritigenin treatment induces apoptosis by increasing intracellular ROS levels in HeLa cells," *Journal of Asian Natural Products Research*, vol. 14, no. 8, pp. 789–798, 2012.

[28] Y. Wang, J. Ma, X. Yan et al., "Isoliquiritigenin inhibits proliferation and induces apoptosis via alleviating hypoxia and reducing glycolysis in mouse melanoma B16F10 cells," *Recent Patents on Anti-Cancer Drug Discovery*, vol. 11, no. 2, pp. 215–227, 2016.

[29] C. Quoilin, A. Mouithys-Mickalad, S. Lécart, M. P. Fontaine-Aupart, and M. Hoebeke, "Evidence of oxidative stress and mitochondrial respiratory chain dysfunction in an *in vitro* model of sepsis-induced kidney injury," *Biochimica et Biophysica Acta (BBA) - Bioenergetics*, vol. 1837, no. 10, pp. 1790–1800, 2014.

[30] H. Ichikawa, X. Wang, and T. Konishi, "Role of component herbs in antioxidant activity of Shengmai San — a traditional Chinese medicine formula preventing cerebral oxidative damage in rat," *The American Journal of Chinese Medicine*, vol. 31, no. 4, pp. 509–521, 2003.

[31] R. Tian, S. Xu, X. Lei, W. Jin, M. Ye, and H. Zou, "Characterization of small-molecule-biomacromolecule interactions: from simple to complex," *TrAC Trends in Analytical Chemistry*, vol. 24, no. 9, pp. 810–825, 2005.

[32] F. Peng, Q. Du, C. Peng et al., "A review: the pharmacology of isoliquiritigenin," *Phytotherapy Research*, vol. 29, no. 7, pp. 969–977, 2015.

[33] S. K. Jung, M. H. Lee, D. Y. Lim et al., "Isoliquiritigenin induces apoptosis and inhibits xenograft tumor growth of human lung cancer cells by targeting both wild type and L858R/T790M mutant EGFR," *Journal of Biological Chemistry*, vol. 289, no. 52, pp. 35839–35848, 2014.

[34] D. H. Kim, J. E. Park, I. G. Chae, G. Park, S. Lee, and K. S. Chun, "Isoliquiritigenin inhibits the proliferation of human renal carcinoma Caki cells through the ROS-mediated regulation of the Jak2/STAT3 pathway," *Oncology Reports*, vol. 38, no. 1, pp. 575–583, 2017.

[35] B. Zhang, Y. Lai, Y. Li et al., "Antineoplastic activity of isoliquiritigenin, a chalcone compound, in androgen-independent human prostate cancer cells linked to G2/M cell cycle arrest and cell apoptosis," *European Journal of Pharmacology*, vol. 821, pp. 57–67, 2018.

[36] C. Vizetto-Duarte, L. Custódio, K. N. Gangadhar et al., "Isololiolide, a carotenoid metabolite isolated from the brown alga *Cystoseira tamariscifolia*, is cytotoxic and able to induce apoptosis in hepatocarcinoma cells through caspase-3 activation, decreased Bcl-2 levels, increased p53 expression and PARP cleavage," *Phytomedicine*, vol. 23, no. 5, pp. 550–557, 2016.

[37] G. Jacquemin, D. Margiotta, A. Kasahara et al., "Granzyme B-induced mitochondrial ROS are required for apoptosis," *Cell Death and Differentiation*, vol. 22, no. 5, pp. 862–874, 2015.

[38] H. Chen, B. Zhang, X. Yuan et al., "Isoliquiritigenin-induced effects on Nrf2 mediated antioxidant defence in the HL-60 cell monocytic differentiation," *Cell Biology International*, vol. 37, no. 11, pp. 1215–1224, 2013.

[39] S. Tamir, M. L. Paddock, M. Darash-Yahana-Baram et al., "Structure-function analysis of NEET proteins uncovers their role as key regulators of iron and ROS homeostasis in health and disease," *Biochimica et Biophysica Acta (BBA) - Molecular Cell Research*, vol. 1853, no. 6, pp. 1294–1315, 2015.

[40] N. Shulga and J. G. Pastorino, "Mitoneet mediates TNFα-induced necroptosis promoted by exposure to fructose and ethanol," *Journal of Cell Science*, vol. 127, no. 4, pp. 896–907, 2014.

Hindawi
Oxidative Medicine and Cellular Longevity
Volume 2019, Article ID 4398695, 13 pages
https://doi.org/10.1155/2019/4398695

Research Article

Antioxidant Properties of Fullerene Derivatives Depend on Their Chemical Structure: A Study of Two Fullerene Derivatives on HELFs

Vasilina Sergeeva,[1] **Olga Kraevaya**,[2,3] **Elizaveta Ershova**,[1] **Larisa Kameneva**,[1] **Elena Malinovskaya**,[1] **Olga Dolgikh**,[1] **Marina Konkova**,[1] **Iliya Voronov**,[2] **Alexander Zhilenkov**,[2] **Natalia Veiko**,[1] **Pavel Troshin**,[2,3] **Sergei Kutsev**,[1] **and Svetlana Kostyuk**[1]

[1]*Research Centre for Medical Genetics (RCMG), Moscow 115478, Russia*
[2]*Institute of Problems of Chemical Physics of Russian Academy of Sciences, Moscow Region 142432, Russia*
[3]*Skolkovo Institute of Science and Technology, Skolkovo Innovation Center, Nobel St. 3, Moscow, 143026, Russia*

Correspondence should be addressed to Vasilina Sergeeva; tracytheplane@gmail.com

Received 13 July 2018; Revised 11 October 2018; Accepted 19 November 2018; Published 17 January 2019

Guest Editor: Patricia Morales

Oxidative stress is a major issue in a wide number of pathologies (neurodegenerative, cardiovascular, immune diseases, and cancer). Because of this, the search for new antioxidants is an important issue. One of the potential antioxidants that has been enthusiastically discussed in the past twenty years is fullerene and its derivatives. Although in aqueous solutions fullerene derivatives have shown to be antioxidants, their properties in this regard within the cells are controversially discussed. We have studied two different water-soluble fullerene C60 and C70 derivatives on human embryonic lung fibroblasts at a wide range of concentrations. Both of them cause a decrease in cellular ROS at short times of incubation (1 hour). Their prolonged action, however, is fundamentally different: derivative GI-761 causes secondary oxidative stress whereas derivative VI-419-P3K keeps ROS levels under control values. To gain a better understanding of this effect, we assessed factors that could play a role in the response of cells to fullerene derivatives. Increased ROS production occurred due to NOX4 upregulation by GI-761. Derivative VI-419-P3K activated the transcription of antioxidant master regulator NRF2 and caused its translocation to the nucleus. This data suggests that the antioxidant effect of fullerene derivatives depends on their chemical structure.

1. Introduction

Oxidative stress plays an important role in various diseases (Alzheimer's disease, schizophrenia, rheumatoid arthritis, diabetes, cardiovascular diseases, and cancer) and ageing [1–3]. Healthy cells produce physiological levels of reactive oxygen species (ROS) that can be localized in the cytoplasm, nucleus, or cell membrane. ROS is important for processes connected to cell cycle regulation, proliferation, apoptosis, and signaling, as well as kinase activity regulation and gene expression regulation [4]. Increased amounts of ROS lead to DNA damage, oxidative stress, and cell death [5–7]; therefore, novel antioxidants are of interest.

One of the synthetic antioxidants that gained a lot of attention in the past decades is fullerene and its derivatives. The chemical structure of fullerene derivatives allows them to effectively neutralize ROS [8]. Although it has been shown that fullerene derivatives act as strong antioxidants in solutions, the data concerning their antioxidant properties on cell cultures is controversial. Some studies confirm the antioxidative action of fullerenes whereas others show that cells treated with fullerenes exhibit signs of oxidative stress.

Fullerenes and their derivatives have shown cytoprotective action when cells were treated by ROS-inducing damaging factors. The polyvinylpyrrolidone fullerene C60 derivative registered as Radical Sponge® protects human keratinocytes from the damaging action of ultraviolet light that typically causes ROS production and oxidative stress [9]. In addition, fullerene C60 derivatives are able to neutralize TiO_2-photocatalized ROS in keratinocytes and skin tissues [10]. Fullerenol C60(OH)36 is able to protect human erythrocytes against high-energy electrons [11].

However, the dependence of antioxidant action of fullerene derivatives on their chemical structure still remains unclear. It is believed that derivatives with a higher degree of functionalization have lower antioxidant activities due to disruption of the π-system. However, this generalization is not always correct, for example, malonic acid trisadducts proved to have a higher antioxidant activity than bisadducts containing ethylene glycol chains. It is unclear whether functionalization or the nature of the chemical moieties attached to the fullerene cage is more important for the antioxidant properties. In addition, fullerene derivatives are able to aggregate based on their chemical structure, thus decreasing their concentration and availability, as well as interact with enzymes and other biological molecules based on the structure and charge of the substance. This presents a challenge in discovering the dependence of antioxidant properties on the chemical structure of the fullerene derivative [12]. Antioxidant and prooxidant gene activation by fullerene derivatives remains an open question and requires further investigation. In this work, we have studied two water-soluble derivatives of fullerenes C60 and C70, bearing solubilizing residues of amino acid and aromatic acid on human embryonic lung fibroblasts (HELFs). Fullerene derivative GI-761 comprises five residues of 4-amino-3-phenylbutanoic acid and a chlorine atom arranged around one cyclopentadienyl unit on the [60]fullerene carbon sphere. On the contrary, solubilizing addends in the structure of compound VI-419-P3K are attached at the equator of the fullerene C70 cage. This study provides details and insights on the antioxidant activity of fullerene derivatives.

2. Materials and Methods

2.1. Cell Culture. Human embryonic lung cells (fourth passage) were provided by the Research Centre for Medical Genetics (RCMG). Approval#5 was obtained from the Committee for Medical and Health Research Ethics of RCMG. Cells were seeded at 1.7×104 per ml in DMEM (Paneco, Moscow, Russia) with 10% fetal calf serum (PAA, Vienna, Austria), 50 U/ml penicillin, 50 μg/ml streptomycin, and 10 μg/ml gentamycin, and cultured at 37°C for 2 or 24 h as previously described in [13, 14]. Investigated fullerene derivatives were added to the medium, and the cells were cultured for periods ranging from 15 min to 48 h.

2.2. Antibodies. Primary antibodies FITC-γH2AX (pSer139) (Chemicon, Temecula, USA), NRF2, BRCA2 (Santa Cruz Biotechnology, Dallas, USA), NOX4, pNRF2, and FITC goat anti-rabbit IgG (Abcam, Cambridge, UK) were used.

2.3. Flow Cytometry Analysis (FCA). Cells were washed with Versene solution, then treated with 0.25% trypsin, washed with culture medium, and suspended in PBS. Paraformaldehyde (PFA, Sigma-Aldrich, Saint Louis, USA) treatment at 37°C for 10 min was performed to fix the cells. Cells were washed three times with 0.5% BSA-PBS and permeabilized with 0.1% Triton X-100 in PBS for 15 min at 20°C or with 90% methanol at 4°C, then washed with 0.5% BSA-PBS (3 times) and stained with antibodies (1 μg/ml) for 2 h at 4°C, and washed three times with 0.5% BSA-PBS. The cells were then incubated for 2 h (20°C) with FITC goat anti-rabbit IgG (1 μg/ml) and analyzed.

2.4. Fluorescence Microscopy. The Axio Scope.A1 microscope (Carl Zeiss) and the confocal microscopy platform Leica TCS SP8 (Germany) were used for fluorescent microscopy of stained cells.

2.5. Immunocytochemistry. Cells were grown in slide flasks (25 cm^3, Thermo Fisher Scientific, Waltham, USA), fixed in 3% paraformaldehyde at 4°C for 20 min, washed with PBS, and then permeabilized with 0.1% Triton X-100 in PBS for 15 min at room temperature, followed by blocking with 0.5% BSA in PBS for 1 h and incubation overnight at 4°C with the antibodies. After washing with 0.1% Triton X-100 in PBS, fibroblasts were incubated for 2 h at room temperature with the FITC goat anti-mouse IgG, washed with PBS, and then stained with DAPI as described in [13, 14].

2.6. Reactive Oxygen Species (ROS) Assays. Cells were grown in 96-well plates, incubated with investigated derivatives, washed with PBS, and treated with 10 μM solution of H2DCFH-DA in PBS (Molecular Probes/Invitrogen, Carlsbad, USA) for 20 min. Cells were washed three times with PBS and analyzed at 37°C using the total fluorescence assay in a plate reader at λex = 488 nm and λem = 528 nm (EnSpire Equipment, Turku, Finland). The ROS analysis was performed with three techniques: flow cytometry, fluorescent microscopy, and total fluorescence assay in a 96-well plate. The reaction rate constant for the formation of DCF (k) was calculated using the dependence of the DCF signal intensity on the time of cell incubation with H2DCFH-DA. The data are presented as the k_i/k_0 ratio, where k_i and k_0 are the rate constants in the exposed and unexposed cells, respectively. The average value of the DCF signal for 16 wells ± standard deviation is reported.

2.7. MTT Assay. Cells were grown in a 96-well plate for 72 h. Survival was measured using the 3-(4,5-dimethylthiazol-2-yl)-2,5-diphenyltetrazolium bromide (MTT) assay, as described previously [13, 14]. The plates were read at 550 nm (EnSpire reader).

2.8. Quantification of mRNA Levels. Total mRNA was isolated using the RNeasy Mini Kit (Qiagen, Hilden, Germany), treated with DNAse I, and then reverse transcribed by the Reverse Transcriptase kit (Sileks, Moscow, Russia). The expression profiles were obtained using qRT-PCR with SYBR Green PCR Master Mix (Applied Biosystems, Foster City, USA). The mRNA levels were analyzed using StepOnePlus

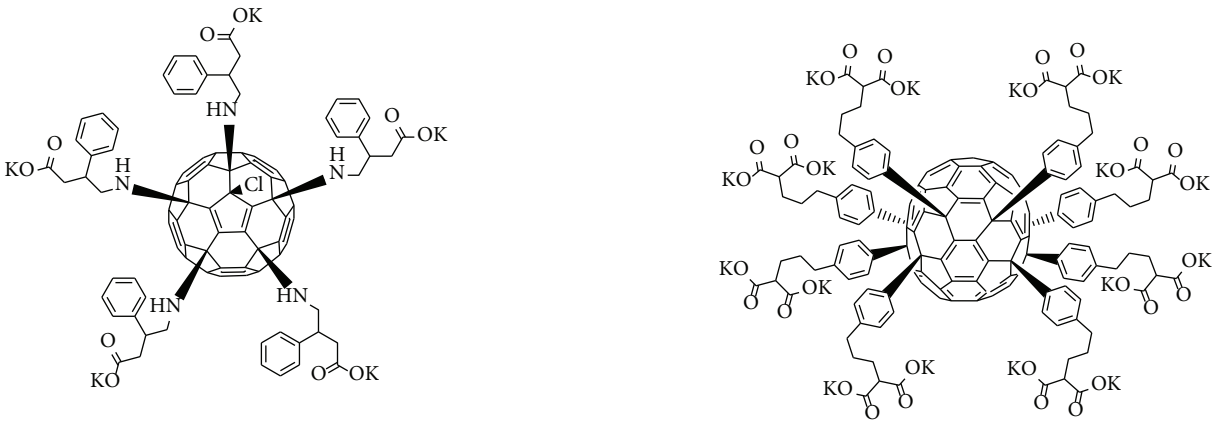

Figure 1: Molecular structures of the investigated water-soluble fullerene derivatives GI-761 and VI-419-P3K.

(Applied Biosystems); the technical error was approximately 2%. *TBP* was used as a reference gene. The following primers were used (Sintol, Moscow, Russia): *BRCA1* (F: TGTGAGGCACCTGTGGTGA, R: CAGCTC CTGGCACTGGTAGAG); *NRF2* (*NFE2L2*) (F: TCCAGT CAGAAACCAGTGGAT, R: GAATGTCTGCGCCAAA AGCTG); *NOX4* (F: TTGGGGCTAGGATTGTGTCTA; R: GAGTGTTCGGCACATGGGTA); *BRCA2* (F: CCTC TGCCCTTATCATCACTTT; R: CCAGATGATGTCTT CTCCATCC); *CCND1* (F: TTCGTGGCCTCTAAGATGA AGG; R: GAGCAGCTCCATTTGCAGC); and *TBP* (reference gene) (F: GCCCGAAACGCCGAATAT, R: CCGTGG TTCGTGGCTCTCT).

2.9. Comet Assay. Cells were suspended in low-melting-point agarose and placed onto slides precoated with 1% normal-melting-point agarose. The slides were placed in a solution of 10 mM Tris-HCl (pH 10), 2.5 M NaCl, 100 mM EDTA, 1% Triton X-100, and 10% DMSO at 4°C for 1 h. Electrophoresis was performed for 20 min at 1 V/cm and 300 mA in an electrophoresis buffer (300 mM NaOH, 1 mM EDTA, and pH > 13). The slides were fixed in 70% ethanol and stained with SYBR Green I (Invitrogen, USA).

Images of comets were analyzed using CASP v.1.2.2 software.

2.10. Statistics. The results were repeated at least three times as independent biological replicates. In FCA, the medians of the signal intensities were analyzed. The figures show the mean and standard deviation (SD). The significance of the observed differences was analyzed with nonparametric Mann-Whitney U tests. P values < 0.05 were considered statistically significant and marked on figures with "$*$." Data were analyzed with StatPlus2007 professional software (http://www.analystsoft.com).

2.11. Synthesis of the Fullerene Derivatives. Polycarboxylic water-soluble fullerene derivatives GI-761 and VI-419-P3K (Figure 1) were synthetized in three steps from the readily available precursors $C_{60}Cl_6$ and $C_{70}Cl_8$ [15] following previously developed methodology [16, 17].

Details of the synthesis of the compounds and their spectral characterization data are provided in the supporting information. Both compounds showed high solubility in water and culture medium in the presence as well as in the absence of serum.

3. Results and Discussion

Investigated derivatives were prescreened for toxicity towards HELFs by the MTT assay as described in [13, 14]. When the concentration of the used derivatives was higher than 20 μM, at least 50% of the treated cells died within 3 days.

3.1. GI-761 and VI-419-P3K Affect ROS Production in HELFs. ROS production level was measured with the DCF reagent in a plate reader (EnSpire, Finland). The dependence of DCF fluorescence on time is shown in Figure 2. The inclination (k) reflects the ROS production rate. Linear approximation was used to calculate the inclination. The DCF synthesis rate shows the amount of ROS in the cell culture. The results are shown as a ratio of k_i/k_0, where k_i is the inclination for the time and concentration of interest and k_0 is the inclination in control cells.

Initially (1 h), GI-761 at both low (4 nM and 0.4 μM) and high (4 μM and 20 μM) concentrations significantly reduces the amount of ROS in the cells. In 3 h, the amount of ROS in cells in the presence of 0.4, 4, and 20 μM of fullerene increases. The concentration of 4 nM of GI-761 keeps ROS levels below the control level. GI-761 caused a significant increase in ROS levels at all investigated concentrations (4 nM, 0.4, 4, and 20 μM) after 24 h of incubation with HELFs.

Derivative VI-419-P3K at low (4 nM and 0.4 μM) and high (20 μM) concentrations significantly reduces the amount of ROS in the cells after 1 h of incubation. The concentration of 4 μM, however, stimulates the synthesis of ROS. ROS production increases after 3 h of incubation with 0.4 and 20 μM of VI-419-P3K. At a concentration of 4 nM, the ROS levels do not change. At a concentration of 4 μM of fullerene, VI-419-P3K stimulates ROS synthesis to the greatest extent.

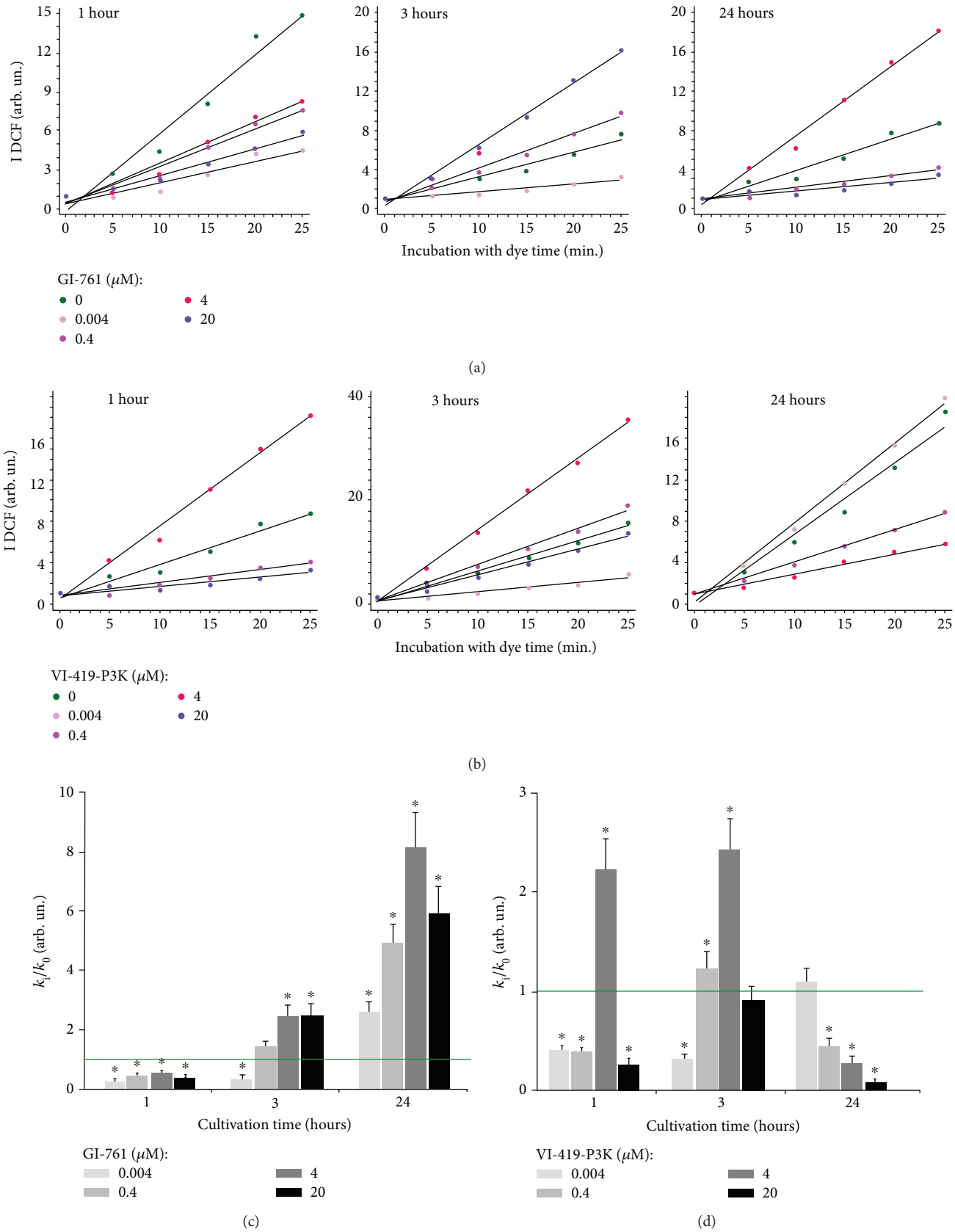

FIGURE 2: ROS levels in cells treated with fullerene derivatives. (a, b) Fluorescence plate reader: dependence of DCF signal intensity on GI-761 (a) and VI-419-P3K (b) concentration and exposure time. (c, d) Dependence of the k_i/k_0 index on GI-761 (c) and VI-419-P3K (d) concentration and exposure time.

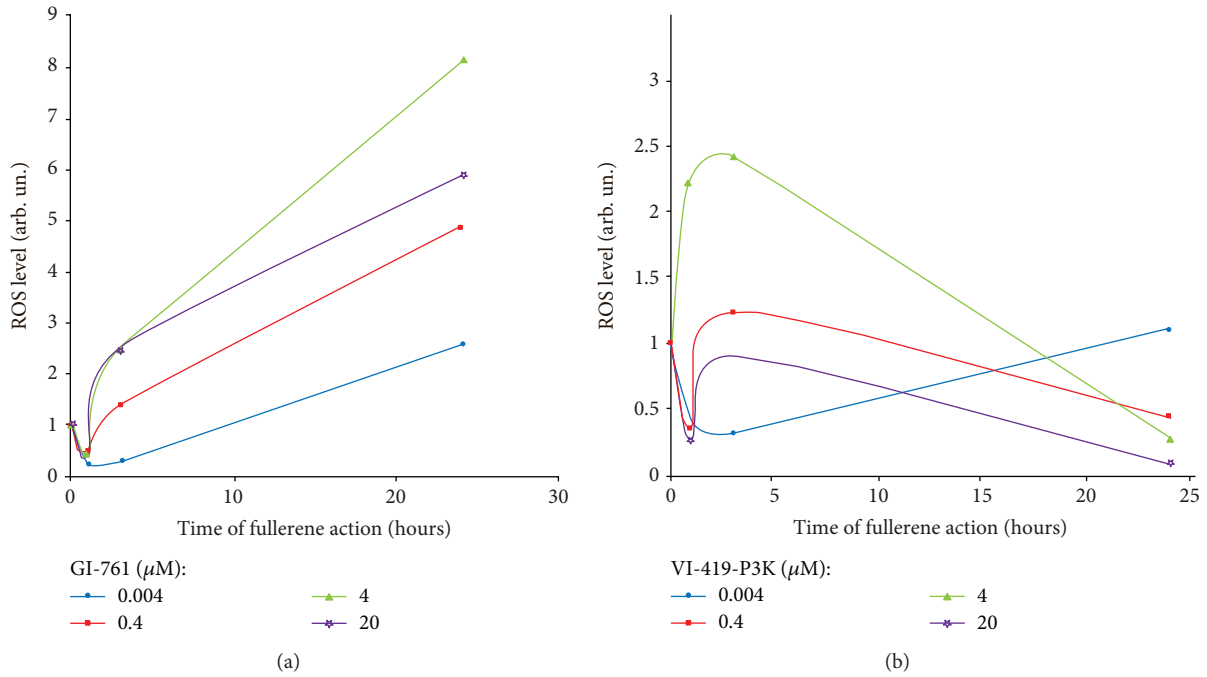

Figure 3: Dependence of ROS levels in HELFs treated with GI-761 (a) and VI-419-P3K (b) on time of incubation.

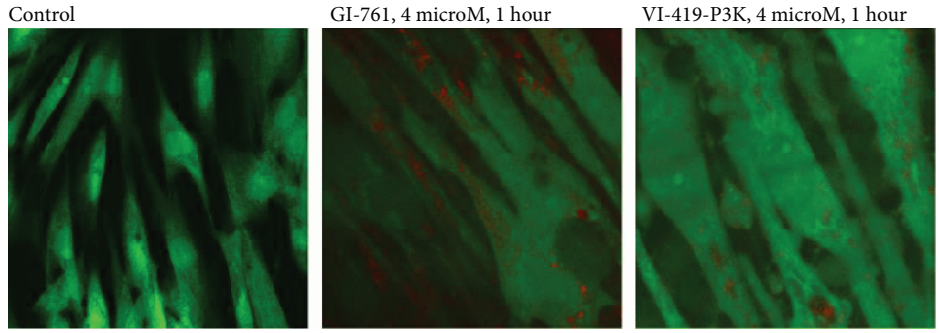

Figure 4: Colocalization of fullerene derivatives GI-761 and VI-419-P3K (red stains) and ROS stained with DCF, fluorescent microscopy.

After a day of incubation with VI-419-P3K (0.4, 4, and 20 μM), a significant decrease in ROS levels is observed. The ROS levels were increased in the presence of 4 nM of fullerene, but did not exceed the control level.

The scheme illustrating the change of ROS levels in fibroblasts under the action of fullerenes GI-761 and VI-419-P3K is shown in Figure 3. All studied concentrations of GI-761 cause rapid decrease of ROS levels in cells 1 h after addition, but in 3 h, it is replaced by increasing ROS levels (Figure 3(a)). The maximum increase in ROS levels is observed after 24 hours of cultivation at a concentration of 4 μM. At very low concentrations (4 nM), VI-419-P3K causes a rapid decrease in ROS levels in cells, which lasts at least three hours and returns to the control values after 24 hours of cultivation (Figure 3(b)). At a low concentration (0.4 μM), ROS levels drop after 1 hour, then after 3 hours, increase above the control, and after 24 hours, decrease again. At a concentration of 4 μM, VI-419-P3K causes a significant increase in ROS levels after 1-3 hours of exposure. In 24 hours of incubation with VI-419-P3K, the synthesis of ROS was below the control values. High concentration of fullerene induced a rapid decrease in ROS levels after 1 hour, a return to the control level after 3 hours, and again a very sharp decrease after 24 hours.

Nonlinear dependence of the ROS changes indicates a complex nature of fullerenes' effect on ROS levels in cells. It is possible that ROS levels in cells are affected by two countervailing processes. The first process is the binding of ROS by nanoparticles of fullerenes (a similar effect for carbon-based nanomaterials is shown in [18]). However, in response to the primary reduction of ROS, processes aimed at ROS production are rapidly activated. The resulting effect is determined by the concentration of fullerenes and the time of action. To determine what is the cause of the detected nonlinear dependence of the cell response to GI-761 and VI-419-P3K, several cellular parameters that can affect ROS levels were analyzed.

Colocalization of investigated fullerene derivatives and ROS (stained with DCF) is shown in Figure 4. Red stains of

fullerene derivatives are surrounded by black spots where there is no ROS indicating that the derivatives neutralize ROS in their surroundings.

3.2. GI-761 and VI-419-P3K Affect Prooxidant and Antioxidant Gene Expressions in HELFs. One of the main producers of physiological amounts of ROS in cells is NADPH oxidases [19] (NOX family). We have previously shown that ROS production in cells treated with fullerene derivatives increased due to NOX4 activation [13]. We measured the amount of NOX4 using the method of flow cytometry.

Average signals of FL1-NOX4 per cell are shown in Figures 5(d) and 5(e). After 1 hour of cultivation with GI-761 at concentrations of 4 nM or 4 μM, a decrease in the expression of NOX4 protein was detected. At a concentration of 20 μM, GI-761 increases the level of NOX4. In 3 h, GI-761 causes an increase in the amount of NOX4 protein levels at all studied concentrations. Maximal amount of NOX4 was seen at 20 μM of fullerene. Longer cultivation (24 hours) is accompanied by a repeated decline in the amount of NOX4 in fibroblasts at 4 and 20 μM concentrations of fullerene derivative GI-761. In 48 hours, an increased level of protein expression was observed for all used concentrations of fullerenes.

One hour after the addition of the compound to the culture medium of HELFs at a concentration of 4 μM, VI-419-P3K fullerene derivative causes an increase in the level of NOX4 in cells. 4 nM and 20 μM reduce the amount of NOX4. In 3 hours, a decrease in the amount of NOX4 is observed for all studied concentrations of VI-419-P3K. Maximal amounts of NOX4 in HELFs were at 4 μM of fullerene. Longer cultivation (24 hours) is accompanied by a repeated increase in the NOX4 levels in fibroblasts at all tested concentrations of fullerene VI-419-P3K. In 48 hours, an increased level of the protein expression was observed only for 4 μM fullerene VI-419-P3K.

Thus, both ROS levels and NOX4 protein levels have a nonlinear dependence on the time of incubation and the concentration of the studied substances.

The gene expression of NOX4 on the mRNA levels was assessed with quantitative real-time PCR. The data is shown in Figure 6. Data concerning the amount of NOX4 mRNA in cells treated with 4 nM of GI-761 and VI-419-P3K fullerenes correlate with the protein NOX4 data. Thus, we can say that regulation of the gene expression of NOX4 in response to the action of 4 nM fullerene is regulated mainly on the level of gene transcription. The amount of protein in the case of 4 μM of GI-761 is different from the amount of mRNA. Despite the same amount of mRNA of a gene, the amount of protein in the case of 4 μM fullerene was much higher than that in the case of 4 nM. Another exception was the data for VI-419-P3K after 48 h of cultivation. Apparently, under certain conditions, fullerenes can regulate amounts of protein on a posttranscriptional level.

As NOX4 catalyzes the formation of ROS, it is important to know where the enzyme is located in the cell. The accumulation of the enzyme close to the nucleus or in the nucleus itself can contribute to enhance the synthesis of ROS there and oxidative DNA damage. The localization of NOX4 in cells treated with fullerene derivatives was assessed with fluorescent microscopy (Figures 5(a) and 5(b)).

In the control cells, NOX4 is localized mainly in the cytoplasm and near the plasma membrane of cells. Small amounts of protein can be found in the nuclei of some cells. Concentrations of 4 nM, 4 μM, and 20 μM of fullerenes GI-761 and VI-419-P3K had a similar effect on the change of NOX4 localization depending on time. The most significant change was observed in the case of 4 μM of fullerene. Fullerene stimulates the expression of NOX4 in the nuclei of the cells. After 1 hour, the NOX4 signal is clearly visible in the nucleus compared to the cytoplasm of cells. In 3 h, NOX4 is still present in the cell nucleus but is also increased in other structures of the cell. After prolonged cultivation (48 hours), the level of NOX4 expression reduced in the nuclei of cells and is increased in the cytoplasm of cells.

Short-term cultivation of HELFs with fullerene increases the amount of NOX4 in the nuclei of the cells, and this should lead to increased synthesis of ROS in the nuclei of the cells. Localization of ROS in nonfixed cells treated with 4 μM of fullerene for 1 hour was assessed in order to confirm the immunofluorescence data. The data is shown in Figure 5.

In control cells, the ROS synthesis occurs in the cytoplasm, mainly in the mitochondria (meandering bright lines) and on the surface of the cell membrane (bright spots, remote from the nuclei). In the presence of fullerenes GI-761 and VI-419-P3K, the main signal of DCF is visible in the cell nucleus. This change in the localization of ROS in the cell may be responsible for the apparent small decrease in ROS levels.

We analyzed the dependence of ROS levels on the amounts of NOX4 in the treated cells. Figure 6 shows the dependence for three time points and three different concentrations of fullerenes GI-761 and VI-419-P3K.

GI-761 causes an increase in the NOX4 expression after 3 h of incubation. This is accompanied by an increase in ROS levels in the cells. In 24 h, despite a decrease in NOX4, increased levels of ROS are present in the cells. VI-419-P3K at concentrations of 4 μM and 20 μM increases the NOX4 expression in 1 h of incubation, which leads to an increased ROS amount in 3 h. In 24 h, however, the NOX4 expression is increased, but the ROS levels are decreased.

This response can be divided into two stages: early (1-3 hours) and late (24-48 hours) stages. After 1 hour of cultivation with GI-761 (4 nM-4 μM) and VI-419-P3K (4 nM-20 μM), there is a decline in the physiological level of ROS in cells, which indicates the ability of fullerenes GI-761 and VI-419-P3K to effectively neutralize ROS and the possibility of their use as antioxidants (with the exception of 4 μM for VI-419-P3K). However, the "late" response of cells to the fullerenes GI-761 and VI-419-P3K is different—VI-419-P3K has a prolonged (up to 24 hours) antioxidant effect, whereas fullerene GI-761 causes a secondary peak in the ROS synthesis after 24 hours of incubation.

Thus, the effect of fullerene derivatives on the ROS production in HELFs depends on the chemical moieties attached to the fullerene core and on the shape and size of the fullerene cage. To assess the possible cause of time dependence and to explain the difference between the actions of the two

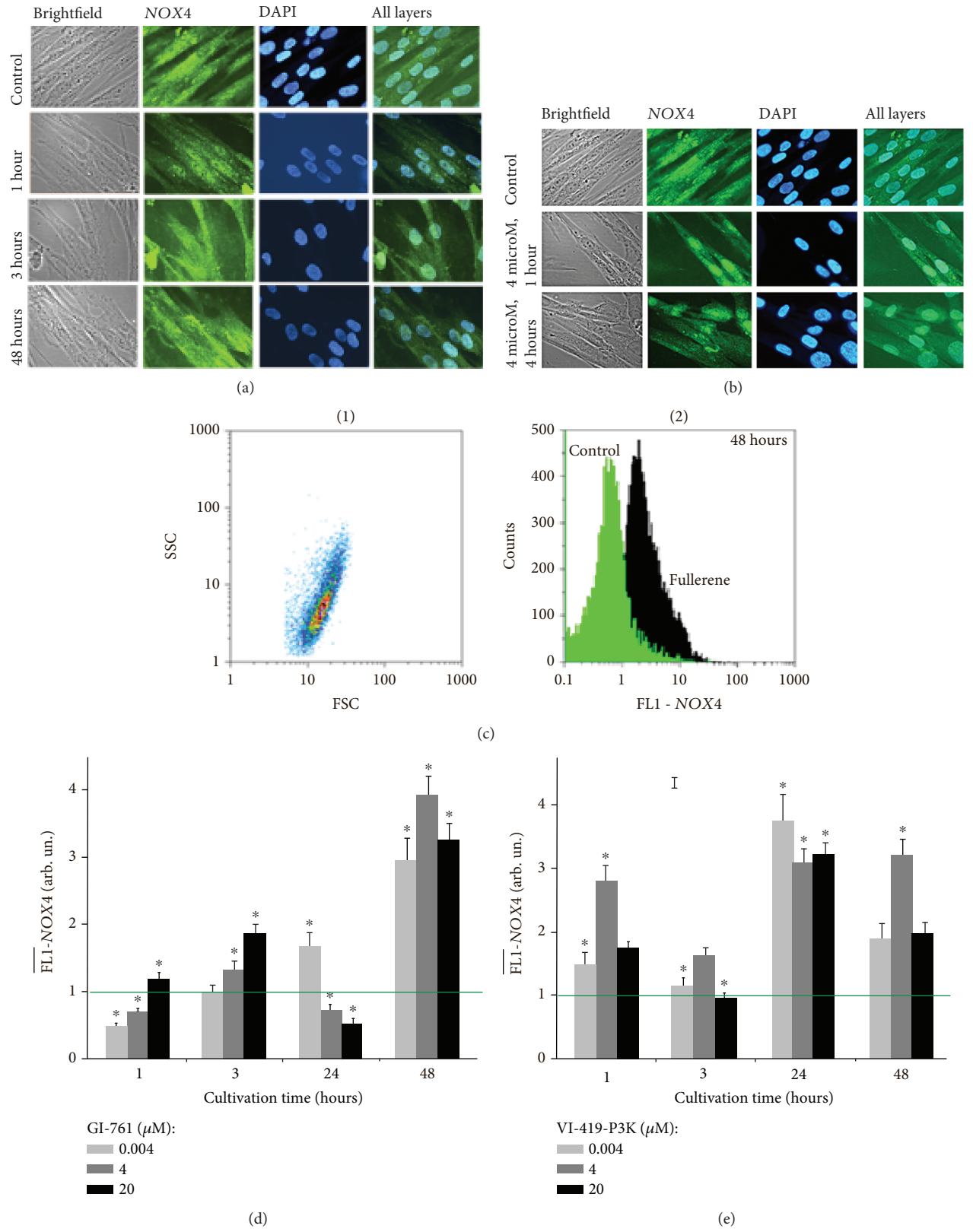

Figure 5: NOX4 expression in HELFs incubated with GI-761 and VI-419-P3K. (a, b) Fluorescent microscopy: localization of NOX4 within fixed cells stained with DAPI and antibodies to NOX4 in HELFs treated with (a) GI-761 and (b) VI-419-P3K. (d, e) FCA: FL1-NOX4 levels for HELFs treated with GI-761 (d) and VI-419-P3K (e). Concentrations and times of exposure shown in graphs.

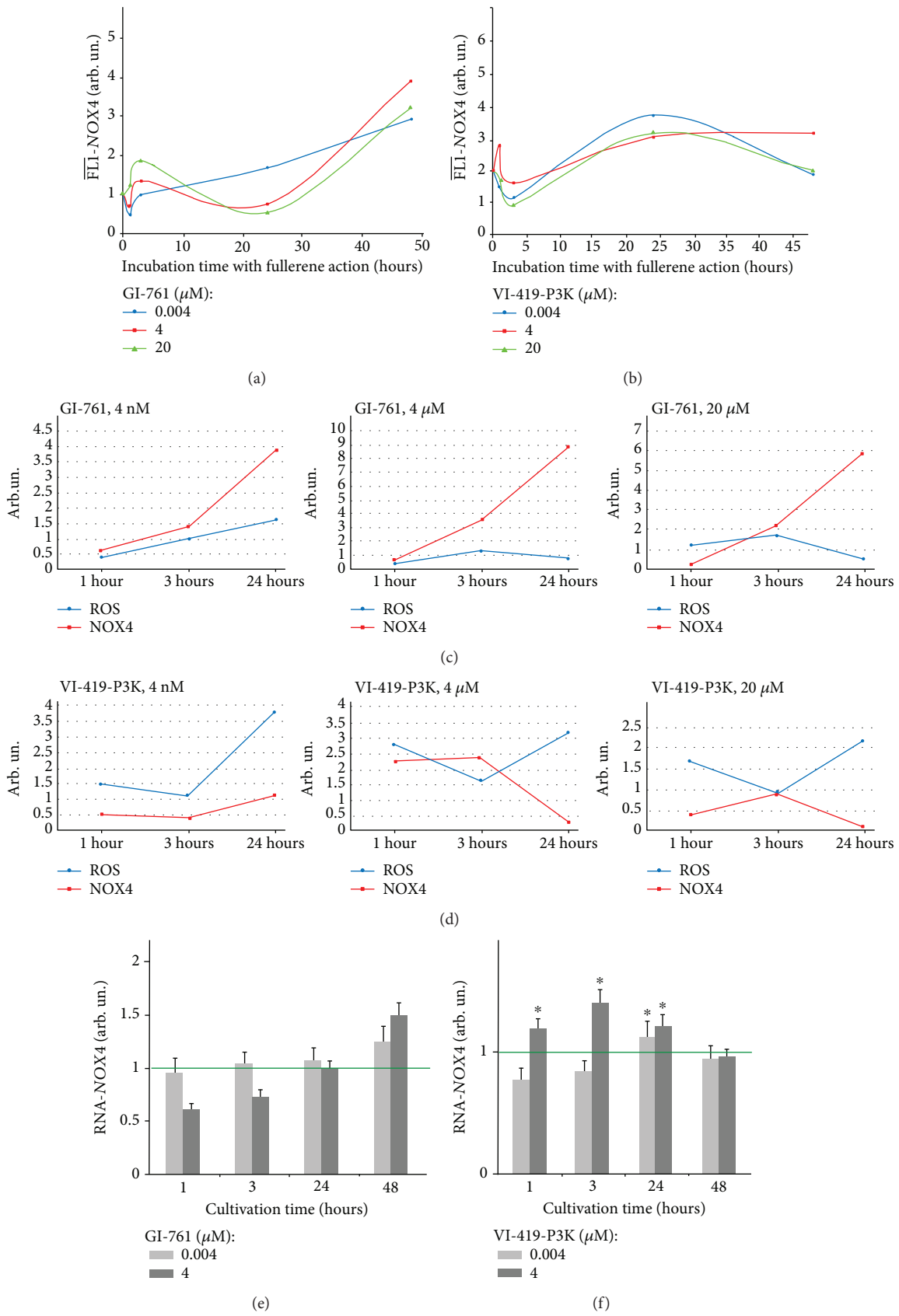

Figure 6: Dependence of NOX4 protein levels on time for HELFs treated with GI-761 (a) and VI-419-P3K (b). Concentrations and times of exposure shown in graphs. (c, d) Dependence of NOX4 protein levels and ROS levels shown in one graph. NOX4 mRNA levels in HELFs treated with GI-761 (e) and VI-419-P3K (f).

investigated fullerene derivatives on HELFs, we looked at the antioxidant response system of the cells.

NRF2 (erythroid-derived factor 2) is one of the main transcription factors that determine antioxidant response of the cells to the action of the internal and external ROS. NRF2 controls constitutive inducible expressions of several genes that contain ARE in their promotor region [20]. NRF2 is regulated both at the level of amount of protein and at the level of its localization in the cells as the factor only affects the gene expression within the nucleus [21]. It is known that NRF2 regulates ROS production by the mitochondria and NADPH oxidases [22]. The change in the NOX4 expression and ROS levels suggests that the activity of NRF2 can be altered in the presence of fullerenes. The amount of NRF2 in the cells was assessed with flow cytometry (Figure 7); an average signal intensity of FL1-NRF2 per cell was detected.

Within the first 3 h of incubation, GI-761 (4 nM, 4, and 20 μM) causes no increase in the NRF2 expression in HELFs, but in 24-48 h, a slight increase (1.2–1.7-fold) is detected. Unlike GI-761, derivative VI-419-P3K induces the activation of NRF2. After 1 h of incubation of VI-419-P3K (4 nM, 4 μM, and 20 μM), an increase of NRF2 (1.5, 2.8, and 1.8 times, respectively) is observed (Figure 7(b)). After 3 h with 4 nM of fullerene, the amount of NRF2 is reduced. After 24 h of incubation with all investigated concentrations, VI-419-P3K caused an increase in the NRF2 levels 3-4-fold (Figure 7(b)).

The change in the NRF2 mRNA amount under the action of fullerenes is shown in Figure 7(c). GI-761 does not affect the level of NRF2 gene expression at all investigated concentrations and times of incubation. These data indicate that GI-761 can regulate the expression of the transcription factor NRF2 at both the transcription level and the posttranscriptional level. Most likely, fullerene can promote the release of NRF2 from the complex with its inhibitor KEAP1 [23], resulting in a better recognition of free NRF2 by antibodies.

Unlike GI-761, derivative VI-419-P3K causes the activation of NRF2 gene expression in 24 and 48 hours, which correlates with the increased levels of NRF2 protein (Figure 7(b)). Increase in the NRF2 protein level 1 hour after addition of VI-419-P3K is likely to be explained with the release of NRF2 from its complex with KEAP1.

The determining factor in the activity of NRF2 as a transcription factor is its localization in the cell. Cells treated with fullerenes were studied using fluorescence microscopy. There was no translocation of NRF2 to the nucleus of HELFs after 3 h of incubation with any of the studied concentrations of GI-761 (Figure 7(e)). On the contrary, at 4 μM of GI-761, the factor NRF2 was migrating from the nuclei of those cells where it was present in the nucleus, to the cytoplasm. Even though after 24 hours of incubation with GI-761 the NRF2 amount increases in the cytoplasm, NRF2 does not translocate to the nucleus. Thus, fullerene GI-761 appears to be blocking the activity of NRF2, despite the increase of the factor at some concentrations.

All investigated concentrations of VI-419-P3K cause an increase in the NRF2 expression within 3 h of incubation, but NRF2 does not translocate to the nucleus. In 24 h, the NRF2 expression increases both in the cytoplasm and the nucleus. Thus, derivative VI-419-P3K causes the activation of the transcription factor NRF2 both on the gene and the protein level and the translocation of the factor to the nucleus. Most likely, the prolonged antioxidant action of VI-419-P3K can be explained with NRF2 activation.

3.3. DNA Breaks. Since investigated substances affect ROS production in HELFs and increased levels of ROS usually lead to DNA damage [24], we investigated the level of DNA breaks in the treated cells. As the addition of GI-761 to HELFs caused increased ROS levels already at a concentration of 4 μM, the level of DNA breaks after 24 h of incubation when GI-761 (4 nM) was assessed. In 24 hours, fullerene GI-761 at a concentration of 4 nM induces a 4.6-fold increase in the amount of DNA breaks as was shown by single cell electrophoresis (comet assay) (Figure 8(a)). This fact correlates with the early ROS production in the treated cells. To confirm this result, we used the gamma-foci method. Gamma-foci is a well-known method of double-strand DNA break detection that is based on the antibody labelling of a phosphorylated form of histone protein H2AX. This form appears at the double-strand DNA break sites [25]. Medians of H2AX levels in the cells obtained by flow cytometry confirmed single cell electrophoresis data. 4 nM of GI-761 increases the amount of double-strand DNA breaks in treated HELFs after 24 hours of incubation (Figures 8(d) and 8(e)).

In 48 h, the amount of double-strand DNA breaks returned to control levels. This could be either due to activation of the DNA reparation system or due to the death of cells with damaged DNA. As we did not detect increased levels of cell death in the population, we assessed the activation of the reparation systems in treated HELFs. Two main genes that are activated in the DNA reparation are *BRCA1* and *BRCA2*. 4 nM of GI-761 increased the expression of the *BRCA1* and *BRCA2* genes 1.5-fold after 24 h of incubation. These data show that cells effectively respond to the DNA breaks induced by GI-761. Activation of DNA reparation systems is usually accompanied by cell cycle arrest.

Cyclin D1 plays a key role in regulating the transition of cells from the G1 phase to the S phase and is encoded by the CCND1 gene. The expression of cyclin D1 protein is regulated at the transcription level, so CCND1 gene expression levels determine the progression of the cell cycle [26]. GI-761 at a concentration of 4 nM caused a 2-3-fold decrease in CCND1 in 24 hours.

Derivative VI-419-P3K at a concentration up to 300 μg/ml has no effect on the number of double-strand DNA breaks and oxidative DNA damage in HELFs.

4. Conclusion

The antioxidant action of fullerene C60 and C70 derivatives is determined by their chemical structure. The difference in the chemical moieties attached to the fullerene core and the difference in the shape and size of the C60 and C70 cages lead to different cell responses to the derivatives. Antioxidative response master regulator NRF2 plays a key role in the

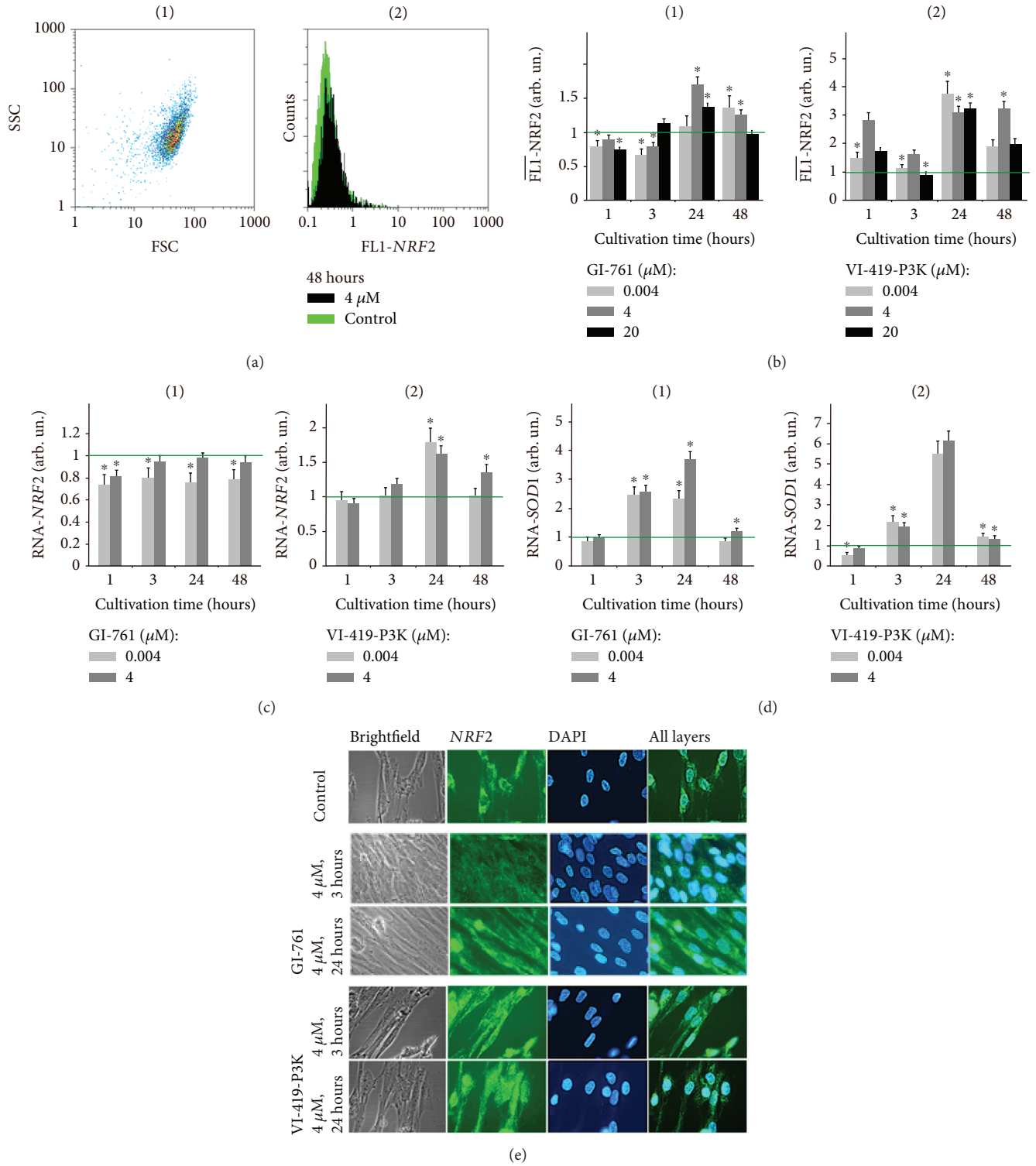

Figure 7: NRF2 levels in HELFs treated with investigated substances. (b) FCA: levels of FL1-NRF2 in cells treated with GI-761 and VI-419-P3K. (c) Real-time PCR: levels of NRF2 mRNA in cells treated with GI-761 and VI-419-P3K. (e) Fluorescent microscopy: localization of NRF2 protein in cells treated with GI-761 and VI-419-P3K, nuclei of the cells stained with DAPI.

determination of the prolonged antioxidant effect of fullerene derivatives on HELFs: activation of this transcription factor downregulates ROS production in cells. Derivative VI-419-P3K causes activation of NRF2 transcription both at gene and protein levels and induces translocation of NRF2 to the nucleus. This enables VI-419-P3K to have a prolonged antioxidant activity.

GI-761 does not increase the NRF2 expression, and the factor does not translocate to the nucleus. Because of this, GI-761 causes a secondary response of the cells that consists

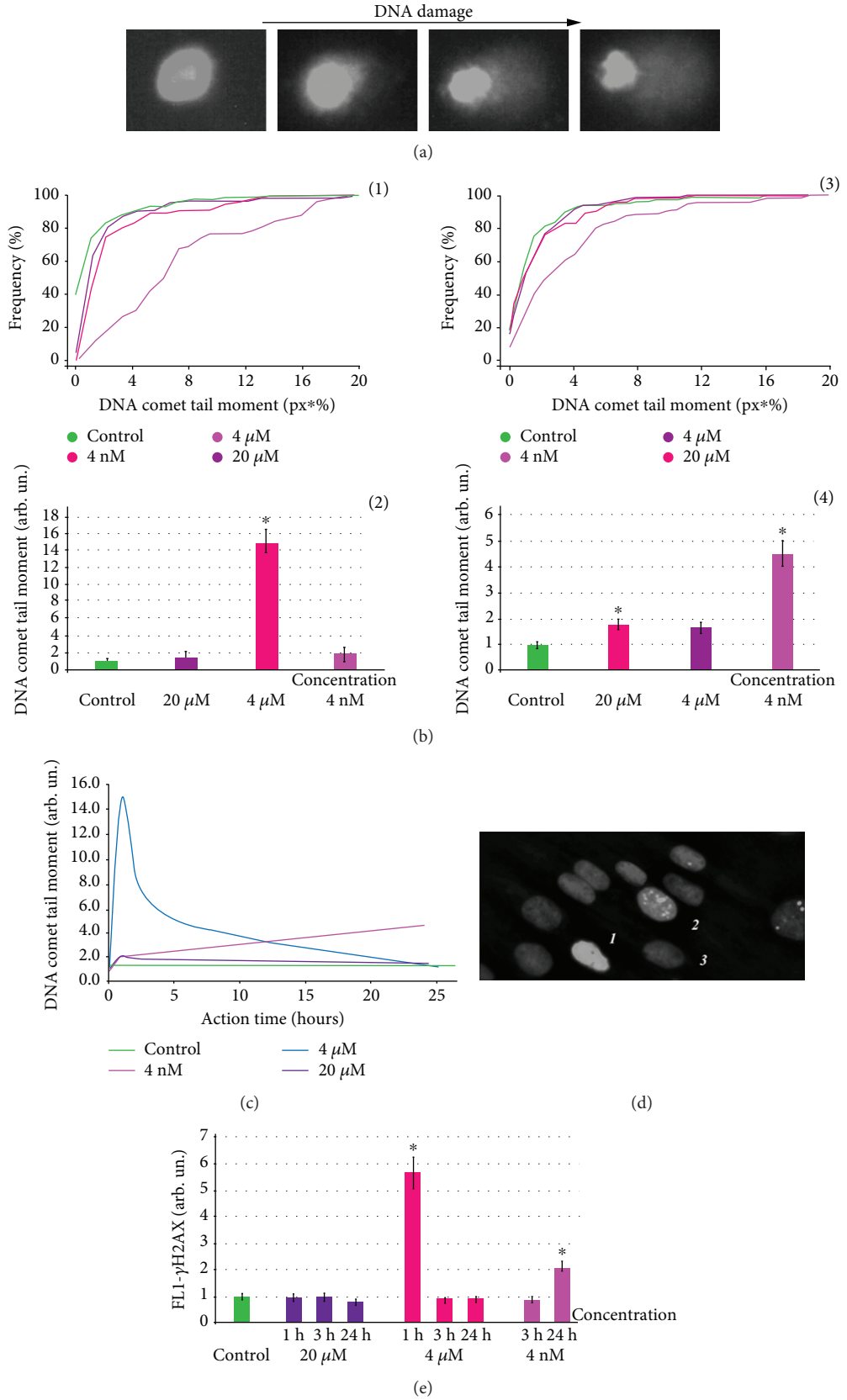

Figure 8: DNA damage in cells incubated with GI-761 and VI-419-P3K. (a–c) Comet assay: (a) digital photography of nuclei with varying degree of DNA damage; (b) dependence of "% of tail DNA" on fullerene derivative concentration; (c) dependence of DNA comet tail moment on the time of incubation with fullerene derivatives. (d) Fluorescent microscopy: cells stained with antibodies for H2AX. (e) FCA: average signal intensity of FL1-γH2AX given for times and concentrations of investigated fullerene derivatives.

of an increased NOX4 expression accompanied by ROS production that leads to DNA damage. GI-761 could only potentially be used as a short-time antioxidant. The antioxidant action of GI-761 could be prolonged either by NOX4 inhibition or by NRF2 activation.

Data Availability

The data used to support the findings of this study are included within the article.

Conflicts of Interest

The authors declare that they have no conflicts of interest.

Acknowledgments

This work was supported by the bilateral Taiwanese-Russian research project (RFBR No. 16-53-52030), by the Russian Federal Agency for Scientific Organizations (project no. 0089-2019-0010), and by the Research Program of the Presidium of Russian Academy of Sciences No. 0089-2018-0248 "Nanostructures: physics, chemistry, biology, and basic technology."

Supplementary Materials

Data concerning the method by which the compounds were obtained as well as the results of their 1H and 13C NMR and LS MS analysis. *(Supplementary Materials)*

References

[1] B. Uttara, A. V. Singh, P. Zamboni, and R. T. Mahajan, "Oxidative stress and neurodegenerative diseases: a review of upstream and downstream antioxidant therapeutic options," *Current Neuropharmacology*, vol. 7, no. 1, pp. 65–74, 2009.

[2] L. A. Pham-Huy, H. He, and C. Pham-Huy, "Free radicals antioxidants in disease and health," *International Journal of Biomedical Science*, vol. 4, no. 2, pp. 89–96, 2008.

[3] S. Sheykhansari, K. Kozielski, J. Bill et al., "Redox metals homeostasis in multiple sclerosis and amyotrophic lateral sclerosis: a review," *Cell Death & Disease*, vol. 9, no. 3, p. 348, 2018.

[4] K. Brieger, S. Schiavone, F. J. Miller Jr., and K. H. Krause, "Reactive oxygen species: from health to disease," *Swiss Medical Weekly*, vol. 142, article w13659, pp. 1–14, 2012.

[5] U. Weyemi and C. Dupuy, "The emerging role of ROS-generating NADPH oxidase NOX4 in DNA-damage responses," *Mutation Research*, vol. 751, no. 2, pp. 77–81, 2012.

[6] O. A. Sedelnikova, C. E. Redon, J. S. Dickey, A. J. Nakamura, A. G. Georgakilas, and W. M. Bonner, "Role of oxidatively induced DNA lesions in human pathogenesis," *Mutation Research*, vol. 704, no. 1-3, pp. 152–159, 2010.

[7] J. D. Lambeth, "Nox enzymes, ROS, and chronic disease: an example of antagonistic pleiotropy," *Free Radical Biology and Medicine*, vol. 43, no. 3, pp. 332–347, 2007.

[8] C. McEwen, R. G. McKay, and B. S. Larsen, "C60 as a radical sponge," *Journal of the American Chemical Society*, vol. 114, no. 11, pp. 4412–4414, 1992.

[9] L. Xiao, H. Takada, X. Gan, and N. Miwa, "The water-soluble fullerene derivative "Radical Sponge" exerts cytoprotective action against UVA irradiation but not visible-light-catalyzed cytotoxicity in human skin keratinocytes," *Bioorganic & Medicinal Chemistry Letters*, vol. 16, no. 6, pp. 1590–1595, 2006.

[10] S. Kato, H. Aoshima, Y. Saitoh, and N. Miwa, "Fullerene-C60 derivatives prevent UV-irradiation/TiO_2-induced cytotoxicity on keratinocytes and 3D-skin tissues through antioxidant actions," *Journal of Nanoscience and Nanotechnology*, vol. 14, no. 5, pp. 3285–3291, 2014.

[11] J. Grebowski, P. Kazmierska, G. Litwinienko, A. Lankoff, M. Wolszczak, and A. Krokosz, "Fullerenol $C_{60}(OH)_3$6 protects human erythrocyte membrane against high-energy electrons," *Biochimica et Biophysica Acta (BBA) - Biomembranes*, vol. 1860, no. 8, pp. 1528–1536, 2018.

[12] F. Beuerle, R. Lebovitz, and A. Hirsch, "Antioxidant properties of water-soluble fullerene derivatives," in *Medicinal Chemistry and Pharmacological Potential of Fullerenes and Carbon Nanotubes*, F. Cataldo and T. Ros, Eds., vol. 1 of Carbon Materials: Chemistry and Physics, Springer, Dordrecht, 2008.

[13] E. S. Ershova, V. A. Sergeeva, V. J. Tabakov et al., "Functionalized fullerene increases NF-κB activity and blocks genotoxic effect of oxidative stress in serum-starving human embryo lung diploid fibroblasts," *Oxidative Medicine and Cellular Longevity*, vol. 2016, Article ID 9895245, 17 pages, 2016.

[14] E. S. Ershova, V. A. Sergeeva, A. I. Chausheva et al., "Toxic and DNA damaging effects of a functionalized fullerene in human embryonic lung fibroblasts," *Mutation Research/Genetic Toxicology and Environmental Mutagenesis*, vol. 805, pp. 46–57, 2016.

[15] P. A. Troshin, O. Popkov, and R. N. Lyubovskaya, "Some new aspects of chlorination of fullerenes," *Fullerenes, Nanotubes and Carbon Nanostructures*, vol. 11, no. 2, pp. 165–185, 2003.

[16] A. B. Kornev, A. S. Peregudov, V. M. Martynenko, J. Balzarini, B. Hoorelbeke, and P. A. Troshin, "Synthesis and antiviral activity of highly water-soluble polycarboxylic derivatives of [70]fullerene," *Chemical Communications*, vol. 47, no. 29, pp. 8298–8300, 2011.

[17] A. B. Kornev, E. A. Khakina, S. I. Troyanov et al., "Facile preparation of amine and amino acid adducts of [60]fullerene using chlorofullerene $C_{60}Cl_6$ as a precursor," *Chemical Communications*, vol. 48, no. 44, pp. 5461–5463, 2012.

[18] A. V. Singh, K. K. Mehta, K. Worley, J. S. Dordick, R. S. Kane, and L. Q. Wan, "Carbon nanotube-induced loss of multicellular chirality on micropatterned substrate is mediated by oxidative stress," *ACS Nano*, vol. 8, no. 3, pp. 2196–2205, 2014.

[19] A. C. Cave, A. Brewer, R. Narayanapanicker et al., "NADPH oxidases in cardiovascular health and disease," *Antioxidants & Redox Signaling*, vol. 8, no. 5-6, pp. 691–728, 2006.

[20] T. Nguyen, P. Nioi, and C. B. Pickett, "The Nrf2-antioxidant response element signaling pathway and its activation by oxidative stress," *Journal of Biological Chemistry*, vol. 284, no. 20, pp. 13291–13295, 2009.

[21] B. Harder, T. Jiang, T. Wu et al., "Molecular mechanisms of Nrf2 regulation and how these influence chemical modulation for disease intervention," *Biochemical Society Transactions*, vol. 43, no. 4, pp. 680–686, 2015.

[22] S. Kovac, P. R. Angelova, K. M. Holmström, Y. Zhang, A. T. Dinkova-Kostova, and A. Y. Abramov, "Nrf2 regulates ROS production by mitochondria and NADPH oxidase,"

Biochimica et Biophysica Acta (BBA) - General Subjects, vol. 1850, no. 4, pp. 794–801, 2015.

[23] H. J. Kim and N. D. Vaziri, "Contribution of impaired Nrf2-Keap1 pathway to oxidative stress and inflammation in chronic renal failure," *American Journal of Physiology-Renal Physiology*, vol. 298, no. 3, pp. F662–F671, 2010.

[24] N. R. Jena, "DNA damage by reactive species: mechanisms, mutation and repair," *Journal of Biosciences*, vol. 37, no. 3, pp. 503–517, 2012.

[25] J. Lee, Y. Kim, S. Lim, and K. Jo, "Single-molecule visualization of ROS-induced DNA damage in large DNA molecules," *Analyst*, vol. 141, no. 3, pp. 847–852, 2016.

[26] Z. Du, X. Tong, and X. Ye, "Cyclin D1 promotes cell cycle progression through enhancing NDR1/2 kinase activity independent of cyclin-dependent kinase 4," *Journal of Biological Chemistry*, vol. 288, no. 37, pp. 26678–26687, 2013.

Hindawi
Oxidative Medicine and Cellular Longevity
Volume 2018, Article ID 9620684, 12 pages
https://doi.org/10.1155/2018/9620684

Research Article

Curcumin Exerted Neuroprotection against Ozone-Induced Oxidative Damage and Decreased NF-κB Activation in Rat Hippocampus and Serum Levels of Inflammatory Cytokines

Sendar Daniel Nery-Flores,[1] María Luisa Mendoza-Magaña,[1] Mario Alberto Ramírez-Herrera,[1] José de Jesús Ramírez-Vázquez,[1] Marina María de Jesús Romero-Prado,[1] César Ricardo Cortez-Álvarez,[2] and Abraham Alberto Ramírez-Mendoza[1]

[1]*Laboratorio de Neurofisiología, Departamento de Fisiología, Centro Universitario de Ciencias de la Salud, Guadalajara, Jalisco, Mexico*
[2]*Departamento de Farmacobiología, Centro Universitario de Ciencias Exactas e Ingenierías, Universidad de Guadalajara, Guadalajara, Jalisco, Mexico*

Correspondence should be addressed to María Luisa Mendoza-Magaña; mmendoza@cucs.udg.mx

Received 2 July 2018; Revised 1 October 2018; Accepted 23 October 2018; Published 30 December 2018

Academic Editor: Isabel C. F. R. Ferreira

Ozone is a harmful tropospheric pollutant, causing the formation of reactive oxygen and nitrogen species that lead to oxidative damage in living beings. NF-κB can be activated in response to oxidative damage, inducing an inflammatory response. Nowadays, there are no reliable results that consolidate the use of antioxidants to protect from damage caused by ozone, particularly in highly polluted cities. Curcumin has a strong antioxidant activity and is a potent inhibitor of NF-κB activation with no side effects. The aim of this study is to evaluate the effect of curcumin in preventive and therapeutic approaches against oxidative damage, NF-κB activation, and the rise in serum levels of IL-1β and TNF-α induced by acute and chronic exposure to ozone in rat hippocampus. One hundred male Wistar rats were distributed into five groups; the intact control, curcumin-fed control, the ozone-exposed group, and the preventive and therapeutic groups. These last two groups were exposed to ozone and received food supplemented with curcumin. Lipid peroxidation was determined by spectrophotometry, and protein oxidation was evaluated by immunodetection of carbonylated proteins and densitometry analysis. Activation of NF-κB was assessed by electrophoretic mobility shift assay (EMSA), and inflammatory cytokines (IL-1β and TNF-α) were determined by ELISA. Curcumin decreased NF-κB activation and serum levels of inflammatory cytokines as well as protein and lipid oxidation, in both therapeutic and preventive approaches. Curcumin has proven to be a phytodrug against the damage caused by the environmental exposure to ozone.

1. Introduction

Air pollution is a direct consequence of industrialization and is defined as an abnormally high concentration of any hazardous gas or particulate matter [1]. Worldwide, millions of human beings are chronically exposed to highly polluted air far above the security limits established by the World Health Organization (WHO). Ozone (O_3) is an allotrope of oxygen generated by photochemical reactions and has high oxidizing power. The tropospheric O_3 is a product generated by intense sunlight radiation acting on nitrogen oxides and volatile organic compounds derived from combustion of fossil fuels; thus, it is produced in densely populated cities [2, 3].

Several studies have documented that the high oxidizing power of O_3 affects human health causing pulmonary and cardiovascular dysfunction [4]. Furthermore, exposure to ozone is capable of affecting the central nervous system (CNS) especially in regions susceptible to oxidative stress

such as the hippocampus [5]. The oxidizing activity of O_3 in living beings occurs through sequential and overlapped processes where the nasal exposure and inhalation of O_3 induce the formation of reactive oxygen and nitrogen species (RONS) that can cause damage in two main forms: (a) by affecting the olfactory mucosa where RONS diffuse through the olfactory tract and spread in the CNS and (b) by acting on the respiratory epithelium and causing alterations in cellular homeostasis and endothelial integrity, resulting in pulmonary dysfunction. RONS subsequently damage the blood-brain barrier (BBB) and reach the CNS, causing an oxidative state and neuroinflammation [6–8]. Additional damages include altered neurogenesis, reactive astrocytosis, reduced dendritic spines, neurotransmitter imbalance, increased activity of superoxide dismutase, DNA fragmentation, neuronal apoptosis, and cognitive, memory, and motor impairment [8–12]. Also, chronic exposure to O_3 has been associated to an increased risk of certain neurodegenerative diseases, such as Alzheimer's and Parkinson's [13, 14].

Nuclear factor kappa B (NF-κB) is a key transcriptional factor which is activated by reactive oxygen species (ROS) and inflammatory cytokines. Under normal conditions, NF-κB is present in the cytoplasm coupled to its inhibitor (IkBα). On activation, IkBα undergoes phosphorylation by IKK and ubiquitination-dependent degradation by the proteosome, and then, NF-κB (p65-p50 heterodimer) is released and translocates into the nucleus where it binds to DNA-response elements, resulting in an increased expression of proinflammatory and prooxidant genes, among others [15, 16]. Furthermore, NF-κB promotes the expression of its own inhibitor, IkBα. After IkBα is synthesized, it is transported into the nucleus where it binds to the heterodimer blocking the binding to response elements [17].

Some studies suggest that the elimination of RONS should be accomplished with the administration of exogenous antioxidants without decreasing or even improving the activity of the endogenous antioxidant system [18, 19]. The use of natural antioxidants as complementary therapies has been proposed to limit the effects of RONS.

A natural alternative is the phytodrug named curcumin (CUR) which is isolated from the rhizome of *Curcuma longa* and chemically defined as diferuloylmethane. CUR has powerful antioxidant and anti-inflammatory activities, among others as well important [20, 21]. Furthermore, it has been documented that CUR modulates signal transduction and gene expression. Benefic effects of CUR are due to its interactions with growth factors, receptors, transcriptional factors, cytokines, enzymes, and genes that regulate apoptosis. It has been shown that CUR acts as a scavenger against RONS, and *in vivo*, CUR enhances the activity of superoxide dismutase, catalase, and glutathione peroxidase [20, 22, 23]. Such properties support its potential for preventive and therapeutic applications.

The aim of the present study was to analyze the neuroprotective effect exerted by CUR in preventive and therapeutic approaches against the increase of lipid peroxidation (LPO), protein oxidation (PO), activation of NF-κB, in the rat hippocampus; and serum cytokines, IL-1β and TNF-α, induced by acute and chronic exposure to O_3 as a model of oxidative stress.

2. Materials and Methods

2.1. Animals. Animals were treated in accordance with the guidelines and requirements of the World Medical Association, of the Declaration of Helsinki, and with the National Institutes of Health guide for the care and use of laboratory animals (NIH publication no. 8023, revised 1978) which are established in the Ethical Committee of the Health Science Center (CUCS, Universidad de Guadalajara). All analytical procedures used in the experiments were performed according to established guidelines. For this study, we used 100 male Wistar rats (*Rattus norvegicus*), 21 days old, weighing ≈130 g. We choose this age because it is well known that young and old animals are more susceptible than mature ones to lipid peroxidation [24]. Thus, young animals could be more important to protect than older ones. This could be based on the results reported by Calderón-Garcidueñas et al. [13, 25] which suggest that neurodegenerative markers are present in the brains of young human inhabiting highly polluted cities. Animals were kept under light/dark cycles 12×12 h, 22 ± 2°C, and relative humidity of 50–60% with free access to water and food (Prolab®RMH Laboratory Animal Diet, 2500 Rodent 5P14).

2.2. Diet. An alcoholic extract was prepared with commercial curcumin (Curcuma Kosher, Batch no. 09076). The concentration of CUR in the extract was determined by UV spectrophotometry at λ 230 nm, and the molecular identity was determined by the infrared spectrum compared with a CUR standard (Sigma Chemical Co., St. Louis, MO, USA). The food pellets were impregnated with the alcoholic extract; the ethanol was evaporated at 60°C for 4 hours, and the homogeneous distribution of CUR in the food pellets was corroborated by UV-spectrophotometry at λ 230 nm in the ethanolic extract obtained from samples of food pellets [26, 27]. The daily amount of CUR administered was approximately 5.6 mg/kg body weight in the food. This dose corresponds to a daily intake of 400 mg for humans in average.

2.3. Experimental Design. Animals were randomly distributed into ten experimental groups with ten rats each. All rats were subjected to an adaptation period of seven days before the beginning of the experiment. The adaptation was done to minimize the effect of human contact, food, and the lodging place in the experimental model. The design was established considering two periods of O_3 exposure: an acute phase (A, 15 days) and a chronic one (C, 60 days). Also, the manner of exposure to O_3 and the CUR supplementation in the experimental groups were defined as preventive (P) or therapeutic (T) for each period, considering their respective control groups. This design led to the following groups: the acute intact control (AIC) ($n = 10$) and the chronic intact control (CIC) ($n = 10$) groups that were exposed to O_3-free air, without CUR; the CUR control groups that received the CUR supplementation, with no exposition to O_3 in the same periods, are ACC ($n = 10$) and CCC ($n = 10$); and the O_3 control groups that were exposed to 0.7 ppm of O_3 during the same phases are AOC ($n = 10$) and COC ($n = 10$). The therapeutic groups were exposed to 0.7 ppm of O_3 for 7 days and,

subsequently, were fed with CUR until the end of the exposure time, covering the acute phase (AT) ($n = 10$) and chronic phase (CT) ($n = 10$). The preventive groups (AP, $n = 10$ and CP, $n = 10$) received supplemented food with CUR for 7 days prior to and during O_3 exposure, in both phases.

2.4. Ozone Exposure. Animals were daily exposed to O_3 for 4 h at a constant concentration of 0.7 ppm. The animals were exposed for 15 days for the acute phase and during 60 days for the chronic phase. Animals were placed in a hermetic acrylic chamber ($65 \times 25 \times 45$ cm L/H/D), which was connected to a gas premix chamber ($40 \times 24 \times 45$ cm). The premix chamber received O_3 generated by a Certizon C100 apparatus (Sander Elektroapparatebau GmbH, Uetze, Germany), which was fed with medical-grade oxygen. The O_3 generated was mixed with O_3-free air to adjust an aforementioned concentration. The O_3 concentration was monitored with a semiconductor sensor (ES-600, Ozone Solutions Inc., Hull, Iowa) to adjust the flow of oxygen and air needed for a proper atmosphere with a constant flow of 1.6–1.2 l/min. As part of the biosecurity actions, the O_3 expelled from the chamber was inactivated with a neutralizing filter containing a solution of sodium nitrite, potassium carbonate, glycerol, methanol, and water before being released to the air.

2.5. Tissue Samples. After the exposure period was completed, animals were euthanized by an intraperitoneal injection of sodium pentobarbital at a dose of 36 mg/kg. Blood was extracted by intracardiac puncture from all rats, serum was separated, and an antiprotease cocktail was added to samples that were frozen at −80°C until use.

Five rats of each group, in the acute and chronic phases, ($n = 5$) were decapitated, one at a time, and the head was chilled on ice. Brains were dissected and two cuts were done in the stereotaxic coordinates of −6.04 to −2.80 bregma. Hippocampi were dissected from both hemispheres. The left hippocampi were 10% homogenized in PBS with 10 μl/ml of butyl hydroxy toluene 0.5 M (BHT) for LPO assay. The right hippocampi were homogenized in PBS with antiproteases (EDTA, EGTA, leupeptin, aprotinin, bestatin, and PMSF) with 0.2 mM mercaptoethanol (Sigma Chemical Co., St. Louis, MO) for PO assay. Samples were stored at −80°C until processed. The protein concentration was determined using the micro-Bradford method (Cat. # 500-0201, Bio-Rad, Hercules, CA, USA), and absorbance was determined with a microplate reader (EZ Read 400, Biochrom, Miami, FL, USA) at λ 595 nm.

The remaining five rats of each group, in acute and chronic phases ($n = 5$), were anesthetized and decapitated. Both hippocampi were dissected and homogenized in 1.2 ml of lysis buffer (0.6% NP10, 0.15 M NaCl, 10 mM Tris pH 7.9, 1 mM EDTA, 0.1 mM EGTA, 0.5 mM 2-mercaptoethanol, and 0.5 mM PMSF). Immediately, the homogenate was incubated for 5 min on ice and centrifuged at 1250 g, at 4°C, for 5 min. Nuclear proteins, contained in the pellet, were resuspended in 100 μl of cold extraction buffer (10 mM HEPES pH 7.9, 0.1 mM EGTA, 0.1 mM EDTA, 1.5 mM MgCl 2, 420 mM NaCl, 0.5 mM 2-mercaptoethanol, 0.5 mM PMSF, and 25% glycerol) and were incubated on ice for 20 min. Then, the nuclear membrane debris was removed by centrifugation at 1250 g for 5 min at 4°C. The supernatants containing the nuclear proteins were stored at −80°C until further analysis by electrophoretic mobility shift assay (EMSA).

2.6. Determination of Lipid Peroxidation. LPO was performed by determining the concentration of malondialdehyde (MDA) and 4-hydroxynonenal (4-HNE), according to the manufacturer's instructions (Cat. # FR12, Oxford Biomedical Res., Oxford, MI, USA). Samples were centrifuged at 3000 g for 5 min at 4°C, and 250 μl of each sample was transferred to assay tubes. Then, 812.5 μl of N-methyl-2-phenylindole was added, mixed, and incubated at 45°C for 40 min. Next, 187.5 μl of methanesulfonic acid was added and samples were immediately chilled in an ice bath. Samples were incubated at 45°C for 45 min. Then, the reaction was stopped in an ice bath and tubes were centrifuged at 15000 g at 4°C for 15 min. Samples were kept on ice, and 200 μl of supernatants was transferred in triplicate to a microplate of 96 wells, and absorbance was determined at λ 595 nm. The standard curve was prepared by adding 650 μl chromogen solution to increasing concentrations of 1,1,3,3-tetrametoxipropane (0.315–10 nmol/ml).

2.7. Detection of Oxidized Protein. This assay was performed to detect the carbonyl groups in oxidized proteins, which reflect the oxidative damage caused by O_3. We used the OxyBlot kit according to the manufacturer's instructions (Cat. # S7150, Merck Millipore Corp., Billerica, MA, USA). Briefly, samples were adjusted at 4 μg of protein/μl; then, 5 μl of each sample was denaturalized with 5 μl of 12% sodium dodecyl sulfate. Five samples of each group were derivatized with dinitrophenylhydrazine (DNPH) and a replica of samples reacted with the derivatization control solution. A stop solution was added, and proteins were separated by 10% PAGE in a mini-PROTEAN chamber (Bio-Rad, Hercules, CA, USA) at 100 V. Proteins were electrotransferred overnight to PVDF membranes at 25 V and 4°C. Membranes were blocked overnight with 5% nonfat milk in PBS and incubated with rabbit anti-DNPH (1 : 150). The reaction was detected with peroxidase-labeled anti-rabbit IgG, and oxidized protein bands were visualized with Immobilon Chemiluminescent HRP substrate (Millipore Corp., Billerica, MA, USA). Digital images were obtained and analyzed with the software Image Studio Lite Ver 5.2® to determine the value of integrated optical density (IOD) per sample and per group obtaining data for statistical analysis.

2.8. Electrophoretic Mobility Shift Assay for NF-κB. NF-κB activation was analyzed by EMSA. Five μg of protein from the nuclear fraction was incubated with biotinylated double-stranded NF-κB oligonucleotide 5′-TTGTTACAAGGGACTTTCCGCTGGGGACTTTCGGGAGGCGTGG-3′; underlining indicates the NF-κB binding site, following supplier instructions (Cat. # 20148X, LightShift Chemiluminescent EMSA, Thermo Fisher Scientific). The DNA-protein complex was resolved on 6% nondenaturing polyacrylamide gel at 100 V in TBE (45 mM Tris-borate, 1 mM EDTA, pH 8.3).

DNA-protein complexes were electrotransferred onto a nylon membrane (Hybond-XL Amersham Pharmacia Biotech), and DNA was crosslinked to the membrane with a transilluminator (UVP model 2UV) at 302 nm for 15 min. After crosslinking, the membranes were blocked for 15 min and then incubated with streptavidin-HRP conjugate for 15 min and reactive bands were detected by chemiluminescence. Blot images were digitally acquired with an HP ScanJet 4670 scanner, and densitometry analysis of images was performed with the GelQuant.Net software. The results were expressed as integrated optical density (IOD).

2.9. Enzyme-Linked Immunosorbent Assay (ELISA). The concentration of IL-1β and TNF-α was determined by ELISA kits (Cat. # RLB00, Cat. # RTA00, R&D Systems, Minneapolis, MN, USA). Fifty micrograms of total protein from serum was used. Absorbance was measured with a microplate reader (EZ Read 400, Biochrom) at λ 492 nm, and the concentration of cytokines was determined and expressed in pg/ml.

2.10. Statistical Analysis. LPO data and cytokine levels were analyzed with one-way ANOVA and Tukey's test as post hoc. The data of oxidized proteins were analyzed by estimated marginal means (EMM) and with the Bonferroni post hoc test. The data obtained from NF-κB activation was analyzed through nonparametric Kruskal-Wallis and Mann–Whitney U tests. Significant differences were considered for a value of $p < 0.05$. GraphPad Prism 6.01 software (GraphPad Software Inc., La Jolla, CA) was employed for all analyses.

3. Results

The results of the control groups AIC and CIC represent the basal oxidative damage without O_3 exposure and without dietary supplementation. The results of the control groups ACC and CCC represent the oxidative damage without exposure to O_3 and with dietary supplementation. These groups were used to establish differences with the control group exposed to O_3 in the acute phase (AOC) and the chronic phase (COC) without dietary supplementation. Also, they were used to compare the neuroprotective effect of CUR observed in the preventive or the therapeutic modes.

3.1. Curcumin Decreased Lipoperoxidation Levels. The quantitation of LPO was performed with the spectrophotometric method in hippocampal homogenate samples as previously described. The one-way ANOVA test applied to LPO among all experimental groups was statistically significant ($F[9, 40]=80.13$; $p < 0.001$). As the maximum oxidative state in our design, the control group exposed to O_3 showed a significantly increased level of LPO in the acute phase (AOC, 9.72 ± 2.36 nmol/ml; $p < 0.001$) in comparison with AIC (0.61 ± 0.18 nmol/ml) and ACC (1.13 ± 0.48 nmol/ml). The preventive and therapeutic supplementation of CUR in the acute phase caused a significant decrease of LPO (AT, 0.31 ± 0.11 nmol/ml; AP, 0.59 ± 0.12 nmol/ml; $p < 0.001$) in comparison with AOC (Figure 1(a)).

A similar pattern was observed in the chronic phase: the control group exposed to O_3 showed a significantly increased concentration of MDA+4-HNE (COC, 9.03 ± 0.15 nmol/ml; $p < 0.001$), in comparison with the CIC (0.58 ± 0.21 nmol/ml) and CCC (0.36 ± 0.19 nmol/ml) groups. Furthermore, the diet supplemented with CUR caused a significant decrease in the concentration of MDA+4-HNE in the chronic phase (CT, 0.21 ± 0.06 nmol/ml and CP, 1.14 ± 0.47 nmol/ml; $p < 0.001$) in comparison with that of the COC group (Figure 1(b)).

3.2. Curcumin Reduced Protein Oxidation. The protein carbonylation is an evidence of protein oxidation. The conjugation of DNPH with carbonyl residues was detected with antibodies against DNP. A representative example of the PO profile for each group is shown in Figure 2(a), which illustrates the immunodetection of carbonylated proteins in hippocampal homogenates. The statistical analysis of EMM showed that the IOD value of the AOC group had a significant increase in the PO profile (2078800 ± 435724; $p < 0.001$) in comparison with the AIC (75979 ± 75571) and ACC (77528 ± 6552) groups. When CUR was included as part of their diet in the therapeutic and preventive approaches, the IOD values were significantly reduced (71776 ± 6035 and 6437 ± 7412, respectively; $p < 0.001$) (Figure 2(b)).

In the chronic phase, the COC group showed a significant increase in the PO profile (2077276 ± 214471; $p < 0.001$) in comparison with the CIC and CCC groups (103843 ± 80734 and 30048 ± 3595, respectively). PO was decreased by the diet supplemented with CUR in the therapeutic group (CT, 89366 ± 15348) and in the preventive group (CP, 12644 ± 1686.19) when compared against the COC group (Figure 2(c)).

3.3. Curcumin Decreased the Activation and Translocation of NF-κB. One of the major effects of O_3 was the generation of RONS that caused the subsequent activation of NF-κB. As we show in Figure 3(a), the acute response in rat hippocampus to this oxidant gas produced a strong activation of NF-κB (AOC, 373727.63 ± 18362). The increase of NF-κB activation was statistically significant compared with the those of AIC and ACC groups (0.00 ± 0.00 and 6.57 ± 2.63, respectively, $p < 0.001$). The ability of CUR to reverse or prevent the activation of NF-κB in the acute phase was observed in the experimental groups AT (47333.40 ± 4081) and AP (109.13 ± 11.69). Furthermore, the AP group showed a significant decrease ($p < 0.001$) with respect to the AT group, suggesting that preventive administration of CUR has a greater effect on NF-κB activation than the therapeutic administration after a 15-day exposure to O_3 (Figure 3(b)). The NF-κB activation in the chronic phase was increased in the COC group (207308.59 ± 11250) compared to the CIC and CCC groups (159.40 ± 17.70 and 777.82 ± 116, respectively, $p < 0.001$), demonstrating the ability of O_3 to induce NF-κB activation. Similarly, animals fed with CUR-supplemented diet in the therapeutic and preventive approaches had a significant decrease ($p < 0.001$) in NF-κB activation, in both the CT and CP groups. Additionally, the CT and CP groups showed a similar activation of NF-κB (Figure 3(c)). However, the

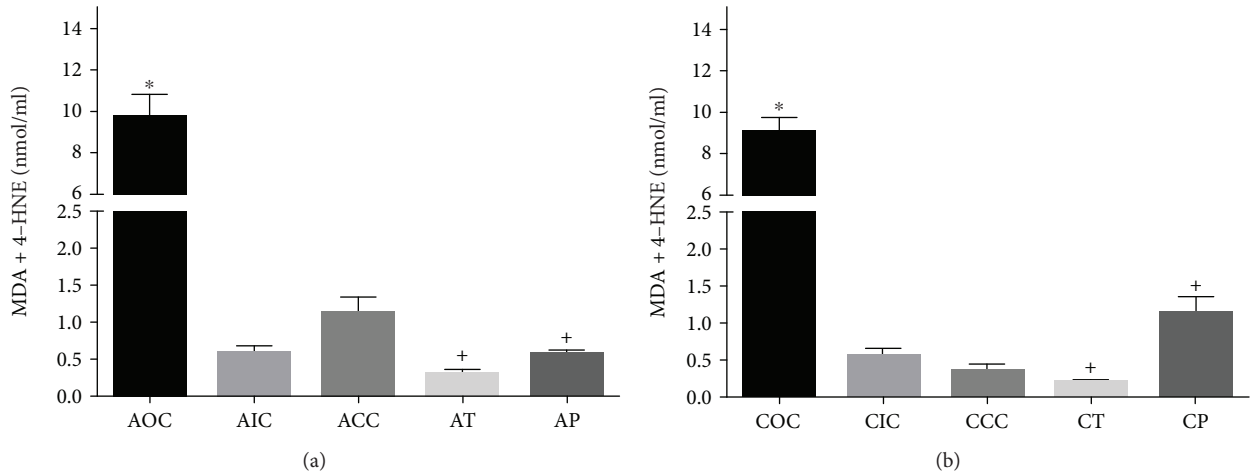

Figure 1: (a) Acute lipid peroxidation profile. AOC: acute O_3 control; AIC: acute intact control; ACC: acute CUR control; AT: acute therapeutic; AP: acute preventive. *Statistical difference between the AOC vs AIC and ACC groups. +Statistical difference between the AOC vs AT and AP groups. (b) Chronic lipid peroxidation profile. COC: chronic O_3 control; CIC: chronic intact control; CCC: chronic CUR control; CT: chronic therapeutic; CP: chronic preventive. *Statistical difference between the COC vs CIC and CCC groups. +Statistical difference between the COC vs CT and CP groups. Bars represent the concentration of MDA+4-HNE. Values are expressed as mean ± SEM.

COC showed a significant reduced NF-κB activation compared to the AOC ($p < 0.001$).

3.4. Curcumin Reduced the Serum Concentration of IL-1β and TNF-α. The activation of NF-κB by acute and chronic exposure to O_3 induced the rise of proinflammatory cytokine levels of IL-1β and TNF-α. The one-way ANOVA test applied to IL-1β and TNF-α among the experimental groups was statistically significant ($F[9, 36]=33.51$; $p < 0.001$ and $F[9, 34]=6.24$; $p < 0.001$, respectively). Furthermore, the diet supplementation with CUR exerted a strong reduction on cytokine serum levels. In the acute phase, the AOC group showed a significant increase in serum concentration for IL-1β (89.63 ± 6.78 pg/ml, $p < 0.0001$) compared with the groups AIC and ACC (24.88 ± 2.33 pg/ml and 23.83 ± 1.19 pg/ml, respectively). Meanwhile, the groups treated with CUR exhibited a significant decrease of IL-1β serum concentration (AT, 41.68 ± 3.41 pg/ml, $p < 0.0001$; AP, 61.49 ± 3.16 pg/ml, $p < 0.0006$) compared with the AOC group. Additionally, the AT group showed a significantly lower level than the AP group ($p < 0.05$, Figure 4(a)). In the chronic phase, the CIC and CCC groups did not show a significant difference between them (25.12 ± 5.15 pg/ml and 25.16 ± 5.96 pg/ml, respectively) nor among the levels found in the acute phase. On the contrary, the COC group displayed an increased concentration of IL-1β (67.87 ± 1.74 pg/ml, $p < 0.0001$) compared to the CIC and CCC groups. The effect of CUR in the chronic phase was significant as shown in data for the CT and CP groups (40.48 ± 1.52 pg/ml and 36.29 ± 2.92 pg/ml, respectively; $p < 0.001$) compared to the COC group (Figure 4(b)). When comparing the IL-1β level of the COC versus AOC groups, it seems to decrease in a time-dependent manner ($p < 0.01$), similar to that observed in the activation of NF-κB.

The effect of O_3 was observed in the AOC group with a significant increase in the serum concentration of TNF-α (40.30 ± 6.14 pg/ml, $p < 0.05$) compared against the AIC and ACC groups (25.48 ± 1.95 pg/ml and 21.16 ± 3.24 pg/ml, respectively). The supplemented diet with CUR caused a decrease of TNF-α concentration in the AT and AP groups (19.67 ± 1.36 pg/ml; 24.73 ± 1.53 pg/ml, $p < 0.05$) compared with the AOC group (Figure 5(a)). The concentration of TNF-α in the chronic phase was not different among the AIC, ACC, COC, and CP groups, but the CT group showed a significantly lower level (18.55 ± 0.74 pg/ml, $p < 0.05$) when compared with the other groups (Figure 5(b)).

4. Discussion

In this work, the antioxidant and anti-inflammatory activities of CUR were evaluated in a model of oxidative stress caused by experimental exposure to O_3. Here, we report that CUR exerted a neuroprotective effect in preventive or therapeutic approaches against oxidative damage, NF-κB activation, and the rise of IL-1β and TNF-α serum levels caused by acute or chronic exposure to O_3.

A considerable number of studies have evaluated and demonstrated the excellent antioxidant activity of CUR against damage induced by different oxidant substances [27–30] and as anti-inflammatory agent against the damage caused by the particulate matter [31, 32]. Oxidative stress is a common process that pollutants and other physical and chemical agents are able to induce [2]. Among air pollutants, O_3 is by far the most powerful pollutant due its ubiquity, high reactivity, and oxidant power [33]. Oxidative stress is strongly related to chronic inflammation, and both processes are involved in the pathogenesis of chronic degenerative diseases and cancer [34]. Thus, it is important to reduce the impact of such harmful factors in human health. Some efforts have been made to reduce the impact of oxidative stress in experimental models using natural and synthetic antioxidants against the oxidative damage caused by O_3 as taurine,

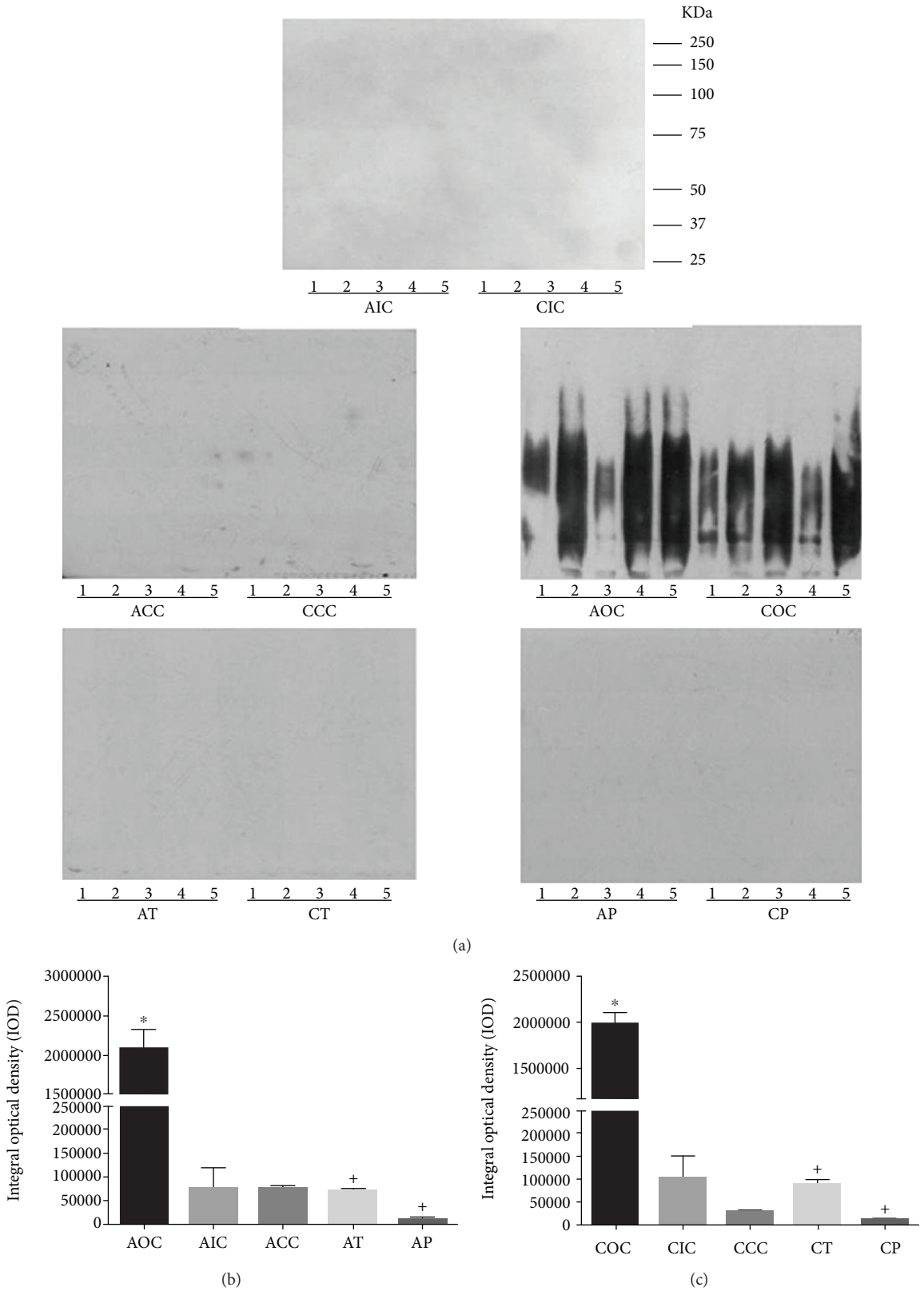

Figure 2: (a) Protein oxidation profile. Representative example of the control and experimental groups. Lanes are numbered for each sample used ($n = 5$). (b) Densitometry analysis of the protein oxidation profile in the acute phase. *Statistical difference between the AOC vs AIC and ACC groups. +Statistical difference between the AOC vs AT and AP groups. (c) Densitometry analysis of the protein oxidation profile in the chronic phase. *Statistical difference between COC vs CIC and CCC groups. +Statistical difference between the COC vs CT and CP groups. Values are expressed as mean ± SEM.

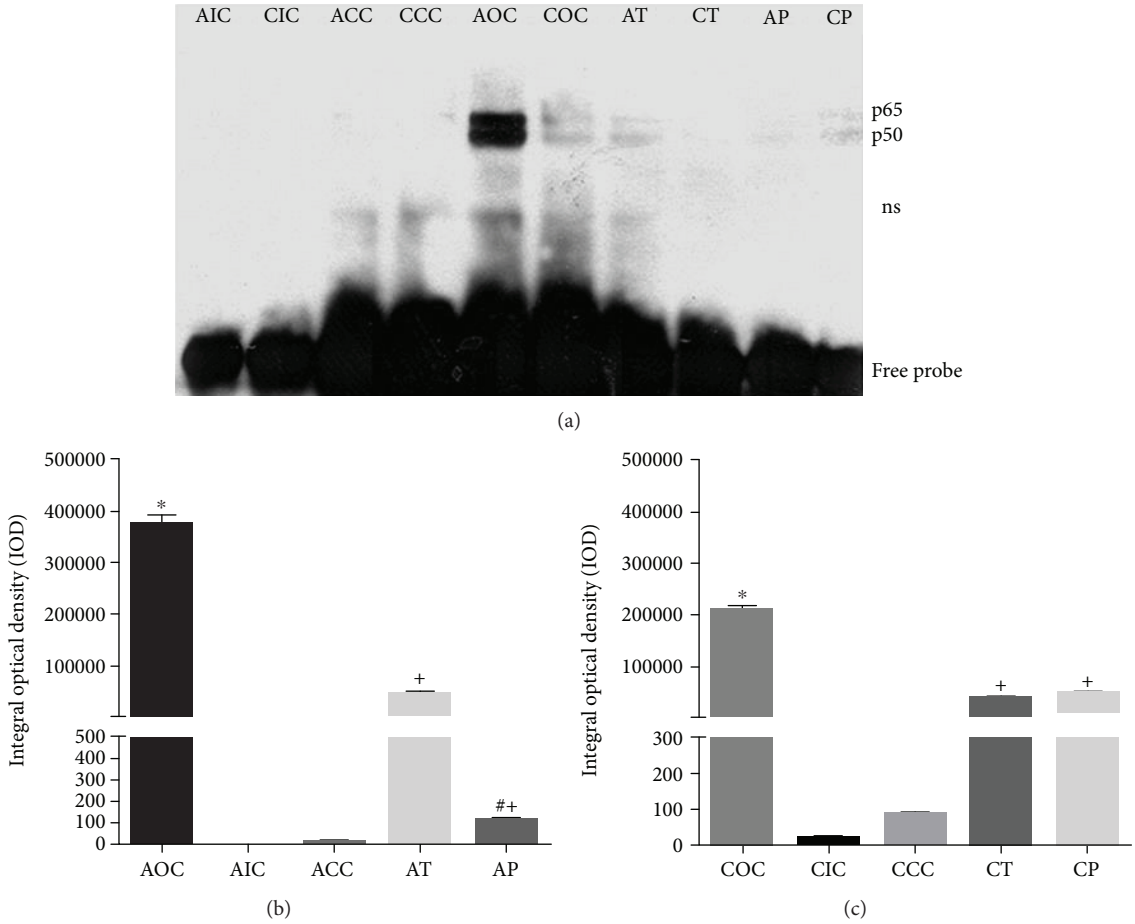

Figure 3: (a) Representative image of NF-κB activation. AOC showed a strong binding to NF-κB and remained activated at a lower level in the COC group. CUR showed an inhibitory effect against NF-κB activation in the therapeutic and preventive approaches; ns: nonspecific binding. (b) Densitometry analysis of the NF-κB activation profile in the acute exposure to O_3. *Statistical difference between the AOC vs AIC and ACC groups. +Statistical difference between AOC vs AT and AP groups. #Statistical difference between the AT and AP groups. (c) Densitometry analysis of the NF-κB activation profile in the chronic phase. *Statistical difference between the COC vs CIC and CCC groups. +Statistical difference between the COC vs CT and CP groups. Values are expressed as mean ± SEM.

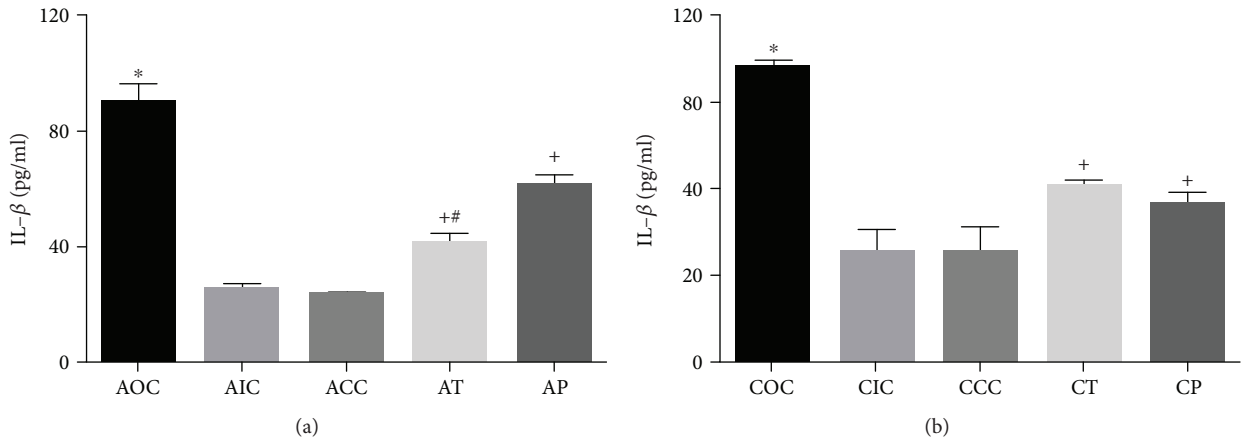

Figure 4: (a) Serum concentration of IL-1β in the acute exposure to O_3. *Statistical difference between the AOC vs AIC and ACC groups. +Statistical difference between the AOC vs AT and AP groups. #Statistical difference between the AT and AP groups. (b) Serum concentration of IL-1β in the chronic exposure to O_3. *Statistical difference between the COC and CIC and CCC groups. +Statistical difference between the COC vs CT and CP groups. Values are expressed as mean ± SEM.

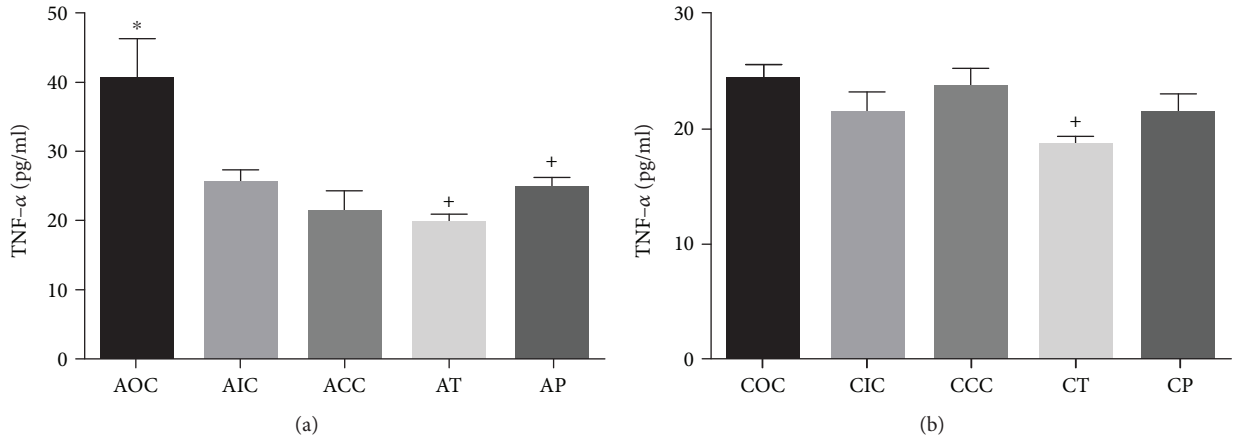

Figure 5: (a) Serum concentration of TNF-α in the acute exposure to O_3. *Statistical difference between the AOC vs AIC and ACC groups. +Statistical difference between the AOC vs AT and AP groups. (b) Serum concentration of TNF-α in the chronic exposure to O_3. +Statistical difference between the COC and CT groups. Values are expressed as mean ± SEM.

tibolone, imipramine, and vitamin E. These molecules have demonstrated antioxidant activity, but their long-term administration could lead to the onset of undesirable side effects [35–38].

We propose the use of CUR, a natural diphenolic compound that has multiple desirable properties as a neuroprotective molecule based on its antioxidant and anti-inflammatory effects [21, 39]. CUR has been administered for long periods and at high doses (8 g/day) without adverse side effects [40, 41]. Previous studies have well demonstrated that CUR is able to cross the blood-brain barrier and is mainly concentrated in the hippocampus; therefore, CUR is able to carry out its activities in the CNS [42, 43].

It has been reported that acute and chronic O_3 exposure causes oxidative stress and inflammation in the CNS, particularly in the hippocampus because it is a highly susceptible region to oxidative damage [5, 8]. The experimental model based on damage in the hippocampus induced by O_3 acute and chronic exposure was corroborated by the oxidation of lipids and proteins.

Lipid peroxidation generates toxic aldehydes such as 4-HNE and MDA, which alter the structural and functional integrity of the plasma membrane that could trigger an inflammatory process in the CNS [44]. The concentration of these aldehydes is increased in several neurodegenerative diseases, which demonstrates its involvement in such pathological conditions [45]. Protein oxidation generated by O_3 exposure occurs through a carbonylation process caused by ROS and reactive aldehydes, which induce covalent modification of proteins via nonenzymatic Michael addition. The carbonyl adducts lead to a dysfunctional behavior or loss of protein function that promotes the development of neuroinflammation and neurodegenerative diseases [46–48].

Our results show that the levels of lipid peroxidation and protein oxidation were increased in the rat hippocampus after acute exposure to O_3 compared to controls. These oxidative levels were maintained in the chronic phase. However, other studies report that the oxidative damage caused by O_3 increased progressively as a function of time [8, 49]. The difference observed in this effect may be attributable to the dose of O_3 used in our study (0.7 ppm), compared to those used in other studies where the O_3 dose was lower (0.25 ppm) and leading to an oxidative damage progressively increased in a time-dependent manner [8, 48]. Our data suggests that at the dose of 0.7 ppm, the endogenous antioxidant defenses had been overcome in the acute phase and this condition remained until the end of the chronic exposure.

We demonstrated that the dietary supplementation with CUR in the preventive and therapeutic approaches effectively decreased the oxidative damage to lipids and proteins in the CNS caused by acute or chronic exposure to O_3. This effect may be due to direct or indirect antioxidant mechanisms. The direct mechanism occurs when CUR acts as a RONS scavenger molecule [50, 51]. The reaction of peroxyl radicals with CUR produces CUR-phenoxyl radicals yielding protective effect against lipoperoxidation generated by O_3 exposure [52]. The indirect mechanism could be through the ability of CUR to induce the activation of Nrf2 to stimulate the expression of antioxidant enzymes that might play a protective role in the CNS against oxidative damage [53–55]. Additional studies are necessary to determine if the antioxidant effect of curcumin on oxidative damage by O_3 is mediated in part by the activation of Nrf2.

NF-κB plays a vital role in regulating the inflammation response in many diseases including brain injury and neurodegenerative diseases [56]. Exposure to O_3 induces the formation of RONS and inflammatory cytokines in the lung tissue and the olfactory tract. In the CNS, these molecules are capable of activating NF-κB that promotes the expression of proinflammatory genes [57, 58]. Our results showed an increase in the activation of NF-κB in the acute phase of exposure while chronic exposure to O_3 showed a decreased activation of NF-κB in the rat hippocampus. This decreased activation of NF-κB in our study is similar to that reported by Rivas et al. [48], where NF-κB translocation occurred in the substantia nigra at 7 days of exposure and decreased after 60 days. The decrease of NF-κB activation during chronic exposure could be due to a compensatory regulation that

may involve the synthesis of IκBα, the activation of Nrf2, the oxidative damage of NF-κB p50 subunit, or the expression of anti-inflammatory cytokines [59–62].

CUR was able to significantly reduce the activation of NF-κB in both the preventive and therapeutic approaches, in acute and chronic exposure. This demonstrates the ability of CUR to inhibit NF-κB activation caused by O_3. CUR acts on the signaling pathway of NF-κB by inhibiting the activity of IKK and thus suppressing the phosphorylation and degradation of IκBα; consequently, the nuclear translocation of NF-κB is prevented [63, 64]. In addition, the scavenger activity of CUR could inhibit the activation of IKK by ROS [65]. In our experiments, we found that the greater effect occurred when CUR was administrated in the preventive mode in the acute phase. This could be related to the ability of CUR to activate the Nrf2 pathway previously to the oxidative insult, leading to the expression of antioxidant enzymes and, therefore, prevent the activation of NF-κB by ROS [53, 66].

O_3 inhalation activates alveolar macrophages through IL-1 receptor and Toll-like receptor 4, which in turn leads to the activation of NF-κB; this induces an increased expression of inflammatory mediators such as IL-1, IL-6, and TNF-α [67, 68]. The high levels of IL-1β and TNF-α found in our experiments in rats exposed to O_3 revealed a systemic inflammatory status that may predict an inflammatory process in the CNS [69–71]. As these cytokines are able to cross the BBB, they are capable of stimulating the activation of NF-κB and increasing the neuroinflammation previously developed in situ [56]. The highest levels of IL-1β and TNF-α were observed in our study during the acute phase of O_3 exposure. At the end of the chronic phase, the levels of IL-1β decreased, while TNF-α levels returned to the steady state; this phenomenon could be due to a compensatory anti-inflammatory response. A similar effect was reported by González-Guevara et al. [57] in a dynamically scalable O_3 exposure model, where TNF-α decreased to basal levels in the cerebral cortex. This effect may be due to the regulation of the chronic inflammatory response. "Early-response cytokines," such as IL-1β and TNF-α, increase during acute inflammation and begin to decrease due to the regulation exerted by anti-inflammatory cytokines such as IL-10 and IL-13, which interfere with the signaling pathway of NF-κB and therefore reduce the production of these inflammatory mediators [62]. Additional studies are needed to determine whether the inflammatory regulation during the chronic exposure to O_3 is due to the secretion of anti-inflammatory cytokines. In addition, the decrease in IL-1β and TNF-α levels in the chronic phase can be related to the lower activation of NF-κB in the hippocampus due to a lower stimulation of the pathway by peripheral cytokines as shown in our results. The anti-inflammatory effect of CUR as a modulator for IL-1β and TNF-α has been reported elsewhere in a variety of experimental conditions [72–77]. In our model, the therapeutic and preventive administration of CUR reduced the concentration of IL-1β during acute and chronic exposure to O_3. Moreover, the effect of CUR caused a significant decrease of TNF-α in the acute phase in the therapeutic and preventive administration modes. Thus, CUR exerts an anti-inflammatory activity by suppressing the transcription of proinflammatory cytokine genes through the NF-κB signaling pathway [65, 78].

The results obtained in our experiments have led us to propose that the oxidative damage was established in the acute phase and remained unchanged throughout the chronic exposure phase; because the endogenous antioxidant system had been overcome at early time, such dynamics has been previously documented [5, 8, 48]. However, the inflammatory process has regulatory mechanisms that temporarily could lead to a diminution of the local or systemic inflammatory cytokines. Furthermore, this regulatory process could not be perpetuated and future insults could provoke a new imbalance manifested with an increase of inflammatory cytokine levels. To elucidate this point, we will design future experiments considering other strategies for the insult process.

Overall, it seems a very plausible idea that beneficial effects of CUR are more reliable in the preventive approach than in the therapeutic one [74, 76]. Therefore, it would be preferable to have a preventive protection against harmful factors especially if the protective strategy is free of side effects.

Our future work will explore whether early degenerative changes occur in the hippocampus of rats after a short-term exposure to O_3 and whether CUR may prevent such deleterious changes.

5. Conclusions

The results presented in this study demonstrate the neuroprotective effect of CUR against the damage caused by exposure to O_3. The administration of CUR decreased oxidative stress markers, such as LPO and PO, as well as the inflammatory profile by decreasing the activation of NF-κB and inflammatory cytokines levels (IL-1β and TNF-α).

Data Availability

The data related to lipid peroxidation, cytokine levels, densitometry determination, and images used to support the findings of this study are available from the corresponding author upon request.

Conflicts of Interest

The authors declare no conflict of interests.

Authors' Contributions

Nery-Flores S. D., Ramírez-Vázquez J. J., and Ramírez-Herrera M. A. contributed equally to this research work.

Acknowledgments

This work was supported by the Consejo Nacional de Ciencia y Tecnología, México (CONACyT) and a fellowship to Sendar Daniel Nery-Flores (589920), Program for Incorporation and Permanence of Postgraduate (PROIMPEP), CONACyT (2228554). The authors thank Dr. Michelle Brennan for the language correction work.

References

[1] W. Yang and S. T. Omaye, "Air pollutants, oxidative stress and human health," *Mutation Research/Genetic Toxicology and Environmental Mutagenesis*, vol. 674, no. 1-2, pp. 45–54, 2009.

[2] M. Lodovici and E. Bigagli, "Oxidative stress and air pollution exposure," *Journal of Toxicology*, vol. 2011, Article ID 487074, 9 pages, 2011.

[3] W. H. White, "Considerations in the use of ozone and PM(2.5) data for exposure assessment," *Air Quality, atmosphere & Health*, vol. 2, no. 4, pp. 223–230, 2009.

[4] A. Raza, M. Dahlquist, T. Lind, and P. L. S. Ljungman, "Susceptibility to short-term ozone exposure and cardiovascular and respiratory mortality by previous hospitalizations," *Environmental Health*, vol. 17, no. 1, p. 37, 2018.

[5] C. Dorado-Martínez, C. Paredes-carbajal, D. Mascher, G. Borgonio-Pérez, and S. Rivas-arancibia, "Effects of different ozone doses on memory, motor activity and lipid peroxidation levels, in rats," *The International Journal of Neuroscience*, vol. 108, no. 3-4, pp. 149–161, 2001.

[6] J. C. Martínez-Lazcano, E. González-Guevara, V. Custodio et al., "Activity of nitric oxide synthase isoforms in acute brain oxidative damage induced by ozone exposure," *Nitric Oxide: Biology and Chemistry*, vol. 75, pp. 42–52, 2018.

[7] W. A. Pryor, K. N. Houk, C. S. Foote et al., "Free radical biology and medicine: it's a gas, man!," *American Journal of Physiology-Regulatory Integrative and Comparative Physiology*, vol. 291, no. 3, pp. R491–R511, 2006.

[8] S. Rivas-Arancibia, R. Guevara-Guzmán, Y. López-Vidal et al., "Oxidative stress caused by ozone exposure induces loss of brain repair in the hippocampus of adult rats," *Toxicological Sciences*, vol. 113, no. 1, pp. 187–197, 2010.

[9] M. R. Avila-Costa, L. Colín-Barenque, T. I. Fortoul et al., "Memory deterioration in an oxidative stress model and its correlation with cytological changes on rat hippocampus CA1," *Neuroscience Letters*, vol. 270, no. 2, pp. 107–109, 1999.

[10] D. Santiago-Lopez, J. A. Bautista-Martinez, C. I. Reyes-Hernandez, M. Aguilar-Martinez, and S. Rivas-Arancibia, "Oxidative stress, progressive damage in the substantia nigra and plasma dopamine oxidation, in rats chronically exposed to ozone," *Toxicology Letters*, vol. 197, no. 3, pp. 193–200, 2010.

[11] E. Rodríguez-Martínez, C. Nava-Ruiz, E. Escamilla-Chimal, G. Borgonio-Perez, and S. Rivas-Arancibia, "The effect of chronic ozone exposure on the activation of endoplasmic reticulum stress and apoptosis in rat Hippocampus," *Frontiers in Aging Neuroscience*, vol. 8, 2016.

[12] S. Rivas-Arancibia, R. Vazquez-Sandoval, D. Gonzalez-Kladiano, S. Schneider-Rivas, and A. Lechuga-Guerrero, "Effects of ozone exposure in rats on memory and levels of brain and pulmonary superoxide dismutase," *Environmental Research*, vol. 76, no. 1, pp. 33–39, 1998.

[13] L. Calderón-Garcidueñas, R. Reynoso-Robles, J. Vargas-Martínez et al., "Prefrontal white matter pathology in air pollution exposed Mexico City young urbanites and their potential impact on neurovascular unit dysfunction and the development of Alzheimer's disease," *Environmental Research*, vol. 146, pp. 404–417, 2016.

[14] L. Calderón-Garcidueñas, A. Mora-Tiscareño, E. Ontiveros et al., "Air pollution, cognitive deficits and brain abnormalities: a pilot study with children and dogs," *Brain and Cognition*, vol. 68, no. 2, pp. 117–127, 2008.

[15] S. C. Gupta, C. Sundaram, S. Reuter, and B. B. Aggarwal, "Inhibiting NF-κB activation by small molecules as a therapeutic strategy," *Biochimica et Biophysica Acta (BBA) - Gene Regulatory Mechanisms*, vol. 1799, no. 10–12, pp. 775–787, 2010.

[16] M. J. Morgan and Z. G. Liu, "Crosstalk of reactive oxygen species and NF-κB signaling," *Cell Research*, vol. 21, no. 1, pp. 103–115, 2011.

[17] B. Hoesel and J. A. Schmid, "The complexity of NF-κB signaling in inflammation and cancer," *Molecular Cancer*, vol. 12, no. 1, p. 86, 2013.

[18] B. Poljšak and R. Fink, "The protective role of antioxidants in the defence against ROS/RNS-mediated environmental pollution," *Oxidative Medicine and Cellular Longevity*, vol. 2014, Article ID 671539, 22 pages, 2014.

[19] A. Ndhlala, M. Moyo, and J. Van Staden, "Natural antioxidants: fascinating or mythical biomolecules?," *Molecules*, vol. 15, no. 10, pp. 6905–6930, 2010.

[20] A. B. Kunnumakkara, D. Bordoloi, G. Padmavathi et al., "Curcumin, the golden nutraceutical: multitargeting for multiple chronic diseases," *British Journal of Pharmacology*, vol. 174, no. 11, pp. 1325–1348, 2017.

[21] B. B. Aggarwal and K. B. Harikumar, "Potential therapeutic effects of curcumin, the anti-inflammatory agent, against neurodegenerative, cardiovascular, pulmonary, metabolic, autoimmune and neoplastic diseases," *The International Journal of Biochemistry & Cell Biology*, vol. 41, no. 1, pp. 40–59, 2009.

[22] S. C. Gupta, G. Kismali, and B. B. Aggarwal, "Curcumin, a component of turmeric: from farm to pharmacy," *BioFactors*, vol. 39, no. 1, pp. 2–13, 2013.

[23] A. Barzegar and A. A. Moosavi-Movahedi, "Intracellular ROS protection efficiency and free radical-scavenging activity of curcumin," *PLoS One*, vol. 6, no. 10, article e26012, 2011.

[24] S. Servais, A. Boussouar, A. Molnar, T. Douki, J. M. Pequignot, and R. Favier, "Age-related sensitivity to lung oxidative stress during ozone exposure," *Free Radical Research*, vol. 39, no. 3, pp. 305–316, 2005.

[25] L. Calderón-Garcidueñas, E. Leray, P. Heydarpour, R. Torres-Jardon, and J. Reis, "Air pollution, a rising environmental risk factor for cognition, neuroinflammation and neurodegeneration: the clinical impact on children and beyond," *Revue Neurologique*, vol. 172, no. 1, pp. 69–80, 2016.

[26] S. A. Frautschy, W. Hu, P. Kim et al., "Phenolic anti-inflammatory antioxidant reversal of Aβ-induced cognitive deficits and neuropathology," *Neurobiology of Aging*, vol. 22, no. 6, pp. 993–1005, 2001.

[27] A. A. Canales-Aguirre, U. A. Gomez-Pinedo, S. Luquin, M. A. Ramírez-Herrera, M. L. Mendoza-Magaña, and A. Feria-Velasco, "Curcumin protects against the oxidative damage induced by the pesticide parathion in the hippocampus of the rat brain," *Nutritional Neuroscience*, vol. 15, no. 2, pp. 62–69, 2012.

[28] P. Srivastava, R. S. Yadav, L. P. Chandravanshi et al., "Unraveling the mechanism of neuroprotection of curcumin in arsenic induced cholinergic dysfunctions in rats," *Toxicology and Applied Pharmacology*, vol. 279, no. 3, pp. 428–440, 2014.

[29] C. Sharma, J. Kaur, S. Shishodia, B. B. Aggarwal, and R. Ralhan, "Curcumin down regulates smokeless tobacco-induced NF-κB activation and COX-2 expression in human oral premalignant and cancer cells," *Toxicology*, vol. 228, no. 1, pp. 1–15, 2006.

[30] J. A. dos Santos Jaques, P. H. Doleski, L. G. Castilhos et al., "Free and nanoencapsulated curcumin prevents cigarette smoke-induced cognitive impairment and redox imbalance," *Neurobiology of Learning and Memory*, vol. 100, pp. 98–107, 2013.

[31] Z. Zhang, X. Niu, C. Lu, M. Jiang, G. G. Xiao, and A. Lu, "The effect of curcumin on human bronchial epithelial cells exposed to fine particulate matter: a predictive analysis," *Molecules*, vol. 17, no. 10, pp. 12406–12426, 2012.

[32] A. Nemmar, D. Subramaniyan, and B. H. Ali, "Protective effect of curcumin on pulmonary and cardiovascular effects induced by repeated exposure to diesel exhaust particles in mice," *PLoS One*, vol. 7, no. 6, article e39554, 2012.

[33] S. Genc, Z. Zadeoglulari, S. H. Fuss, and K. Genc, "The adverse effects of air pollution on the nervous system," *Journal of Toxicology*, vol. 2012, Article ID 782462, 23 pages, 2012.

[34] N. Khansari, Y. Shakiba, and M. Mahmoudi, "Chronic inflammation and oxidative stress as a major cause of age-related diseases and cancer," *Recent Patents on Inflammation & Allergy Drug Discovery*, vol. 3, no. 1, pp. 73–80, 2009.

[35] S. Rivas-Arancibia, C. Dorado-Martínez, G. Borgonio-Pérez et al., "Effects of taurine on ozone-induced memory deficits and lipid peroxidation levels in brains of young, mature, and old rats," *Environmental Research*, vol. 82, no. 1, pp. 7–17, 2000.

[36] E. D. Farfán-García, M. C. Castillo-Hernández, R. Pinto-Almazán, S. Rivas-Arancibia, J. M. Gallardo, and C. Guerra-Araiza, "Tibolone prevents oxidation and ameliorates cholinergic deficit induced by ozone exposure in the male rat hippocampus," *Neurochemical Research*, vol. 39, no. 9, pp. 1776–1786, 2014.

[37] M. L. Mokoena, B. H. Harvey, D. W. Oliver, and C. B. Brink, "Ozone modulates the effects of imipramine on immobility in the forced swim test, and nonspecific parameters of hippocampal oxidative stress in the rat," *Metabolic Brain Disease*, vol. 25, no. 2, pp. 125–133, 2010.

[38] A. L. Guerrero, C. Dorado-Martinez, A. Rodriguez, K. Pedroza-Rios, G. Borgonio-Perez, and S. Rivas-Arancibia, "Effects of vitamin E on ozone-induced memory deficits and lipid peroxidation in rats," *Neuroreport*, vol. 10, no. 8, pp. 1689–1692, 1999.

[39] G. M. Cole, B. Teter, and S. A. Frautschy, "Neuroprotective Effects of Curcumin," *Advances in Experimental Medicine and Biology*, vol. 595, pp. 197–212, 2007.

[40] C. J. Cooksey, "Turmeric: old spice, new spice," *Biotechnic & Histochemistry*, vol. 92, no. 5, pp. 309–314, 2017.

[41] S. C. Gupta, S. Patchva, and B. B. Aggarwal, "Therapeutic roles of curcumin: lessons learned from clinical trials," *The AAPS Journal*, vol. 15, no. 1, pp. 195–218, 2013.

[42] K. Maiti, K. Mukherjee, A. Gantait, B. P. Saha, and P. K. Mukherjee, "Curcumin–phospholipid complex: preparation, therapeutic evaluation and pharmacokinetic study in rats," *International Journal of Pharmaceutics*, vol. 330, no. 1-2, pp. 155–163, 2007.

[43] Y.-M. Tsai, C.-F. Chien, L.-C. Lin, and T.-H. Tsai, "Curcumin and its nano-formulation: the kinetics of tissue distribution and blood–brain barrier penetration," *International Journal of Pharmaceutics*, vol. 416, no. 1, pp. 331–338, 2011.

[44] S. Pizzimenti, E. Ciamporcero, M. Daga et al., "Interaction of aldehydes derived from lipid peroxidation and membrane proteins," *Frontiers in Physiology*, vol. 4, 2013.

[45] M. Perluigi, R. Coccia, and D. A. Butterfield, "4-Hydroxy-2-nonenal, a reactive product of lipid peroxidation, and neurodegenerative diseases: a toxic combination illuminated by redox proteomics studies," *Antioxidants & Redox Signaling*, vol. 17, no. 11, pp. 1590–1609, 2012.

[46] P. Dkhar and R. Sharma, "Effect of dimethylsulphoxide and curcumin on protein carbonyls and reactive oxygen species of cerebral hemispheres of mice as a function of age," *International Journal of Developmental Neuroscience*, vol. 28, no. 5, pp. 351–357, 2010.

[47] P. A. Grimsrud, H. Xie, T. J. Griffin, and D. A. Bernlohr, "Oxidative stress and covalent modification of protein with bioactive aldehydes," *The Journal of Biological Chemistry*, vol. 283, no. 32, pp. 21837–21841, 2008.

[48] S. Rivas-Arancibia, L. F. H. Zimbrón, E. Rodríguez-Martínez, P. D. Maldonado, G. Borgonio Pérez, and M. Sepúlveda-Parada, "Oxidative stress-dependent changes in immune responses and cell death in the substantia nigra after ozone exposure in rat," *Frontiers in Aging Neuroscience*, vol. 7, p. 65, 2015.

[49] R. Pinto-Almazán, J. J. Segura-Uribe, M. A. Soriano-Ursúa, E. D. Farfán-García, J. M. Gallardo, and C. Guerra-Araiza, "Effect of tibolone pretreatment on kinases and phosphatases that regulate the expression and phosphorylation of Tau in the hippocampus of rats exposed to ozone," *Neural Regeneration Research*, vol. 13, no. 3, pp. 440–448, 2018.

[50] T. Ak and İ. Gülçin, "Antioxidant and radical scavenging properties of curcumin," *Chemico-Biological Interactions*, vol. 174, no. 1, pp. 27–37, 2008.

[51] J. Trujillo, Y. I. Chirino, E. Molina-Jijón, A. C. Andérica-Romero, E. Tapia, and J. Pedraza-Chaverrí, "Renoprotective effect of the antioxidant curcumin: recent findings()," *Redox Biology*, vol. 1, no. 1, pp. 448–456, 2013.

[52] K. Priyadarsini, "The chemistry of curcumin: from extraction to therapeutic agent," *Molecules*, vol. 19, no. 12, pp. 20091–20112, 2014.

[53] S. González-Reyes, S. Guzmán-Beltrán, O. N. Medina-Campos, and J. Pedraza-Chaverri, "Curcumin pretreatment induces Nrf2 and an antioxidant response and prevents hemin-induced toxicity in primary cultures of cerebellar granule neurons of rats," *Oxidative Medicine and Cellular Longevity*, vol. 2013, Article ID 801418, 14 pages, 2013.

[54] Z. Liu, W. Dou, Y. Zheng et al., "Curcumin upregulates Nrf2 nuclear translocation and protects rat hepatic stellate cells against oxidative stress," *Molecular Medicine Reports*, vol. 13, no. 2, pp. 1717–1724, 2016.

[55] W. Dong, B. Yang, L. Wang et al., "Curcumin plays neuroprotective roles against traumatic brain injury partly via Nrf2 signaling," *Toxicology and Applied Pharmacology*, vol. 346, pp. 28–36, 2018.

[56] R.-H. Shih, C. Y. Wang, and C. M. Yang, "NF-kappaB signaling pathways in neurological inflammation: a mini review," *Frontiers in Molecular Neuroscience*, vol. 8, p. 77, 2015.

[57] E. González-Guevara, J. C. Martínez-Lazcano, V. Custodio, M. Hernández-Cerón, C. Rubio, and C. Paz, "Exposure to ozone induces a systemic inflammatory response: possible source of the neurological alterations induced by this gas," *Inhalation Toxicology*, vol. 26, no. 8, pp. 485–491, 2014.

[58] C. L. Mumaw, S. Levesque, C. McGraw et al., "Microglial priming through the lung-brain axis: the role of air pollution-induced circulating factors," *The FASEB Journal*, vol. 30, no. 5, pp. 1880–1891, 2016.

[59] L. Gan and J. A. Johnson, "Oxidative damage and the Nrf2-ARE pathway in neurodegenerative diseases," *Biochimica et Biophysica Acta (BBA) - Molecular Basis of Disease*, vol. 1842, no. 8, pp. 1208–1218, 2014.

[60] H. E. Marshall and J. S. Stamler, "Inhibition of NF-κB by S-Nitrosylation," *Biochemistry*, vol. 40, no. 6, pp. 1688–1693, 2001.

[61] T. Nishi, N. Shimizu, M. Hiramoto et al., "Spatial redox regulation of a critical cysteine residue of NF-κB *in vivo*," *Journal of Biological Chemistry*, vol. 277, no. 46, pp. 44548–44556, 2002.

[62] P. A. Ward and A. B. Lentsch, "The acute inflammatory response and its regulation," *Archives of Surgery*, vol. 134, no. 6, pp. 666–669, 1999.

[63] A. C. Bharti, N. Donato, S. Singh, and B. B. Aggarwal, "Curcumin (diferuloylmethane) down-regulates the constitutive activation of nuclear factor–κB and IκBα kinase in human multiple myeloma cells, leading to suppression of proliferation and induction of apoptosis," *Blood*, vol. 101, no. 3, pp. 1053–1062, 2003.

[64] C. Jobin, C. A. Bradham, M. P. Russo et al., "Curcumin blocks cytokine-mediated NF-κB activation and proinflammatory gene expression by inhibiting inhibitory factor I-κB kinase activity," *Journal of Immunology*, vol. 163, no. 6, pp. 3474–3483, 1999.

[65] S. Singh and B. B. Aggarwal, "Activation of transcription factor NF-κB is suppressed by curcumin (diferuloylmethane)," *Journal of Biological Chemistry*, vol. 270, no. 42, pp. 24995–25000, 1995.

[66] G. Scapagnini, C. Colombrita, M. Amadio et al., "Curcumin activates defensive genes and protects neurons against oxidative stress," *Antioxidants & Redox Signaling*, vol. 8, no. 3-4, pp. 395–403, 2006.

[67] J.-W. Park, C. Taube, C. Swasey et al., "Interleukin-1 receptor antagonist attenuates airway hyperresponsiveness following exposure to ozone," *American Journal of Respiratory Cell and Molecular Biology*, vol. 30, no. 6, pp. 830–836, 2004.

[68] A. J. Connor, J. D. Laskin, and D. L. Laskin, "Ozone-induced lung injury and sterile inflammation. Role of Toll-like receptor 4," *Experimental and Molecular Pathology*, vol. 92, no. 2, pp. 229–235, 2012.

[69] S. Rivest, "How circulating cytokines trigger the neural circuits that control the hypothalamic–pituitary–adrenal axis," *Psychoneuroendocrinology*, vol. 26, no. 8, pp. 761–788, 2001.

[70] R. A. Johnston, J. P. Mizgerd, L. Flynt, L. J. Quinton, E. S. Williams, and S. A. Shore, "Type I interleukin-1 receptor is required for pulmonary responses to subacute ozone exposure in mice," *American Journal of Respiratory Cell and Molecular Biology*, vol. 37, no. 4, pp. 477–484, 2007.

[71] M. D. Nguyen, J.-P. Julien, and S. Rivest, "Innate immunity: the missing link in neuroprotection and neurodegeneration?," *Nature Reviews Neuroscience*, vol. 3, no. 3, pp. 216–227, 2002.

[72] H. Ni, W. Jin, T. Zhu et al., "Curcumin modulates TLR4/NF-κB inflammatory signaling pathway following traumatic spinal cord injury in rats," *The Journal of Spinal Cord Medicine*, vol. 38, no. 2, pp. 199–206, 2015.

[73] J. Wang, H. Wang, R. Zhu, Q. Liu, J. Fei, and S. Wang, "Anti-inflammatory activity of curcumin-loaded solid lipid nanoparticles in IL-1β transgenic mice subjected to the lipopolysaccharide-induced sepsis," *Biomaterials*, vol. 53, pp. 475–483, 2015.

[74] V. Sorrenti, G. Contarini, S. Sut et al., "Curcumin prevents acute neuroinflammation and long-term memory impairment induced by systemic lipopolysaccharide in mice," *Frontiers in Pharmacology*, vol. 9, p. 183, 2018.

[75] Y.-Z. Guo, P. He, and A.-M. Feng, "Effect of curcumin on expressions of NF-κBp65, TNF-α and IL-8 in placental tissue of premature birth of infected mice," *Asian Pacific Journal of Tropical Medicine*, vol. 10, no. 2, pp. 175–178, 2017.

[76] P. Kumar, K. Sulakhiya, C. C. Barua, and N. Mundhe, "TNF-α, IL-6 and IL-10 expressions, responsible for disparity in action of curcumin against cisplatin-induced nephrotoxicity in rats," *Molecular and Cellular Biochemistry*, vol. 431, no. 1-2, pp. 113–122, 2017.

[77] M. E. Kelany, T. M. Hakami, and A. H. Omar, "Curcumin improves the metabolic syndrome in high-fructose-diet-fed rats: role of TNF-α, NF-κB, and oxidative stress," *Canadian Journal of Physiology and Pharmacology*, vol. 95, no. 2, pp. 140–150, 2016.

[78] Y. Yu, Q. Shen, Y. Lai et al., "Anti-inflammatory effects of curcumin in microglial cells," *Frontiers in Pharmacology*, vol. 9, p. 386, 2018.

Hindawi
Oxidative Medicine and Cellular Longevity
Volume 2018, Article ID 7890291, 12 pages
https://doi.org/10.1155/2018/7890291

Research Article

Estradiol Alleviates Intervertebral Disc Degeneration through Modulating the Antioxidant Enzymes and Inhibiting Autophagy in the Model of Menopause Rats

Lin-Yu Jin,[1] Zhen-Dong Lv,[1] Kun Wang,[1] Lie Qian,[1] Xiao-Xing Song,[2] Xin-Feng Li,[1] and Hong-Xing Shen[1]

[1]*Department of Spine Surgery, Renji Hospital, Shanghai Jiao Tong University School of Medicine, Shanghai 200240, China*
[2]*Department of Anesthesiology, Ruijin Hospital, Shanghai Jiao Tong University School of Medicine, Shanghai, China*

Correspondence should be addressed to Xiao-Xing Song; sxx11493@rjh.com.cn, Xin-Feng Li; lxfrenji@126.com, and Hong-Xing Shen; shenhxgk@126.com

Received 4 July 2018; Accepted 1 October 2018; Published 23 December 2018

Guest Editor: Marina Sokovic

Objective. To investigate the effects of menopause on redox balance in the intervertebral disc and to examine whether oxidative stress and autophagy were associated with disc degeneration in menopause rats. *Methods*. Thirty female Sprague-Dawley rats were randomly divided into three groups (sham, ovariectomized with vehicle, and ovariectomized with estrogen). At the end of the 3-month treatment, the rats were examined by 3.0 T MRI. Serum estradiol (E2) level was measured. Redox balance of nucleus pulposus was determined by measuring total antioxidant capacity (T-AOC), superoxide dismutase (SOD), catalase (CAT), glutathione peroxidase (GSH-Px), glutathione (GSH), and oxidized glutathione (GSSG). Transmission electron microscopy (TEM), immunohistochemical staining, and Western blot were used to determine the nucleus pulposus autophagy level. At the same time, Spearman's correlation coefficient was used to describe the relationship between intervertebral disc grade, oxidative stress status, serum E2, and autophagy level. *Results*. The level of serum E2 was significantly decreased by ovariectomy and can be corrected by the estrogen replacement therapy (ERT). In OVX rats, an increased oxidative stress and high level of autophagy were observed in nucleus pulposus tissue. ERT prevented the intervertebral disc degeneration (IVDD), restored the redox balance, and reduced autophagy level. *Conclusion*. Ovariectomy induced oxidative stress, autophagy, and intervertebral disc degeneration. Autophagy of the intervertebral disc was negatively correlated with oxidative stress, and the level of autophagy can be reduced by ERT through modulating the redox balance and downregulating the autophagy level. Regulating the redox balance of IVD may be a potential therapeutic option for degeneration of the disc in the postmenopausal women.

1. Introduction

Menopause occurs gradually between the ages of 45 and 55 years during women's life, leading to a significant depression of estrogen level [1]. This process influences many organs and system metabolism in postmenopausal women. Recently, accumulating evidences showed that older women had a higher prevalence and severity of disc degeneration compared with older men [2–5]. An intervertebral disc (IVD) is a fibrocartilaginous tissue and is composed of three distinct but interdependent tissues: annulus fibrosis (AF), nucleus pulposus (NP), and cartilage endplate (EP). IVDs, as a shock absorber system, can transfer loads and weaken energy that are imposed on the skeletal spine [6]. Intervertebral disc degeneration (IVDD) is characterized by reduced water content, depression of proteoglycan synthesis, inappropriate collagen types, and abnormal production of the extracellular matrix (ECM) [7, 8]. Commonly, the NP tissue plays a major role in the functional composition of IVD, and the pathological changes of the NP tissue are important causes of disc degeneration [9]. Degeneration of the intervertebral disc is the main contributor to back pain. The back pain imposes

heavy economic burdens on human society [10]. Regrettably, the current therapy strategies, such as conservative treatment and/or surgery, do not keep the normal function of IVD. Therefore, pathogenesis of IVD and remedial methods for IVDD are still the main area in research about IVD. Several articles indicated that 17β-estradiol (E2) could promote AF cell and NP cell proliferation by reducing the level of apoptosis in vitro [11–13]. Interestingly, postmenopausal women, receiving estrogen replacement treatment (ERT), can sustain a higher IVD height than untreated menopausal women [14]. For animal intervertebral discs, previous studies have shown that OVX female rats are sensitive to IVDD, and E2 supplementation can retard the progress of pathology of the IVDD [15, 16]. However, although significant advances have been made in order to understand the protective effects of E2 that can reverse or retard the pathogenesis of IVDD, the underlying mechanisms are not well understood.

The process of IVDD induced by estrogen depletion may be partly caused by oxidative stress, which is defined as imbalance between oxidants and antioxidants [17]. Recent studies have reported that the occurrence and development of IVDD are related to oxidative stress [18, 19]. More importantly, postmenopausal women have higher levels of oxidative stress, suggesting that antioxidant capacity may be associated with decreased estrogen [20, 21]. Interestingly, estrogen replacement therapy (ERT) could be able to restore antioxidant status [22]. Autophagy, an important cellular protective mechanism, can respond to different kinds of cellular stress. Furthermore, several in vitro studies suggested that autophagy has an important protective effect on IVD cells [23, 24]. Evidences mainly obtained from the above studies suggest that the oxidative stress induced by the estrogen loss may be a risk factor for the IVDD, and autophagy level may play a protective role with the absence of estrogen. Nevertheless, the relationships between estrogen and redox system/autophagy level have not been addressed so far in intervertebral discs. Therefore, our objective was to investigate the effects of changes in estrogen levels, redox balance, and autophagy on intervertebral discs in ovariectomized rats.

2. Methods and Materials

2.1. Study Design. The present study included thirty six-week-old female Sprague-Dawley rats, and they were randomized and divided into three groups, which were sham surgery (sham), oophorectomy (OVX), and 10 μg/kg/day 17β-estradiol (OVX + E2). Bilateral oophorectomy was performed under anesthesia with pentobarbital for the sham, OVX + veh, and OVX + E2 groups. E2 supplementation was performed for 12 weeks; then, we used the 3.0 T MRI (Siemens Symphony, Erlangen, Germany) to examine the IVD of rats. The IVDD was evaluated by the quantitative T2 mapping in the MRI sagittal plane. Immediately after radiographic examinations, the intervertebral discs and blood samples were acquired from the rats treated with overdose pentobarbital. No rat died during the research before they were treated with euthanasia. All experiments were in accordance with the *Guide for the Care and Use of Laboratory Animals* and have been approved by the Ethics Committee of Renji Hospital.

2.2. Magnetic Resonance Imaging Examination. T2 mapping magnetic resonance (MR) imaging sequence is a reliable method for monitoring the dipolar interaction of water proton molecule movements in the extracellular matrix of collagen and proteoglycan [25]. Lumbar MRI images of the three groups were obtained with a 3.0 T MR machine (Siemens), covering the L1–L6 IVDs. The same procedure was used to scan the spines: acquisition time of the T2 mapping sequence of L5–6 disc for each spine was approximately 15 min. Then, the regions of interest (ROIs), which were displayed in Figure 1(a), were evaluated by T2 mapping relaxation time; ROI 1 covered the ventral annulus fibrosus (VAF), ROI 2 covered the ventral border zone (BZ), ROI 3 covered the NP, ROI 4 covered the dorsal BZ, and ROI 5 covered the dorsal annulus fibrosus (DAF). The standard ratio of these ROIs was determined based on microstructure evaluation under a microscope: ROI 1 accounted for 25.3% of the disc diameter, ROIs 2 and 4 each were 13.8%, ROI 3 was 35.9%, and ROI 5 measured 11.2%.

2.3. Histological Evaluation. 4% paraformaldehyde was used to fix the spinal tissues, which were washed twice with phosphate-buffered saline (PBS). 24 hours later, the tissues underwent the procedure of decalcification for one month. Immediately after that, the tissues were embedded in paraffin. Then, the L5–L6 disc segments were sliced into 4 μm thick sections. Obtained in the sagittal plane, it was treated with xylene to remove paraffin, rehydrated in a gradient alcohol bath, and then rinsed 3 times with PBS. Sections were stained with either hematoxylin-eosin (HE), safranin-O (SO) green, or picrosirius rend (PR). The slides were observed with a digital microscope (Olympus, Japan), and a scoring system, according to the previous study [16], was used to evaluate the disc degeneration. These slides were independently and blindly assessed by 2 observers, and the average results of the 2 observers were regarded as the final data.

2.4. Immunohistochemistry for Autophagy Level of IVD. The paraffin-embedded L5–L6 segments were cut into 4 μm thickness, and then the slides underwent paraffin removal and were rehydrated in graded alcohol baths. After being treated with antigen retrieval and blocking solution, slides were incubated with an LC-3B monoclonal antibody (1 : 100, CST Inc., USA) at 4°C overnight. Then, the sections were incubated with a secondary antibody dilution (1 : 500, CST Inc., USA) for 30 min. Finally, slides were treated with DAB solution for 5 min after a double wash by PBS. Finished works were observed with a digital microscope (Olympus, Japan). The semiquantitative analysis method was used to evaluate the density of sections by the Image-Pro Plus (IPP) 6.0 software, and the average results were addressed under 400x magnification images.

2.5. Measurement of Redox Balance in IVD. The fresh NP tissue of IVD was ground and made into protein homogenate,

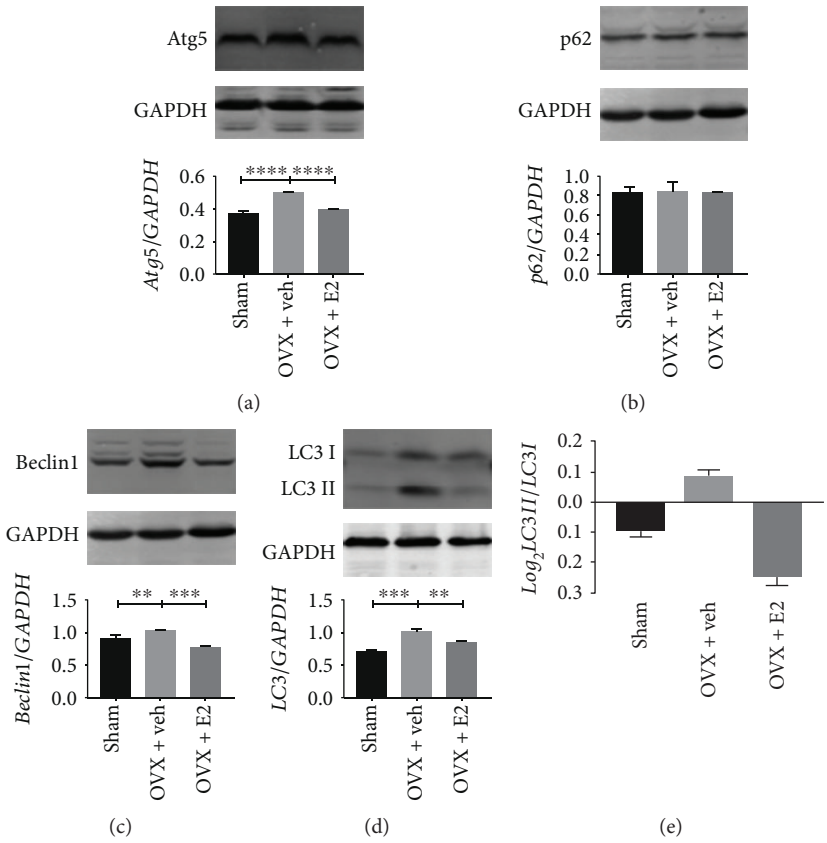

Figure 1: Autophagy level in the NP tissue of OVX was higher than that of the other two groups. An increase in protein levels of Atg5 (a), Beclin1 (c), and LC3-II (d) and the LC3 I/LC3 II ratio (e). However, there are no significant differences in the p62 (b). $^{**}P < 0.05$; $^{****}P < 0.01$.

and it was centrifuged at 3000 rpm for 15 min. An antioxidant enzyme activity test kit (Nanjing Jiancheng Bioengineering Institute, Jiangsu, China) was used to detect the activities of T-AOC, SOD, CAT, and GSH-Px and the level of T-GSH and GSSG. All procedures were performed according to the instruction book of the kit.

2.6. Detection of Serum E2. The blood samples after standing at room temperature for 2 hours were centrifuged at 3000 rpm for 15 min at 4°C, and then the supernatant was collected to prepare serum samples. The estrogen detection ELISA kit was used to determine the level of serum E2 (Shanghai Institute of Biological Product, Shanghai, China). All experimental steps referred to the product manual.

2.7. Autophagosome Observed by a Transmission Electron Microscope. The fresh NP tissue samples were immediately fixed in 1% glutaraldehyde for one day at room temperature and demineralized for 3 weeks. After that, the NP tissues were cut into 1 mm^3. These samples were postfixed with 1% osmium tetroxide for 1 hour after washing with PBS. The treated samples were embedded in Durcupan ACM for 7 hours, cut into thin sections, which was stained with uranyl acetate and lead citrate, and finally examined with a Philips CM-80 transmission electron microscope (Eindhoven, Netherlands).

2.8. Western Blot Analysis. All the NP tissues were lysed in RIPA buffer (Beyotime, Jiangsu, China) containing PMSF and inhibitor of protease. The BCA kit (Beyotime, Jiangsu, China) was used to determine the concentration of protein in the tissue lysate according to the product manual. The tissue lysates (35 μg) were separated by 12% SDS-PAGE using electrophoresis, and then the proteins were transferred to the nitrocellulose membrane. After blocking with 5% nonfat milk for 1 hour, the membranes were incubated with primary antibodies against LC3-B (1 : 1000, Novus, USA), Beclin1 (1 : 1000, Abcam, USA), p62 (1 : 1000, CST, USA), Atg5 (1 : 1000, CST, USA), and GAPDH (1 : 5000, Proteintech, China) at 4°C overnight. After being washed three times with PBS, the membranes were incubated with a LI-COR 800W secondary antibody (LI-COR Biosciences, USA). Finally, the membranes were determined by Odyssey machine (LI-COR Biosciences, USA) and were quantified by the IPP software.

2.9. Statistical Analyses. The present data were calculated and presented as means ± standard deviation (SD). One-way analysis of variance and t-test were used to analyze the significant difference by the SPSS 21.0 software. The correlation analysis was performed to correlate the serum estrogen level, autophagy level, status of redox balance, H-score, and the value of T2 mapping of IVD using Spearman's rank correlation

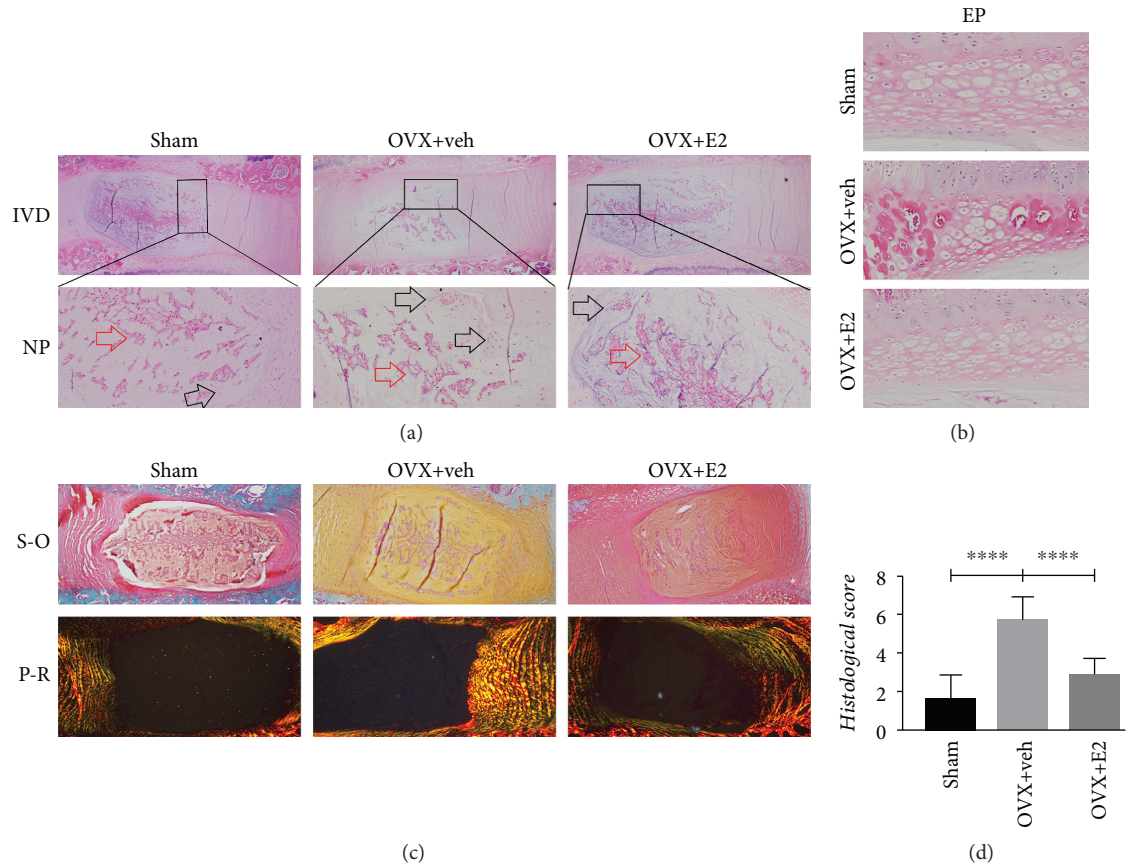

Figure 2: (a) Histological illustration of the L5–L6 IVDs 3 months postsurgery (original magnification, 4x). The arrows indicate the certain cell types in the NP tissue (red arrows: notochord cells; black arrows: chondrocyte-like cells; original magnification, 20x). (b) Ectopic bone tissue in EP. (c) Safranin-O (S-O) staining and picric acid-sirius red (P-R) staining of the IVD (original magnification, 4x). The red staining intensity for proteoglycan decreased in the NP and AF tissue with ovariectomy; estrogen supplementation can reverse the degeneration changes; collagen II was mainly displayed in the inner AF of the sham and OVX + E2 groups, but it was replaced by collagen I in the OVX group. (d) Histological score of disc degeneration of the three groups (****$P < 0.01$ compared with the sham group and OVX + E2 group).

coefficients. $P < 0.05$ demonstrated significant differences and $P < 0.01$ demonstrated highly significant differences.

3. Results

3.1. Verification of the Rat Lumbar IVDD. To investigate whether menopause plays a side role in causing IVDD, we established an ovariectomy rat model according to previous studies [15, 16]. Hematoxylin and eosin (HE) staining was used to assess the intervertebral disc (Figure 2(a)). In the OVX + veh group, the change of the cell phenotype occurred in the NP tissue. In the NP tissue, there were a significant number of notochord cells that are reduced, while many chondrocyte-like cells appeared in groups, and they were surrounded by the decrease in ECM in the NP tissue. The junction zone between AF and NP became blurring due to fissures, disorganized collagen fibers, and proliferation of fibrocartilage. However, the situation of the sham group was different because there were more notochord cells and a small number of cartilage-like cells. There was an intact and tightly arranging structure in the AF tissue of the sham group. The protective effects of estrogen were observed in the OVX + E2 group in which situations of the NP tissues were similar to those observed in the sham group.

The intervertebral discs were assessed using the scoring system. A good label was given to the sham group and its H-score was the lowest (1.6 ± 1.26). There were obvious pathological changes of the intervertebral disc in the OVX + veh group with a score of 5.7 ± 1.25, which was higher than the others ($P < 0.05$). Estrogen supplementation can partly alleviate the intervertebral disc degeneration; the score was 2.9 ± 0.88, which was lower than that of the OVX group ($P < 0.05$).

3.2. Estrogen Retards Degeneration of Disc Components. To assess the protective effects of estrogen in vivo, estrogen supplementation was performed in the OVX + E2 group daily. The content of proteoglycan and collagen was determined by SO and PR staining. As shown in Figure 2(c), the decreased red staining intensity demonstrated the degradation of proteoglycan in the nucleus pulposus and annulus fibrosus tissues in the OVX rats, which indicated that estrogen supplementation can reverse the degradation. Polarization microscopy was used to determine the types of collagen, under which collagen type I

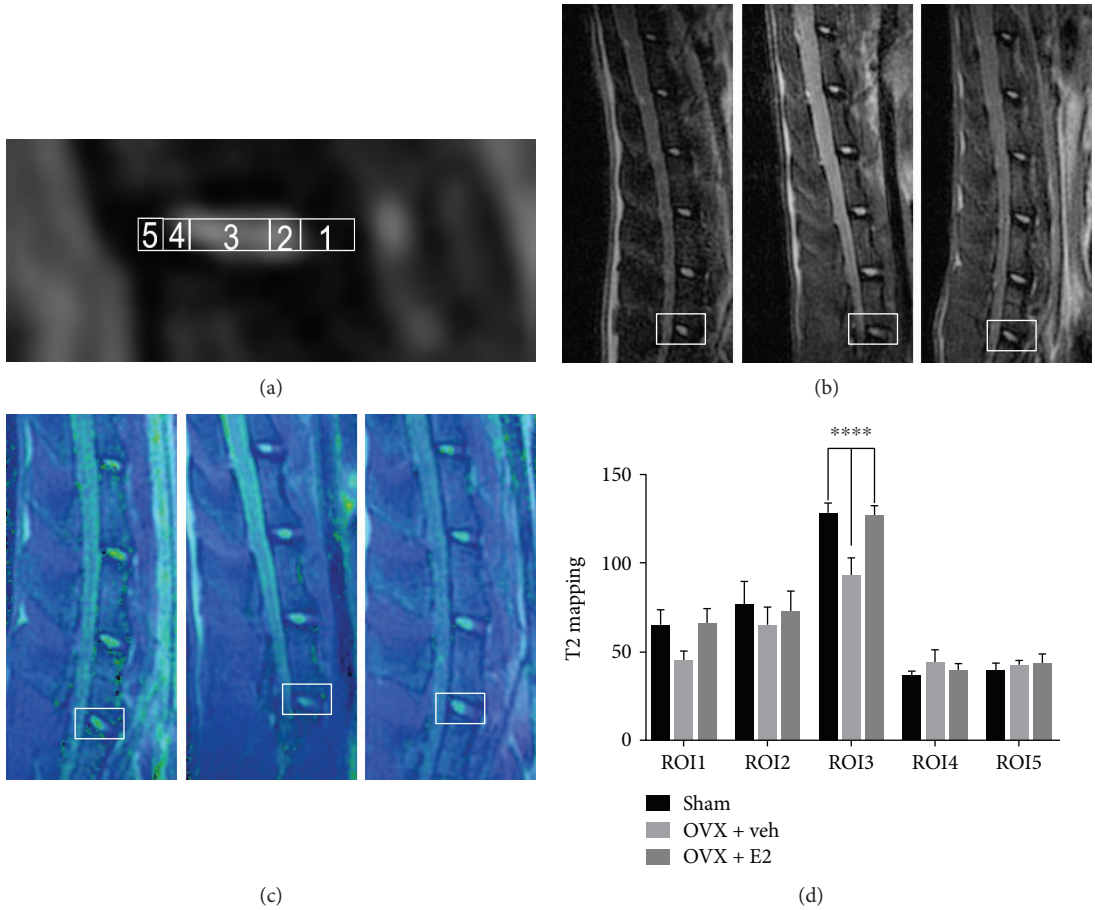

Figure 3: (a) Five regions of interest (ROIs) in the L5–L6 IVD were displayed. (b) MRI data of the discs were acquired at 3 months after surgery. (c) T2 mapping heatmap of the three groups was presented. (d) The values of T2 mapping (****$P < 0.01$ compared with the sham group and OVX + E2 group).

fibrils exhibit strong yellow birefringence, while collagen type II fibrils exhibit slight multicolor birefringence. In the sham and OVX + E2 groups, the inner layer AF exhibited multicolor, and the outer layer AF showed strong density of yellow color, indicating that AF closest to the NP tissue was mainly collagen type II. However, the AF of the OVX group's discs presented yellow staining, which proves that their main component was composed of type I collagen (Figure 2(c)). Traditional methods of clinically evaluating IVD degeneration are typically performed using T2-weighted magnetic resonance imaging sequences. Regrettably, it failed to diagnose the early stage of degeneration of the intervertebral disc. A new kind of sequence, called T2 mapping, was believable to be a credible and sensitive tool to monitor the degradation of intervertebral disc content [26]. According to our data, the depression of the T2 mapping value is positively correlated with IVDD. The value acquired from T2 mapping of the NP (ROI3) decreased in the OVX groups compared with the sham group. Furthermore, such degradation can be reversed by drug intervention (Figure 3). The MR results have an inverse correlation with histological scores (Figure 4(a)).

3.3. Estrogen Supplementation Restored Redox Balance by Promoting Antioxidant Capacity. As shown in Table 1, the results of ELISA demonstrated that serum E2 level in OVX rats was significantly reduced (216.51 ± 88.08 pg/ml). Furthermore, the ovariectomy decreased the level of GSH (5.46 ± 1.33 U/mg prot) and increased the level of GSSG (4.92 ± 1.4 U/mg prot), which consequently increased the ratio of GSSG/GSH (1.30 ± 0.75). Moreover, ovariectomy resulted in a decrease in the capacity of T-AOC (1.69 ± 0.89 U/mg prot), SOD (22.65 ± 8.73 U/mg prot), and GSH-Px (34.47 ± 11.92 U/mg prot), while no changes were observed in the capacity of CAT (29.28 ± 10.86 U/mg prot). Estrogen supplementation in OVX rats made serum E2 level (906.14 ± 104.2 pg/ml) close to the sham group. The detection of redox balance showed a significant accumulation of oxidized glutathione (GSSG) and a consumption of reduced glutathione (GSH), suggesting that redox imbalance stress can be corrected by estrogen supplementation (Table 1). In the OVX + E2 group, the level of GSH (GSH 8.12 ± 1.33 U/mg prot) was higher and the GSSG (3.56 ± 0.87 U/mg prot) was lower than the OVX + veh group; as a consequence, the GSSG/GSH of the NP tissue was diminished by estrogen supplementation. Our data suggested that estrogen deprivation decreased the antioxidant capacity of the NP tissue. This imbalance of redox may be restored by estrogen replacement. The capacities of T-AOC (2.64 ± 0.92 U/mg prot), SOD (44.24 ± 13.74 U/

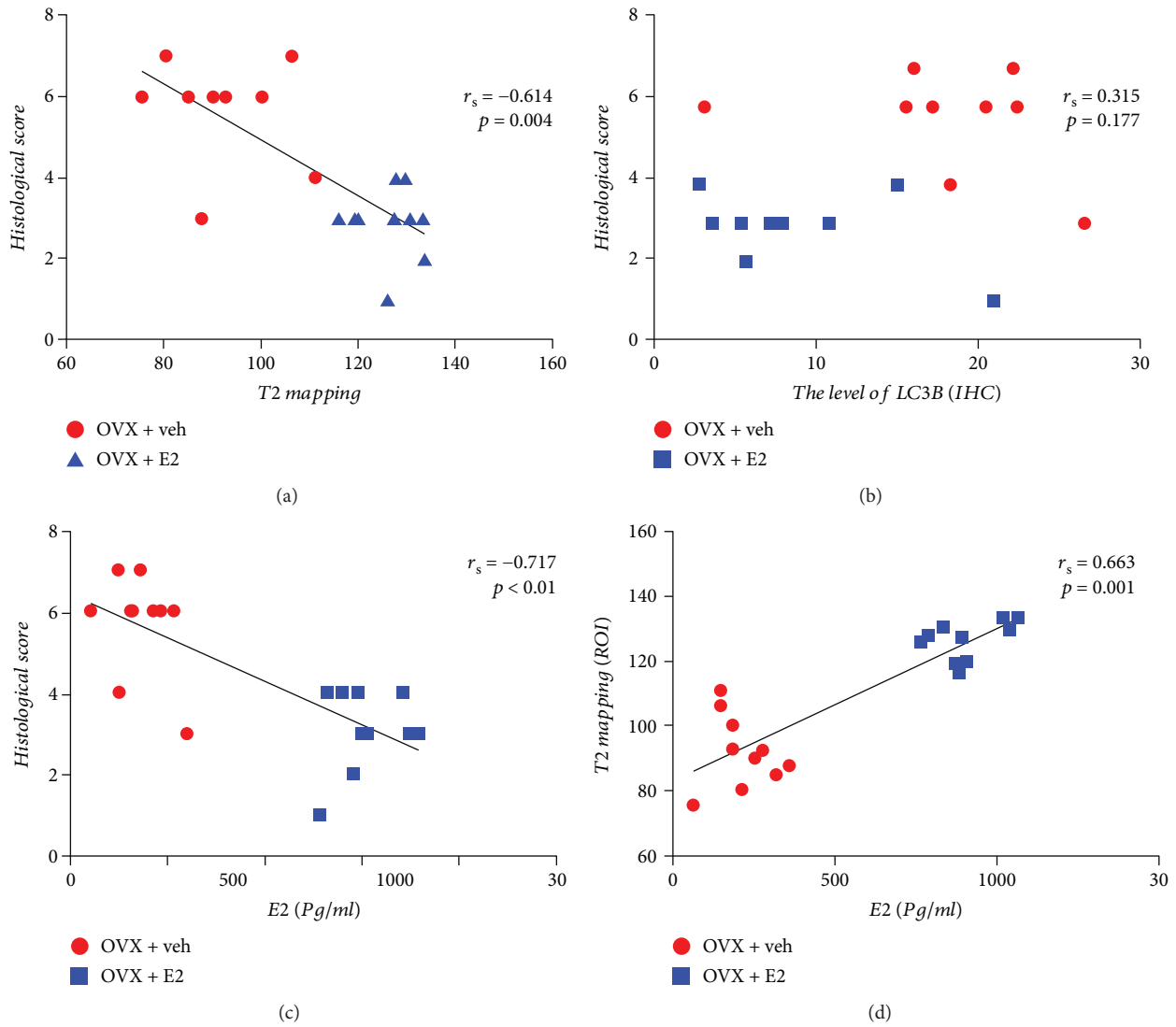

Figure 4: Spearman's correlation between the histological score and T2 mapping (a), level of LC3 (IHC) (b), and serum E2 level (c). Spearman's correlation between T2 mapping and serum E2 level.

Table 1: The level of E2 in serum and oxidative stress in IVD.

	Sham	OVX + veh	OVX + E2
Serum E2 (pg/ml)	949.18 ± 104.4	216.51 ± 88.08**	906.14 ± 104.2##
T-AOC (units/mg protein)	3.88 ± 0.95	1.69 ± 0.89**	2.64 ± 0.92##
CAT (units/mg protein)	28.73 ± 11.67	29.28 ± 10.86	30.08 ± 11.73
SOD (units/mg protein)	45.90 ± 12.29	22.65 ± 8.73**	44.24 ± 13.74##
GSH-Px (units/mg protein)	35.67 ± 13.31	14.15 ± 7.46**	34.47 ± 11.92##
GSSG (units/mg protein)	3.12 ± 1.13	5.46 ± 1.33*	3.56 ± 0.87#
GSH (units/mg protein)	7.71 ± 2.26	4.92 ± 1.4*	8.12 ± 1.33#
Ratio of GSSG/GSH	0.50 ± 0.24	1.30 ± 0.75**	0.46 ± 0.19##

Data are expressed as mean ± SD. **$P < 0.01$, significant difference between OVX and sham. *$P < 0.05$, significant difference between OVX and sham. ##$P < 0.01$, significant difference between OVX and OVX + E2. #$P < 0.05$, significant difference between OVX and OVX + E2.

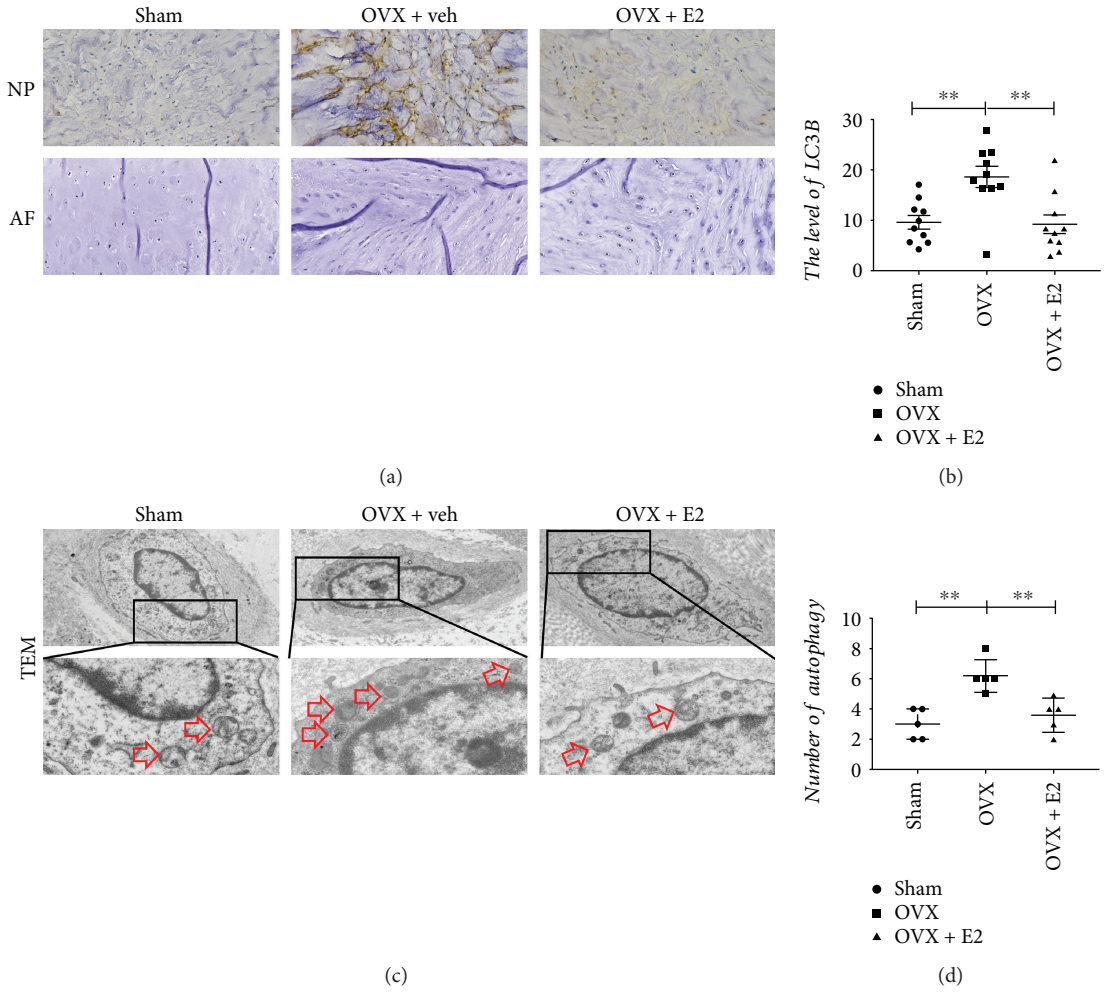

Figure 5: Autophagy in IVD assessed by IHC staining and TEM. (a) IHC staining for LC3 protein expression in the NP (original magnification, 20x). No significant difference in the AF. (b) Quantification of LC3 in the NP tissue, $^{**}P < 0.01$. (c) The autophagosome was displayed in the cytoplasm of the NP cell as the red arrow showed among the three groups (original magnification, 2 K and 8 K). (d) Quantification of the number of autophagosomes per cell. Data were shown as mean ± SD ($n = 5$, $^{**}P < 0.01$).

mg prot), and GSH-Px (34.47 ± 11.92 U/mg prot) were enhanced by estrogen replacement. In contrast, CAT (30.08 ± 11.73 U/mg prot) capacity seemed not to be modulated by estrogen.

3.4. The Increasing Level of Autophagy in the OVX + veh Group. Autophagy plays as a protective effect when the NP cells are stimulated by inflammatory, compression stress, starvation, and/or oxidative stress. The hallmarkers of autophagy in the NP tissue, such as LC3-II/I, p62, Atg5, and Beclin1, were assessed by Western blot. Protein bolt results revealed that the protein level of Atg5, LC3, and Beclin1 increased in the OVX + veh group, while E2 therapy decreased the levels of Atg5, LC3, and Beclin1. However, the level of p62 had no difference compared with the other two groups (Figure 1). To further confirm that NP cells do produce the autophagy, immunohistochemistry was adopted. The similar trend of LC3 levels was determined compared with protein blot's result (Figure 5). Furthermore, TEM was used to detect the autophagosome of NP cells. As shown in Figure 5(d), NP cells of the OVX group possessed more autophagosomes than that of the other two groups. The present results indicated that there was a high level of autophagy in NP cells of the OVX group. In addition, there was no correlation between histological score and the level of LC3 ($r_s = 0.315$, $P = 0.177$) (Figure 4(b)).

3.5. Correlation between Serum E2 Levels and H-Score, Antioxidative Biomarkers, and Autophagy Levels in the NP Tissue. To assess the relationship between E2 changes and redox balance, Spearman's correlation method was used to describe the correlation of serum E2 level with H-score, the value of T2 mapping, the capacity of T-AOC, SOD, CAT, GSH-Px, GSSG, GSH, and GSSG/GSH ratio, and autophagy levels in IVD of OVX rats and OVX + E2 rats. The results are reported in Figures 4 and 6. There was a significant correlation between the E2 and T2 mapping value ($r_s = 0.663$, $P = 0.001$), T-AOC ($r_s = 0.6$, $P = 0.005$), SOD ($r_s = 0.558$, $P = 0.006$), GSH-Px ($r_s = 0.795$, $P < 0.01$), and GSH ($r_s = 0.614$, $P = 0.004$); in contrast, changes in E2 were

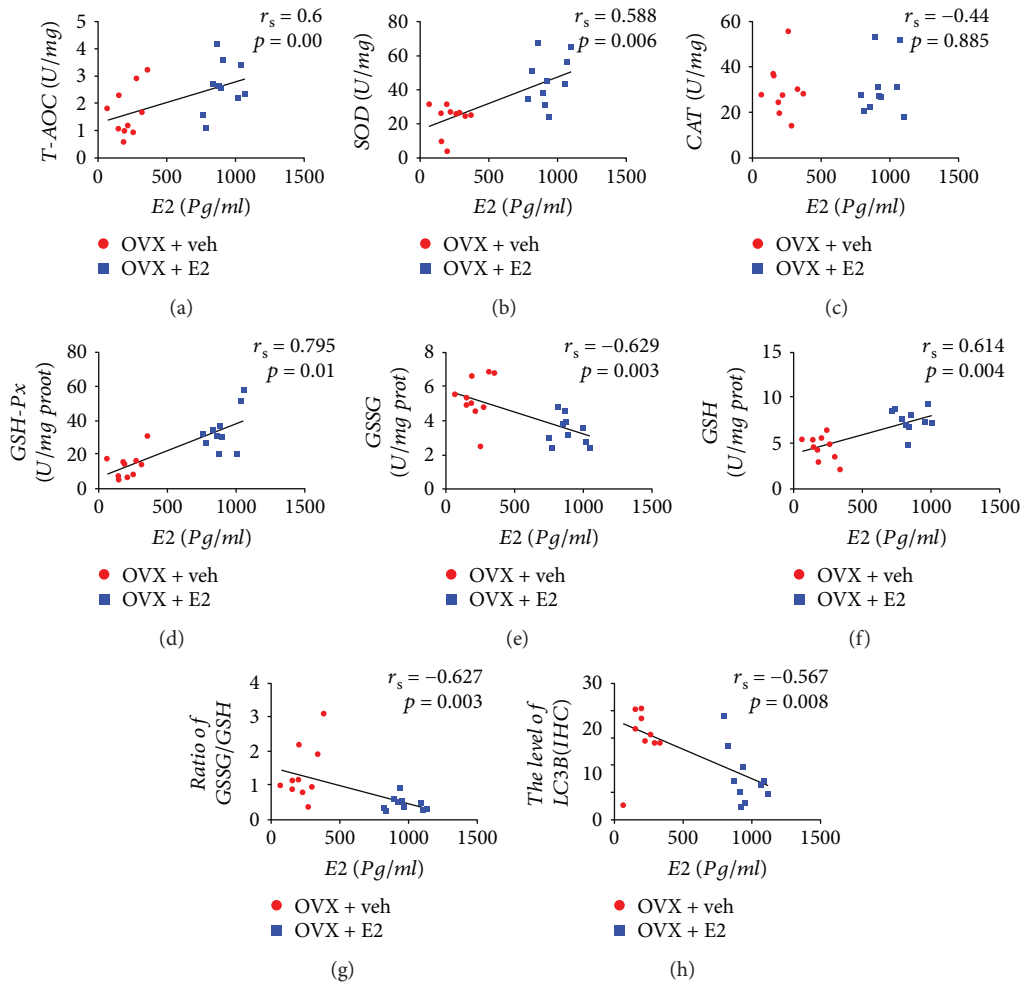

Figure 6: Spearman's correlation between serum E2 level and T-AOC (a), SOD (b), CAT (c), GSH-Px (d), GSSG (e), GSH (f), ratio of GSSG/GSH (g), and level of LC3 (IHC) (h).

negatively correlated with H-score ($r_s = -0.717$, $P < 0.01$), GSSG ($r_s = -0.629$, $P = 0.03$), GSSG/GSH ratio ($r_s = -0.627$, $P = 0.003$), and LC3B ($r_s = -0.576$, $P = 0.08$). The changes in E2 level, however, cannot indicate variation of CAT capacity ($r_s = 0.44$, $P = 0.885$). In addition, there was a significant negative correlation between the LC3B level and T-AOC activity ($r_s = -0.519$, $P = 0.019$) and GSH ($r_s = -0.45$, $P = 0.0.047$). However, no significant correlation was found between LC3B level and SOD ($r_s = -0.042$, $P = 0.079$), CAT ($r_s = 0.005$, $P = 0.985$), GSH-Px ($r_s = -0.042$, $P = 0.061$), and GSSG ($r_s = 0.361$, $P = 0.118$).

4. Discussion

Due to the high prevalence of low back pain associated with IVDD in postmenopausal women and the limitation of treatment methods [2, 4, 6], it is important to find novel ways to retard IVDD and restore normal disc function. Many previous studies have demonstrated the effects of ERT on osteoporosis in postmenopausal women, but few reports focused on disc degeneration [2, 14]. Interestingly, our study showed that a negative correlation between degeneration of disc and level of estrogen was addressed in OVX rats. Low level of antioxidant status was correlated with degeneration of intervertebral disc and induced high autophagy level in the NP tissue. In addition, the imbalance in the redox status of disc can be corrected by ERT; meanwhile, the IVD degeneration can be reversed and autophagy can be downregulated by estrogen. Very interestingly, here we reported that ERT acted as a protective factor in the degeneration of intervertebral disc by modulating the redox balance and downregulating the autophagy level.

IVDD, caused by abnormal axial load and inappropriate internal environment of discs [27], is the major pathogenesis leading to low back pain, and higher prevalence of the pain associated with menopause has been reported in several literatures [25, 28, 29]. Evidences suggested that depression of estrogen level may be the main factor to IVDD in postmenopausal women [4, 5, 30]. However, there are few investigations to address the regulatory effect of estrogen on IVDD. In this study, we employed ovariectomy rat model to induce lumbar IVDD as performed in previous reports [15, 16] and found that OVX rats were susceptible to IVDD, in which the pathogenesis displayed in early stage of degeneration. The early stage of IVDD often starts with changing of cellular phenotype, degradation of extracellular matrix, and blurred

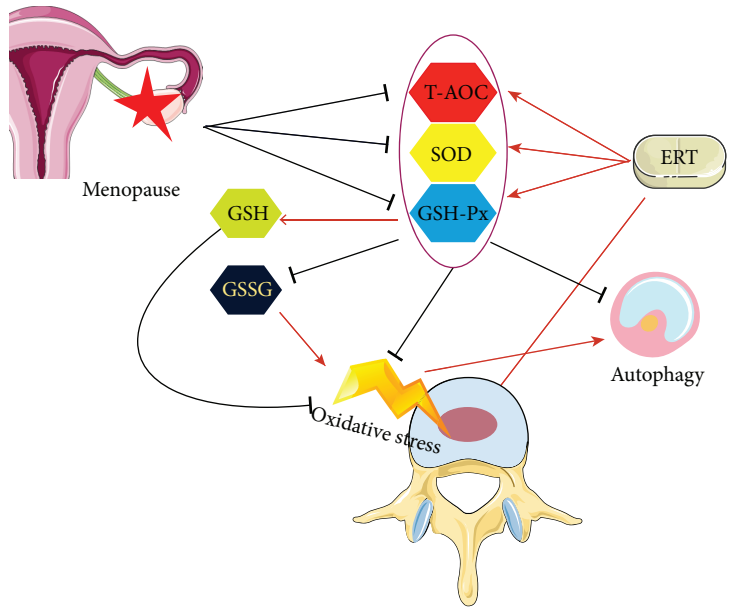

Figure 7: Schematic of the working hypothesis. Low level of estrogen leads to oxidative stress in the NP tissue of IVD, and at the same time, the level of autophagy increased as a response to the stress. ERT could modulate the redox balance, by which IVDD can be retarded partly.

border zone between AF and NP [8, 31–33]. In the OVX group, there was a reduced number of notochord cells and appearance of chondrocyte-like cells in the NP tissue, whereas estrogen supplementation can halt the above pathological process in the OVX + E2 group. Previous studies suggested that estrogen directly regulated the synthesis and function of collagen and proteoglycans [34]. In fact, IVDD contains various collagens and proteoglycans. The type II collagen, playing an important role in NP and the boundary between NP and AF, provides tensile strength to the disc [35]. The major proteoglycan of the NP tissue in IVD, aggrecan, played a major role in maintaining osmotic pressure and tissue hydration [36]. Here, the present study showed that IVDD, induced by low level of estrogen, started with the degradation of aggrecan and type II collagen in the OVX rats compared with the sham and OVX + E2 rats. Jia et al. [16] reported that the gene level of aggrecan and collagen II decreased in OVX rats, and at the same time, the ECM enzymes can be inhibited by the E2 treatment.

Oxidative stress, induced by redox imbalance, could cause damage to cellular and tissue components [37]. Recent studies have reported that the pathological morphology and development of IVDD are correlated with oxidative stress [18, 19], and oxidative stress targeted treatment may be a potential method to reverse the IVDD [38]. Importantly, estrogen depletion deranges redox balance in postmenopausal women [39], whereas ERT can decrease the lipid peroxides and promote antioxidant capacity [40]. Previous studies have reported that E2 promoted the capability to scavenge free radicals, suggesting that E2 could exert protective effect against oxidative damage by controlling the antioxidant signaling pathways [41, 42]. This study showed, for the first time, that the status of redox in IVD is closely managed by serum E2. Glutathione, a tripeptide and a major factor in cell survival, acts as cornerstone for intracellular antioxidant system [43]. There are two states of glutathione in cell and tissue, glutathione (GSH) and GSH disulfide (GSSG) [44]. The ratio of GSSG/GSH represents oxidative status of cell and tissue, and the normal ratio is critical for the cell to survival [45, 46]. Baeza et al. reported that OVX rats had a higher ratio of GSSG/GSH [47], and a recent report showed that depletion of estrogen induced high level of GSH-Px in OVX rats [48]. Otherwise, a series of antioxidant enzymes, including T-AOC, SOD, CAT, and GSH-Px, are the main tools to remove overproduction of active free radicals. Accumulating evidences about the effects of estrogen on the activities of these enzymes have been reported [20]. Kawvised et al. reported that, in hippocampus homogenates of OVX rats, the activities of SOD, CAT, and GSH-Px were reduced [48]. Recent studies reported the promotion effects of estrogen on antioxidant enzyme system [22, 40]. Estrogen promotes the expression of antioxidant enzymes system through activating MAPK and NFκB pathways in vitro [49]. Another evidence provided on circulation of ovariectomized female showed that ERT increased antioxidant gene expression [22]. Our present results definitively supported such observations.

In addition to redox balance, Shen et al. [23] addressed that autophagy acted as a protective factor against oxidative stress through reducing oxidative stress. We, firstly, showed that autophagy levels increased in intervertebral disc in OVX rats. Our results suggested that autophagy might play a protective role to oxidative stress under hormone deprivation. Furthermore, we find that autophagy levels had inverse tendency compared with antioxidative biomarkers (T-AOC and GSH). Autophagy may protect cells by digesting oxidative damaged proteins and organelles [50]. Our results suggested that autophagy of the intervertebral disc

is a response to the oxidative damage, and the levels of autophagy were decreased after that estrogen restored the redox balance.

There are some limitations that should be considered in this study. First, there was only one time point to investigate the effect of ERT on the redox balance in intervertebral disc. It may be better that the dynamic redox balance and treatment effects of ERT to IVDD should be evaluated under multitime points. Second, future studies could be included to confirm our conclusion, such as treating the OVX rats with antioxidative stress drugs to address whether IVDD can be retard by regulating the redox balance in IVD. Finally, the pathogenesis environment of IVD is different between rats and human; further studies should discuss the matter of human IVD.

In summary, the data demonstrated that disc redox balance was correlated with E2 levels; furthermore, IVDs in OVX rats were susceptible to degeneration due to estrogen deficiency. ERT was able to enhance the antioxidant capacity and reverse the degeneration of IVD, even though there were too few studies investigating the menopause-related intervertebral disc degeneration. These findings strongly suggested that estrogen may partly control antioxidant enzyme proteins' expression (Figure 7). Moreover, IVDD associated with menopause may depend on redox biology, and ERT may bring a positive effect for disc degeneration.

Data Availability

The data used to support the findings of this study are available from the corresponding author upon request.

Disclosure

Jin LY and Lv ZD are co-first authors.

Conflicts of Interest

The authors declare that they have no conflicts of interest.

Authors' Contributions

Li XF and Jin LY designed the experiments. Jin LY, Lv ZD, Wang K, and Qian L performed the experiments and acquired the data. Song XX and Shen HX analyzed the data. Jin LY and Li XF supervised the project and wrote the manuscript. Jin LY and Lv ZD contributed equally to this work.

Acknowledgments

This work was supported by grants from the National Natural Science Foundation of China (81772292, 81400910, 81802139, and 81270027), the Development Fund for Shanghai Talents (201453), and the Medico-Engineering Cooperation Fund of Shanghai Jiao Tong University (no. YG2012MS25 and no. YG2016MS54).

References

[1] F. Al-Azzawi and S. Palacios, "Hormonal changes during menopause," *Maturitas*, vol. 63, no. 2, pp. 135–137, 2009.

[2] Y.-X. J. Wang, J. F. Griffith, H. T. Ma et al., "Relationship between gender, bone mineral density, and disc degeneration in the lumbar spine: a study in elderly subjects using an eight-level MRI-based disc degeneration grading system," *Osteoporosis International*, vol. 22, no. 1, pp. 91–96, 2011.

[3] Y.-X. J. Wang, J. F. Griffith, X.-J. Zeng et al., "Prevalence and sex difference of lumbar disc space narrowing in elderly Chinese men and women: osteoporotic fractures in men (Hong Kong) and osteoporotic fractures in women (Hong Kong) studies," *Arthritis and Rheumatism*, vol. 65, no. 4, pp. 1004–1010, 2013.

[4] C. Lou, H. Chen, L. Mei et al., "Association between menopause and lumbar disc degeneration: an MRI study of 1,566 women and 1,382 men," *Menopause*, vol. 24, no. 10, pp. 1136–1144, 2017.

[5] Y. X. J. Wang, "Postmenopausal Chinese women show accelerated lumbar disc degeneration compared with Chinese men," *Journal of Orthopaedic Translation*, vol. 3, no. 4, pp. 205–211, 2015.

[6] J. Dowdell, M. Erwin, T. Choma, A. Vaccaro, J. Iatridis, and S. K. Cho, "Intervertebral disk degeneration and repair," *Neurosurgery*, vol. 80, no. 3s, pp. S46–s54, 2017.

[7] C. Le Maitre, A. J. Freemont, and J. Hoyland, "The role of interleukin-1 in the pathogenesis of human intervertebral disc degeneration," *Arthritis Research & Therapy*, vol. 7, no. 4, pp. R732–R745, 2005.

[8] J. I. Sive, P. Baird, M. Jeziorsk, A. Watkins, J. A. Hoyland, and A. J. Freemont, "Expression of chondrocyte markers by cells of normal and degenerate intervertebral discs," *Molecular Pathology*, vol. 55, no. 2, pp. 91–97, 2002.

[9] X. Wu, Y. Liu, X. Guo et al., "Prolactin inhibits the progression of intervertebral disc degeneration through inactivation of the NF-κB pathway in rats," *Cell Death & Disease*, vol. 9, no. 2, p. 98, 2018.

[10] G. Waddell, "Low back pain: a twentieth century health care enigma," *Spine*, vol. 21, no. 24, pp. 2820–2825, 1996.

[11] H. E. Gruber, D. Yamaguchi, J. Ingram et al., "Expression and localization of estrogen receptor-β in annulus cells of the human intervertebral disc and the mitogenic effect of 17-β-estradiol in vitro," *BMC Musculoskeletal Disorders*, vol. 3, no. 1, p. 4, 2002.

[12] S. D. Yang, et al.L. Ma, T. X. Gu et al., "17β-Estradiol protects against apoptosis induced by levofloxacin in rat nucleus pulposus cells by upregulating integrin $\alpha_2\beta_1$," *Apoptosis*, vol. 19, no. 5, pp. 789–800, 2014.

[13] S. D. Yang, D. L. Yang, Y. P. Sun et al., "17β-Estradiol protects against apoptosis induced by interleukin-1β in rat nucleus pulposus cells by down-regulating MMP-3 and MMP-13," *Apoptosis*, vol. 20, no. 3, pp. 348–357, 2015.

[14] Y. M. Baron, M. P. Brincat, R. Galea, and N. Calleja, "Intervertebral disc height in treated and untreated overweight postmenopausal women," *Human Reproduction*, vol. 20, no. 12, pp. 3566–3570, 2005.

[15] T. Wang, L. Zhang, C. Huang, A. G. Cheng, and G. T. Dang, "Relationship between osteopenia and lumbar intervertebral disc degeneration in ovariectomized rats," *Calcified Tissue International*, vol. 75, no. 3, pp. 205–213, 2004.

[16] H. Jia, et al.J. Ma, J. Lv et al., "Oestrogen and parathyroid hormone alleviate lumbar intervertebral disc degeneration in ovariectomized rats and enhance Wnt/β-catenin pathway activity," *Scientific Reports*, vol. 6, no. 1, article 27521, 2016.

[17] J. Miquel, A. Ramirez-Bosca, J. V. Ramirez-Bosca, and J. D. Alperi, "Menopause: a review on the role of oxygen stress and favorable effects of dietary antioxidants," *Archives of Gerontology and Geriatrics*, vol. 42, no. 3, pp. 289–306, 2006.

[18] A. Dimozi, Laboratory of Cell Proliferation and Ageing, Institute of Biosciences and Applications, National Centre for Scientific Research, E. Mavrogonatou, A. Sklirou, and D. Kletsas, "Oxidative stress inhibits the proliferation, induces premature senescence and promotes a catabolic phenotype in human nucleus pulposus intervertebral disc cells," *European Cells & Materials*, vol. 30, pp. 89–103, 2015.

[19] G. Hou, H. Lu, M. Chen, H. Yao, and H. Zhao, "Oxidative stress participates in age-related changes in rat lumbar intervertebral discs," *Archives of Gerontology and Geriatrics*, vol. 59, no. 3, pp. 665–669, 2014.

[20] S. S. Signorelli, S. Neri, S. Sciacchitano et al., "Behaviour of some indicators of oxidative stress in postmenopausal and fertile women," *Maturitas*, vol. 53, no. 1, pp. 77–82, 2006.

[21] M. A. Sánchez-Rodríguez, M. Zacarías-Flores, A. Arronte-Rosales, E. Correa-Muñoz, and V. M. Mendoza-Núñez, "Menopause as risk factor for oxidative stress," *Menopause*, vol. 19, no. 3, pp. 361–367, 2012.

[22] F. Bellanti, M. Matteo, T. Rollo et al., "Sex hormones modulate circulating antioxidant enzymes: impact of estrogen therapy," *Redox Biology*, vol. 1, no. 1, pp. 340–346, 2013.

[23] C. Shen, J. Yan, L. S. Jiang, and L. Y. Dai, "Autophagy in rat annulus fibrosus cells: evidence and possible implications," *Arthritis Research & Therapy*, vol. 13, no. 4, article R132, 2011.

[24] J. W. Chen, B. B. Ni, X. F. Zheng, B. Li, S. D. Jiang, and L. S. Jiang, "Hypoxia facilitates the survival of nucleus pulposus cells in serum deprivation by down-regulating excessive autophagy through restricting ROS generation," *The International Journal of Biochemistry & Cell Biology*, vol. 59, pp. 1–10, 2015.

[25] R. C. Lawrence, C. G. Helmick, F. C. Arnett et al., "Estimates of the prevalence of arthritis and selected musculoskeletal disorders in the United States," *Arthritis and Rheumatism*, vol. 41, no. 5, pp. 778–799, 1998.

[26] S. E. L. Detiger, R. M. Holewijn, R. J. W. Hoogendoorn et al., "MRI T2* mapping correlates with biochemistry and histology in intervertebral disc degeneration in a large animal model," *European Spine Journal*, vol. 24, no. 9, pp. 1935–1943, 2015.

[27] M. Hangai, K. Kaneoka, S. Kuno et al., "Factors associated with lumbar intervertebral disc degeneration in the elderly," *The Spine Journal*, vol. 8, no. 5, pp. 732–740, 2008.

[28] A. C. Papageorgiou, P. R. Croft, S. Ferry, M. I. V. Jayson, and A. J. Silman, "Estimating the prevalence of low back pain in the general population. Evidence from the South Manchester Back Pain Survey," *Spine*, vol. 20, no. 17, pp. 1889–1894, 1995.

[29] S. Muraki, H. Oka, T. Akune et al., "Prevalence of radiographic lumbar spondylosis and its association with low back pain in elderly subjects of population-based cohorts: the ROAD study," *Annals of the Rheumatic Diseases*, vol. 68, no. 9, pp. 1401–1406, 2009.

[30] C. Lou, H. L. Chen, X. Z. Feng et al., "Menopause is associated with lumbar disc degeneration: a review of 4230 intervertebral discs," *Climacteric*, vol. 17, no. 6, pp. 700–704, 2014.

[31] J. Antoniou, T. Steffen, F. Nelson et al., "The human lumbar intervertebral disc: evidence for changes in the biosynthesis and denaturation of the extracellular matrix with growth, maturation, ageing, and degeneration," *The Journal of Clinical Investigation*, vol. 98, no. 4, pp. 996–1003, 1996.

[32] B. Li, Y. J. Su, X. F. Zheng, Y. H. Yang, S. D. Jiang, and L. S. Jiang, "Evidence for an important role of *Smad-7* in intervertebral disc degeneration," *Journal of Interferon & Cytokine Research*, vol. 35, no. 7, pp. 569–579, 2015.

[33] Y. Zhang, C. Xiong, M. Kudelko et al., "Early onset of disc degeneration in SM/J mice is associated with changes in ion transport systems and fibrotic events," *Matrix Biology*, vol. 70, pp. 123–139, 2018.

[34] P. Li, Y. Xu, Y. Gan et al., "Estrogen enhances matrix synthesis in nucleus pulposus cell through the estrogen receptor β-p38 MAPK pathway," *Cellular Physiology and Biochemistry*, vol. 39, no. 6, pp. 2216–2226, 2016.

[35] P. P. Raj, "Intervertebral disc: anatomy-physiology-pathophysiology-treatment," *Pain Practice*, vol. 8, no. 1, pp. 18–44, 2008.

[36] S. Fukuta, K. Miyamoto, K. Suzuki et al., "Abundance of calpain and aggrecan-cleavage products of calpain in degenerated human intervertebral discs," *Osteoarthritis and Cartilage*, vol. 19, no. 10, pp. 1254–1262, 2011.

[37] H. Sies, "Oxidative stress: oxidants and antioxidants," *Experimental Physiology*, vol. 82, no. 2, pp. 291–295, 1997.

[38] S. Suzuki, N. Fujita, N. Hosogane et al., "Excessive reactive oxygen species are therapeutic targets for intervertebral disc degeneration," *Arthritis Research & Therapy*, vol. 17, no. 1, p. 316, 2015.

[39] G. Serviddio, G. Loverro, M. Vicino et al., "Modulation of endometrial redox balance during the menstrual cycle: relation with sex hormones," *The Journal of Clinical Endocrinology & Metabolism*, vol. 87, no. 6, pp. 2843–2848, 2002.

[40] C. Escalante Gómez and S. Quesada Mora, "HRT decreases DNA and lipid oxidation in postmenopausal women," *Climacteric*, vol. 16, no. 1, pp. 104–110, 2012.

[41] O. Y. Kim, J. S. Chae, J. K. Paik et al., "Effects of aging and menopause on serum interleukin-6 levels and peripheral blood mononuclear cell cytokine production in healthy nonobese women," *Age*, vol. 34, no. 2, pp. 415–425, 2012.

[42] A. F. Bokov, D. Ko, and A. Richardson, "The effect of gonadectomy and estradiol on sensitivity to oxidative stress," *Endocrine Research*, vol. 34, no. 1-2, pp. 43–58, 2009.

[43] N. Kaplowitz, "Physiological significance of glutathione S-transferases," *The American Journal of Physiology*, vol. 239, no. 6, pp. G439–G444, 1980.

[44] R. Matsui, Y. Watanabe, and C. E. Murdoch, "Redox regulation of ischemic limb neovascularization - what we have learned from animal studies," *Redox Biology*, vol. 12, pp. 1011–1019, 2017.

[45] D. M. Townsend, K. D. Tew, and H. Tapiero, "The importance of glutathione in human disease," *Biomedicine & Pharmacotherapy*, vol. 57, no. 3-4, pp. 145–155, 2003.

[46] S. Jaswal, H. C. Mehta, A. K. Sood, and J. Kaur, "Antioxidant status in rheumatoid arthritis and role of antioxidant therapy," *Clinica Chimica Acta*, vol. 338, no. 1-2, pp. 123–129, 2003.

[47] I. Baeza, J. Fdez-Tresguerres, C. Ariznavarreta, and M. De la Fuente, "Effects of growth hormone, melatonin, oestrogens and phytoestrogens on the oxidized glutathione (GSSG)/reduced glutathione (GSH) ratio and lipid peroxidation in

aged ovariectomized rats," *Biogerontology*, vol. 11, no. 6, pp. 687–701, 2010.

[48] S. Kawvised, J. Wattanathorn, and W. Thukham-Mee, "Neuroprotective and cognitive-enhancing effects of microencapsulation of mulberry fruit extract in animal model of menopausal women with metabolic syndrome," *Oxidative Medicine and Cellular Longevity*, vol. 2017, Article ID 2962316, 13 pages, 2017.

[49] C. Borrás, J. Gambini, M. C. Gómez-Cabrera et al., "17β-Oestradiol up-regulates longevity-related, antioxidant enzyme expression via the ERK1 and ERK2$^{[MAPK]}$/NFκB cascade," *Aging Cell*, vol. 4, no. 3, pp. 113–118, 2005.

[50] P. Haberzettl and B. G. Hill, "Oxidized lipids activate autophagy in a JNK-dependent manner by stimulating the endoplasmic reticulum stress response," *Redox Biology*, vol. 1, no. 1, pp. 56–64, 2013.

Hindawi
Oxidative Medicine and Cellular Longevity
Volume 2018, Article ID 1324173, 8 pages
https://doi.org/10.1155/2018/1324173

Research Article

Pyrrolidine Dithiocarbamate (PDTC) Inhibits DON-Induced Mitochondrial Dysfunction and Apoptosis via the NF-κB/iNOS Pathway

Dan Wan,[1,2,3,4] **Qinghua Wu**,[5,6] **Wei Qu**,[2,3] **Gang Liu**,[1] **and Xu Wang**[2,3,4]

[1]*Hunan Provincial Key Laboratory of Animal Nutritional Physiology and Metabolic Process, Key Laboratory of Agro-Ecological Processes in Subtropical Region, Institute of Subtropical Agriculture, Chinese Academy of Sciences, National Engineering Laboratory for Pollution Control and Waste Utilization in Livestock and Poultry Production, Changsha, Hunan 410125, China*
[2]*National Reference Laboratory of Veterinary Drug Residues (HZAU) and MAO Key Laboratory for Detection of Veterinary Drug Residues, Wuhan 430070, China*
[3]*MOA Laboratory for Risk Assessment of Quality and Safety of Livestock and Poultry Products, Wuhan 430070, China*
[4]*Hubei Collaborative Innovation Center for Animal Nutrition and Feed Safety, Wuhan 430070, China*
[5]*College of Life Science, Yangtze University, Jingzhou, China*
[6]*Department of Chemistry, Faculty of Science, University of Hradec Kralove, Hradec Kralove, Czech Republic*

Correspondence should be addressed to Gang Liu; gangle.liu@gmail.com and Xu Wang; wangxu@mail.hzau.edu.cn

Received 6 July 2018; Accepted 16 October 2018; Published 25 November 2018

Guest Editor: Marina Sokovic

Oxidative stress is closely linked to the toxic responses of various cell types in normal and pathophysiological conditions. Deoxynivalenol (DON), an inducer of stress responses in the ribosome and the endoplasmic reticulum (ER), causes mitochondrial dysfunction and mitochondria-dependent apoptosis through oxidative stress in humans and animals. The NF-κB pathway, which is closely linked to oxidative stress, is hypothesized to be a critical signaling pathway for DON-induced toxicity and is a potential target for intervention. The present study was conducted to explore the protective effects of pyrrolidine dithiocarbamate (PDTC) from the toxic effects of DON in rat anterior pituitary GH3 cells. Our results showed that DON activated the NF-κB transcription factors and induced cellular oxidative stress, mitochondrial dysfunction, and apoptosis. Morphological studies using transmission electron microscopy (TEM) and cell apoptosis analyses suggested that PDTC prevented DON-induced mitochondrial dysfunction and apoptosis, probably by preventing the DON-induced translocation of NF-κB p65 into the nucleus, and by inhibiting DON-induced iNOS expression. This led to the blocking of the NF-κB pathway and inhibition of iNOS activity.

1. Introduction

Oxidative stress is closely linked to toxic responses of various cell types in normal and pathophysiological conditions. Deoxynivalenol (DON), produced by the *Fusarium graminearum* and *F. culmorum* species, is an inducer of stress responses in the ribosome and the endoplasmic reticulum (ER). It causes mitochondrial dysfunction and mitochondria-dependent apoptosis through oxidative stress [1, 2]. The consumption of DON-contaminated products causes a wide range of disorders in animals and humans, affecting the gastrointestinal, reproductive, neuroendocrine, and immune systems [3–5].

The main cellular targets of DON are the ribosome and the ER [6, 7]. However, studies have indicated that DON-induced toxicity also induced oxidative stress and endocrine imbalance [8]. DON targets the mitochondria and causes the mitochondrial membrane potential ($\Delta\Psi m$) to decrease, leading to the deformation of the mitochondria and the subsequent release of cytochrome *c* into the cytoplasm [9–11]. Mitochondrial impairment occurred in the livers of fetuses when their mothers consumed DON [12]. Moreover, DON

reduced intracellular hormone levels, including those of insulin, leptin, insulin-like growth factor 1 (IGF-1), and IGF acid-labile subunit (IGFALS), which could potentially cause DON-induced growth retardation [13, 14]. We recently discovered that DON inhibited the synthesis of growth hormone (Gh1) in rat GH3 cells, by reducing the cell viability and by inducing apoptosis [15]. Thus, we hypothesized that protecting cells from DON-induced cytotoxicity would prevent growth retardation.

Previous studies have identified that the NF-κB signaling pathway, which occurs downstream of MAPK signaling, can be widely activated after DON treatment in the human Caco-2 and HT-29 cell lines [16, 17]. NF-κB is activated by cytokines, such as TNFα and interleukin (IL), and regulates downstream effects on cell function [18, 19]. It regulates downstream antioxidant and prooxidant genes such as inducible nitric oxide synthase (iNOS), neuronal nitric oxide synthase, superoxide dismutase, catalase, heme oxygenase-1, xanthine oxidoreductase, NADPH : quinone oxidoreductase, and cyclooxygenase-2 [20]. We previously found that the T-2 toxin induced the transcription of *Nfkbil1* and *Nfrkb* in GH3 cells [15], suggesting that the NF-κB signaling pathway was critical to mycotoxin-induced toxicity.

The rat GH3 cell line is a clonal strain of rat pituitary tumor that can synthesize and secrete prolactin and growth hormone. Trichothecenes induce considerable toxicity in endocrine GH3 cells by causing mitochondrial dysfunction, growth hormone synthesis inhibition, cell apoptosis, and inflammation [15, 21]. Therefore, we used an *in vitro* model of GH3 cells to study the effects of the NF-κB inhibitor, pyrrolidine dithiocarbamate (PDTC), on DON-induced mitochondrial dysfunction and apoptosis. We discovered the mechanisms of DON-induced cytotoxicity in relation to nitric oxide (NO) generation, oxidant-antioxidant balance, and NF-κB activation. The morphological changes in DON-treated cells were determined using flow cytometry and transmission electron microscopy (TEM). The effect of PDTC on DON-induced cytotoxicity was evaluated by TEM, with particular focus on phosphoryl-NF-κB p65 nuclear localization, iNOS expression, and mitochondrial injury. Protection from apoptosis was monitored by flow cytometry.

2. Materials and Methods

2.1. Reagents and Chemicals. DON was obtained from Sigma-Aldrich (St. Louis, MO, USA). PDTC was obtained from Beyotime (Shanghai, P.R. China). Anti-iNOS (ab15323) and anti-actin (ab1801) antibodies were purchased from Abcam (Cambridge, MA, USA). Anti-phospho-IκBα (Ser32/36; 5A5), anti-phosphoryl-NF-κB p65 (Ser536; 93H1), and peroxidase-coupled goat anti-rabbit and mouse IgG (H + L) secondary antibodies were obtained from CST (Danvers, MA, USA). The apoptosis detection kit (Annexin V-FITC) was purchased from BestBio (Shanghai, China).

2.2. Cell Culture. The cells were cultivated as previously reported [15, 21]. Briefly, the GH3 cells from passages 5 to 15 were cultivated in high-glucose DMEM (HyClone Laboratories, Inc., Logan, Utah, USA) with 10% heat-inactivated fetal bovine serum (FBS; Gibco BRL, Gaithersburg, MD, USA) and 1% penicillin-streptomycin (HyClone Laboratories, Inc., Logan, Utah, USA) at 37°C, in the presence of 5% CO_2. After 24 hours of incubation, the culture medium was changed to high-glucose DMEM, and the cells were incubated with or without the test reagents (DON and PDTC) for the indicated time intervals.

For cytotoxicity analysis, the cells were seeded in a 96-well plate (at a density of 1×10^4 cells per well) and treated with 0, 300, 600, or 1200 mg/L of DON [15]. For quantitative real-time PCR, western blot, and chemoimmunological assays, GH3 cells were seeded in a six-well plate (at a density of 1×10^5 cells per well) with 2 mL of medium. For TEM, the cells were seeded in a 75 cm^2 flask (at a density of 5×10^5 cells per flask) with 12 mL of medium. In some experiments, the cells were treated with inhibitors for 45 min to an hour, then exposed to DON for 12 hours. All experiments were performed in triplicate on at least three independent occasions.

2.3. Quantitative Real-Time PCR (qRT-PCR). Total RNA was extracted using TRIzol (Invitrogen, Breda, The Netherlands) [15] and analyzed by quantitative real-time RT-PCR using the iNOS gene specific primers (S: 5′CCTCAGGCTTGGGT CTTGTTA3′; AS: 5′ATCCTGTGTTGTTGGGCTGG3′) as previously described. Fold changes in mRNA expression levels were calculated using the $2^{-\Delta\Delta Ct}$ method [11].

2.4. Western Blotting. Total protein was extracted, quantified, separated on a 12% SDS-PAGE gel, and transferred onto a polyvinylidene fluoride membrane (Millipore, Billerica, MA, USA) as previously described [15]. Membranes were incubated with anti-actin (ab1801), anti-phospho-NF-κB p65 (Ser536; 93H1; diluted 1 : 1000), anti-phospho-IκBα (Ser32/36; 5A5; diluted 1 : 1000), and anti-iNOS (ab15323; diluted 1 : 500) antibodies overnight at 4°C, according to the manufacturer's instructions.

2.5. Oxidative Stress Indices. The CAT activity, malondialdehyde (MDA), SOD, and glutathione peroxidase (GSH-Px) levels were assessed using commercial kits (Nanjing Jiancheng BioEngineering Institute Co. Ltd., Nanjing, China).

2.6. Chemoimmunology of Phosphoryl-NF-κB p65. Immunofluorescence was used to determine phosphoryl-NF-κB p65 localization. GH3 cells were fixed with paraformaldehyde (v/v, 1/25) at 37°C for 10 minutes. They were then permeabilized with cold acetone at −20°C for 3 minutes. After a PBS wash (0.1 mM, pH 7.4), cells were saturated with 3% BSA in PBS for 30 minutes, and incubated with the anti-phosphoryl-NF-κB p65 antibody (diluted 1 : 100) at 4°C overnight. After another PBS wash (0.1 mM, pH 7.4), the cells were incubated with the secondary antibody for 30 minutes at room temperature. Coverslips were washed twice with PBS (0.1 mM, pH 7.4), incubated with the goat anti-mouse IgG antibody conjugated with Alexa Fluor 555 (Cell Signaling Technology, Danvers, MA, USA) for 30 minutes in the dark, incubated in 5 μM DAPI staining solution (Invitrogen) for 5 minutes, and then washed in PBS. The

Table 1: Activities of GSH-Px, GST, CAT, and SOD in GH3 cells.

Group (ng/mL)	CAT activity (U/mg protein)	SOD (U/mL)	GSH-Px (U/mg protein)	MDA (μmol/mg protein)
0	0.407 ± 0.008	1.907 ± 0.224	150.262 ± 0.001	1.476 ± 0.023
300	$0.949 \pm 0.012^{*}$	$2.938 \pm 0.426^{*}$	$134.592 \pm 0.034^{*}$	$1.736 \pm 0.032^{*}$
600	$1.129 \pm 0.006^{*}$	$4.630 \pm 0.075^{**}$	$85.149 \pm 0.217^{**}$	$1.698 \pm 0.038^{*}$
1200	$2.326 \pm 0.005^{**}$	$5.798 \pm 0.257^{**}$	$53.719 \pm 0.421^{**}$	$1.777 \pm 0.042^{*}$

Note: CAT 1 U = the amount of enzyme that consumes 1 nmole H_2O_2/min. GST 1 U = the amount of enzyme that conjugates 1 μmole CDNB/min. GSH-Px 1 U = the amount of enzyme that converts 1 μM GSH to GSSG in the presence of H_2O_2/min. SOD 1 U = the amount of enzyme required for 50% inhibition of pyrogallol autooxidation. Data are shown as means ± SD ($n = 3$) from three separate experiments performed in triplicate. * indicates P values < 0.05, and ** indicates P values < 0.01.

fluorescence was monitored using an UltraVIEW VoX confocal system (PerkinElmer, Co., Norwalk, CT, USA).

2.7. GH3 Cell Morphology by Transmission Electron Microscopy (TEM). The morphological variation in mitochondria was investigated as described earlier [21]. Briefly, the cells were fixed with glutaraldehyde (v/v, 2.5/100), post-fixed in osmium tetroxide (w/v, 1/100), dehydrated in absolute ethanol, then embedded stepwise by polymerization at 45°C for 12 hours and at 60°C for 36–48 hours. The 70 nm ultrathin slices were stained with lead citrate for 10 minutes and with uranyl acetate for 30 minutes. Finally, they were washed thrice with ddH_2O and dried. The slices were viewed with the H-7650 TEM (Hitachi, Japan).

2.8. Cell Apoptosis. The cells were harvested, washed, and centrifuged (2000 ×g, 4°C, 10 min). Then, they were suspended in Annexin V-FITC binding buffer at a density of 1×10^6 cells per mL. They were then incubated with 10 μL of propidium iodide (PI) solution (BD BioScience, San Jose, CA, USA) in the dark for 15 minutes. Apoptosis was measured using CyAn ADP as described previously [11].

2.9. Statistical Analyses. Data were analyzed by performing a two-way analysis of variance using the SPSS software (SPSS Inc., version 17.0, Chicago, IL, USA). P values < 0.05 indicated statistical significance.

3. Results and Discussion

Oxidative stress plays a major role in the mediation of cellular damage and dysfunction. It is inseparably linked to mitochondrial dysfunction and cell apoptosis [22, 23]. Free radicals contribute to the development of mycotoxicosis by inducing lipid peroxidation and changes in antioxidant status, and by causing the loss of cellular mitochondrial membrane potential [24, 25]. In this study, we found that after DON treatment, the activity of MDA and antioxidant enzymes such as CAT and SOD significantly increased, whereas the activity of GSH-Px significantly decreased (Table 1). This result corroborates other studies [26, 27] in which T-2 toxin exposure was associated with significant decreases in GSH-Px activity in granulosa cells from rats and in hepatic cells from chicken. However, a significant increase in GSH-Px activity was observed in DON-treated HT-29 cells [16]. Because GSH-Px functions as a scavenger of lipid peroxides and is induced by reactive oxygen species

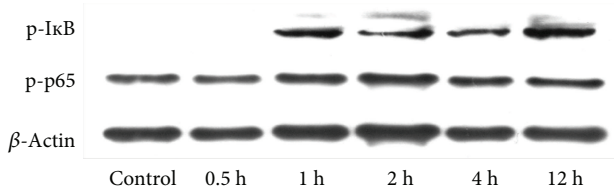

Figure 1: DON-induced IκBα and NF-κB p65 phosphorylation in GH3 cells.

and hydroxyl free radicals in cells, the reduction in GSH-Px activity indicates a serious oxidant-antioxidant imbalance in cells. This implies that the rat GH3 cell line is likely more sensitive to DON toxicity than the human HT-29 cell line.

The NF-κB transcription factors control many processes such as immunity, oxidative stress, and apoptosis. Phosphorylation of p65 NF-κB at serine 536 is mediated by multiple protein kinases, including the IκB kinase [28]. We found that DON induced the phosphorylation of IκBα kinase as well as the phosphorylation and nuclear translocation of the p65 proteins (Figure 1). The pretreatment of cells with PDTC before DON treatment resulted in reduced p65 phosphorylation and translocation (Figure 2). In the nucleus, NF-κB p65 binds to the iNOS gene promoter and upregulates its gene expression [29]. Therefore, we also investigated the iNOS mRNA and protein levels. The quantitative RT-PCR showed that *iNOS* gene expression increased after DON treatment, but decreased significantly with PDTC pretreatment (Figure 3(a)). The immunoblotting analysis showed similar patterns for the protein levels (Figure 3(b)). Reactive nitrogen species (RNS) and ROS are free radicals that cause oxidative stress. ROS generation did not significantly increase after DON treatment in human HT-29 cells [30] and RAW264.7 cells [31], whereas it increased significantly in HepG-2 cells [24]. At doses of 250 and 500 ng/mL, DON resulted in increased ROS and RNS production in human HT-29 cells [16]. Taken together, the PDTC appears to act as an antioxidant for DON-induced oxidative stress.

In several cell lines, treatment with DON results in a loss of $\Delta\Psi m$, mitochondrial damage, caspase activation, and apoptosis [9–12, 16, 32]. PDTC relieves oxidative stress and improves mitochondrial structural integrity [33]. Hence, we tested the effects of PDTC pretreatment in DON-treated GH3 cells, with particular focus on mitochondrial ultrastructure and apoptosis. The control cells and PDTC-treated cells exhibited normal mitochondria (Figures 4(a), 4(b), 4(e), and

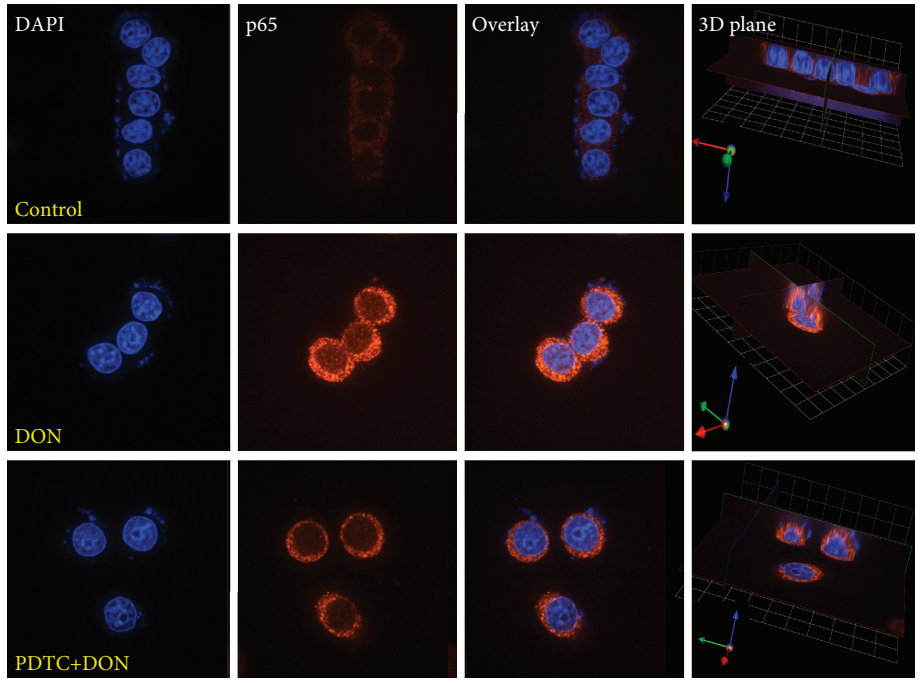

Figure 2: Nuclear translocation of phosphoryl-NF-κB p65 (p-p65 (Ser536)) induced by DON treatment (1200 ng/mL) and PDTC pretreatment (20 μM, 45 min) followed by DON treatment (1200 ng/mL) in GH3 cells, visualized through indirect immunofluorescence, using Alexa Fluor-conjugated secondary antibody. The nucleus was stained with PI. The panels show PI staining, Alexa Fluor staining, overlay, and the 3D plane of the cells. All photos were captured at 400x magnification. Phosphoryl-NF-κB p65 was upregulated and can be observed in the nucleus.

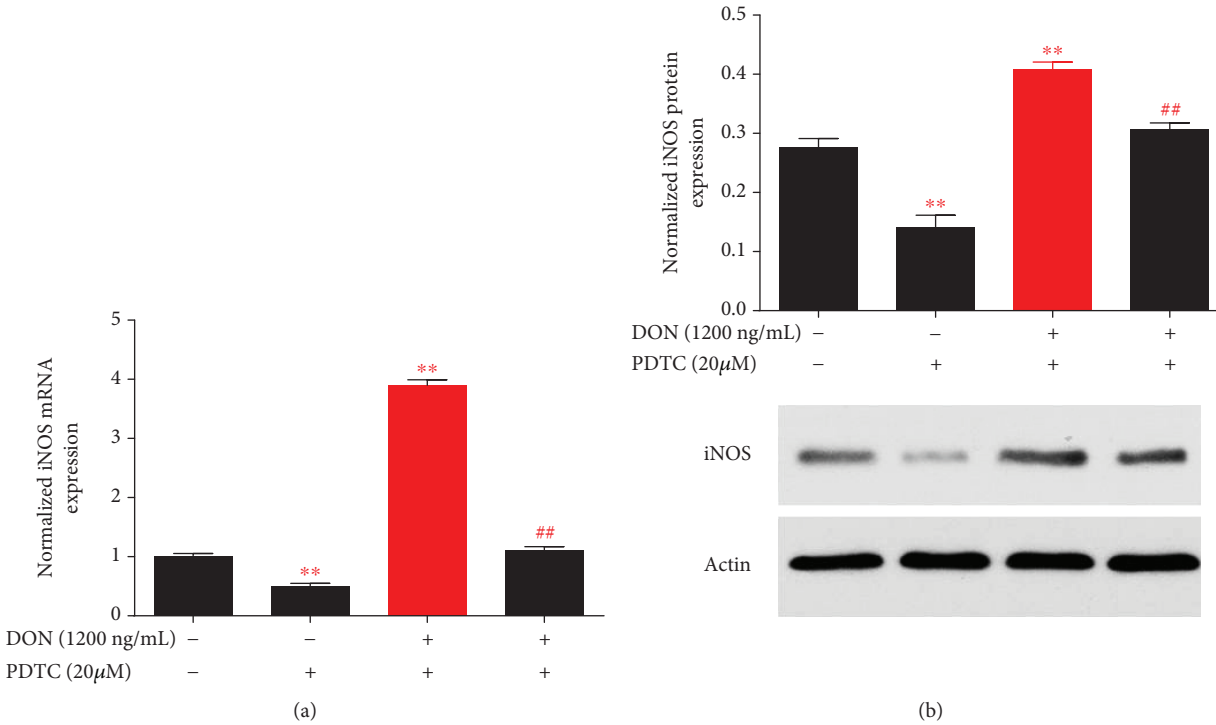

Figure 3: PDTC protects cells from DON-induced iNOS expression. (a) Cells were treated with DON, PDTC, and PDTC pretreatment followed by DON to assess iNOS transcription by qRT-PCR. (b). Cells were treated with DON, DON, PDTC, and PDTC pretreatment followed by DON to assess iNOS expression by western blotting. P values < 0.05 are indicated by a single asterisk, *. P values < 0.01 are indicated by double asterisks, **.

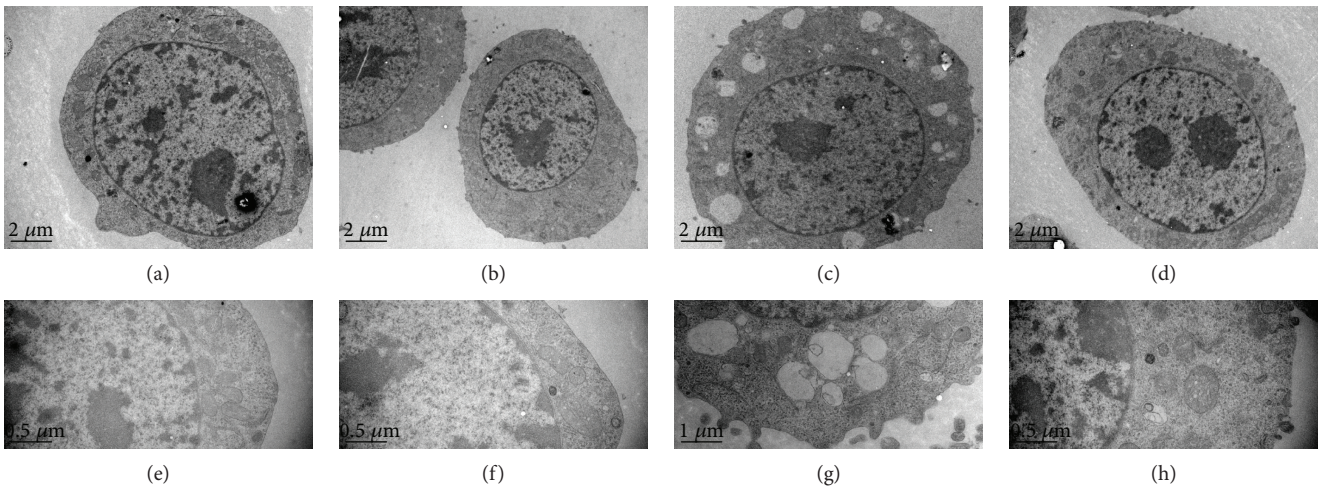

Figure 4: PDTC protects cells from DON-induced mitochondrial injury in GH3 cells. Cells were treated with DON, PDTC, and PDTC pretreatment, followed by treatment with DON for 12 hours. (a, e) Cell treated with DON showing normal mitochondria. (b, f) Cell treated with PDTC showing normal mitochondria. (c, g) Cells with PDTC pretreatment, followed by treatment with DON for 12 hours showing normal mitochondria and tiny vacuoles.

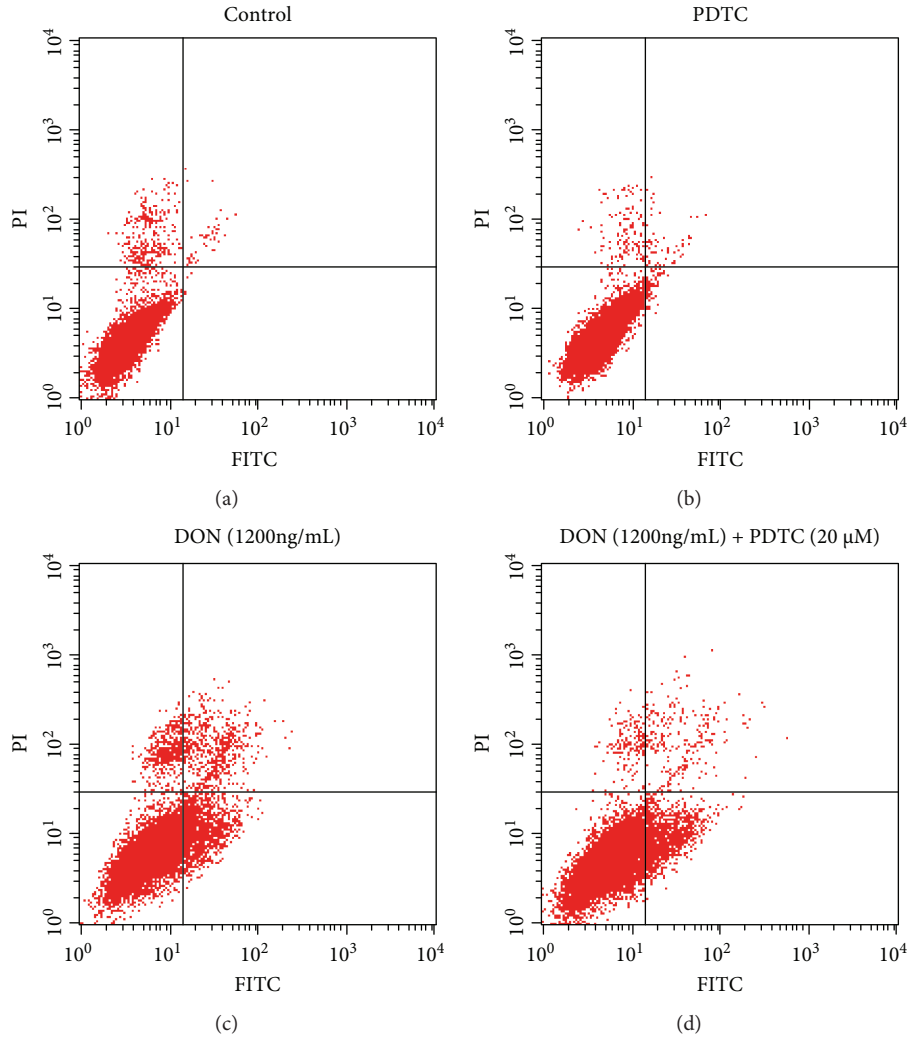

Figure 5: PDTC protects cells from DON-induced apoptosis in GH3 cells. Cells in the control group (a), cells treated with PDTC (b) and DON (c), and cells pretreated with PDTC followed by DON treatment (d) were used to assess the apoptosis rate. Data are shown as means for three separate experiments performed in triplicate.

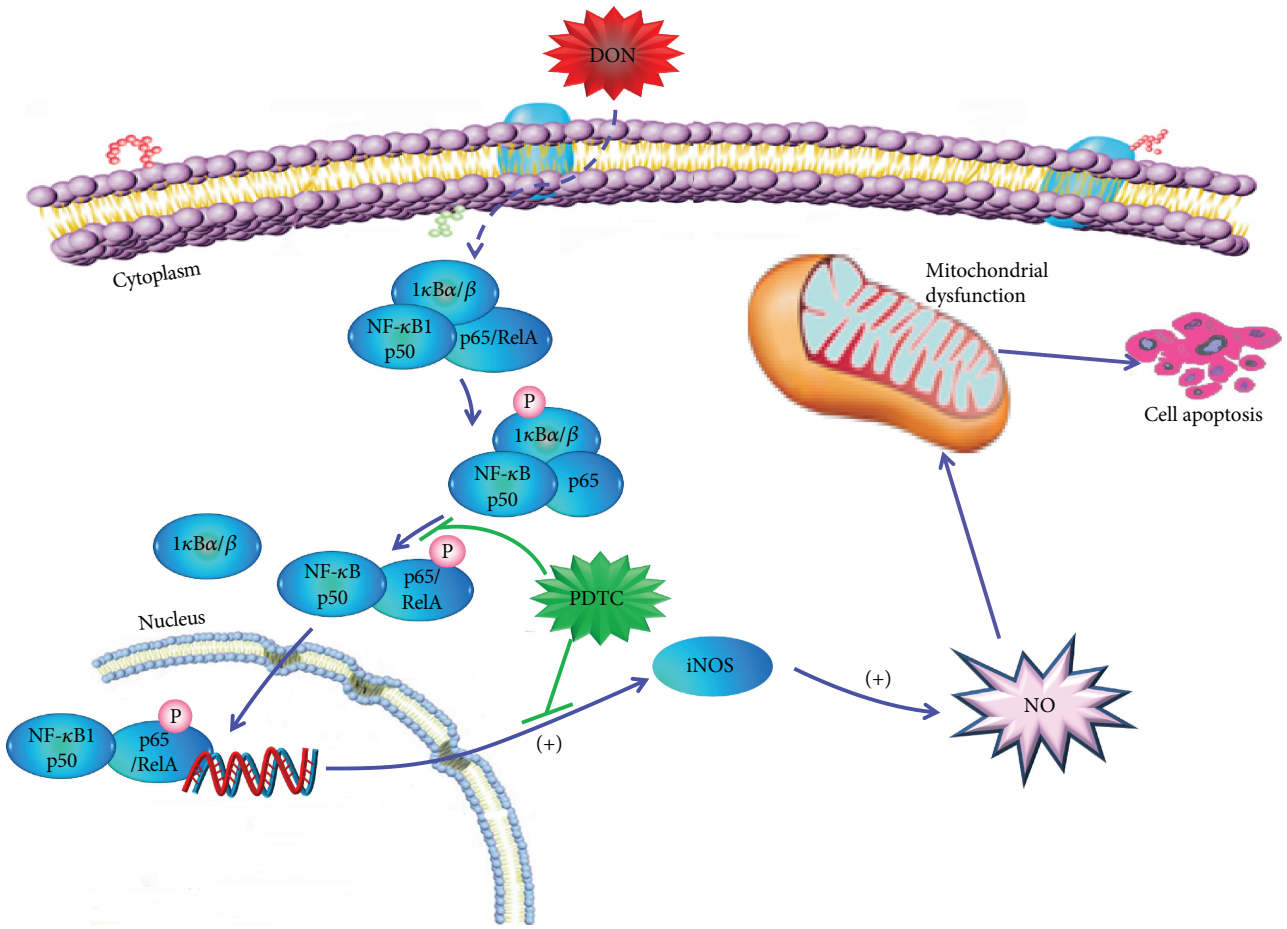

Figure 6: A proposed mechanism of action for the protective effect of PDTC in DON-mediated mitochondrial dysfunction and apoptosis. DON indirectly activates the NF-κB signal pathway via the classical route of IκB/NF-κB p65 signaling. PDTC inhibits the translocation of NF-κB p65 and the transcription of iNOS, and thereby protects cells from mitochondrial dysfunction and cell apoptosis.

4(f)), whereas cells treated with DON for 12 hours displayed dose-dependent mitochondrial swelling, serious vacuolar degeneration, disarrayed cristae, and reduced electron density of the matrix (Figures 4(c) and 4(g)). PDTC reduced the DON-induced toxicity, and normal mitochondria were observed despite the reduction in vacuole size observed in the PDTC-pretreated cells (Figures 4(d) and 4(h)). DON treatment led to a significant increase in the number of early and late apoptotic cells. The proportion of apoptotic cells significantly decreased in DON-treated cells that were pretreated with PDTC (Figure 5). All of our findings suggest that PDTC inactivates NF-κB, inhibits iNOS expression, and protects cells from cytotoxicity and mitochondrial toxicity via antioxidant effects (Figure 6). Our results are consistent with the known activity of another antioxidant, lutein, that protects cells from DON-induced mitochondrial structural damage, probably via inhibition of NF-κB [16].

4. Conclusion

In DON-treated GH3 cells, DON caused the translocation of NF-κB and induced iNOS expression. PDTC prevented the DON-induced migration of phosphoryl-NF-κB p65 into the nucleus, inhibited DON-induced iNOS expression, and prevented DON-induced mitochondrial dysfunction and apoptosis.

Abbreviations

DON: Deoxynivalenol
ERK: Extracellular signal-regulated kinase
FBS: Fetal bovine serum
FITC: Fluorescein isothiocyanate
GSH-Px: Glutathione peroxidase
Hck: Hematopoietic cell kinase
iNOS: Inducible nitric oxide synthase
LDH: Lactate dehydrogenase
L-NAME: L-NG-nitro arginine methyl ester
MDA: Malondialdehyde
NF-κB: Nuclear factor-kappa B
PBS: Phosphate-buffered saline
PDTC: Pyrrolidine dithiocarbamate
PI: Propidium iodide
qRT-PCR: Quantitative real-time PCR
ROS: Reactive oxygen species
SMT: S-methyl-isothiourea
SOD: Superoxide dismutase
TEM: Transmission electron microscopy.

Data Availability

The data used to support the findings of this study are available from the corresponding author upon request.

Conflicts of Interest

The authors declare that there is no conflict of interest.

Acknowledgments

This work was financially supported by the National Key R&D Program of China (2016YFD0501201), National Science Foundation of China (31702127, 31772642, 31572575, 31602114, and 51403072), and by the Fundamental Research Funds for the Central Universities (2662016PY115), as well as the long-term development plan UHK.

References

[1] G. S. Bondy, L. Coady, I. Curran et al., "Effects of chronic deoxynivalenol exposure on p 53 heterozygous and p 53 homozygous mice," *Food and Chemical Toxicology*, vol. 96, pp. 24–34, 2016.

[2] C. Kosawang, M. Karlsson, D. Jensen, A. Dilokpimol, and D. B. Collinge, "Transcriptomic profiling to identify genes involved in *Fusarium* mycotoxin deoxynivalenol and zearalenone tolerance in the mycoparasitic fungus *Clonostachys rosea*," *BMC Genomics*, vol. 15, no. 1, p. 55, 2014.

[3] P. Pinton and I. Oswald, "Effect of deoxynivalenol and other type B trichothecenes on the intestine: a review," *Toxins*, vol. 6, no. 5, pp. 1615–1643, 2014.

[4] O. Rocha, K. Ansari, and F. M. Doohan, "Effects of trichothecene mycotoxins on eukaryotic cells: a review," *Food Additives and Contaminants*, vol. 22, no. 4, pp. 369–378, 2005.

[5] Q. Wu, V. Dohnal, L. Huang, K. Kuča, and Z. Yuan, "Metabolic pathways of trichothecenes," *Drug Metabolism Reviews*, vol. 42, no. 2, pp. 250–267, 2010.

[6] J. J. Pestka, "Deoxynivalenol-induced proinflammatory gene expression: mechanisms and pathological sequelae," *Toxins*, vol. 2, no. 6, pp. 1300–1317, 2010.

[7] Y. Shi, K. Porter, N. Parameswaran, H. K. Bae, and J. J. Pestka, "Role of GRP 78/BiP degradation and ER stress in deoxynivalenol-induced interleukin-6 upregulation in the macrophage," *Toxicological Sciences*, vol. 109, no. 2, pp. 247–255, 2009.

[8] Q. H. Wu, X. Wang, W. Yang et al., "Oxidative stress-mediated cytotoxicity and metabolism of T-2 toxin and deoxynivalenol in animals and humans: an update," *Archives of Toxicology*, vol. 88, no. 7, pp. 1309–1326, 2014.

[9] F. Bensassi, C. Gallerne, O. Sharaf el Dein, C. Lemaire, M. R. Hajlaoui, and H. Bacha, "Involvement of mitochondria-mediated apoptosis in deoxynivalenol cytotoxicity," *Food and Chemical Toxicology*, vol. 50, no. 5, pp. 1680–1689, 2012.

[10] Y. Ma, A. Zhang, Z. Shi et al., "A mitochondria-mediated apoptotic pathway induced by deoxynivalenol in human colon cancer cells," *Toxicology in Vitro*, vol. 26, no. 3, pp. 414–420, 2012.

[11] X. Wang, Q. Liu, A. Ihsan et al., "JAK/STAT pathway plays a critical role in the proinflammatory gene expression and apoptosis of RAW264.7 cells induced by trichothecenes as DON and T-2 toxin," *Toxicological Sciences*, vol. 127, no. 2, pp. 412–424, 2012.

[12] U. Tiemann, K. P. Brüssow, D. Dannenberger et al., "The effect of feeding a diet naturally contaminated with deoxynivalenol (DON) and zearalenone (ZON) on the spleen and liver of sow and fetus from day 35 to 70 of gestation," *Toxicology Letters*, vol. 179, no. 3, pp. 113–117, 2008.

[13] C. J. Amuzie and J. J. Pestka, "Suppression of insulin-like growth factor acid-labile subunit expression—a novel mechanism for deoxynivalenol-induced growth retardation," *Toxicological Sciences*, vol. 113, no. 2, pp. 412–421, 2010.

[14] K. A. Voss, "A new perspective on deoxynivalenol and growth suppression," *Toxicological Sciences*, vol. 113, no. 2, pp. 281–283, 2010.

[15] D. Wan, X. Wang, Q. Wu et al., "Integrated transcriptional and proteomic analysis of growth hormone suppression mediated by trichothecene T-2 toxin in rat GH 3 cells," *Toxicological Sciences*, vol. 147, no. 2, pp. 326–338, 2015.

[16] R. Krishnaswamy, S. N. Devaraj, and V. V. Padma, "Lutein protects HT-29 cells against deoxynivalenol-induced oxidative stress and apoptosis: prevention of NF-κB nuclear localization and down regulation of NF-κB and cyclo-oxygenase-2 expression," *Free Radical Biology and Medicine*, vol. 49, no. 1, pp. 50–60, 2010.

[17] J. Van De Walle, B. Romier, Y. Larondelle, and Y.-J. Schneider, "Influence of deoxynivalenol on NF-κB activation and IL-8 secretion in human intestinal Caco-2 cells," *Toxicology Letters*, vol. 177, no. 3, pp. 205–214, 2008.

[18] M. Karin and Y. Ben-Neriah, "Phosphorylation meets ubiquitination: the control of NF-κB activity," *Annual Review of Immunology*, vol. 18, no. 1, pp. 621–663, 2000.

[19] K. A. Steinbrecher, W. Wilson, P. C. Cogswell, and A. S. Baldwin, "Glycogen synthase kinase 3β functions to specify gene-specific, NF-κB-dependent transcription," *Molecular and Cellular Biology*, vol. 25, no. 19, pp. 8444–8455, 2005.

[20] M. J. Morgan and Z. G. Liu, "Crosstalk of reactive oxygen species and NF-κB signaling," *Cell Research*, vol. 21, no. 1, pp. 103–115, 2011.

[21] X. Liu, P. Guo, A. Liu et al., "Nitric oxide (NO)-mediated mitochondrial damage plays a critical role in T-2 toxin-induced apoptosis and growth hormone deficiency in rat anterior pituitary GH3 cells," *Food and Chemical Toxicology*, vol. 102, pp. 11–23, 2017.

[22] A. J. Kowaltowski and A. E. Vercesi, "Mitochondrial damage induced by conditions of oxidative stress," *Free Radical Biology and Medicine*, vol. 26, no. 3-4, pp. 463–471, 1999.

[23] J. Lee, S. Giordano, and J. Zhang, "Autophagy, mitochondria and oxidative stress: cross-talk and redox signalling," *The Biochemical Journal*, vol. 441, no. 2, pp. 523–540, 2012.

[24] X. Zhang, L. Jiang, C. Geng, J. Cao, and L. Zhong, "The role of oxidative stress in deoxynivalenol-induced DNA damage in HepG2 cells," *Toxicon*, vol. 54, no. 4, pp. 513–518, 2009.

[25] M. Chaudhari, R. Jayaraj, A. S. B. Bhaskar, and P. V. Lakshmana Rao, "Oxidative stress induction by T-2 toxin causes DNA damage and triggers apoptosis via caspase pathway in human cervical cancer cells," *Toxicology*, vol. 262, no. 2, pp. 153–161, 2009.

[26] J. E. Dvorska, A. C. Pappas, F. Karadas, B. K. Speake, and P. F. Surai, "Protective effect of modified glucomannans and organic selenium against antioxidant depletion in the chicken liver due to T-2 toxin-contaminated feed consumption,"

Comparative Biochemistry and Physiology Part C: Toxicology & Pharmacology, vol. 145, no. 4, pp. 582–587, 2007.

[27] J. Wu, D. Tu, L. Y. Yuan, H. Yuan, and L. X. Wen, "T-2 toxin exposure induces apoptosis in rat ovarian granulosa cells through oxidative stress," *Environmental Toxicology and Pharmacology*, vol. 36, no. 2, pp. 493–500, 2013.

[28] H. Buss, A. Dörrie, M. L. Schmitz, E. Hoffmann, K. Resch, and M. Kracht, "Constitutive and interleukin-1-inducible phosphorylation of p65 NF-κB at serine 536 is mediated by multiple protein kinases including IκB kinase (IKK)-α, IKKβ, IKKϵ, TRAF family member-associated (TANK)-binding kinase 1 (TBK1), and an unknown kinase and couples p65 to TATA-binding protein-associated factor II31-mediated interleukin-8 transcription," *Journal of Biological Chemistry*, vol. 279, no. 53, pp. 55633–55643, 2004.

[29] W. Eberhardt, D. Kunz, R. Hummel, and J. Pfeilschifter, "Molecular cloning of the rat inducible nitric oxide synthase gene promoter," *Biochemical and Biophysical Research Communications*, vol. 223, no. 3, pp. 752–756, 1996.

[30] F. Bensassi, E. el Golli-Bennour, S. Abid-Essefi, C. Bouaziz, M. R. Hajlaoui, and H. Bacha, "Pathway of deoxynivalenol-induced apoptosis in human colon carcinoma cells," *Toxicology*, vol. 264, no. 1-2, pp. 104–109, 2009.

[31] G. E. Ji, S. Y. Park, S. S. Wong, and J. J. Pestka, "Modulation of nitric oxide, hydrogen peroxide and cytokine production in a clonal macrophage model by the trichothecene vomitoxin (deoxynivalenol)," *Toxicology*, vol. 125, no. 2-3, pp. 203–214, 1998.

[32] C. Bouaziz, C. Martel, O. Sharaf el dein et al., "Fusarial toxin-induced toxicity in cultured cells and in isolated mitochondria involves PTPC-dependent activation of the mitochondrial pathway of apoptosis," *Toxicological Sciences*, vol. 110, no. 2, pp. 363–375, 2009.

[33] N. Mariappan, C. M. Elks, S. Sriramula et al., "NF-κB-induced oxidative stress contributes to mitochondrial and cardiac dysfunction in type ii diabetes," *Cardiovascular Research*, vol. 85, no. 3, pp. 473–483, 2010.

Hindawi
Oxidative Medicine and Cellular Longevity
Volume 2018, Article ID 4061901, 10 pages
https://doi.org/10.1155/2018/4061901

Clinical Study

Dark Chocolate Intake Positively Modulates Redox Status and Markers of Muscular Damage in Elite Football Athletes: A Randomized Controlled Study

Elena Cavarretta,[1,2] **Mariangela Peruzzi**,[1] **Riccardo Del Vescovo**,[2,3] **Fabio Di Pilla**,[3] **Giuliana Gobbi**,[4] **Andrea Serdoz**,[5] **Roberto Ferrara**,[5] **Leonardo Schirone**,[1] **Sebastiano Sciarretta**,[1,6] **Cristina Nocella**,[6] **Elena De Falco**,[1] **Sonia Schiavon**,[6] **Giuseppe Biondi-Zoccai**,[1,6] **Giacomo Frati**,[1,6] **and Roberto Carnevale**[1]

[1]*Department of Medical-Surgical Sciences and Biotechnologies, Sapienza University of Rome, Latina, Italy*
[2]*Villa Stuart Sport Clinics, FIFA Medical Center of Excellence, via Trionfale 5952, 00136 Rome, Italy*
[3]*A.S. Roma Football Club, piazzale Dino Viola 1, 00128 Rome, Italy*
[4]*Department of Medicine and Surgery, University of Parma, Ospedale Maggiore, Parma, Italy*
[5]*Department of Physiology and Pharmacology, Sapienza University of Rome, Rome, Italy*
[6]*IRCCS Neuromed, Pozzilli (IS), Italy*

Correspondence should be addressed to Elena Cavarretta; elena.cavarretta@gmail.com
and Roberto Carnevale; roberto.carnevale@uniroma1.it

Received 25 May 2018; Accepted 18 October 2018; Published 21 November 2018

Guest Editor: Marina Sokovic

Intensive physical exercise may cause increase oxidative stress and muscular injury in elite football athletes. The aim of this study was to exploit the effect of cocoa polyphenols on oxidative stress and muscular injuries induced by intensive physical exercise in elite football players. Oxidant/antioxidant status and markers of muscle damage were evaluated in 24 elite football players and 15 controls. Furthermore, the 24 elite football players were randomly assigned to either a dark chocolate (>85% cocoa) intake ($n = 12$) or a control group ($n = 12$) for 30 days in a randomized controlled trial. Oxidative stress, antioxidant status, and muscle damage were assessed at baseline and after 30 days of chocolate intake. Compared to controls, elite football players showed lower antioxidant power and higher oxidative stress paralleled by an increase in muscle damage markers. After 30 days of dark chocolate intake, an increased antioxidant power was found in elite athletes assuming dark chocolate. Moreover, a significant reduction in muscle damage markers (CK and LDH, $p < 0.001$) was observed. In the control group, no changes were observed with the exception of an increase of sNox2-dp, H_2O_2, and myoglobin. A simple linear regression analysis showed that sNox2-dp was associated with a significant increase in muscle damage biomarker release ($p = 0.001$). An *in vitro* study also confirmed that polyphenol extracts significantly decreased oxidative stress in murine myoblast cell line C2C12-derived. These results indicate that polyphenol-rich nutrient supplementation by means of dark chocolate positively modulates redox status and reduced exercise-induced muscular injury biomarkers in elite football athletes. This trial is registered with NCT03288623.

1. Introduction

Intensive physical exercise may increase oxidative stress and cause muscular injury in elite athletes [1]. This represents a significant problem for professional football players representing more than one third of all time-loss injuries and causing more than a quarter of the total injury-dependent absence in high-level European professional football clubs [2]. Consequently, the overall burden of muscle injuries is the main reason for player unavailability in training and official matches for professional football clubs [3]. Accordingly, injuries during a regular season or a particular tournament

can have considerable impact on team performance as well as on the economics of the club. Hereafter, prevention and reduction of muscle injuries in professional football should be of paramount importance.

The generation of reactive oxygen species (ROS) is a fundamental and physiological process of normal human biology. However, when ROS production and endogenous antioxidant ability are imbalanced, a maladaptive biological response occurs leading to both oxidative stress and inflammation [4, 5]. In muscle cells, aerobic energy production generates a significant amount of ROS, which can increase up to 10- to 20-fold during physical exercise [6]. Notably, previous evidence suggests that high ROS levels are able to induce muscular injury [1, 7, 8] with a consequent decrease in physical performance [9]. Several mechanisms contribute to the generation of ROS in skeletal muscles in response to intensive exercise. Among them, NADPH oxidase-derived formation of ROS may result in an altered redox state in muscles which may lead to contractile muscle dysfunction, accelerated muscle fatigue, longer recovery time, and reduced exercise performance [10].

Many studies have identified the potential antioxidant effect of polyphenols, a large group of natural compounds found in food and beverages [11]. Banerjee et al. highlighted that a supplementation with antioxidants is able to accelerate recovery from fatigue and to prevent exercise tissue damage [12]. Moreover, supplementation with other antioxidant nutrients, such as vitamin C and vitamin E, has been able to prevent exercise-induced oxidative damage but not inflammation in ultra-marathon runners [13]. Finally, previous work demonstrated a reduced exercise-induced muscular injury and a downregulation of monocytes expressing toll-like receptor 4 in kendo athletes by means of coenzyme Q10 administration [14, 15]. Overall, these data indicate that the administration of antioxidant nutrients may be a beneficial intervention to reduce the rate of muscular injury in endurance athletes. Cocoa may be appropriate for this purpose since it is a polyphenol-rich nutrient eliciting antioxidant effects [16]. A recent work demonstrated that acute cocoa-derived flavonoid intake may reduce oxidative stress and muscle damage induced by exercise [17]. However, there are few studies examining the effect of chronic cocoa flavonoid intake during exercise training.

Accordingly, the purpose of this study was to exploit the effect of chronic dark chocolate supplementation on muscular injury and oxidative stress during training exercise in elite football players.

2. Material and Methods

The study was performed on 24 young (17.2 ± 0.7 years) elite male football players during the first month of the regular season and 15 physically active male subjects who did not practice football but practice aerobic sports such as running, swimming, or gymnastics (engaging in at least 3-day·week^{-1} of moderate-to-intense physical activity, ranging from 3.0 to 6.0 METs and/or >6.0 METs) (24.8 ± 3.5 years) (Table 1). Players had at least 10 years of previous football training and were members of the Italian first-league A.S. Roma youth (17-19 years) team (Primavera). They were engaged in a 120-minute training (including a 15-minute warm-up, 30-minute technical/tactical skills, 30-minute aerobic training reaching 75% of the maximal heart rate, 30-minute strength training, and 15-minute cooldown) 6 times per week and a 90-minute match per week. The training program of the youth team was the same of the first A.S. Roma team (Serie A league). During the study, two players of the youth team also made their debut in the Serie A league with the first team and played regularly with the first team.

Table 1: Baseline characteristics of controls and elite football players.

	Controls ($n = 15$)	Football elite players ($n = 24$)	p
Age (years)	24.8 ± 3.5	17.2 ± 0.7	<0.001
Gender (male/female)	15/0	24/0	1
WBC ($\times 10^3$ μl)	7.1 ± 1.4	5.6 ± 1.3	0.001
PLT ($\times 10^3$ μl)	233.8 ± 48.4	228 ± 39.7	0.357
RBC ($\times 10^6$ μl)	5.3 ± 0.3	5.8 ± 0.3	0.559
Cholesterol (mg/dl)	185.1 ± 30.8	172.3 ± 29.4	0.130
BMI	24.3 ± 1.4	22.5 ± 1.5	<0.01
Glycaemia (mg/dl)	89.0 ± 28.8	83.5 ± 15.2	0.276
LDH (U/l)	179.5 ± 23.5	387.0 ± 50.7	<0.01
CK (U/l)	192.3 ± 28.7	342.6 ± 70.2	<0.01
Myoglobin (ng/ml)	50.6 ± 11.3	100.1 ± 42.9	<0.01
sNox2-dp (pg/ml)	13.8 ± 7.7	19.5 ± 6.9	<0.01
H_2O_2 (μM)	22.6 ± 13.2	38.8 ± 7.3	<0.0001
HBA (%)	52.9 ± 23.0	37.5 ± 11.4	<0.0001
Training per week (h)	7.2 ± 1.5	18 ± 2	<0.0001
Football practice (yrs.)	0	10 ± 1.2	<0.0001

WBC: white blood cells; PLT: platelet; RBC: red blood cells; BMI: body mass index; LDH: lactate dehydrogenase; CK: creatine kinase; HBA: hydrogen peroxide (H_2O_2) breakdown activity.

All participants and the head coach were explained the study's purposes, risks, and benefits; they were familiarized with the study's protocol during the pre-season screening; and they gave a written informed consent. The institutional review board approved this study (C.E. 4662), and the randomized controlled trial was registered on ClinicalTrials.gov (Identifier: NCT03288623).

Elite male athlete volunteers, aged between 18 and 35 years, were included in the study. Subjects were excluded if they suffer from an allergy to cocoa or any of the ingredients contained within either of the chocolate bars; they have a low platelet count ($<170 \times 10^{09}$/L); they are taking aspirin or aspirin-containing drugs, other anti-inflammatory drugs, or any drugs or herbal medicines known to alter platelet function or the haemostatic system in general (without a minimum washout period of one month); they are taking fish oils or evening primrose oil, or fat-soluble vitamin supplements within the last 4 weeks; they have unsuitable veins for blood sampling and/or cannulation; they have a BMI below 18 or above 35 kg/m^2; they are taking any medicine

known to affect lipid and/or glucose metabolism; they are suffering from alcohol or any other substance abuse or are having eating disorders; they have any known clinical signs of diabetes, hypertension, renal, hepatic, and haematological diseases, gastrointestinal disorders, endocrine disorders, coronary heart disease, infection, or cancer.

2.1. Study Design. In the first phase, we performed a cross-sectional study to compare oxidative stress, as assessed by blood levels of soluble Nox2 (sNox2-dp), H_2O_2 production, H_2O_2 breakdown activity (HBA) which is a method evaluating the antioxidant capacity of serum, and markers of muscle damage such as creatine kinase (CK), lactate dehydrogenase (LDH), and myoglobin in 24 young well-trained male elite football athletes and 15 sex-matched amateur controls. In the second phase, we performed a randomized controlled trial in elite football athletes to investigate the effect of daily supplementation with normal diet and 40 g of dark chocolate (20 g every 12 h) vs normal diet, for 30 days, on markers of oxidative stress and muscle damage.

Elite football athletes were randomly allocated to a treatment sequence with normal diet plus 40 g/day of commercially available dark chocolate in tablet (cocoa solids >85%, cocoa mass, fat-reduced cocoa, cocoa butter, sugar, and vanilla) or normal diet for 30 days. The content of total polyphenols in the dark chocolate employed in our study was 799 μg GAE/ml.

Blood levels of CK, LDH, myoglobin, total polyphenols, and oxidative stress biomarkers were assessed at baseline and at 30 days after the last ingestion of chocolate. During the trial, participants were required to follow a diet adjusted according to their anthropometric and clinical characteristics and to the amount of calories coming from chocolate intake; furthermore, participants were restrained by having foods with high polyphenol content (blueberry, sweet cherry, strawberry, blackberry, red raspberry, chestnut, black tea, green tea, pure apple juice, hazelnut, red wine, and pomegranate juice) and/or additional chocolate.

Blood samples were collected in the morning (between 08 : 00 and 09 : 00 hours) after a fasting period of 8 h at baseline and 30 days after the last ingestion of chocolate.

2.2. Randomisation and Blinding. An individual not involved in the study assigned codes to the study treatments, randomly allocated the participants to a treatment sequence with normal diet plus dark chocolate or normal diet, and kept the key in a sealed envelope. The randomisation was carried out by a procedure based on a random numeric sequence. The authors and laboratory technicians were unaware of the treatment allocation.

2.3. Sample Size, Randomisation, and Blinding. Sample size calculation was computed with G*Power [18] based on preliminary data, by means of a two tailed one-sample Student *t*-test with Welch correction: 1,69 (d) as effect size for sNox2-dp, 0.05 (a) as type I error probability, and 0.90 as power 1-b. Therefore, at least 22 elite soccer players (11 athletes per group, allocation ratio = 1) need to be randomly assigned to dark chocolate implementation or normal diet.

2.4. Extraction of Phenolic Fraction from Chocolate and Total Polyphenol Content Evaluation. One g of chocolate was weighted, and fat was removed by using 1 ml of n-hexane. Polyphenols were extracted from the defatted pellet using a total volume of 3 ml (1×3 ml) with 80% (*v*/*v*) of acetone : water at 80°C. This aqueous acetone solution, which contained most of all polyphenols, was used for polyphenols analysis and for *in vitro* study.

Total polyphenol content in extracted phenolic fraction from chocolate was evaluated by a modified Folin–Ciocalteu colorimetric method [19] and in plasma samples by the Folin–Ciocalteu method according to Serafini et al. [20]. Results were expressed as μg gallic acid equivalent (GAE)/ml.

2.5. Extraction and Quantification of Catechin and Epicatechin from Chocolate. Catechin and epicatechin were extracted and quantified according to Gottumukkala et al. [21]. Briefly, about 10 g of chocolate sample was extracted with methanol on a hot water and all methanolic fractions were combined, filtered, and evaporated. Catechin and epicatechin stock solutions were prepared in methanol in the concentration range of 100–600 μg/ml. HPLC analysis was performed using an HPLC system (Agilent 1200 Infinity Series HPLC system, Santa Clara, USA). The column temperature was maintained at 30°C. The HPLC mobile phase was as follows: solution A, 0.1 ml of orthophosphoric acid dissolved in 900 ml of HPLC-grade water; solution B, acetonitrile. The mobile phase was run using a gradient elution: at the time of 0.01 minutes, 11% B; at the time of 30 minutes, 25% B; at the time of 35 to 39 minutes, 100% B; and at the time of 40 to 50 minutes, 11% B. The mobile phase flow rate was 1.0 ml/minute, and the injection volume was 10 μl. The eluents were detected and analyzed at 280 nm.

2.6. Plasma Extraction and Quantification of Epicatechin. Plasma samples were extracted by the method described by Spadafranca et al. [22]. Briefly, 20 μl vitamin C-EDTA (200 mg vitamin C and 1 mg EDTA in 1 ml 0.4 mol/l NaH_2PO_4) and 20 μl glucuronidase/sulfatase type II (Sigma, St. Louis, MO) were added to 200 μl plasma and incubated at 37°C for 45 minutes. Flavonoids were extracted by addition of 500 μl acetonitrile, and the mixture was centrifuged at 10,000 g for 5 minutes at room temperature. After centrifugation, the supernatant was removed, dried under nitrogen, and reconstituted in the aqueous HPLC mobile phase. After centrifugation, 50 μl supernatant was injected into the HPLC column for separation, detection, and analysis.

The HPLC analysis was performed using an HPLC system (Agilent 1200 Infinity Series HPLC system, Santa Clara, USA). Separations were carried out at a flow rate of 1.5 ml/min with an isocratic mobile phase of 85% Na_2PO_4 10 mol/l, pH 3, and 15% acetonitrile. Chromatograms were recorded at 279 nm, and plasma epicatechin identification was made by comparison of retention times with those of commercially available authentic (-)-epicatechin (Sigma, St. Louis, MO) through the same procedures as the plasma samples.

2.7. Determination of % HBA in Serum. Serum hydrogen peroxide (H_2O_2) breakdown activity (HBA) was measured with

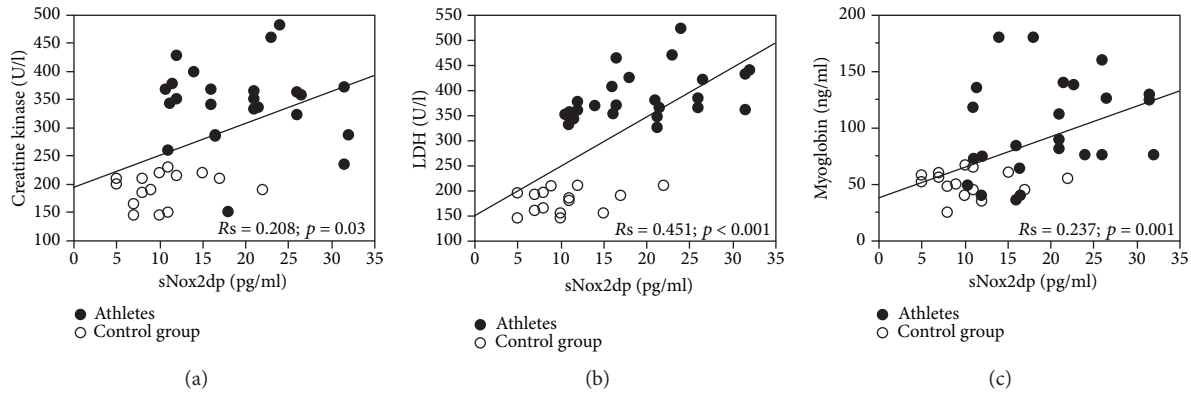

Figure 1: Linear correlation between sNox2-dp and creatine kinase (a), between sNox2-dp and LDH (b), and between sNox2-dp and myoglobin (c) in 15 controls (circle empty mark) and 24 elite football players (circle full mark).

HBA assay kit (Aurogene, code HPSA-50). The % of HBA was calculated according to the following formula: % of HB A = $[(Ac - As)/Ac] \times 100$ where Ac is the absorbance of H_2O_2 1.4 mg/ml as is the absorbance in the presence of the serum sample.

2.8. Serum Nox2 Activation. Serum Nox2 was measured as soluble Nox2-derived peptide (sNox2dp) with an ELISA method, according to Pignatelli et al. [23].

2.9. H_2O_2 Production. Hydrogen peroxide (H_2O_2) was evaluated by a Colorimetric Detection Kit (Arbor Assays) and expressed as μmol/l. Intra-assay and interassay coefficients of variation were 2.1% and 3.7%, respectively.

2.10. Muscle Damage Markers. Serum creatine kinase (CK), lactate dehydrogenase (LDH), and myoglobin levels were analyzed using a commercial ELISA kit (Antibodies, Germany; EIAab, China; DRG Instruments GmbH, Germany); the intra- and interassay coefficients were <10%.

2.11. In Vitro Study

2.11.1. Cell Culture and Reagents. The murine myoblast cell line C2C12 was cultured in DMEM/20% heat-inactivated foetal bovine serum (FBS), 2 mM glutamine, and 1% antibiotics (all Gibco) for expansion and maintenance of the undifferentiating state. When cultures reached 80% confluence, myogenic differentiation was induced by replacing the expansion media with DMEM/0.2% FBS. Afterwards, cells were stimulated with H_2O_2 (5 mM, Solarbio, Beijing, China) alone or in combination with cocoa-derived polyphenols (50, 100, and 150 μg/ml) for 30 minutes. Conditioned media were harvested and tested for the quantification of soluble Nox2 and H_2O_2 as described.

2.12. Statistical Methods. Continuous variables are reported as mean ± standard deviation unless otherwise indicated. Differences between categorical variables were tested using the χ^2 test. The crossover study data were analyzed for the assessment of treatment and period effects, by performing a split-plot ANOVA with one between-subject factor (treatment sequence) and two within-subject factors (period 1 vs 2; pre- vs post-treatment). The full model was considered, allowing for the assessment of all main effects and interactions. Pairwise comparisons were corrected by *t*-test for paired data. Bivariate analysis was performed with the Spearman linear regression test. Multiple linear regression analysis was performed using a forward selection. $p < 0.05$ was considered statistically significant. All analyses were carried out with SPSS V.18.0 (Armonk, USA).

Table 2: Total polyphenol content in dark chocolate.

Compounds	Dark chocolate
Total polyphenols (μg GAE/ml)	799
Epicatechin (mg/g)	0.65
Catechin (mg/g)	0.26

3. Results

3.1. Cross-Sectional Study. Clinical characteristics of elite football players and controls are reported in Table 1. WBC, BMI, and HBA were higher in controls compared to elite football athletes. Conversely, LDH, CK, myoglobin sNox2-dp, and H_2O_2 were higher in elite athletics compared to controls (Table 1). A simple linear regression analysis showed that sNox2-dp was associated with CK ($R = 0.208$; $p = 0.03$), LDH ($R = 0.451$; $p < 0.001$), and myoglobin ($R = 0.237$; $p = 0.001$) (Figures 1(a)-1(c)).

3.2. Randomized Controlled Trial. Total polyphenol, catechin, and epicatechin contents of dark chocolate are reported in Table 2.

No significant differences between clinical characteristics and biochemical parameters were found at baseline in the elite athlete groups allocated to dark chocolate intake and no dark chocolate intake (Table 3, Figures 2 and 3). Four athletes dropped out of the study to transfer to another team.

After 30 days of training, the control group showed increased levels of sNox2-dp and H_2O_2 compared to baseline (from 18.9 ± 7.0 pg/ml to 34.6 ± 7.5 pg/ml, $p < 0.0001$, and from 38.7 ± 10.2 μM to 48.9 ± 4.3 μM, $p < 0.0001$, respectively) (Figures 2(a) and 2(b)). Conversely, HBA and plasma total polyphenols resulted to be unchanged (from 37.78 ±

Table 3: Baseline characteristics of elite football players before treatment.

	No dark chocolate ($n = 10$)	Dark chocolate ($n = 10$)	p
Age (years)	17.0 ± 0.9	17.4 ± 0.5	0.859
Gender (male/female)	10/0	10/0	1
WBC ($\times 10^3$ ml)	5.0 ± 1.3	6.2 ± 1.1	0.983
PLT ($\times 10^3$ ml)	226.6 ± 55.4	230.0 ± 12.8	0.580
RBC ($\times 10^6$ ml)	5.3 ± 0.3	5.5 ± 0.3	0.950
LDL (mg/dl)	82.9 ± 18.3	84.3 ± 22.2	0.566
Glycaemia (mg/dl)	84.0 ± 11.2	83.1 ± 19.1	0.448
LDH (U/l)	389.7 ± 59.9	384.2 ± 42.2	0.398
CK (U/l)	363 ± 21.83	341.1 ± 20.13	0.880
Myoglobin (ng/ml)	97.4 ± 40.8	105.8 ± 41.9	0.579
hs-PCR (mg/l)	0.6 ± 0.4	0.7 ± 0.6	0.759
sNox2-dp (pg/ml)	18.9 ± 7.0	19.5 ± 6.7	0.844
H_2O_2 (μM)	38.7 ± 10.1	37.7 ± 6.6	0.746
HBA (%)	37.8 ± 27.8	34.9 ± 29.8	0.775

WBC: white blood cells; PLT: platelet; RBC: red blood cells; LDL: low-density lipoprotein; LDH: lactate dehydrogenase; CK: creatine kinase; HBA: hydrogen peroxide (H_2O_2) breakdown activity.

27.8% to 43.7 ± 16.3%, $p = 0.402$, and from 152.6 ± 35.3 μg GAE/ml to 144.7 ± 48.06 μg GAE/ml, $p = 0.573$, respectively) (Figures 2(c) and 2(d)). The pairwise comparisons showed that sNox2-dp levels and H_2O_2 production did not change after 30 days of dark chocolate intake compared to baseline (from 19.5 ± 6.7 pg/ml to 23.55 ± 5.6 pg/ml, $p = 0.224$, and from 37.7 ± 6.7 μM to 32.6 ± 4.5 μM, $p = 0.06$, respectively) (Figures 2(a) and 2(b)). Conversely, HBA and plasma total polyphenols increased after treatment (from 34.9 ± 29.8% to 66.0 ± 7.3%, $p = 0.003$, and from 151.9 ± 44.2 μg GAE/ml to 187.1 ± 7.1 μg GAE/ml, $p = 0.02$, respectively) (Figures 2(c) and 2(d)).

A significant difference between the two treatments (no dark chocolate vs dark chocolate) was found regarding sNox2-dp (34.6 ± 7.5 pg/ml vs 23.55 ± 5.6 pg/ml, $p = 0.002$) (Figure 2(a)), H_2O_2 production (48.9 ± 4.3 μM vs 32.6 ± 4.5 μM, $p < 0.002$) (Figure 2(b), HBA (43.7 ± 16.3% vs 66.0 ± 7.3%, $p = 0.008$) (Figure 2(c)) and total polyphenols (144.7 ± 48.1 μg GAE/ml vs 187.1 ± 7.16 μg GAE/ml, $p = 0.02$) (Figure 2(d)).

Serum *muscle enzymes* highlighted in the control group increased myoglobin levels (from 97.4 ± 40.8 ng/ml to 168.0 ± 20.2 ng/ml, $p = 0.0004$), and there was no change in CK and LDH levels (from 363.0 ± 69.1 U/l to 341.1 ± 63.67 U/l, $p = 0.475$, and 384.7 ± 59.6 U/l to 367.5 ± 52.9 U/l, $p = 0.06$, respectively) (Figures 3(a)-3(c)). Conversely, we observed a significant decrease of CK (from 337.4 ± 36.5 U/l to 283.9 ± 41.0 U/l, $p = 0.0007$) and LDH (from 381.6 ± 44.3 U/l to 273.4 ± 55.5 U/l, $p = 0.0008$) (Figures 3(b) and 3(c)) after dark chocolate treatment. Myoglobin levels decreased without reaching statistical significance (from 105.8 ± 41.9 ng/ml to 81.4 ± 25.7 ng/ml, $p = 0.06$) (Figure 3(a)). A significant difference between the two treatments (no dark chocolate vs dark chocolate) was found regarding myoglobin (168.0 ± 20.3 ng/ml vs 81.4 ± 25.7 ng/ml, $p < 0.001$) (Figure 3(a)), CK (341.1 ± 63.67 U/l vs 283.9 ± 41.1 U/l, $p = 0.028$) (Figure 3(b)), and LDH (367.5 ± 53.0 U/l vs 273.4 ± 55.5 U/l, $p = 0.001$) (Figure 3(c)).

To assess the adherence to the protocol, we analyzed the levels of epicatechin which is a major component of dark chocolate. The results showed a significant increase of epicatechin in the dark chocolate group compared to the control group (189.8 ± 54.0 ng/ml vs <10 ng/ml, $p < 0.0001$).

A sensitivity analysis was then conducted by using generalized estimating equations (GLM), and point estimates of effect, 95% confidence intervals, and corresponding p values were reported. Chocolate exerted a significant beneficial effect on the following several variables at repeated measurement: sNox2-dp (point estimate of effect = −11.6 [95% -18.8; -4.4] pg/ml, $p = 0.002$), H_2O_2 (point estimate of effect = −15.2 [95% -23.3; -7.2] μM, $p < 0.0001$), HBA (point estimate of effect = 25.2 [95% 3.8; 46.5] %, $p = 0.021$), total polyphenols (point estimate of effect = 43.1 [95% 7.6; 78.6] μg GAE/ml, $p = 0.01$), CK (point estimate of effect = −31.6 [95% -52.8; -10.3] U/l, $p = 0.004$), LDH (point estimate of effect = −91.0 [95% -153.8; -28.1] U/L, $p = 0.005$), and myoglobin (point estimate of effect = −95.0 [95% -126.7; -63.2] U/L, $p < 0.001$).

No significant correlation was found between baseline blood parameters and days of unavailability days of FKT and occurrence of muscular and joint lesions (all $p > 0.05$), with the notable exception of baseline myoglobin levels, which were lower in subjects requiring more FKT afterwards (spearman rho = −0.553, $p = 0.011$).

No significant effect of chocolate intake was found on days of unavailability, days of FKT, and occurrence of muscular and joint lesions (all $p > 0.05$). Accordingly, changes in blood parameters were not significantly associated with days of unavailability, FKT, and occurrence of muscular and joint lesions (all $p > 0.05$).

3.3. In Vitro Study. In order to corroborate the clinical effects of cocoa-derived polyphenols on muscle redox state, we performed an in vitro study with a polyphenol extract at concentrations (50-150 μg/ml) relatively similar to that found in serum of elite football athletes after dark chocolate intake. Murine myoblast cell line C2C12-derived conditioned media after stimulation with H_2O_2 showed both enhanced levels of Nox2 activation and H_2O_2 production (Figures 4(a) and 4(b)). Polyphenol extract significantly decreased Nox2 activation and H_2O_2 production (Figures 4(a) and 4(b)).

4. Discussion

This study showed that (1) oxidative stress and markers of muscle damage are significantly increased in elite football players compared to controls and (2) chronic intake of dark chocolate is able to reduce oxidative stress and muscle damage biomarkers during elite football players' training session.

The novel finding of the present study is the improvement of oxidative stress and muscle damage enzymes after 30 days by ingestion of dark chocolate in elite football athletes during intensive physical exercise. The effect of dark

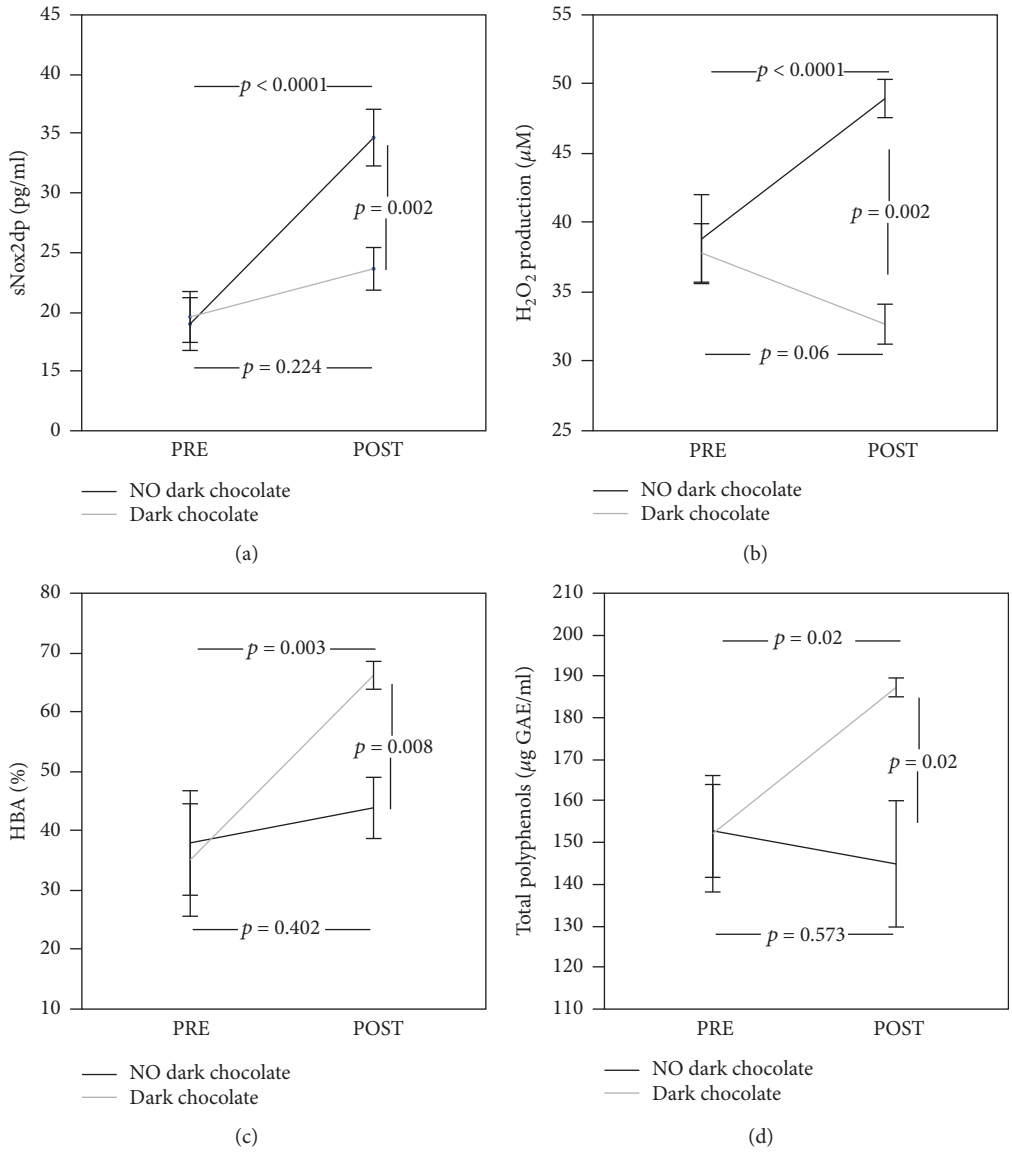

Figure 2: sNox2-dp levels (a), H_2O_2 production (b), hydrogen peroxide breakdown activity (HBA) (c), and total polyphenol (d) before and 30 days after daily intake of 40 g of dark chocolate (grey line) or without dark chocolate (black line) in elite football players.

chocolate supports the hypothesis that polyphenol content, in particular epicatechin, may be responsible for this effect. Accordingly, total polyphenol content and epicatechin plasma levels were increased in the group of athletes randomized for dark chocolate intake.

The scientific background of our research was based on the evidence that intensive physical exercise implies a wide range of multifaceted biological activities challenging the physiological homeostasis of the body. The relationship between exercise and oxidative stress is extremely complex and mainly depends on mode, frequency, intensity, and duration of exercise. On the one hand, several experimental and epidemiological evidences have underlined the key role of physical exercise (PE) in decreasing oxidative stress, especially if associated to aging, and to prevent and positively modulate cardiovascular-associated risk factors [24, 25]. It was suggested that the reduction of oxidative stress triggered by PE could be associated with the improvement of the nitric oxide function. Regular exercise was also recently demonstrated to activate eNOS and nitrite production and to reduce oxidative stress in spontaneously hypertensive rats [26]. Moreover, PE was suggested to exert cardioprotective effects in ischemic rats in which high-intensity interval training increases NO metabolite levels and reduce myocardial infarction [27]. Oppositely, other reports have demonstrated that exercise increases the production of ROS, particularly suggesting that high-intensity, but not moderate, physical exercise can cause redox imbalance overwhelming the antioxidant defence ability, leading to several types of injuries [12, 28–30]. These emerging data have nonnegligible theoretical and applicative implications.

According to this premise, professional training programs including those for elite football players could indirectly and physiologically induce oxidative stress in athletes

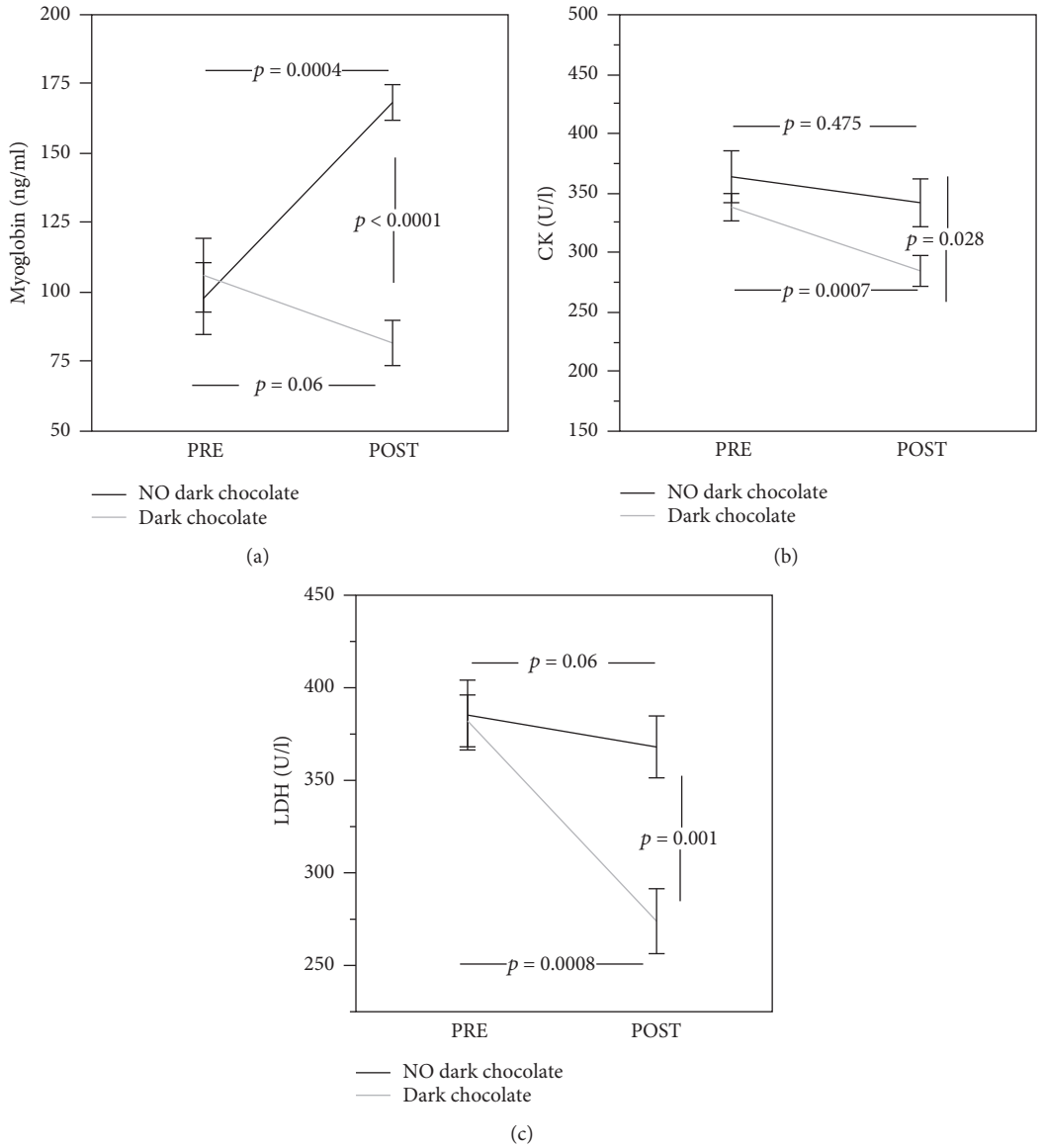

Figure 3: Myoglobin (a), creatine kinase (CK) (b), and lactate dehydrogenase (LDH) (c) concentration before and 30 days after daily intake of 40 g of dark chocolate (grey line) or without dark chocolate (black line) in elite football players.

and significantly influence biological antioxidant patterns. Accordingly, in our cross-sectional study, we found an increase in Nox2 activation and H_2O_2 production with reduced antioxidant property as indicated by decreased HBA in elite football players compared to controls. Moreover, at the same time, we observed an increase in muscle damage markers such as CK, LDH, and myoglobin.

These aspects represent a serious issue since a recent study showed that levels of oxidative stress markers are directly correlated with markers of muscular damage in elite football players playing in the Italian Serie A league [1].

For this reason, dietary regimens including antioxidant supplementation are now considered important interventions able to counteract the hazardous effects of free radicals by increasing the antioxidant profile and regulating the equilibrium between oxidant and antioxidant species [31]. These beneficial effects were observed in both animals and healthy subjects and in other chronic conditions that are accompanied by enhanced levels of oxidative stress [31–33]. Supporting endogenous defences with oral antioxidant supplementation may represent a suitable noninvasive tool for preventing or reducing oxidative stress during intensive physical training. The protective effects against oxidative stress elicited by antioxidant-rich nutrients have been partially ascribable to the high content of polyphenols (a class of chemicals characterized by the presence of phenol units in their chemical structure). The best-characterized biological property of all flavonoids as for polyphenols in general is their ability to act as antioxidants, by inhibiting ROS accumulation by scavenging ROS or by inhibiting enzymes involved in ROS production or by enhancing the natural antioxidant defences [34, 35]. In particular, a recent study suggests that daily supplementation with flavonol-rich cocoa over 4 weeks may improve oxidative stress biomarkers as

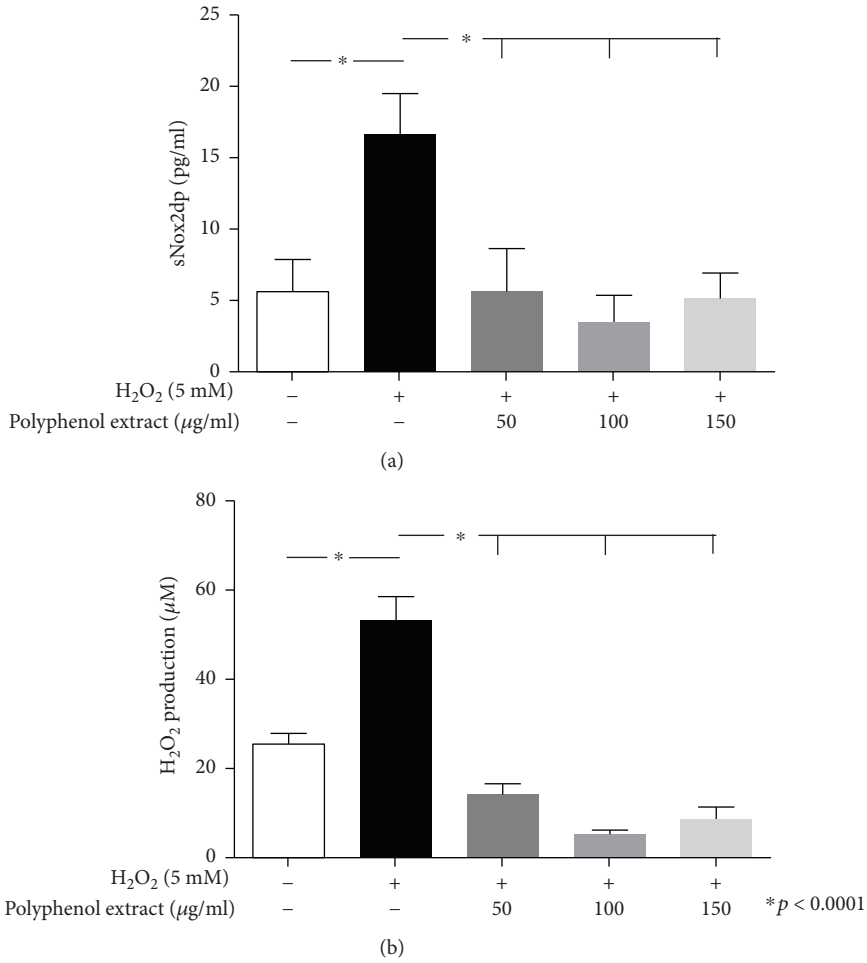

Figure 4: sNox2-dp levels (a) and H_2O_2 production (b) in murine myoblast cell line C2C12 stimulated with H_2O_2 (5 mM), alone or in combination with cocoa-derived polyphenols (50, 100, and 150 μg/ml). All values are expressed as means ± SD.

indicated by an increase in total GSH levels and a decrease in urinary F2-isoprostane excretion [30].

We planned to use this body of evidence as a benchmark for the development of new strategies in the setting of elite athlete training programs. In this interventional study, we thus demonstrated for the first time that polyphenol-rich nutrient supplementation of dark chocolate reduces exercise-induced oxidative stress and muscular injury biomarkers in elite football athletes.

The antioxidative effects induced by cocoa-derived polyphenols were also confirmed on skeletal muscle cells *in vitro*. Our experiments were conducted using concentrations of polyphenol extract relatively close to that achieved in blood circulation of athletes after dark chocolate intake. Notably, the lower dose of polyphenols was able to completely counter the effects of induced oxidative stress, restoring the physiological redox state in treated murine myoblasts.

In conclusion, the present study provides the first direct relationship between cocoa-based polyphenol-rich nutrient supplementation and the effect of high-intensity training on elite athletes' antioxidant status. Based on our results, the development and improvement of training techniques focusing also on new nutrition strategies may help to reduce muscular damage in elite football players.

Data Availability

The data used to support the findings of this study are available from the corresponding author upon request.

Ethical Approval

The institutional review board approved this study (C.E. 4662), and the randomized controlled trial was registered on ClinicalTrials.gov (Identifier: NCT03288623).

Conflicts of Interest

The authors declare that they have no conflict of interest.

Authors' Contributions

Giacomo Frati, Roberto Carnevale, Elena Cavarretta, and Mariangela Peruzzi have equal contribution to this work.

Acknowledgments

This work was partially supported by an unrestricted grant from Villa Stuart Sport Clinic, FIFA Medical Centre of Excellence, and Sapienza University of Rome (grant number 2016/

43780) to Elena Cavarretta. The authors are grateful to Dr. Vincenzo Costa, MD, for his invaluable help in the athletes' follow-up.

References

[1] M. Becatti, A. Mannucci, V. Barygina et al., "Redox status alterations during the competitive season in élite soccer players: focus on peripheral leukocyte-derived ROS," *Internal and Emergency Medicine*, vol. 12, no. 6, pp. 777–788, 2017.

[2] J. Ekstrand, M. Hägglund, and M. Waldén, "Epidemiology of muscle injuries in professional football (soccer)," *The American Journal of Sports Medicine*, vol. 39, no. 6, pp. 1226–1232, 2011.

[3] M. Hägglund, M. Waldén, H. Magnusson, K. Kristenson, H. Bengtsson, and J. Ekstrand, "Injuries affect team performance negatively in professional football: an 11-year follow-up of the UEFA Champions League injury study," *British Journal of Sports Medicine*, vol. 47, no. 12, pp. 738–742, 2013.

[4] A. Phaniendra, D. B. Jestadi, and L. Periyasamy, "Free radicals: properties, sources, targets, and their implication in various diseases," *Indian Journal of Clinical Biochemistry*, vol. 30, no. 1, pp. 11–26, 2015.

[5] H. Sies, "Oxidative stress: a concept in redox biology and medicine," *Redox Biology*, vol. 4, pp. 180–183, 2015.

[6] B. Sjödin, Y. H. Westing, and F. S. Apple, "Biochemical mechanisms for oxygen free radical formation during exercise," *Sports Medicine*, vol. 10, no. 4, pp. 236–254, 1990.

[7] J. Finaud, G. Lac, and E. Filaire, "Oxidative stress: relationship with exercise and training," *Sports Medicine*, vol. 36, no. 4, pp. 327–358, 2006.

[8] J. Peake, K. Nosaka, and K. Suzuki, "Characterization of inflammatory responses to eccentric exercise in humans," *Exercise Immunology Review*, vol. 11, pp. 64–85, 2005.

[9] Z. Radák, J. Pucsok, S. Mecseki, T. Csont, and P. Ferdinandy, "Muscle soreness-induced reduction in force generation is accompanied by increased nitric oxide content and DNA damage in human skeletal muscle," *Free Radical Biology & Medicine*, vol. 26, no. 7-8, pp. 1059–1063, 1999.

[10] S. K. Powers, E. E. Talbert, and P. J. Adhihetty, "Reactive oxygen and nitrogen species as intracellular signals in skeletal muscle," *The Journal of Physiology*, vol. 589, no. 9, pp. 2129–2138, 2011.

[11] C. Manach, A. Scalbert, C. Morand, C. Rémésy, and L. Jiménez, "Polyphenols: food sources and bioavailability," *The American Journal of Clinical Nutrition*, vol. 79, no. 5, pp. 727–747, 2004.

[12] A. K. Banerjee, A. Mandal, D. Chanda, and S. Chakraborti, "Oxidant, antioxidant and physical exercise," *Molecular and Cellular Biochemistry*, vol. 253, no. 1/2, pp. 307–312, 2003.

[13] A. Mastaloudis, J. D. Morrow, D. W. Hopkins, S. Devaraj, and M. G. Traber, "Antioxidant supplementation prevents exercise-induced lipid peroxidation, but not inflammation, in ultramarathon runners," *Free Radical Biology & Medicine*, vol. 36, no. 10, pp. 1329–1341, 2004.

[14] M. Kon, K. Tanabe, T. Akimoto et al., "Reducing exercise-induced muscular injury in kendo athletes with supplementation of coenzyme Q10," *The British Journal of Nutrition*, vol. 100, no. 4, pp. 903–909, 2008.

[15] K. Shimizu, M. Kon, Y. Tanimura et al., "Coenzyme Q10 supplementation downregulates the increase of monocytes expressing toll-like receptor 4 in response to 6-day intensive training in kendo athletes," *Applied Physiology, Nutrition, and Metabolism*, vol. 40, no. 6, pp. 575–581, 2015.

[16] I. Andújar, M. C. Recio, R. M. Giner, and J. L. Ríos, "Cocoa polyphenols and their potential benefits for human health," *Oxidative Medicine and Cellular Longevity*, vol. 2012, Article ID 906252, 23 pages, 2012.

[17] J. A. González-Garrido, J. R. García-Sánchez, S. Garrido-Llanos, and I. M. Olivares-Corichi, "An association of cocoa consumption with improved physical fitness and decreased muscle damage and oxidative stress in athletes," *The Journal of Sports Medicine and Physical Fitness*, vol. 57, no. 4, pp. 441–447, 2017.

[18] F. Faul, E. Erdfelder, A. Buchner, and A. G. Lang, "Statistical power analyses using G*Power 3.1: tests for correlation and regression analyses," *Behavior Research Methods*, vol. 41, no. 4, pp. 1149–1160, 2009.

[19] L. Mosca, C. de Marco, F. Visioli, and C. Cannella, "Enzymatic assay for the determination of olive oil polyphenol content: assay conditions and validation of the method," *Journal of Agricultural and Food Chemistry*, vol. 48, no. 2, pp. 297–301, 2000.

[20] M. Serafini, G. Maiani, and A. Ferro-Luzzi, "Alcohol-free red wine enhances plasma antioxidant capacity in humans," *The Journal of Nutrition*, vol. 128, no. 6, pp. 1003–1007, 1998.

[21] R. V. S. S. Gottumukkala, N. Nadimpalli, K. Sukala, and G. V. Subbaraju, "Determination of catechin and epicatechin content in chocolates by high-performance liquid chromatography," *International Scholarly Research Notices*, vol. 2014, Article ID 628196, 5 pages, 2014.

[22] A. Spadafranca, C. Martinez Conesa, S. Sirini, and G. Testolin, "Effect of dark chocolate on plasma epicatechin levels, DNA resistance to oxidative stress and total antioxidant activity in healthy subjects," *The British Journal of Nutrition*, vol. 103, no. 7, pp. 1008–1014, 2010.

[23] P. Pignatelli, R. Carnevale, R. Cangemi et al., "Atorvastatin inhibits gp91phox circulating levels in patients with hypercholesterolemia," *Arteriosclerosis, Thrombosis, and Vascular Biology*, vol. 30, no. 2, pp. 360–367, 2010.

[24] V. Conti, G. Corbi, G. Russomanno et al., "Oxidative stress effects on endothelial cells treated with different athletes' sera," *Medicine & Science in Sports & Exercise*, vol. 44, no. 1, pp. 39–49, 2012.

[25] V. Conti, G. Russomanno, G. Corbi et al., "Aerobic training workload affects human endothelial cells redox homeostasis," *Medicine & Science in Sports & Exercise*, vol. 45, no. 4, pp. 644–653, 2013.

[26] Z. N. Kumral, G. Sener, S. Ozgur et al., "Regular exercise alleviates renovascular hypertension-induced cardiac/endothelial dysfunction and oxidative injury in rats," *Journal of Physiology and Pharmacology*, vol. 67, no. 1, pp. 45–55, 2016.

[27] A. Fallahi, A. Gaeini, S. Shekarfroush, and A. Khoshbaten, "Cardioprotective effect of high intensity interval training and nitric oxide metabolites (NO2−, NO3 −)," *Iranian Journal of Public Health*, vol. 44, no. 9, pp. 1270–1276, 2015.

[28] L. Packer, E. Cadenas, and K. J. A. Davies, "Free radicals and exercise: an introduction," *Free Radical Biology & Medicine*, vol. 44, no. 2, pp. 123–125, 2008.

[29] K. Fisher-Wellman and R. J. Bloomer, "Acute exercise and oxidative stress: a 30 year history," *Dynamic Medicine*, vol. 8, no. 1, p. 1, 2009.

[30] G. Metin, M. K. Gümüştaş, E. Uslu, A. Belce, and A. Kayserilioglu, "Effect of regular training on plasma thiols, malondialdehyde and carnitine concentrations in young soccer players," *The Chinese Journal of Physiology*, vol. 46, no. 1, pp. 35–39, 2003.

[31] G. Corbi, V. Conti, K. Komici et al., "Phenolic plant extracts induce Sirt1 activity and increase antioxidant levels in the rabbit's heart and liver," *Oxidative Medicine and Cellular Longevity*, vol. 2018, Article ID 2731289, 10 pages, 2018.

[32] S. Davinelli, G. Corbi, A. Zarrelli et al., "Short-term supplementation with flavanol-rich cocoa improves lipid profile, antioxidant status and positively influences the AA/EPA ratio in healthy subjects," *The Journal of Nutritional Biochemistry*, vol. 61, pp. 33–39, 2018.

[33] S. Davinelli, G. Corbi, S. Righetti et al., "Cardioprotection by cocoa polyphenols and ω-3 fatty acids: a disease-prevention perspective on aging-associated cardiovascular risk," *Journal of Medicinal Food*, vol. 21, no. 10, pp. 1060–1069, 2018.

[34] M. Forte, V. Conti, A. Damato et al., "Targeting nitric oxide with natural derived compounds as a therapeutic strategy in vascular diseases," *Oxidative Medicine and Cellular Longevity*, vol. 2016, Article ID 7364138, 20 pages, 2016.

[35] L. Loffredo, M. del Ben, L. Perri et al., "Effects of dark chocolate on NOX-2-generated oxidative stress in patients with non-alcoholic steatohepatitis," *Alimentary Pharmacology and Therapeutics*, vol. 44, no. 3, pp. 279–286, 2016.

Hindawi
Oxidative Medicine and Cellular Longevity
Volume 2018, Article ID 7408370, 10 pages
https://doi.org/10.1155/2018/7408370

Research Article

Ellagic Acid Suppresses the Oxidative Stress Induced by Dietary-Oxidized Tallow

Alam Zeb[1,2] **and Adnan Akbar**[2]

[1]*Laboratory of Functional Foods Chemistry, Institute of Biochemistry, Technical University of Graz, Graz, Styria, Austria*
[2]*Laboratory of Biochemistry, Department of Biotechnology, Faculty of Biological Sciences, University of Malakand, Chakdara, Khyber Pakhtunkhwa, Pakistan*

Correspondence should be addressed to Alam Zeb; azebuom@gmail.com

Received 2 July 2018; Accepted 17 October 2018; Published 18 November 2018

Guest Editor: Marina Sokovic

Dietary tallow was thermally oxidized at 180°C in an open fryer. The oxidized tallow (OT) and unoxidized tallow were characterized for oxidation parameters and fatty acid composition using GC-MS. Tallow samples were fed to rabbits along with 50, 100, and 150 mg/kg/day of ellagic acid (EA) for three weeks. Results revealed that the peroxide value (PV) and thiobarbituric acid reactive substances (TBARS) significantly increased, while radical scavenging activity (RSA) of the tallow decreased significantly with oxidation. GC-MS analysis showed eight fatty acids in the tallow samples, where palmitic acid (48.5-49.7 g/100 g), linoleic acid (18.7-23.7 g/100 g), stearic acid (13.5-15.6 g/100 g), and margaric acid (6.32-6.42 g/100 g) were the major fatty acids. Animal studies showed that oxidized tallow (OT) alone or in combination with EA significantly altered the body weight of the rabbits. Serum biochemical parameters and renal function tests were affected by OT and ameliorated by EA. The toxic effects of OT on haematological indices were minimized by EA. The supplementation of OT alone had significant effects on the liver structure and functions. The coadministration of EA reduced the toxic properties of OT on the liver, by increasing the antioxidant (GSH) system. The rabbit heart was also affected by the OT, which was ameliorated by EA supplementation. These results suggested that the supplementation of EA was beneficial against the OT-induced oxidative stress and may be considered for foods containing oxidized lipids.

1. Introduction

Foods are prepared in dietary lipids such as fats or oils. During frying or food preparation, triacylglycerols are oxidized to form primary oxidation products. These primary oxidation products may include hydroperoxides, epoxides, hydroxides, and epoxides [1]. The lipid oxidation products formed are highly reactive. Most of these products are either free radicals or highly oxygenated compounds with high affinity for further reactions [2]. During the frying of foods, these products enter the food matrix and consequently consumed by humans [3]. The oxidized lipids then enter the gastrointestinal system, where it is metabolized or reaches the intestine as such. During digestion, these oxidized products alter several biochemical reactions thus causing toxicity [4]. The toxicity of the oxidized lipids may also be due to their capacity to form a complex with proteins. The oxidized products are toxic and are capable of inhibiting enzymatic reactions and cellular respiration and also contribute to ageing. The dietary lipid oxidation induces oxidative stress and increases lipogenesis in animal models [5, 6]. The lipogenesis was more pronounced in the liver and also in adipose tissues.

Dietary oxidized frying oil had been found to upregulate both hepatic acyl-CoA oxidase enzyme and one of the important genes (cytochrome p450 4 a1) in rats [7]. The dietary oxidized oil also activates peroxisome proliferator-activating receptors thus altering lipid metabolism. These effects were independent of the nature of the animal used [8]. The oxidized dietary lipids were also found to alter the glucose metabolism [9]. The oxidized lipids induced glucose intolerance by the mediation of altering the insulin secretion. The oxidized tallow was found to increase significantly the

levels of serum total cholesterol, triglycerides, liver function tests, and liver toxicity [3]. Similarly, oxidized Vanaspati ghee was also causing significant detrimental effects on serum biochemical parameters, haematological parameters, and liver histology [10]. Fat accumulation in the liver was highly favoured by the ingestion of thermally oxidized sunflower oil [5]. Sea buckthorn seed oil [11], tomato products [6], and dietary glycine and glutamic acid [12] were found beneficial in controlling the oxidative stress induced by dietary oxidized lipids. The continuous uses of fried fats or oils in our daily food preparation have therefore warranted to determine other possible alternative ways for protection against the oxidative stress produced by dietary oxidized lipids. Phenolic compounds also played a significant role in the prevention of oxidative stress in animal models [13–15] and in humans [16]. Ellagic acid was found to be a potentially strong antioxidant in different kinds of oxidative stresses [17]. These studies only focused on the chemical-induced oxidative stress, while lacking its role against the oxidative stress produced by dietary oxidized lipids. This study was therefore aimed at determining the role of ellagic acid as a widely known oxidation suppressor against the oxidative stress produced by dietary oxidized oils.

2. Materials and Methods

2.1. Sample Collection. Samples of the animal adipose tissues (buffalos) were collected from the local slaughterhouse in Mingora Swat. Tallow was prepared as per the method of Zheng and Hanna [18]. After sample preparation, tallow was stored in the refrigerator for further analysis.

2.2. Thermal Oxidation of Tallow. Unoxidized tallow was taken as the control. Tallow (1 kg) was thermally oxidized in the open fryer at a controlled temperature of 180°C for 10 hours continuously. The oxidized samples were stored in the refrigerator until feeding to animals or characterization.

2.3. Characterization of Tallow. Peroxide values (meq/kg) were determined using an AOCS official method no Cd 8b-90 [19]. Thiobarbituric acid reactive substances (TBARS) were determined as per the optimized developed method [20]. Briefly, samples (100 mg) were dissolved in 10 mL of the glacial acetic acid. The extract (0.5 mL) was mixed with 0.5 mL of the thiobarbituric acid solution and kept in boiling water bath for 60 min. The absorbance of the samples was calculated at 532 nm against the blank. The values of TBARS were calculated from the standard calibration curve and expressed as mmol/g. The DPPH radical scavenging activity (RSA) was determined with 0.1 mM diphenyl-1-picrylhydrazyl (DPPH) solution using a UV-visible spectrophotometer (Shimadzu Japan) at 515 nm against methanol blank. The RSA was calculated as % RSA.

Fatty acids in the tallow samples were determined using gas chromatography coupled to mass spectrometry (GC-MS). For this purpose, 20 mg of the oil sample was converted to its methyl esters using acidified methanol [11]. The GC-MS system (QP-2010 plus) of the Shimadzu Corporation (Japan) was used for the analysis of fatty acid methyl ester of tallow samples. The total ion chromatograms (TIC) were recorded in the range of m/z 85-400. The amount of fatty acids was quantified using the available authentic standards and also by comparison with fatty acids MS library, where standards were not available. The fatty acids were expressed as g/100 g of the samples.

2.4. Animal Feeding. Rabbits as experimental animals were used. Rabbits were acclimatized to the new environment for one week. The experiments were conducted as per the approved protocols of animal care and experimentation, which are in accordance with the Helsinki Declaration. The experiments were approved by the Advanced Studies and Research Board of the University of Malakand. Male rabbits were randomly divided into six groups with five animals in each group according to the following scheme:

Group 1: control without any treatment on a normal diet

Group 2: fed with 50 mg/kg body weight of ellagic acid and oxidized tallow (3 g/kg) represented as OT + 50EA

Group 3: fed with 100 mg/kg body weight of ellagic acid and oxidized tallow (3 g/kg) represented as OT + 100EA

Group 4: fed with 150 mg/kg body weight of ellagic acid and oxidized tallow (3 g/kg) represented as OT + 150EA

Group 5: fed with 100 mg/kg body weight of ellagic acid only represented as 100EA

Group 6: fed with oxidized tallow (3 g/kg) only represented as OT

The doses of ellagic acid in the present study were lower than the values of 200 mg/kg as reported in the literature [21]. The oral gavage feeding was continued for 7 days, while the 8th day was considered a break for the collection of blood samples from the jugular vein of the rabbit.

2.5. Weight Changes. The changes in the weight of the whole body, heart, and liver were determined using a digital balance with high accuracy.

2.6. Serum Biochemical Parameters. Serum biochemical parameters such as total cholesterol, total triglycerides, and glucose were determined using the available standard reagent kits of HUMAN (Germany).

2.7. Renal Function Tests. The serum was analyzed for renal function tests, i.e., serum creatinine, urea, and uric acid, using the standard reagent kits of HUMAN (Germany).

2.8. Haematological Studies. Blood (3 mL) in the EDTA tubes was processed for the determination of different haematological parameters using the automatic CELL-DYN 3200 of the Abbott Diagnostic Division, Canada. The haematological parameters such as haemoglobin concentration, platelet concentration, monocytes, lymphocytes, eosinophils,

Table 1: Quality characteristic and composition of fatty acids of control and oxidized tallow.

No.	Fatty acid/parameter	Code	Retention time (min)	Composition (g/100 g)*	
				Control	Oxidized
1	Myristic acid	C14:0	12.9	3.56 ± 0.1^{a}	3.24 ± 0.2^{a}
2	Pentadecanoic acid	C15:0	14.6	1.37 ± 0.03^{a}	1.76 ± 0.05^{b}
3	Palmitic acid	C16:0	16.2	48.5 ± 0.2^{a}	49.7 ± 0.1^{b}
4	Margaric acid	C17:0	18.0	6.42 ± 0.2^{a}	6.32 ± 0.2^{a}
5	Stearic acid	C18:0	19.2	13.5 ± 0.2^{a}	15.6 ± 0.1^{b}
6	Linoleic acid	C18:2	19.6	23.7 ± 0.3^{a}	18.7 ± 0.1^{b}
7	Eicosanoic acid	C20:1	22.8	1.39 ± 0.1^{a}	1.19 ± 0.05^{b}
8	Behenic acid	C22:0	26.9	0.45 ± 0.05^{a}	ND^{b}
Quality characteristics					
1	PV (meq/kg)*			9.03 ± 0.5^{a}	111.3 ± 3.0^{b}
2	TBARS (mmol/g)**			0.254 ± 0.01^{a}	0.518 ± 0.01^{b}
3	RSA (%)***			51.1 ± 0.4^{a}	40.5 ± 0.8^{b}

The identification of each fatty acid was based on comparison with authentic standards and comparison with reported in the library. Data are the mean of replicate ($n = 5$) readings and represented as the mean with a standard deviation. Different letters (a-b) in the same parameter showed a significant difference at $\alpha = {}^{*}0.05$, $^{**}0.01$, and $^{***}0.001$ using Tukey's test. PV: peroxide values; TBARS: thiobarbituric acid reactive substances; RSA: radical scavenging activity; C: carbons in fatty acid; ND: not detected.

total leucocyte counts, basophils, platelets, and neutrophils were determined.

2.9. Liver Structure and Function. The liver was analyzed for histological studies. Briefly, a small section of the median lobe of the liver was dissected. The section was then fixed in formalin buffer (10%) for 14 h. The dissected section was then dehydrated with ethanol solutions and further embedded in paraffin. Liver sections of about 8-10 mm in thickness were cut using a microtome, then deparaffinized, rehydrated again with ethanol, and finally stained on the slide [12]. The final slides were then studied using a microscope with a 1.3 MP digital camera. The level of the liver inflammation marker was studied as serum alanine aminotransferase activity was measured using HUMAN (Germany) kits and expressed as U/L.

Lipids from the liver tissues were extracted using the optimized method [10]. The DPPH radical scavenging activity of the liver lipids was determined with 0.1 mM diphenyl-1-picrylhydrazyl (DPPH) solution freshly prepared in methanol. For this purpose, 1.95 mL of the DPPH solution was mixed with 0.05 mL of the sample extract. The mixture was incubated for 30 min in a dark chamber. The absorbance of the mixture was recorded using a UV-visible spectrophotometer (Shimadzu Japan) at λ 515 nm against methanol blank. The RSA was calculated as % RSA.

2.10. Total Reduced Glutathione. Reduced glutathione from the liver was extracted using 10 mL of ice-cold metaphosphoric acid (3%). A sample extract of 0.5 mL was mixed with 5 μg of reduced glutathione, 1.5 mL of potassium sodium phosphate buffer (0.5 M, pH 8.0), and 0.03 mL of dithio nitrobenzene (DTNB). After 3 min of shaking, the absorbance of the sample was determined at 412 nm against the reference blank [22]. The amount of the total reduced glutathione was expressed as mmol/g.

Table 2: Effects of ellagic acid on the net changes in the whole body weight of the rabbits.

Duration (weeks)	Net body weight change (g)					
	Control	OT + 50EA	OT + 100EA	OT + 150EA	100EA	OT
1	0.0^{a}	36.3^{b}	-418.7^{c}	-443.3^{d}	-245.2^{e}	-48.5^{f}
2	26.3^{a}	22.3^{a}	-431.0^{b}	-471.3^{c}	-266.3^{d}	-62.3^{e}
3	37.3^{a}	5.66^{b}	-438.4^{c}	-511.7^{d}	-312.6^{e}	-84.3^{f}

Data are the mean of replicate ($n = 5$) readings and represented as the mean. Different letters (a-f) in the same week represent the significant difference at $\alpha = 0.05$ using Tukey's test. OT represents oxidized tallow; EA is ellagic acid; 50, 100, and 150 represent the respective dose amounts in mg per kg of rabbit body weight.

2.11. Glutathione S-Transferase Activity. The liver was also analyzed for glutathione S-transferase (GST) activity. Glutathione transferase is a highly selective hydrolyzing enzyme for detoxification of glutathione conjugates with different stressing or carcinogenic compounds. GST activity was measured using a 1-choloro-2,4-dinitrobenzene (CDNB) reagent with a concentration of 1 mmol/L. The extract (100 μL) prepared in ethanol and buffer was mixed with 100 μL CDNB, 100 μL of GSH, and 700 μL of potassium phosphate buffer (pH 7.5) [23]. The enzyme activity was expressed as unit/g.

2.12. Histology of the Heart. A rabbit heart was analyzed for histological studies. Briefly, a small section of the heart was dissected. The section was then fixed in formalin buffer (10%) for 14 h. The dissected section was then dehydrated with ethanol solutions and further embedded in paraffin. The sections (8-10 mm in thickness) were cut using a microtome, deparaffinized, rehydrated again with ethanol, and finally stained on the slide [24]. The final

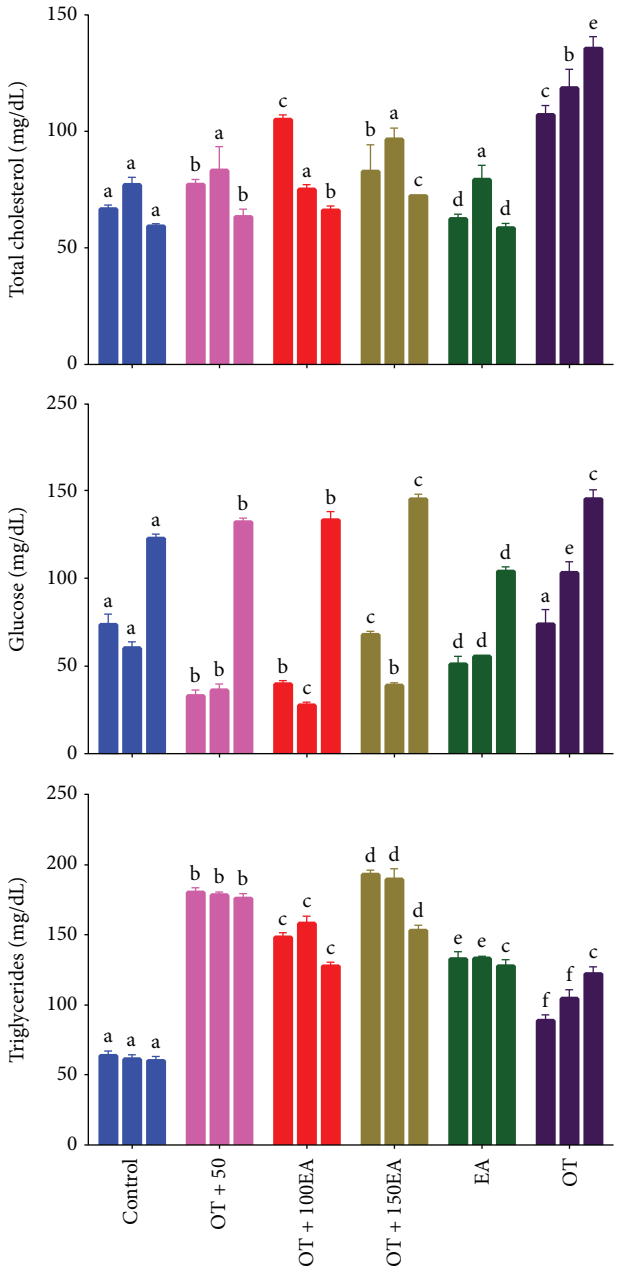

Figure 1: Effects of EA and OT alone or in combination on serum total cholesterol, glucose, and triglycerides. OT is oxidized tallow; EA is ellagic acid; 50, 100, and 150 are dose amounts in mg/kg. The three bars are weekly treatment starting from the left side. Different letters (a-f) in the same treatment week are a significant difference at $\alpha = 0.05$ using Tukey's test.

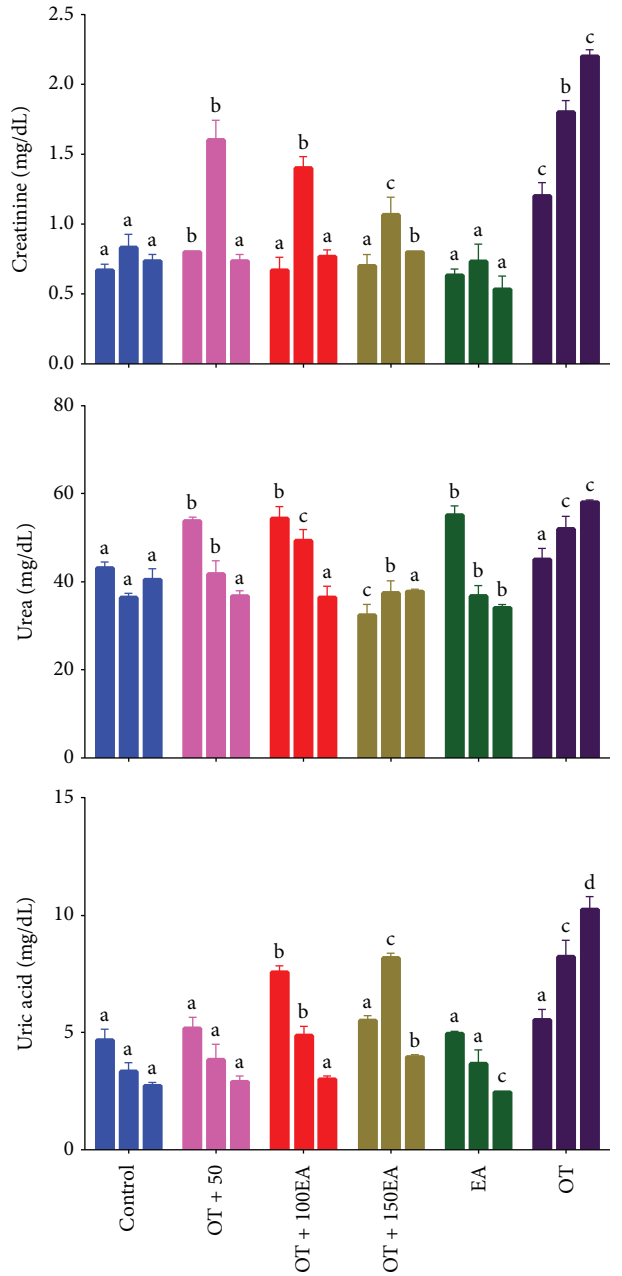

Figure 2: Effects of EA and OT alone or in combination on serum liver function tests. OT is oxidized tallow; EA is ellagic acid; 50, 100, and 150 are dose amounts in mg/kg. The three bars are weekly treatment starting from the left side. Different letters (a-d) in the same treatment week are a significant difference at $\alpha = 0.05$ using Tukey's test.

slides were then studied using a microscope with a 1.3 MP digital camera.

2.13. Statistical Analysis. Each parameter was repeated three to five times and was expressed as the mean with standard deviation. The data were evaluated for the statistical significance using one-way analysis of variance with the post hoc test of Tukey's at $\alpha = 0.05$ using GraphPad Prism 7.0 (GraphPad Software Inc., 2016).

3. Results and Discussion

3.1. Characterization of Tallow. Table 1 shows the peroxide values, TBARS, and radical scavenging activity of oxidized and control tallow. The peroxide value of the control tallow was 9.03 meq/kg and increased to 111.3 meq/kg upon oxidation. This showed that oxidation of tallow increased the PV of the tallow. The results are in agreement with findings [3, 6]. The increase in the PV may be due to the oxidation

Table 3: Effects of ellagic acid and oxidized tallow alone or in combination on the haematological parameters of rabbits.

Parameter	Control			OT + 50EA			OT + 100EA			OT + 150EA			100EA			OT		
	1	2	3	1	2	3	1	2	3	1	2	3	1	2	3	1	2	3
WBC (cells/μL) $\times 10^6$	5.53^a	7.23^b	7.16^b	6.93^b	6.03^a	5.86^a	6.7b	7.83^c	6.76b	6.1^a	5.86^a	6.16^a	9.23^d	7.16^b	8.03^f	6.0^a	5.3^a	5.2^a
LYM (%)	43.0^a	35.0^b	32.0^c	30.9^c	31.1^c	30.8^c	44.9a	40.9^a	39.2a	39.1^a	39.0^a	39.0^a	30.8^a	27.7^d	33.3^c	78.5^e	79.0^e	77.5^e
RBC (cells/μL) $\times 10^6$	5.12^a	5.40^a	5.09^a	4.9^b	5.34^a	4.91^b	3.90c	4.53^c	4.13c	5.13^a	4.36^b	4.79^b	5.01^b	4.97^b	5.69^a	5.27^a	5.94^a	5.39^a
HGB (g/dL)	11.4^a	12.0^a	12.0^a	11.5^a	11.9^a	12.4^a	9.96b	12.2^a	12.1a	11.3^a	9.9^b	8.73^b	10.7^a	10.7^a	10.7^a	11.2^a	12.4^a	12.2^a
HCT (%)	40.0^a	40.6^a	41.0^a	36.8^b	39.0^a	39.7^a	41.5a	41.5^a	40.7a	35.2^b	33.5^b	31.4^b	33.0^b	33.4^b	31.8^b	39.2^a	28.5^c	30.2^b
MCV (fL/cell)	65.5^a	68.4^a	68.9^a	68.1^a	68.8^a	67.3^a	66.6a	63.9^b	64.5a	61.0^b	64.3^a	61.8^b	59.5^b	60.0^b	60.4^b	63.3^b	64.0^b	63.4^b
MCH (pg/cell)	22.4^a	19.7^b	22.7^a	24.8^a	25.8^c	22.4^a	23.0a	23.8^a	21.6a	26.6^c	20.4^b	18.2^b	19.5^b	20.0^b	20.5^b	18.2^b	19.7^b	19.2^b
PLT (cells/μL) $\times 10^3$	3.57^a	3.39^a	2.58^b	2.49^b	2.75^b	2.47^b	2.06c	2.84^b	3.07b	2.10^c	1.75^c	1.74^c	2.17^c	2.04^c	2.14^c	2.45^b	2.47^b	2.56^b

Data are the mean of replicate ($n = 3$) readings and represented as the mean. Different superscript letters (a-e) in the same treatment week represent the significant difference at $\alpha = 0.01$ using Tukey's test. EA is ellagic acid; OT is oxidized tallow; 50, 100, and 150 represent the respective dose amounts in mg per kg of rabbit body weight. WBC: white blood cells; LYM: lymphocytes; RBC: red blood cells; HGB: haemoglobin; HCT: haematocrit; MCV: mean corpuscular volume; MCH: mean corpuscular haemoglobin; PLT: platelet count.

of triacylglycerols present in the tallow to form hydroperoxides, which are measured as PV values. Similarly, the TBARS value of the control tallow was 0.254 mmol/g and increased to 0.518 mmol/g on oxidation. However, the amount of TBARS was relatively very low as compared to the thermally oxidized edible oils under similar conditions of sunflower oil [25] and rapeseed oils [12]. The DPPH radical scavenging activity was 51.1% and decreased to 40.5% upon oxidation. The results are in agreement with previous findings [6]. There was a strong positive correlation coefficient ($R^2 = 0.9999$) between the increase in the PV and TBARS and a strong negative correlation ($R^2 = 0.9999$) between TBARS or PV and RSA values. The formation of peroxides and secondary oxidation compounds resulted in the reduction of antioxidant activity of the tallow.

Eight fatty acids were identified and quantified in the present work using total ion chromatogram (TIC) of GC-MS as shown in Table 1. It has been observed that tallow was rich in palmitic acid, i.e., 48.5 and 49.7 g/100 g, in control and oxidized tallow. Linoleic acid was 23.47 g/100 g and reduced to 18.7 g/100 g on oxidation. Stearic acid was the third most abundant fatty acid in the tallow, while margaric acid and myristic acid were placed on the fourth and fifth positions, respectively. The amount of palmitic acid was higher than that reported by Segura et al. [26], which was 25.7 g/100 g. The authors, however, reported a higher amount of stearic acid (26.7 g/100 g) than the present results. This might be due to the difference in the type of organism used for the extraction of tallow. The presence of a high amount of linoleic acid in tallow may be one of the contributing factors for specific taste and flavour of foods during frying.

3.2. Effects on Body Weight Change. Table 2 shows the comparison of the body weight change with respect to the control values of the first week. In control rabbits, the body weight increased to 26.3 g and 37.3 g in the third week. In the first week of the OT + 50EA group, there was a significant increase in the body weight, which was equal to the body weight in the third week of the control group. The values of the net weight change were reduced with treatment times in the second and third weeks, respectively. There was also a significant decrease in the whole body weight changes with supplementation of OT with 100 mg/kg of EA. The decrease in weight was recorded with respect to the time of treatment. Similarly, for OT with 150EA, body weight increased with treatment time. There was a significant decrease in the body weight by the supplementation of EA at a dose rate of 100 mg/kg and also in the case of OT. However, the EA showed significant weight loss as compared to the OT supplementation. These results suggested that ellagic acid significantly contributed to the weight loss in the rabbits. The antiglycative and antidiabetic properties of the ellagic acid [27] may be contributing to the body weight loss in rabbits.

3.3. Effects on Serum Biochemical Parameters. Figure 1 shows the effects of ellagic acid on the serum total triglycerides, total cholesterol, and serum glucose levels of rabbits administered against the oxidized tallow. Ellagic acid was found to increase the serum triglycerides and total cholesterols upon coadministration with oxidized tallow. The results are in agreement with those of Klingenberg et al. [28], who showed that supplementation of tallow and high oleic sunflower oil increased the serum total triglycerides and cholesterols. These results also confirm the previous findings from our lab [6], where it was shown that thermally oxidized tallow increased the serum lipids in rabbits. In the present work, it was suggested that ellagic acid induced the synthesis of triglycerides in the experimental animals. The reduction in the serum glucose by the ellagic acid alone or in combination with EA for two weeks may be attributed to the antidiabetic potential of the ellagic acid recently reported [29]. It was suggested that ellagic acid stimulates insulin secretion by the β-cells of the pancreas and ultimately decreases glucose intolerance.

3.4. Effects on Renal Function. Figure 2 shows the effects of ellagic acid on the serum renal function tests of rabbits administered against the oxidized tallow. It was observed that

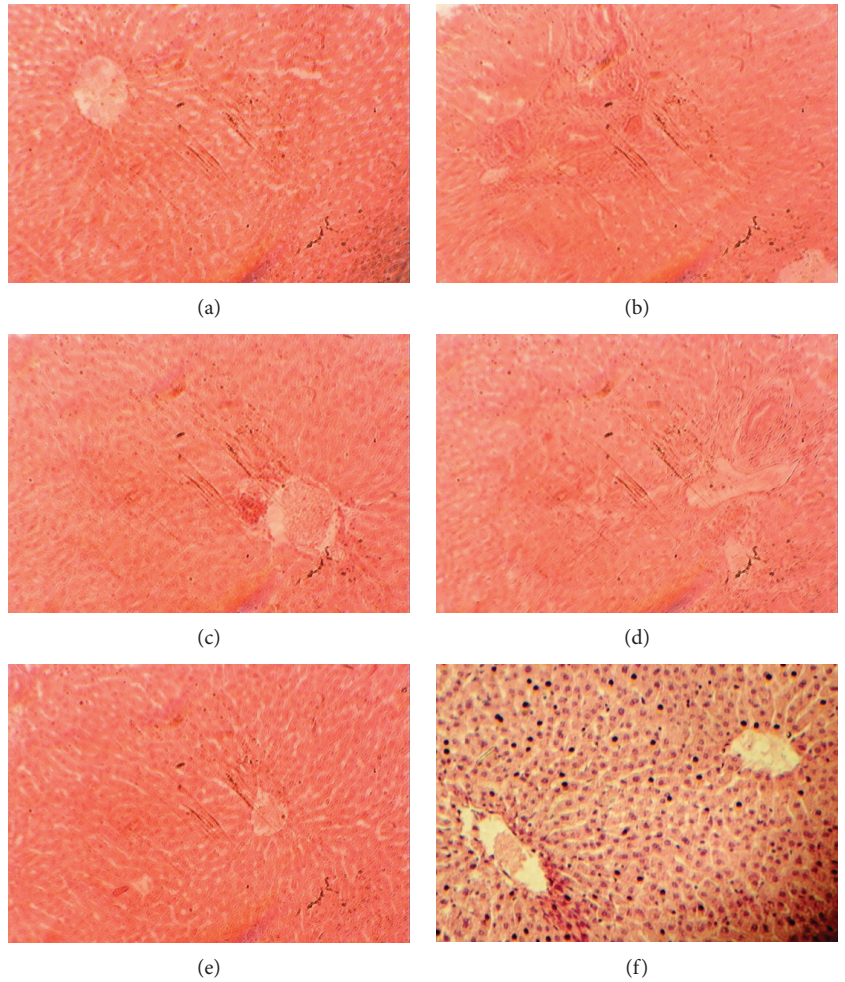

Figure 3: Effects of ellagic acid on the liver structure and function: (a) control, (b) OT + 50EA, (c) OT + 100EA, (d) OT + 150EA, (e) EA, and (f) OT. The pictures were documented at a magnification of 40x.

OT increased the serum creatinine, a marker of renal function, and was significantly reduced by ellagic acid. Similarly, serum urea and uric acid were also controlled by the cosupplementation of OT and EA in a dose-dependent manner. Atessahin et al. [30] showed that EA significantly reduced high plasma creatinine, urea, and calcium and also neutralized the harmful effects of cisplatin on oxidative stress markers. These authors also showed that EA improved cisplatin-induced pathological changes, which include tubular necrosis, degeneration, and tubular dilatation. They concluded that EA has a protective effect against cisplatin-induced oxidative stress and nephrotoxicity in rats, but the effects were not sufficient to prevent cisplatin-induced renal dysfunction. Similarly, Ahad et al. [31] showed that ellagic acid was protective for kidneys in diabetic rats partly through antihyperglycemia, which was believed to be accompanied by a reduction of inflammatory processes through inhibition of the NF-κB pathway system. Thus, it was concluded that EA is beneficial in renal function by controlling the oxidative stress induced by thermally oxidized lipids.

3.5. Effects on Haematological Indices. It has been observed that white blood cells (WBC) increased significantly with

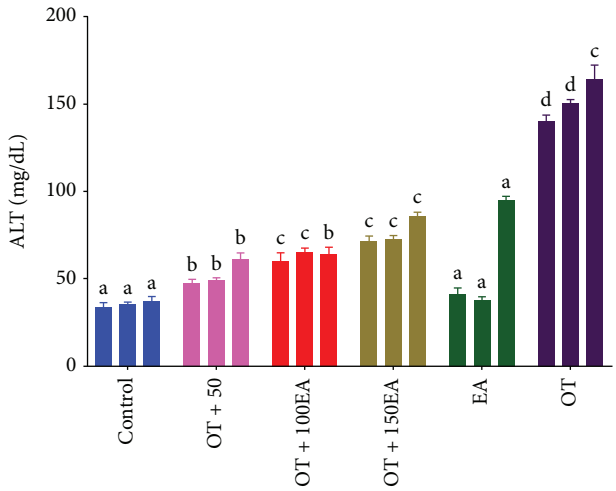

Figure 4: Effects of EA and OT alone or in combination on serum ALT levels. OT is oxidized tallow; EA is ellagic acid; 50, 100, and 150 are dose amounts in mg/kg. The three bars are weekly treatment starting from the left side. Different letters (a-d) in the same treatment week are a significant difference at $\alpha = 0.05$ using Tukey's test.

Table 4: Effects of ellagic acid supplementation against the oxidative stress induced by thermally oxidized tallow on the DPPH radical scavenging activity of the liver lipids.

Duration (weeks)	DPPH radical scavenging activity (%)					
	Control	OT + 50EA	OT + 100EA	OT + 150EA	100EA	OT
1	33.7 ± 2.6^{a}	47.7 ± 2.0^{b}	60.3 ± 4.4^{c}	71.3 ± 3.0^{d}	41.3 ± 3.3^{e}	23.7 ± 2.1^{f}
2	35.3 ± 1.2^{a}	49.3 ± 1.2^{b}	65.3 ± 2.0^{c}	72.7 ± 2.0^{d}	37.7 ± 2.0^{a}	25.2 ± 1.2^{e}
3	37.3 ± 2.4^{a}	61.3 ± 3.2^{b}	64.3 ± 3.6^{b}	76.0 ± 2.1^{c}	95.0 ± 2.1^{d}	27.3 ± 2.0^{e}

Data are the mean of replicate ($n = 5$) readings. Different superscript letters (a-f) in the same treatment week represent the significant difference at $\alpha = 0.05$ using Tukey's test. DPPH represents diphenyl-1-picrylhydrazyl; OT represents oxidized tallow; EA is ellagic acid; 50, 100, and 150 represent the respective dose amounts in mg per kg of rabbit body weight.

EA alone or in combination with OT and EA (Table 3). A significant decline was also observed in lymphocytes (LYM) in the OT + 50EA group, while no significant changes in other treated groups. Granulocytes (GRAN) and red blood cells (RBC) were not affected by any treatment. Haemoglobin was found to decrease only in the OT + 150EA group, while no significant changes were observed in other groups. Similarly, a significant decline was also observed in EA alone or in combination with 150EA in haematocrit (HCT) values. There was no significant difference in the amounts of MCV and MCH, respectively. Platelets were significantly lower in all treated groups as compared to the control. Zeb and Rahman [3] and Zeb and Haq [6] showed that oxidized tallow significantly affected different haematological parameters. Thus, remedies are needed such as tomato powder and sea buckhorn oil, while this study provides the beneficial properties of an ellagic acid. Chao et al. [32] showed that ellagic acid has anticoagulation properties in mice. This means that EA is beneficial for haematological parameters and ultimately the heart. Similarly, Ikewuchi et al. [33] reported that the plant consists of large amounts of ellagic acid ameliorates, haematological indices, and oxidative stress produced in alloxan-induced rats.

3.6. Effects on Liver Structure and Function. The liver of the control rabbits was of normal structure and function. The supplementation of OT induced inflammation and toxicity in the rabbit's liver (Figures 3(a)–3(f)). The OT also elevates serum ALT levels, which was controlled by the EA supplementation (Figure 4). The low dose of EA, i.e., 50 mg/kg, was more effective than other higher doses. Liver RSA was increased by the supplementation of EA (Table 4). It was also found that EA normalizes the negative effects and oxidative stress induced by dietary oxidized tallow on the function and architecture of the liver. Singh et al. [34] showed that ellagic acid provides protection against the carbon tetrachloride-induced hepatotoxicity in rats. Ellagic acid was also found to be protective against the toxicity produced by paracetamol in rats [35] and was much better in CCl_4-induced toxicity [36]. The present study was also in accordance with the study reported by Kannan and Quine [14], who showed that EA significantly ameliorates the toxic properties of isoproterenol in rats. The authors also reported that EA increased the antioxidant enzyme system of the liver.

3.7. Effects on Reduced Glutathione. Reduced glutathione (GSH) level is highly important for studying the oxidative

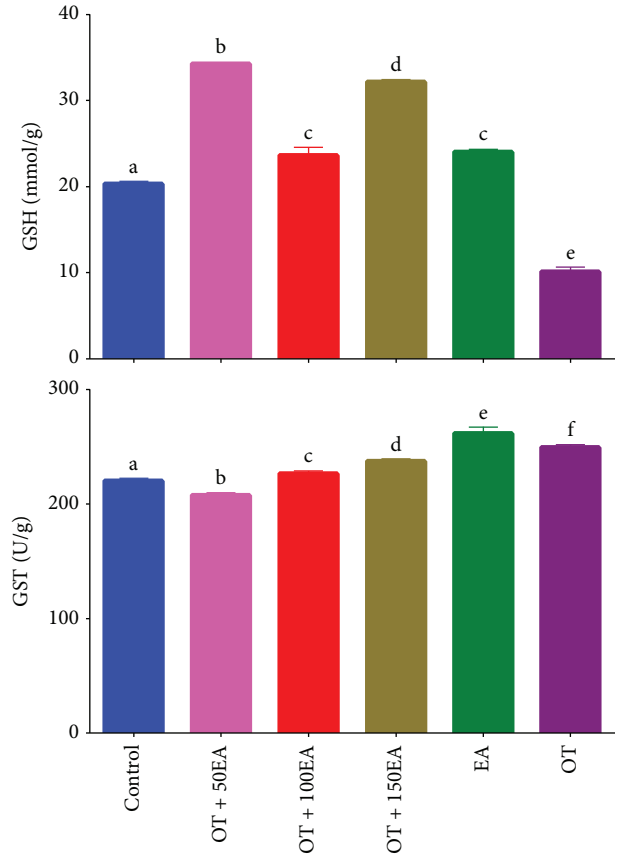

Figure 5: Effects of EA and OT alone or in combination on serum GSH & GST levels. OT is oxidized tallow; EA is ellagic acid; 50, 100, and 150 are dose amounts in mg/kg. Different letters (a-f) in the same parameter are a significant difference at $\alpha = 0.05$ using Tukey's test.

stress on the biological system. Glutathione is a tripeptide with strong biological antioxidant properties. The effects of ellagic acid and oxidized tallow on the reduced glutathione (GSH) levels of the rabbit's liver have been presented. The amount of GSH was 20.3 mmol/g and significantly reduced to 10.2 mmol/g in an OT-fed rabbit's liver (Figure 5). The amount of GSH in the EA-fed group was close to the values of OT with 100EA. Similarly, the amounts of GSH in the OT + 50EA and the OT + 150EA groups were similar. Arafat et al. [37] showed that EA protected the liver and increased the amount of GSH in the liver. Similarly, El-Shitany et al. [38] also showed that EA enhanced the production of GSH

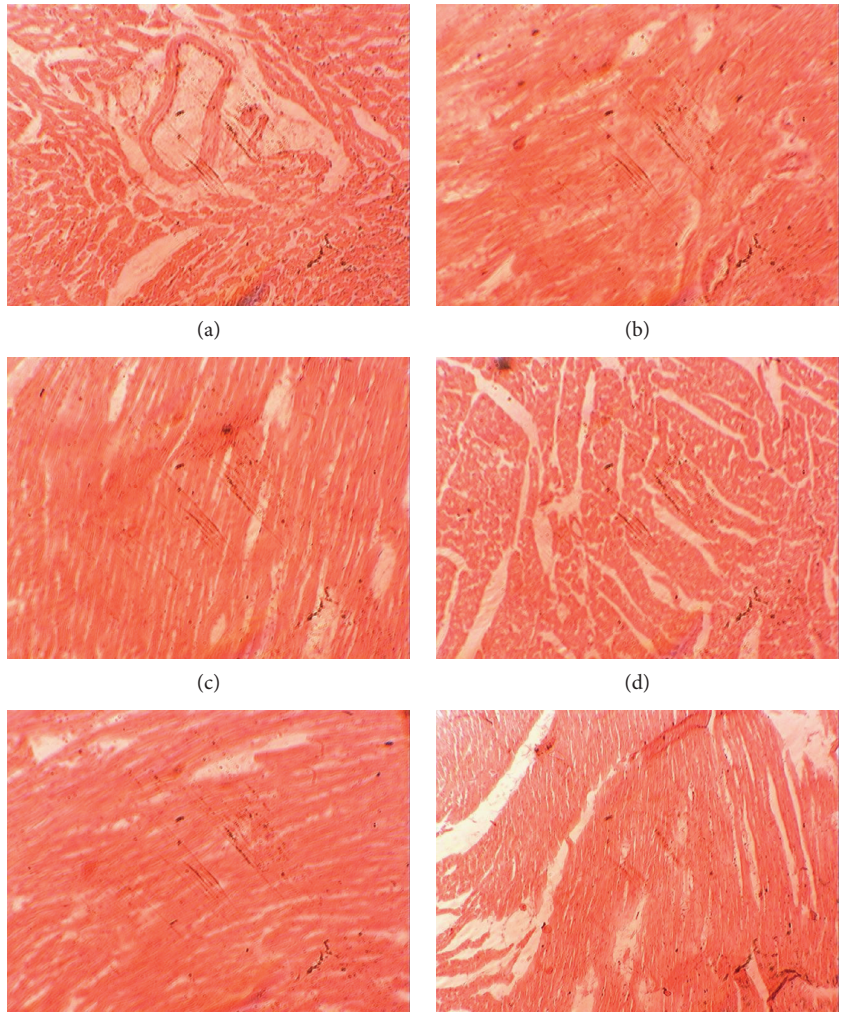

Figure 6: Effects of ellagic acid and oxidized tallow alone or in combination on the histology of the rabbit heart: (a) control, (b) OT + 50EA, (c) OT + 100EA, (d) OT + 150EA, (e) EA, and (f) OT. The pictures were documented at a magnification of 40x.

and consequently the oxidative stress. These results showed that oxidative stress produced by the dietary oxidized lipids can also be counteracted by ellagic acid.

3.8. Glutathione S-Transferase Activity. Glutathione S-transferase (GST) is a highly selective group of enzymes, which are required for the detoxification of foreign chemicals such as dietary oxidized lipids. The liver is the main site for the activity of this enzyme. Figure 5 shows the effects of ellagic acid and thermally oxidized tallow on the GST activity of the rabbit's liver. It was observed that the control group has a GST activity of 220.7 U/g of the tissue, which was significantly increased with the supplementation of OT. The activity was also found to rise by EA alone, which was higher than the OT group. There were no significant changes in the activity levels in the OT with the EA groups except in the OT + 50EA group, where the amount was lower than control levels. Previous results showed that EA enhanced the production of GST of the liver in nickel-induced oxidative stressed rats [39]. Pari and Sivasankari [40] also reported the increase in the GST of the liver, which was depleted by cyclosporine A in rats. Thus, an increase in the GST activity of the liver was due to the supplementation of EA to rabbits.

3.9. Effects on Histology of the Heart. In control rabbits, there was a normal heart structure and function, while the OT + 50EA group revealed mild toxicity or myocarditis. No significant changes were observed in the OT + 100EA group, while the OT + 150EA group showed mild toxicity or myocarditis (Figure 6). This showed that lower doses of EA were protective for the heart against the OT-induced toxicity. Larrosa et al. [41] reviewed that ellagic acid is beneficial for vascular health. Similarly, ellagic acid was found to inhibit the myocardial necrosis and infarction induced by isoproterenol in rats [14] by protecting the mitochondria of the heart cells [42, 43]. It was also found that dietary ellagic acid provides protection against oxidant-induced endothelial dysfunction and atherosclerosis partly via Nrf2 activation [44]. Thus, it was suggested that EA was protective in the dose range of 50-100 mg/kg for the heart against the oxidative stress in the cardiovascular system produced by dietary oxidized tallow in rabbits.

4. Conclusions

Results revealed that PV and TBARS increased, while RSA of the tallow decreased significantly with oxidation at 180°C in an open fryer. A total of eight fatty acids were quantified in the tallow; palmitic acid, stearic acid, linoleic acid, margaric acid, and myristic acid were the major fatty acids. Animal studies showed that OT alone or in combination with EA significantly alters the body weight of the rabbits. Serum biochemical parameters and renal function tests were affected by OT and ameliorated by EA. The toxic effects of OT on haematological indices were minimized by EA. The supplementation of OT alone had significant effects on the liver structure and functions. The coadministration of EA reduced the toxic properties of OT on the liver, by increasing the antioxidant (GSH) system. The rabbit heart was also affected by the OT, while no significant effects were observed by the EA supplementation up to a dose rate of 100 mg/kg, suggesting an ameliorative effect at low doses of EA. These results suggested that the supplementation of EA was beneficial against the OT-induced oxidative stress and may be considered for foods containing oxidized lipids. Studies are therefore required to explore the sources of ellagic acid in different unexplored plants and its uses in food industries.

Data Availability

The data used to support the findings of this study are available from the corresponding author upon request.

Conflicts of Interest

The authors declare no conflict of interests regarding the publication of this paper.

Acknowledgments

The work was kindly financed by the Higher Education Commission (HEC) project no. 2344 under National Research Program for Universities (NRPU). This work was supported by TUG Open Access Publishing Fund.

Supplementary Materials

Figure: representative total ion chromatogram (TIC) of fatty acids using GC-MS of tallow: (A) control tallow and (B) oxidized tallow. *(Supplementary Materials)*

References

[1] A. Zeb, "Chemistry and liquid chromatography methods for the analyses of primary oxidation products of triacylglycerols," *Free Radical Research*, vol. 49, no. 5, pp. 549–564, 2015.

[2] J. T. Handa, M. Cano, L. Wang, S. Datta, and T. Liu, "Lipids, oxidized lipids, oxidation-specific epitopes, and age-related macular degeneration," *Biochimica et Biophysica Acta*, vol. 1862, no. 4, pp. 430–440, 2017.

[3] A. Zeb and W. U. Rahman, "Effects of oxidized tallow on the rabbit serum lipids and antioxidant activity of the in-vitro lipids," *Toxicological Research*, vol. 28, no. 3, pp. 151–157, 2012.

[4] J. Gutierrez, S. W. Ballinger, V. M. Darley-Usmar, and A. Landar, "Free radicals, mitochondria, and oxidized lipids: the emerging role in signal transduction in vascular cells," *Circulation Research*, vol. 99, no. 9, pp. 924–932, 2006.

[5] A. Zeb and S. Hussain, "Sea buckthorn seed powder provides protection in the oxidative stress produced by thermally oxidized sunflower oil in rabbits," *Journal of Food Biochemistry*, vol. 38, no. 5, pp. 498–508, 2014.

[6] A. Zeb and I. Haq, "The protective role of tomato powder in the toxicity, fatty infiltration and necrosis induced by oxidized tallow in rabbits," *Journal of Food Biochemistry*, vol. 40, no. 4, pp. 428–435, 2016.

[7] P.-M. Chao, C.-Y. Chao, F.-J. Lin, and C.-j. Huang, "Oxidized frying oil up-regulates hepatic acyl-CoA oxidase and cytochrome P450 4 A1 genes in rats and activates PPARα," *The Journal of Nutrition*, vol. 131, no. 12, pp. 3166–3174, 2001.

[8] P.-M. Chao, S.-C. Hsu, F.-J. Lin, Y.-J. Li, and C.-j. Huang, "The up-regulation of hepatic acyl-coA oxidase and cytochrome P450 4A1 mRNA expression by dietary oxidized frying oil is comparable between male and female rats," *Lipids*, vol. 39, no. 3, pp. 233–238, 2004.

[9] C.-H. Liao, H.-M. Shaw, and P.-M. Chao, "Impairment of glucose metabolism in mice induced by dietary oxidized frying oil is different from that induced by conjugated linoleic acid," *Nutrition*, vol. 24, no. 7-8, pp. 744–752, 2008.

[10] A. Zeb and A. Mehmood, "Effects of oxidized vanaspati ghee on the serum lipids profile and radical scavenging activity of the in vitro lipids of liver, brain and muscles," *Turkish Journal of Biochemistry*, vol. 37, no. 4, pp. 417–423, 2012.

[11] A. Zeb and S. Ullah, "Sea buckthorn seed oil protects against the oxidative stress produced by thermally oxidized lipids," *Food Chemistry*, vol. 186, no. 1, pp. 6–12, 2015.

[12] A. Zeb and S. U. Rahman, "Protective effects of dietary glycine and glutamic acid toward the toxic effects of oxidized mustard oil in rabbits," *Food and Function*, vol. 8, no. 1, pp. 429–436, 2017.

[13] V. Vijaya Padma, P. Kalai Selvi, and S. Sravani, "Protective effect of ellagic acid against TCDD-induced renal oxidative stress: modulation of CYP1A1 activity and antioxidant defense mechanisms," *Molecular Biology Reports*, vol. 41, no. 7, pp. 4223–4232, 2014.

[14] M. M. Kannan and S. D. Quine, "Ellagic acid ameliorates isoproterenol induced oxidative stress: evidence from electrocardiological, biochemical and histological study," *European Journal of Pharmacology*, vol. 659, no. 1, pp. 45–52, 2011.

[15] A. Galano, R. Castañeda-Arriaga, A. Pérez-González, D.-X. Tan, and R. Reiter, "Phenolic melatonin-related compounds: their role as chemical protectors against oxidative stress," *Molecules*, vol. 21, no. 11, p. 1442, 2016.

[16] B. Baek, S. H. Lee, K. Kim, H. W. Lim, and C. J. Lim, "Ellagic acid plays a protective role against UV-B-induced oxidative stress by up-regulating antioxidant components in human dermal fibroblasts," *Korean Journal of Physiology and Pharmacology*, vol. 20, no. 3, pp. 269–277, 2016.

[17] A. Zeb, "Ellagic acid in suppressing in vivo and in vitro oxidative stresses," *Molecular and Cellular Biochemistry*, vol. 448, no. 1-2, pp. 27–41, 2018.

[18] D. Zheng and M. A. Hanna, "Preparation and properties of methyl esters of beef tallow," *Bioresource Technology*, vol. 57, no. 2, pp. 137–142, 1996.

[19] D. Firestone, *Official Methods and Recommended Practices of the American Oil Chemists' Society*, AOCS Champaign, IL, USA, 1998.

[20] A. Zeb and F. Ullah, "A simple spectrophotometric method for the determination of thiobarbituric acid reactive substances in fried fast foods," *Journal of Analytical Methods in Chemistry*, vol. 2016, Article ID 9412767, 5 pages, 2016.

[21] M. Sakthivel, R. Elanchezhian, E. Ramesh et al., "Prevention of selenite-induced cataractogenesis in Wistar rats by the polyphenol, ellagic acid," *Experimental Eye Research*, vol. 86, no. 2, pp. 251–259, 2008.

[22] C. W. I. Owens and R. V. Belcher, "A colorimetric micro-method for the determination of glutathione," *Biochemical Journal*, vol. 94, no. 3, pp. 705–711, 1965.

[23] M. Habdous, M. Vincent-Viry, S. Visvikis, and G. Siest, "Rapid spectrophotometric method for serum glutathione S-transferases activity," *Clinica Chimica Acta*, vol. 326, no. 1-2, pp. 131–142, 2002.

[24] S. F. Nagueh, H. A. Kopelen, D.-S. Lim et al., "Tissue Doppler imaging consistently detects myocardial contraction and relaxation abnormalities, irrespective of cardiac hypertrophy, in a transgenic rabbit model of human hypertrophic cardiomyopathy," *Circulation*, vol. 102, no. 12, pp. 1346–1350, 2000.

[25] A. Zeb and P. Nisar, "Effects of high temperature frying of spinach leaves in sunflower oil on carotenoids, chlorophylls, and tocopherol composition," *Frontiers in Chemistry*, vol. 5, article 19, 2017.

[26] N. Segura, R. C. da Silva, F. A. S. de M. Soares, L. Antonio Gioielli, and I. Jachmanián, "Valorization of beef tallow by lipase-catalyzed interesterification with high oleic sunflower oil," *Journal of the American Oil Chemists' Society*, vol. 88, no. 12, pp. 1945–1954, 2011.

[27] C. Y. Chao, M. C. Mong, K. C. Chan, and M. C. Yin, "Anti-glycative and anti-inflammatory effects of caffeic acid and ellagic acid in kidney of diabetic mice," *Molecular Nutrition and Food Research*, vol. 54, no. 3, pp. 388–395, 2010.

[28] I. L. Klingenberg, D. A. Knabe, and S. B. Smith, "Lipid metabolism in pigs fed beef tallow or high-oleic acid sunflower oil," *Comparative Biochemistry and Physiology Part B: Biochemistry and Molecular Biology*, vol. 110, no. 1, pp. 183–192, 1995.

[29] N. Fatima, R. M. Hafizur, A. Hameed, S. Ahmed, M. Nisar, and N. Kabir, "Ellagic acid in Emblica officinalis exerts anti-diabetic activity through the action on β-cells of pancreas," *European Journal of Nutrition*, vol. 56, no. 2, pp. 591–601, 2017.

[30] A. Atessahin, A. O. Ceribasi, A. Yuce, O. Bulmus, and G. Cikim, "Role of ellagic acid against cisplatin-induced nephrotoxicity and oxidative stress in rats," *Basic & Clinical Pharmacology & Toxicology*, vol. 100, no. 2, pp. 121–126, 2006.

[31] A. Ahad, A. A. Ganai, M. Mujeeb, and W. A. Siddiqui, "Ellagic acid, an NF-κB inhibitor, ameliorates renal function in experimental diabetic nephropathy," *Chemico-Biological Interactions*, vol. 219, pp. 64–75, 2014.

[32] P. C. Chao, C. C. Hsu, and M. C. Yin, "Anti-inflammatory and anti-coagulatory activities of caffeic acid and ellagic acid in cardiac tissue of diabetic mice," *Nutrition and Metabolism*, vol. 6, no. 1, p. 33, 2009.

[33] J. C. Ikewuchi, E. N. Onyeike, A. A. Uwakwe, and C. C. Ikewuchi, "Effect of aqueous extract of the leaves of Acalypha wilkesiana 'Godseffiana' Muell Arg (Euphorbiaceae) on the hematology, plasma biochemistry and ocular indices of oxidative stress in alloxan induced diabetic rats," *Journal of Ethnopharmacology*, vol. 137, no. 3, pp. 1415–1424, 2011.

[34] K. Singh, A. K. Khanna, P. K. Visen, and R. Chander, "Protective effect of ellagic acid on t-butyl hydroperoxide induced lipid peroxidation in isolated rat hepatocytes," *Indian Journal of Experimental Biology*, vol. 37, no. 9, pp. 939-940, 1999.

[35] C. Girish, B. C. Koner, S. Jayanthi, K. Ramachandra Rao, B. Rajesh, and S. C. Pradhan, "Hepatoprotective activity of picroliv, curcumin and ellagic acid compared to silymarin on paracetamol induced liver toxicity in mice," *Fundamental & Clinical Pharmacology*, vol. 23, no. 6, pp. 735–745, 2009.

[36] C. Girish, B. C. Koner, S. Jayanthi, K. Ramachandra Rao, B. Rajesh, and S. C. Pradhan, "Hepatoprotective activity of picroliv, curcumin and ellagic acid compared to silymarin on paracetamol induced liver toxicity in mice," *The Journal of Pharmacy and Pharmacology*, vol. 23, no. 6, pp. 735–745, 2012.

[37] S. Y. Arafat, M. Nayeem, S. Jahan et al., "Ellagic acid rich Momordica charantia fruit pulp supplementation prevented oxidative stress, fibrosis and inflammation in liver of alloxan induced diabetic rats," *Oriental Pharmacy and Experimental Medicine*, vol. 16, no. 4, pp. 267–278, 2016.

[38] N. A. El-Shitany, E. A. El-Bastawissy, and K. El-desoky, "Ellagic acid protects against carrageenan-induced acute inflammation through inhibition of nuclear factor kappa B, inducible cyclooxygenase and proinflammatory cytokines and enhancement of interleukin-10 via an antioxidant mechanism," *International Immunopharmacology*, vol. 19, no. 2, pp. 290–299, 2014.

[39] S. Ahmed, A. Rahman, M. Saleem, M. Athar, and S. Sultana, "Ellagic acid ameliorates nickel induced biochemical alterations: diminution of oxidative stress," *Human & Experimental Toxicology*, vol. 18, no. 11, pp. 691–698, 1999.

[40] L. Pari and R. Sivasankari, "Effect of ellagic acid on cyclosporine A-induced oxidative damage in the liver of rats," *Fundamental & Clinical Pharmacology*, vol. 22, no. 4, pp. 395–401, 2008.

[41] M. Larrosa, M. T. Garcia-Conesa, J. C. Espin, and F. A. Tomas-Barberan, "Ellagitannins, ellagic acid and vascular health," *Molecular Aspects of Medicine*, vol. 31, no. 6, pp. 513–539, 2010.

[42] M. M. Kannan and S. D. Quine, "Ellagic acid inhibits cardiac arrhythmias, hypertrophy and hyperlipidaemia during myocardial infarction in rats," *Metabolism*, vol. 62, no. 1, pp. 52–61, 2013.

[43] M. M. Kannan and S. D. Quine, "Mechanistic clues in the protective effect of ellagic acid against apoptosis and decreased mitochondrial respiratory enzyme activities in myocardial infarcted rats," *Cardiovascular Toxicology*, vol. 12, no. 1, pp. 56–63, 2012.

[44] Y. Ding, B. Zhang, K. Zhou et al., "Dietary ellagic acid improves oxidant-induced endothelial dysfunction and atherosclerosis: role of Nrf2 activation," *International Journal of Cardiology*, vol. 175, no. 3, pp. 508–514, 2014.

Hindawi
Oxidative Medicine and Cellular Longevity
Volume 2018, Article ID 9765027, 13 pages
https://doi.org/10.1155/2018/9765027

Research Article

ALDH2 Activity Reduces Mitochondrial Oxygen Reserve Capacity in Endothelial Cells and Induces Senescence Properties

G. Nannelli,[1] E. Terzuoli,[1] V. Giorgio,[2,3] S. Donnini,[1] P. Lupetti,[1] A. Giachetti,[1] P. Bernardi,[2,3] and M. Ziche[1]

[1]*Department of Life Sciences, University of Siena, Siena, Italy*
[2]*Department of Biomedical Sciences, University of Padua, Padua, Italy*
[3]*Consiglio Nazionale delle Ricerche, Neuroscience Institute, Padua, Italy*

Correspondence should be addressed to M. Ziche; marina.ziche@unisi.it

Received 21 May 2018; Revised 31 August 2018; Accepted 9 September 2018; Published 14 November 2018

Academic Editor: Márcio Carocho

Endothelial cells (ECs) are dynamic cells that turn from growth into senescence, the latter being associated with cellular dysfunction, altered metabolism, and age-related cardiovascular diseases. Aldehyde dehydrogenase 2 (ALDH2) is a mitochondrial enzyme metabolizing acetaldehyde and other toxic aldehydes, such as 4-hydroxynonenal (4-HNE). In conditions in which lipid peroxidation products and reactive oxygen species (ROS) are accumulated, ECs become dysfunctional and significantly contribute to the progression of vascular-dependent diseases. The aim of the present study has been to investigate whether inhibition of ALDH2 alters endothelial functions together with the impairment of bioenergetic functions, accelerating the acquisition of a senescent phenotype. HUVECs transfected with siRNA targeting ALDH2 or treated with daidzin, an ALDH2 inhibitor, were used in this study. We observed an alteration in cell morphology associated with endothelial dysfunctions. Loss of ALDH2 reduced cell proliferation and migration and increased paracellular permeability. To assess bioenergetic function in intact ECs, extracellular flux analysis was carried out to establish oxygen consumption rates (OCR). We observed a decrease in mitochondrial respiration and reserve capacity that coincided with SA-β-Gal accumulation and an increase in p21 and p53 expression in siALDH2 or daidzin-treated HUVECs. Treatment with N-acetyl-L-cysteine (NAC) reduced endothelial dysfunctions mediated by siALDH2, indicating that oxidative stress downstream to siALDH2 plays an instrumental role. Our results highlight that ALDH2 impairment accelerates the acquisition of a premature senescent phenotype, a change likely to be associated with the observed reduction of mitochondrial respiration and reserve capacity.

1. Introduction

The aging process reflects the age-dependent functional decline of body tissues and organs [1]. The progressive decline also affects the vascular endothelium, resulting in an impairment of its important functions such as the capacity to supply nutrients and growth factors to organs, the barrier function, and the capacity to form new vessels or angiogenesis [2, 3]. Vascular cell senescence is widely considered one of the causative factors of peripheral and central nervous system pathologies [4], as it promotes reactive oxygen species (ROS) production and the ensuing vascular inflammatory responses [5]. For instance, frequent stroke episodes in patients affected by cerebral amyloid angiopathy (CAA) are related to the perivascular deposition of amyloid beta peptides (Aβ), which promote ROS production and, in turn, reduce endothelial cell (EC) responsiveness. Similarly, in MELAS, a disease characterized by encephalomyopathy, high ROS levels, derived from dysfunctional mitochondria, compromise EC-mediated vasodilatation, which explains the susceptibility of these patients to stroke-like episodes [6–8]. Besides increased ROS production, nine hallmarks have been proposed to contribute to the aging phenotype, including the phenomenon of cellular senescence as a stable arrest of cell cycle coupled with phenotypic changes, mitochondrial dysfunction, and activation of the p53 pathway [1].

Even though ECs appear to meet most of their energy needs anaerobically, they have an extensive mitochondrial

network and consume oxygen. Their mitochondria are essential to endothelial functions [9–11]. It is broadly accepted that, as cells are exposed to stressors, mitochondria are able to rely on a "reserve capacity," referred to as the difference between the maximum respiratory capacity and the basal respiratory capacity. This reserve capacity is suitable to provide the increased energy demands to preserve cellular functions and repair or detoxification of reactive species [11, 12].

In this study, we sought to gain insights into the role of endothelial mitochondria in the senescence process, taking advantage of the recent progress gathered on the role of aldehyde dehydrogenases (ALDHs), particularly ALDH2 isozyme (one of 19 enzymes belonging to the same superfamily). The ALDH2 isozyme is located in the mitochondrial matrix and is predominantly responsible for the acetaldehyde detoxification in alcohol metabolism. It is also a key to detoxification of endogenous aldehydes, such as 4-hydroxy-2-nonenal (4-HNE), which arise from lipid peroxidation under oxidative stress, and of exogenous aldehyde products, such as acrolein from tobacco smoke and car exhausts [13, 14]. Increasing evidence has revealed a cardioprotective and neuroprotective role of ALDH2 in myocardial ischemia-reperfusion injury and Aβ-induced damage, respectively. Studies from our laboratory have provided evidence on the contribution of ALDH2 to Aβ-induced endothelial dysfunction and on the possibility of preserving the endothelial function in some pathological conditions by activating the ALDH2 enzyme [15]. In this study, we focused on ALDH2 and its role as a critical metabolic checkpoint for endothelial function. The aim of the study was to move beyond correlative analyses between ALDH2 and hallmarks of aging, providing causal evidence of the implication of ALDH2 in endothelial senescence.

2. Materials and Methods

2.1. Cell Cultures. Human umbilical vein endothelial cells (HUVECs) (Lonza, Basel, Switzerland) were used. Cells were cultured on gelatin-coated dishes with endothelial growth medium (EGM-2) (Lonza) supplemented with antibiotics (100 U/ml penicillin and 100 μg/ml streptomycin, Euroclone, Milan, Italy), glutamine (2 mM, Euroclone), and 10% fetal bovine serum (FBS, Hyclone, GE Healthcare, Little Chalfont, UK). Progressively passaged HUVECs were utilized up to senescence as already described [16]. The formula PD = (ln n_{ch} − ln n_{cs})/ln 2 was used to calculate the number of cumulative population doublings (PD), where n_{ch} is the number of cells harvested and n_{cs} is the number of cells seeded.

2.2. Small Interfering RNA Transfection. Transient knockdown experiments were performed using control and specific siRNAs (OriGene, Rockville, MD, USA). Subconfluent cells were seeded in 60 mm or 100 mm or 6-well plate dishes in EGM-2 plus 10% FBS. After 24 h, cells were transfected in endothelial basal medium (EBM-2) without serum and antibiotics using Lipofectamine® 3000 (Invitrogen, Carlsbad, CA, USA) and 20 nM targeting siRNA (siALDH2) or scrambled control siRNA (siCTR) diluted in Opti-MEM (Gibco, Thermo Fisher Scientific, Waltham, MA, USA). Serum was added 6–8 h posttransfection. Where indicated, cells were harvested 24 h posttransfection. Cells were assayed 2–6 days posttransfection. The transfection was repeated every 72 h. We evaluated the knockdown efficiency using immunoblotting or quantitative RT-PCR (qRT-PCR) analysis at the indicated time.

2.3. Immunoblot Analysis. Subconfluent cells were plated in 60 mm or 100 mm or 6-well plate gelatin-coated dishes and transfected as above or treated with 10 μM daidzin, for 48 h. Daidzin was dissolved in DMSO (Sigma-Aldrich). The treatment with daidzin was repeated every day. Where indicated, siCTR and siALDH2 HUVECs have been pretreated with 5 mM N-acetyl-L-cysteine (NAC), as reported [17]. Next, cells were washed and lysed, and an equal amount of proteins was used for immunoblot analysis, as described [15]. The blotted membranes were incubated with anti-ALDH2 (OriGene), anti-p21, anti-Egr-1, anti-c-Myc (Cell Signaling Technology, Danvers, MA, USA), anti-tubulin, anti-p53 (Santa Cruz, Heidelberg, Germany), anti-β-actin (Sigma-Aldrich), anti-4-HNE (Abcam, Cambridge, United Kingdom), and OXPHOS antibody cocktail kit (Abcam) antibodies. Super-Signal West Pico Chemiluminescent Substrate (Thermo Fisher Scientific) was used to develop signals, which were detected and quantified by the ChemiDoc system and Quantity One software (Bio-Rad, Hercules, CA, USA). For all experiments using whole-cell lysate, β-actin or β-tubulin was used as loading controls.

2.4. Real-Time PCR. The RNeasy Plus Kit (Qiagen, Hilden, Germany) was used according to the manufacturer's instructions to extract and prepare total RNA. A total amount of 1 μg RNA was transcribed, and quantitative RT-PCR was performed as reported [18]. The fold change expression was determined using the comparative Ct method (ΔΔCt) normalized to 60S ribosomal protein L19 expression. Data are reported as fold change relative to siCTR (control), which was set to 1.

2.5. ALDH Enzymatic Activity. The conversion of acetaldehyde to acetic acid was determined in order to evaluate ALDH enzyme activity, as reported [15]. Briefly, 1×10^6 of seeded cells were transfected as described above, and after 48 h, cells were scraped into 100 μl of CelLytic™ MT Cell Lysis (Sigma-Aldrich) supplied with protease inhibitors (Sigma-Aldrich) and sodium orthovanadate (Sigma-Aldrich). Then, lysates were centrifuged for 20 min at 4°C at 14000 × g. The protein content in the supernatant was quantified in a Bradford assay. ALDH2 activity was measured in an assay mix (0.8 ml) containing 100 mM sodium pyrophosphate (Sigma-Aldrich) at pH 9 and 10 mM NAD+ (Sigma-Aldrich) and 300 μg of sample protein. Then, acetaldehyde (10 mM, Sigma-Aldrich) was added to the cuvette to start the reaction. NADH formation from NAD+ was monitored at 25°C in a spectrophotometer Infinite F200 Pro at 340 nm (Tecan Life Sciences, Switzerland). Where indicated, supernatants of HUVECs were challenged with daidzin for 10 min before the acetaldehyde was added; the compound was tested at 1 and 10 μM to monitor the extent of ALDH

inhibition in these cell lysates. Enzyme-specific activity was expressed as % nmol NADH/minute/mg protein.

2.6. Cell Survival and Area. Cells were transfected with siRNA for ALDH2 as described above. Then, cells were harvested and seeded (1.5×10^3/well) in triplicate in 96-multiwell plates. Adherent cells were exposed to EBM-2 with 2% FBS for 2 and 5 days. Where indicated, HUVECs were treated with 5 mM NAC (Sigma-Aldrich) before the administration of 2% FBS. This treatment was repeated every three days. Further, HUVECs were also pretreated for 30 min with 10 μM daidzin in EBM-2 before the administration of 2% FBS for 2 or 5 days. Then, cells were fixed and stained with the PanReac kit (Darmstadt, Germany), and five fields per well were counted. Data are analyzed in triplicate, and results are expressed as the cell number counted/well. To calculate the area of cells, three fields in which cells were at 60% confluence for each condition were measured using ImageJ software and results are expressed as square pixel.

2.7. Senescence-Associated β-Galactosidase (SA-β-Gal) Activity Assay. Cells were seeded in 6-well multiplates (8×10^4 or 1.5×10^5 cells/well). Adherent cells were treated with 10 μM daidzin for 2 days or transfected with siRNA as described above. Where indicated, 24 h posttransfection, a preincubation of 30 min with 5 mM NAC was carried out before the administration of 2% FBS. This treatment was repeated every three days. At 2 and 6 days, SA-β-Gal activity was assessed by using the Senescence β-Galactosidase Staining Kit (Cell Signaling) following the manufacturer's manual. Data are reported as a fold increase vs. siCTR of positive cells for SA-β-Gal activity.

2.8. BrdU Incorporation Assay. Cell proliferative capacity was evaluated using a chemiluminescence ELISA (Roche Diagnostic S.p.A, Monza, Italy) which assesses the 5-bromo-2′-deoxy-uridine (BrdU) incorporation. 3×10^3 cells were seeded in a 96-well plate in triplicate 24 h posttransfection. Adherent cells were exposed to EBM-2 in the presence or absence of serum (2% and 0.1% FBS, respectively) for 48 h. 8 hours before the end of incubation, BrdU was added in each well. Then, the assay was carried out as reported [18].

2.9. Wound Healing Assay. siRNA transfection of adherent cells was conducted as described above, and after 24 h, cells were harvested. siCTR, siALDH2, and wild-type HUVECs were seeded (1×10^5 cells/well) into 24-well plates and incubated until they were grown into a confluent monolayer (24–30 h). Then, a sterile 100–1000 μl micropipette tip was used to scrape the confluent monolayer and create a wound $\pm$ 500 μm. The cells were washed twice with PBS and exposed to fresh EBM-2 medium supplemented with 0.1 or 2% FBS and ARA-C (2.5 mg/ml, Sigma-Aldrich) to suppress cell proliferation. Where indicated, confluent HUVECs were pretreated for 30 min with daidzin and then treated with 2% FBS. Images of the wound in each well were acquired from 0 to 18 h under a phase contrast microscope at 10x magnification. Then, cells were fixed and stained with the PanReac kit. Results were quantified using ImageJ software, and data are reported as % of scratch closure.

2.10. Immunofluorescence Microscopy Analysis. Cells were transfected with siRNA as described above, and 24 h post-transfection, ECs were harvested and seeded (8×10^4 cells) on 8 mm ø glass coverslips in triplicate. After 24 h, cells were exposed to EBM-2 with 0.1% FBS for 8 h. 4% paraformaldehyde/PBS with Ca^{2+} and $Mg^{2+}$and 3% bovine serum albumin (BSA) were used to fix cells and block unspecific binding sites, respectively. Then, cells were incubated with a monoclonal rabbit anti-VE-cadherin diluted to 1 : 400 (Cell Signaling Technology) and a polyclonal rabbit anti-ZO-1 (Life Technologies, Carlsbad, CA, USA) diluted to 1 : 50 in 0.5% BSA in PBS for 18 h at 4°C. After incubation with the secondary antibody, Alexa Fluor© 488-labeled anti-rabbit (1 : 200, 1 h, Invitrogen) and Alexa Fluor© 555-labeled anti-rabbit (1 : 200, 1 h) were used for 1 h at room temperature, and then the protocol was completed according to Terzuoli et al. [19]. Leica SP5 confocal microscopy (63x objective) was used to capture images of stained cells.

2.11. Paracellular Permeability Assay. Cells were seeded (8×10^4 cells/well) 24 h post-ALDH2 silencing on gelatin-coated insert membranes (0.4 μm diameter pores, Corning, New York, USA), and the inserts were placed in 24-multiwell plates and incubated for 24 h. Next, cells were exposed to EBM-2 with 0.1% FBS for 8 h. The assay was carried out as described [20]. Briefly, the fluorescent permeability tracer (3 kDa FITC-Dextran, 10 μM) was added, and the fluorescence was measured after 7 min in the medium present in the bottom of the well, in a multiplate reader (Infinite 200 Pro, SpectraFluor, Tecan), at 485/535 nm (excitation/emission). Results are reported as relative fluorescence units (RFU) [20].

2.12. ROS Measurement. siCTR and siALDH2 cells (24 h posttransfection) were seeded (1.5×10^3 cells/well) in triplicate in a 96-well plate, and after adherence (6–8 h), the medium was replaced with EBM-2 with 0.1% FBS in the presence or absence of 5 mM NAC for 24 h. DCFH2-DA (2,-7-dichlorodihydrofluorescein diacetate, Invitrogen) was used, and intracellular ROS were measured as previously described [20]. The results are reported as fold change vs. siCTR of relative fluorescence units (RFU) corrected for the cell number counted [20].

2.13. Measurement of the Oxygen Consumption Rate. The measurement of oxygen consumption rates (OCR) was carried out using the Seahorse XF24 extracellular flux analyzer as described previously [21, 22]. siCTR and siALDH2 ECs were harvested and seeded 24 h posttransfection in XF24 cell culture plates at 3×10^4 cells/well density in 200 μl of EGM-2 supplemented with 10% FBS and incubated at 37°C in 5% CO_2 for 6–8 h. Then, adherent cells were exposed to EBM-2 supplemented with 2% FBS for 24 h. Assays were performed as reported [22]. Independent titration was routinely carried out to determine the optimal concentration of FCCP (carbonylcyanide-p-trifluoromethoxyphenyl hydrazone), which was ranged between 0.2 and 0.4 μM. Initially, a stable OCR baseline was determined, and then, oligomycin, FCCP,

rotenone, and antimycin A were supplied as reported in the figure legend.

2.14. Transmission Electron Microscopy. 1×10^4 cells transfected with siRNA as above were harvested and seeded 24 h posttransfection in a small chamber prepared with cylinder part of BEEM® (Ted Pella Inc., Redding, CA, USA) capsule glued to the coverslip as previously described [23]. After 6–8 h of incubation needed for adhesion, cells were exposed to EBM-2 with 2% FBS for 24 h. The medium was replaced with 2.5% glutaraldehyde (Ted Pella, Redding, CA, USA) in 0.1 M phosphate buffer (pH 7.2) for 2 h at RT and postfixed with buffered 1% OsO_4 (EMS, Hatfield, PA, USA) for 1 h and processed by standard dehydration through a graded series of ethanol (50°–100°). Specimens were then embedded in pure Epon (EMS, Hatfield, PA, USA) resin. Polymerization was done in an oven at 60°C for 48 h. Then, slides were dropped into liquid nitrogen to detach the resin from coverslips. 60–70 nm thick sections were cut with an Ultracut E (Reichert-Jung, Wien, AT) ultramicrotome, stained with uranyl acetate and lead citrate, and examined in a TEM Jeol 1010 (Peabody, MA, USA) transmission electron microscope.

2.15. Statistical Analysis. Results are expressed as means ± SD or SEM. Statistical analysis was generated by GraphPad software (San Diego, CA, USA). Statistical analysis was performed by Student's t-test and two-way ANOVA. $p < 0.05$ was considered statistically significant.

3. Results

3.1. ALDH2 Silencing or Inhibition Impairs Endothelial Cell Functions. To examine the role of ALDH2 in endothelial function, HUVECs were treated with 1 and 10 μM daidzin, an inhibitor of ALDH2 activity [14], or transiently knocked down for ALDH2 (siALDH2) and compared with wild-type cells transfected with an empty vector (siCTR), throughout this work. 10 μM daidzin was the higher concentration without a significant effect of its solvent on HUVEC survival.

Whereas in siCTR cells ALDH2 protein expression was easily detected by Western blot, the enzyme expression was drastically reduced in siALDH2 (Figure 1(a)). Silencing of ALDH2 also reduced the mRNA levels and activity of the enzyme (Figures 1(b) and 1(c)) and promoted a significant change in HUVEC morphology, characterized by the irregular elongated shape instead of the regular polygonal shape of siCTR cells (Figure 1(d)). As expected, 10 μM daidzin significantly reduced ALDH2 activity, while at 1 μM, it did not affect the enzyme activity (Figure 1(e)).

Next, we determined the involvement of ALDH2 activity on cell viability, proliferation, and migration, as well as on cell permeability, key features of endothelial cell functions. The proliferation of siALDH2 ECs, assessed by the BrdU incorporation assay, was significantly reduced relative to siCTR ECs and not recovered in the presence of serum (Figure 2(a)). Accordingly, both deficiency and pharmacological inhibition of ALDH2 in HUVECs resulted in a consistent reduction of cell viability, particularly visible after 5 days (Figures 2(b) and 2(c)). Moreover, cell migration, evaluated by the scratch assay, was significantly inhibited in both daidzin-treated and siALDH2 ECs (Figure 2(d)). ALDH2 ablation also affected the adherence and tight junctions of HUVECs altering their barrier function. Indeed, in confluent siCTR, the expression of VE-cadherin and ZO-1, examined by immunofluorescence, was mainly localized at cell-cell contacts and disappeared in cells whose ALDH2 was silenced (Figure 2(e)).

To corroborate the immunofluorescence analysis, we evaluated the paracellular flux in a confluent monolayer of siCTR and siALDH2 ECs. Consistent with the above data, we observed an increase in permeability in siALDH2 when compared to siCTR ECs, as shown by increased paracellular flux of fluorescence-conjugated dextran (Figure 2(f)).

Of note, silencing the ALDH2 triggered the accumulation of 4-HNE-induced covalent adducts, as well as ROS products [24] in ECs (Figures 3(a) and 3(b)), suggesting that the intracellular abundance of these toxic products might contribute to the impairment of the endothelium and trigger the premature senescence process seen below.

To get insight into the role of ROS in the dysfunction of ECs whose ALDH2 was silenced, 5 mM NAC, a ROS scavenger, was used. In particular, as shown in Figures 3(b)–3(e), NAC treatment in siALDH2 ECs affected the pattern of 4-HNE protein adducts and reduced their expression, significantly inhibited the production of total ROS levels, and improved viability at 5 days. Taken together, these results indicate that ALDH2 silencing affects the healthy phenotype of HUVECs by increasing the accumulation of 4-HNE-induced adducts and ROS products, leading to changes in morphology and disassembling of intercellular junctions, and impairs endothelial cell barrier function and mobilization capacity.

3.2. ALDH2 Silencing or Inhibition Promotes the Onset of Senescence in Endothelial Cells. In light of the above findings, showing a pervasive dysfunction of endothelial cells upon ALDH2 silencing, we wondered whether this impaired state might be associated with the acquisition of premature senescence. Morphological modifications characterize usually senescent cells in *in vitro* culture: cells become large, flat, vacuolated, and occasionally multinucleated [25]. Therefore, we quantified the size of the cells and reported it as the area of the cells expressed as square pixel. siALDH2 cells presented a larger cell area in comparison to siCTR cells (Figures 4(a) and 4(b)). We next measured the cumulative population doubling (PD) in long-term cultured endothelial cells at predetermined set points, an experimental protocol we devised to study senescence [16]. We performed measurements of PD and of several senescence markers at PD 5 and PD 21, corresponding to the time-dependent progress from premature to moderate-full senescent cells, respectively. Senescent cells vary from other nonproliferating cells by several markers. Besides the expression of signals belonging to the two major senescence-inducing pathways (p53/p21, c-Myc, Egr-1), we also evaluated beta-galactosidase (SA-β-Gal) activity. As shown in Figures 4(c), 4(d), and 4(g), HUVECs at PD 21 overexpressed SA-β-Gal activity and senescence markers

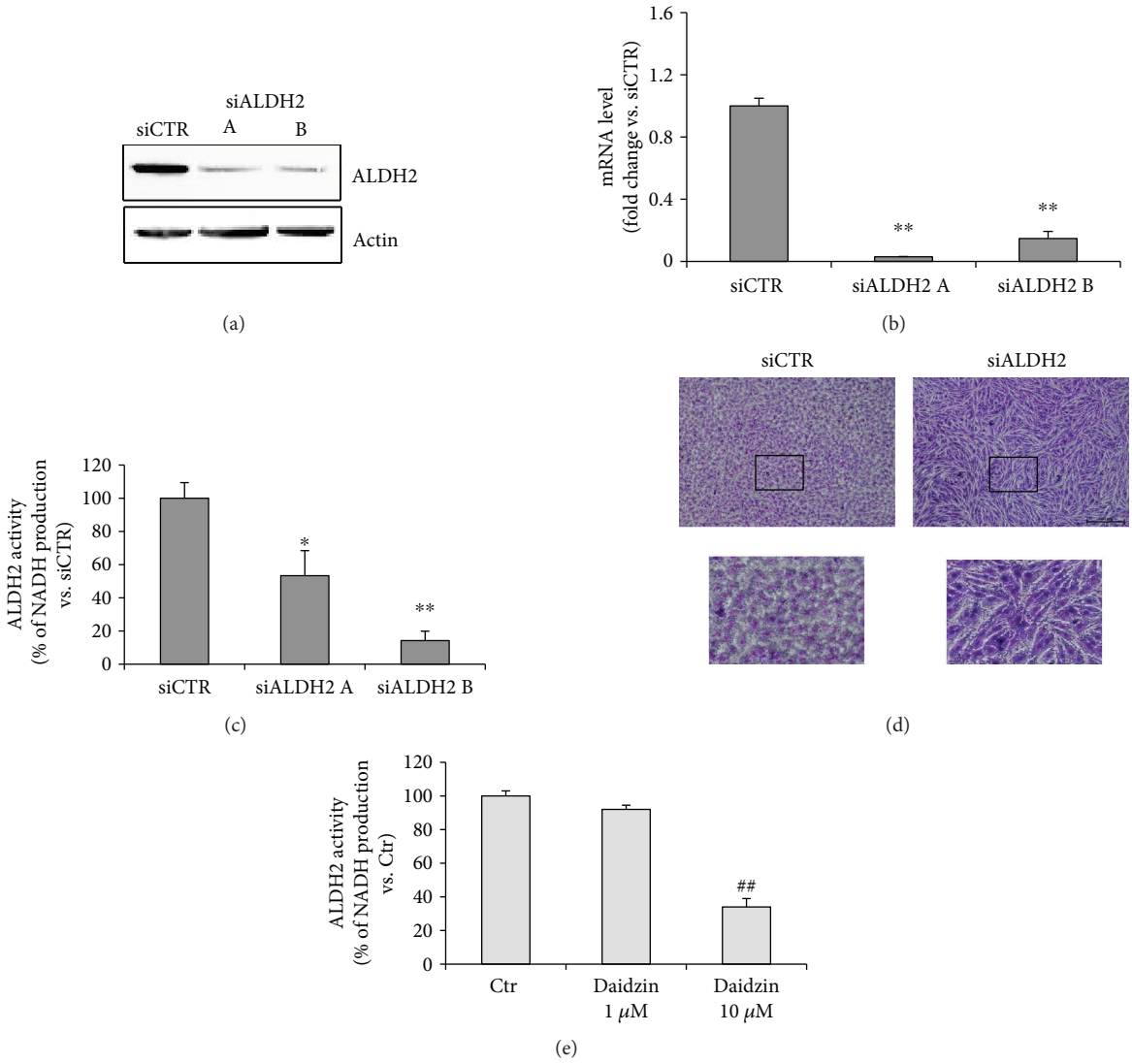

Figure 1: Characterization of siALDH2 and daidzin-treated HUVECs. (a) Immunoblotting and (b) qPCR analysis of ALDH2 silencing (siALDH2) in ECs, 48 h posttransfection. Representative blots of at least 3 with similar results are shown. qPCR data are expressed as the mean of fold change ± SD vs. siCTR cells, which were assigned to 1. $^{**}p < 0.01$ vs. siCTR. (c) ALDH2 activity measured in siALDH2 EC lysates (48 h posttransfection). Data are presented as the mean ± SD of % NADH production vs. siCTR. $^{*}p < 0.05$ and $^{**}p < 0.01$ vs. siCTR. (d) Morphology of confluent monolayers of siCTR and siALDH2 B ECs fixed and stained 48 h posttransfection. A representative image for each condition is shown. Scale bar: 100 μm. (e) ALDH2 activity measured in ECs in the presence or absence of daidzin (1–10 μM). D10: 10 μM daidzin. Data are presented as the mean ± SD of % NADH production vs. Ctr. $^{\#\#}p < 0.01$ vs. Ctr.

compared to HUVECs at PD 5. Of note, in HUVECs at PD 5 whose ALDH2 was silenced, we observed the overexpression of p53 and p21, c-Myc, and Egr-1 (Figures 4(e), 4(f), and 4(h)).

In addition, evaluation of SA-β-Gal revealed significant differences in its expression between siCTR PD 5 cells and those of siALDH2 groups and PD 21 groups (see Figure 4(i)). A time-related increase in SA-β-Gal expression (3- to 5-fold difference) was evident in siALDH2 but not in siCTR cells (Figure 4(j)). Similarly, treatment with 10 μM daidzin significantly increased senescence markers in PD 5 ECs (Figures 4(k) and 4(l)). Of note, 5 mM NAC partially reversed SA-β-Gal expression in siALDH2 ECs (Figure 4(m)), corroborating the instrumental role played by ROS in the impairment of the endothelium whose ALDH2 was silenced.

These data clearly indicate that ALDH2 silencing and inhibition are associated with the onset of early signs of a senescent phenotype.

3.3. ALDH2 Silencing Alters Bioenergetic Functions in Endothelial Cells. Adjusting metabolism to a quiescent state is central to normal vessel function [9, 10]. As we observed that ablation of ALDH2 causes an impairment of permeability leading to a senescent phenotype in HUVECs, we investigated whether ALDH2 would affect cell oxidative metabolism. We evaluated oxygen consumption rates (OCR) in siCTR compared to siALDH2 at baseline and in response to oligomycin (Oligo), fluoro-carbonyl cyanide phenylhydrazone (FCCP), or antimycin A (AA) and rotenone (R). We found that ALDH2 silencing reduced basal

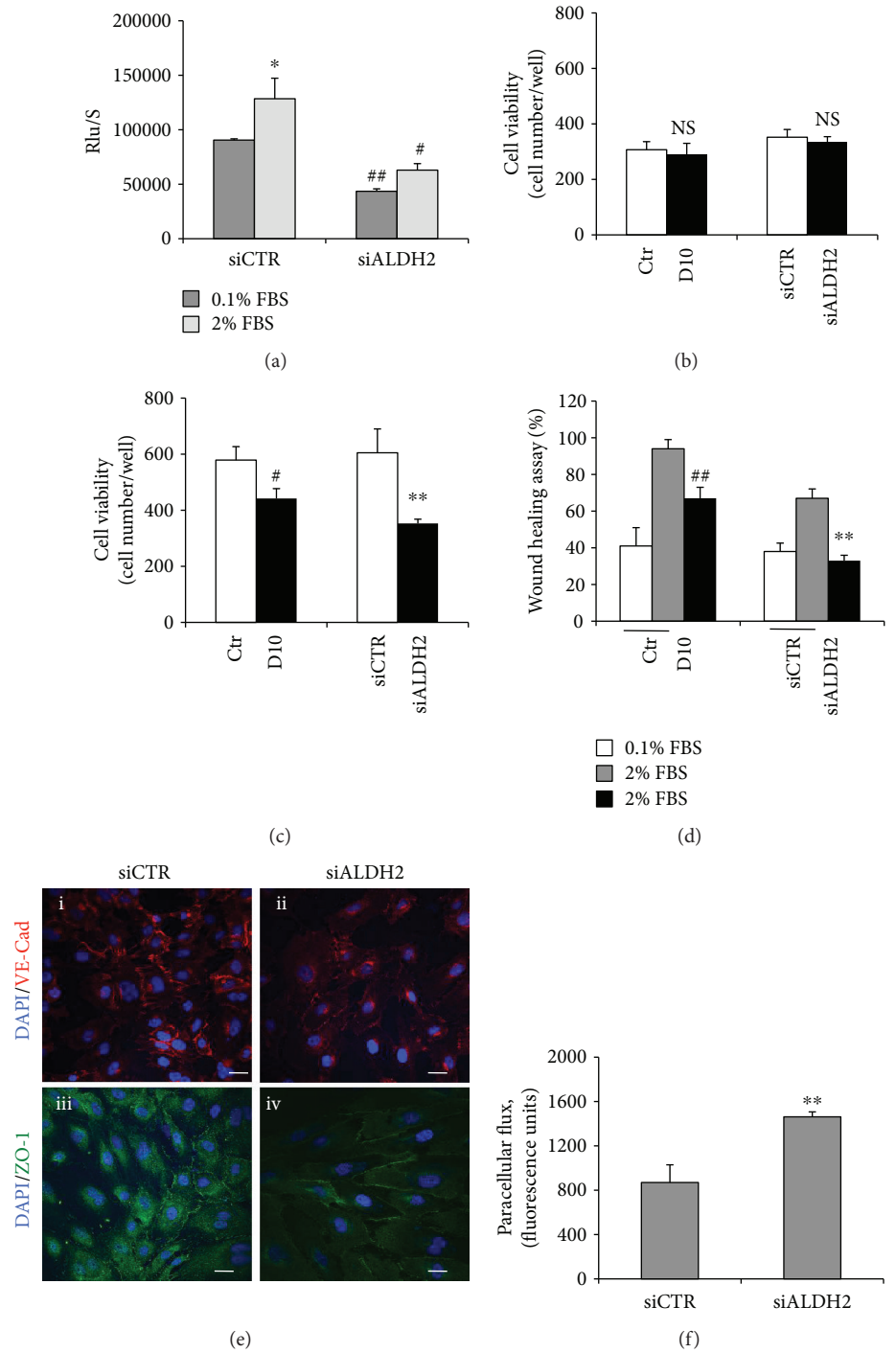

Figure 2: ALDH2 silencing or inhibition impairs endothelial functions. (a) BrdU incorporation in ECs transfected with siRNA for 24 h. Proliferative capacity was assessed after 48 h treatment with 0.1%–2% FBS. Data are reported as mean ± SD. $^{*}p < 0.05$ vs. siCTR with 0.1% FBS; $^{\#}p < 0.05$ and $^{\#\#}p < 0.01$ vs. siCTR. (b) Cell survival in 10 μM daidzin-treated ECs or siCTR and siALDH2 ECs exposed to 2% FBS for 2 and (c) 5 days. Data are expressed as means ± SD of the cell number counted/well. Dimethyl sulfoxide (DMSO) is used as a solvent to dissolve daidzin. No significant effect of DMSO was observed in HUVEC survival (DMSO-treated cell numbers/well: 329 ± 30). NS: not statistically significant; $^{\#}p < 0.05$ vs. Ctr; $^{**}p < 0.01$ vs. siCTR. D10: 10 μM daidzin. (d) Scratch assay in 10 μM daidzin-treated ECs or in siCTR and siALDH2 ECs cultured in 0.1% or 2% FBS for 18 h. Means ± SD of % of scratch closure ($^{\#\#}p < 0.01$ vs. Ctr; $^{**}p < 0.01$ vs. siCTR). (e) Confocal analysis of VE-cadherin and ZO-1 patterns in control (i–iii) and siALDH2 ECs (ii–iv) after exposure to EBM-2 with 0.1% FBS for 8 h. Representative images of three experiments at 63x magnification are shown. Scale bar: 20 μm. (f) Permeability in siCTR and siALDH2 ECs detected as fluorescence-conjugated FITC-dextran diffusion through the confluent monolayers after exposure to EBM-2 with 0.1% FBS for 8 h. $^{**}p < 0.01$ vs. siCTR. Images are representative of results obtained with siALDH2 B.

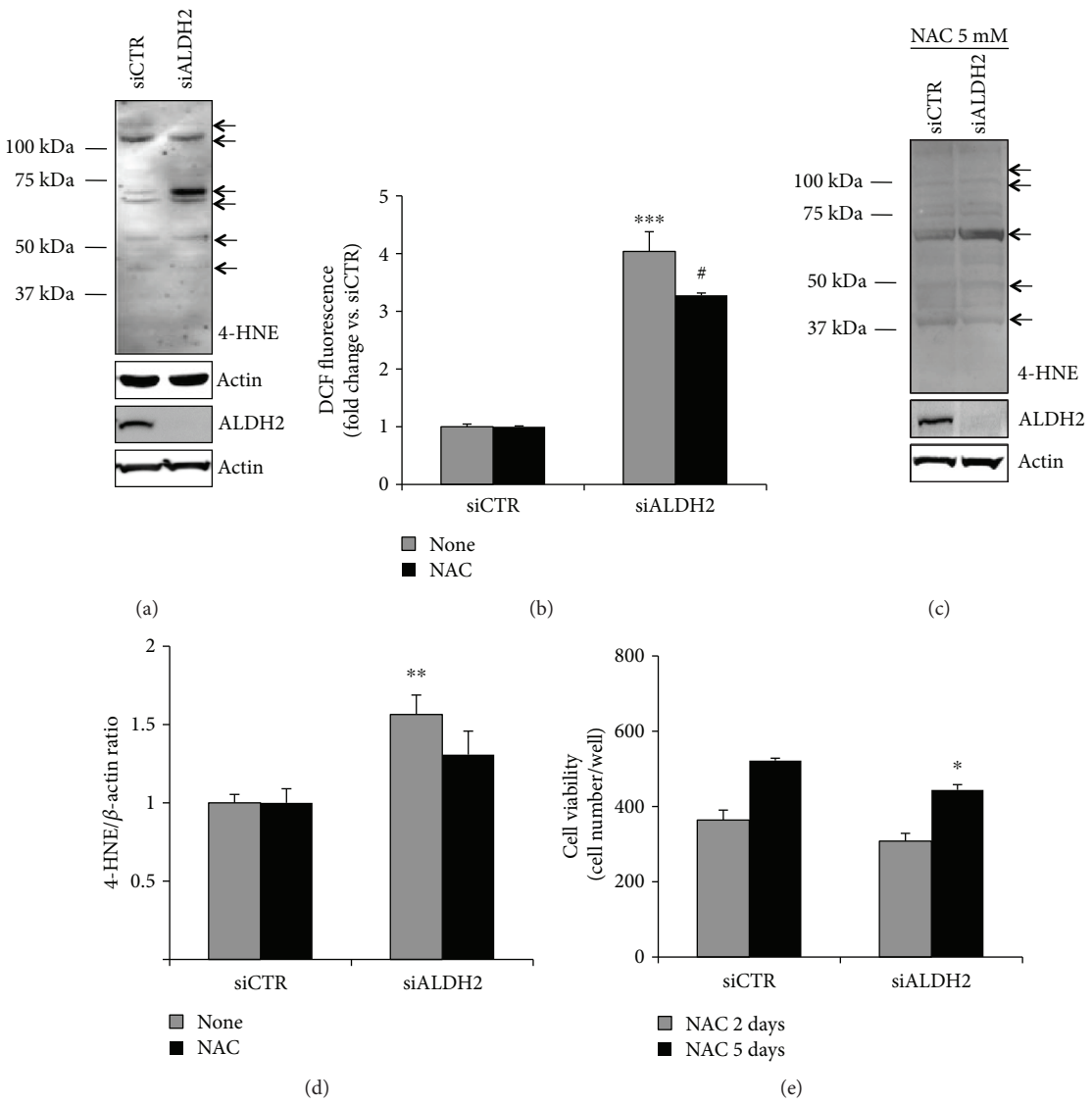

Figure 3: ALDH2 silencing increases 4-HNE protein adducts and ROS levels. (a) Western blot analysis of 4-HNE protein adducts in siCTR and siALDH2 ECs cultured in 2% FBS for 24 h. Knockdown efficiency was checked using immunoblotting with an ALDH2 antibody. The arrows indicate bands quantified in (d). Representative blots of at least 3 with similar results are shown. (b) ROS production in siCTR and siALDH2 ECs cultured in 0.1% FBS for 24 h in the presence/absence of NAC (5 mM). Cells were pretreated for 30 min with NAC before FBS treatment. Data, normalized for the cell number, are expressed as the mean of fold change ± SD vs. siCTR of DCF fluorescence. $^{***}p < 0.01$ vs. siCTR; $^{\#}p < 0.05$ vs. untreated siALDH2 ECs. (c) Western blot analysis of 4-HNE protein adducts in siCTR and siALDH2 ECs cultured in 2% FBS for 24 h with or without pretreatment (30 min) with NAC (5 mM). Knockdown efficiency was checked using immunoblotting with an ALDH2 antibody. The arrows indicate bands quantified in (d). Representative blots of 3 with similar results are shown. (d) Quantification of major bands (indicated with arrows), normalized to actin, is reported as a fold increase ± SD of ADU vs. siCTR. $^{**}p < 0.01$ vs. siCTR. (e) Cell survival in siCTR and siALDH2 ECs exposed to 2% FBS in the presence/absence of NAC (5 mM) for 2 (grey bars) or 5 (black bars) days. Data are expressed as means ± SD of the cell number counted/well. $^{*}p < 0.05$ vs. siCTR. Images are representative of results obtained with siALDH2 B.

and maximal respiration and decreased the respiratory reserve capacity (Figures 5(a) and 5(b)). Importantly, Western blot analysis of constitutive respiratory complexes including CII, CIII, and CIV, known to be sensible to the ROS increase in mitochondria, indicated that ALDH2 did not alter the abundance of these respiratory complexes (Figure 5(c)).

Given the significant changes of the metabolic function reported, we assessed whether they were associated with morphological modification of cellular components. TEM images showed minor morphological changes in mitochondria of siALDH2 cells (Figure 6). In particular, smaller mitochondria in Figure 6(b) were observed when compared to those in Figure 6(a), and cristae in the centre of mitochondria in Figure 6(d) appear to be deleted.

In conclusion, bioenergetic analysis revealed that ALDH2 deficiency specifically reduced both mitochondrial respiration

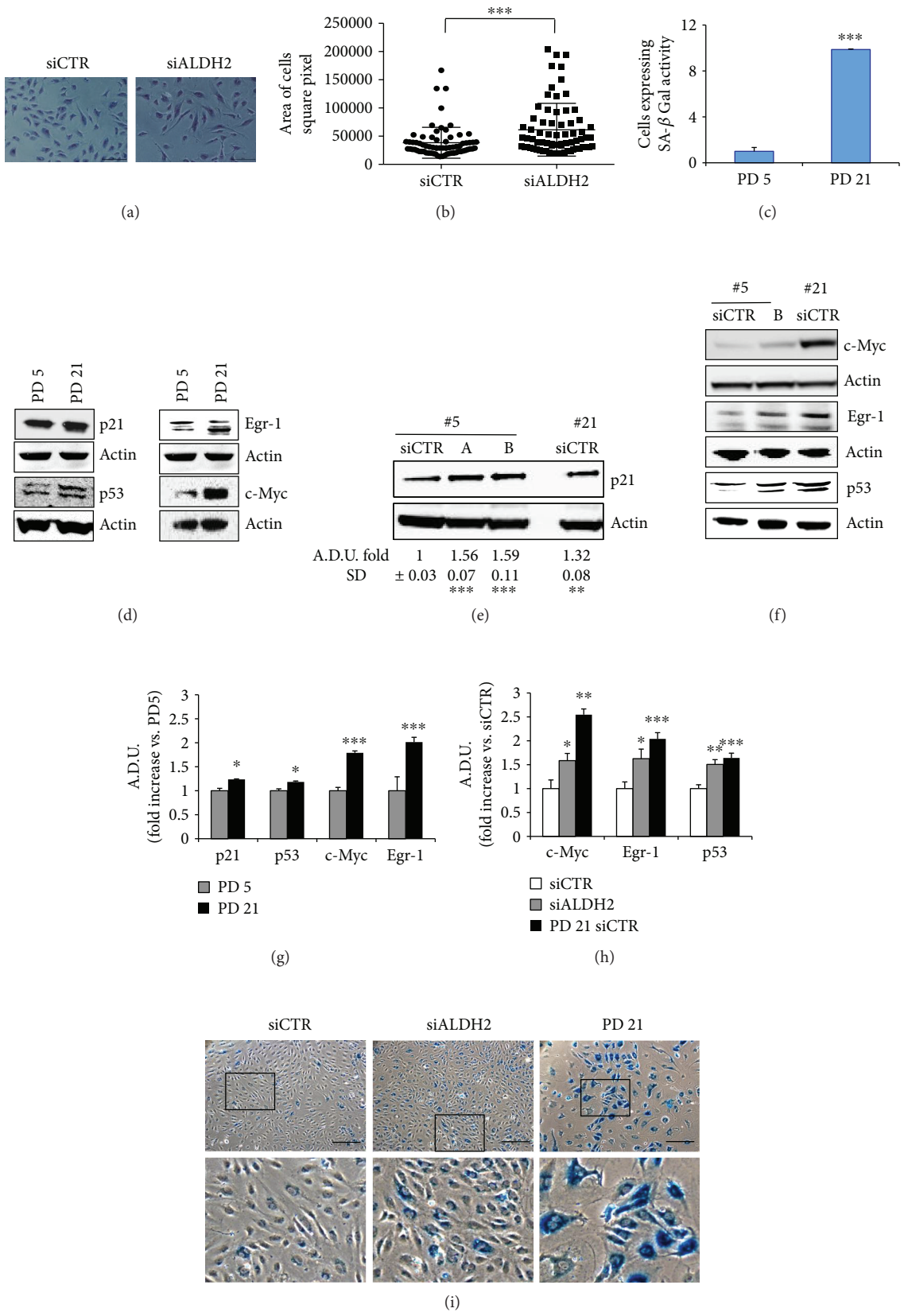

Figure 4: Continued.

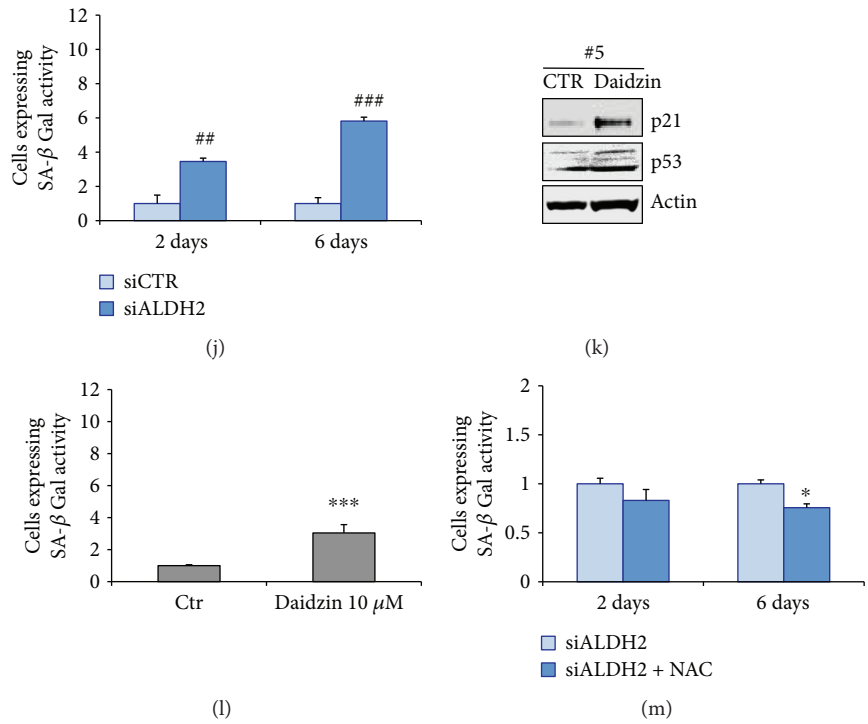

FIGURE 4: ALDH2 silencing or inhibition induces the expression of senescence markers in HUVECs. (a, b) Images and area of cells in siCTR and siALDH2 ECs cultured in EBM-2 supplemented with 2% FBS for 48 h. Data are expressed as a square pixel of cells analyzed using ImageJ. Quantification of 70 cell areas for each condition is reported. $^{***}p < 0.001$ vs. siCTR. Two-way ANOVA was used. (c) SA-β-Gal quantification, expressed as a fold increase in positive cells for SA-β-Gal activity ± SD vs. PD 5. $^{***}p < 0.001$ vs. PD 5. (d, e, f) Western blot analysis of a pattern of senescent markers (d, left: p21 and p53 or right: Egr-1 and c-Myc) in HUVECs at PD 5 (#5, PD 5) and PD 21 (#21, PD 21) or (e, p21 or f c-Myc, Egr-1, and p53) in siCTR and siALDH2 HUVECs, 48 h posttransfection (#5, PD 5; #21, PD 21). Representative blots of 3 with similar results are shown (e, g, h). Quantification of immunoblot in (d), (e), and (f). Data are reported as an ADU fold increase vs. siCTR (e, h) or vs. PD 5 (g). (e) $^{***}p < 0.001$ and $^{**}p < 0.01$ vs. siCTR. (g) $^{***}p < 0.001$ and $^{*}p < 0.05$ vs. PD5. (h) $^{***}p < 0.001$, $^{**}p < 0.01$, and $^{*}p < 0.05$ vs. siCTR. (i) Images of SA-β-Gal staining of siCTR and siALDH2 ECs and PD 21 groups obtained with a Leica DMI4000 microscope. Images of HUVECs at PD 21 were reported as a positive control. Scale bar: 250 μm. The insets show boxed areas in detail. (j) Cells were transfected with siRNA for 2 or 6 days. The transfection was repeated every 72 h. SA-β-Gal quantification, expressed as a fold increase ± SD vs. siCTR of positive cells for SA-β-Gal activity. $^{\#\#}p < 0.01$ and $^{\#\#\#}p < 0.001$. (k) Western blot analysis of senescent markers in HUVECs at PD 5 in the presence/absence of daidzin (10 μM) for 48 h (#5, PD 5). Representative blots of 3 with similar results are shown. (l) SA-β-Gal quantification in ECs treated or not with daidzin (10 μM) for 48 h, expressed as a fold increase in positive cells for SA-β-Gal activity ± SD vs. untreated cells. $^{***}p < 0.001$ vs. untreated cells. (m) Cells were transfected with siRNA for 2 or 6 days in the presence/absence of NAC (5 mM). The transfection was repeated every 72 h. Cells were pretreated for 30 min with NAC, before the treatment with 2% of FBS. The pretreatment with NAC and the treatment with 2% FBS were repeated every 3 days. SA-β-Gal quantification, expressed as a fold decrease ± SD vs. untreated cells positive for SA-β-Gal activity. $^{*}p < 0.05$. Images are representative of results obtained with siALDH2 B.

and reserve capacity, which presumably contribute to the reduction of the endothelial responsiveness.

4. Discussion

ALDH2, a mitochondrial enzyme, is known for its detoxifying properties, which provide living organisms with a protective shield against endogenous and exogenous toxic agents [26], such as acetaldehyde (alcohol metabolism) and products originating from lipid peroxidation (4-HNE) and ROS. The relevance of ALDH2 in providing strong protection toward toxic insults has been described in numerous reports, demonstrating its efficacy in various models of human diseases such as ischemia-reperfusion and ischemic stroke characterized by overwhelming oxidative stress [27]. Note that the above pathologies have the vascular endothelium as an underlying component whose function might be compromised by ROS and aldehyde surge.

Previous data from our group documented that alteration in endothelial function induced by Aβ was restored by the activation of mitochondrial ALDH2 in the endothelium [15]. However, the contribution of ALDH2 to endothelial senescence remains unresolved.

Here, we have described the role of ALDH2 in endothelial growth and function, using HUVECs as a model, whose ALDH2 was silenced through transfection of targeting siRNA or exposure to the pharmacological inhibitor of ALDH2, daidzin. The resulted cellular models displayed a number of morphological and functional changes. Morphologically, we observed a subverted phenotype of silenced cells,

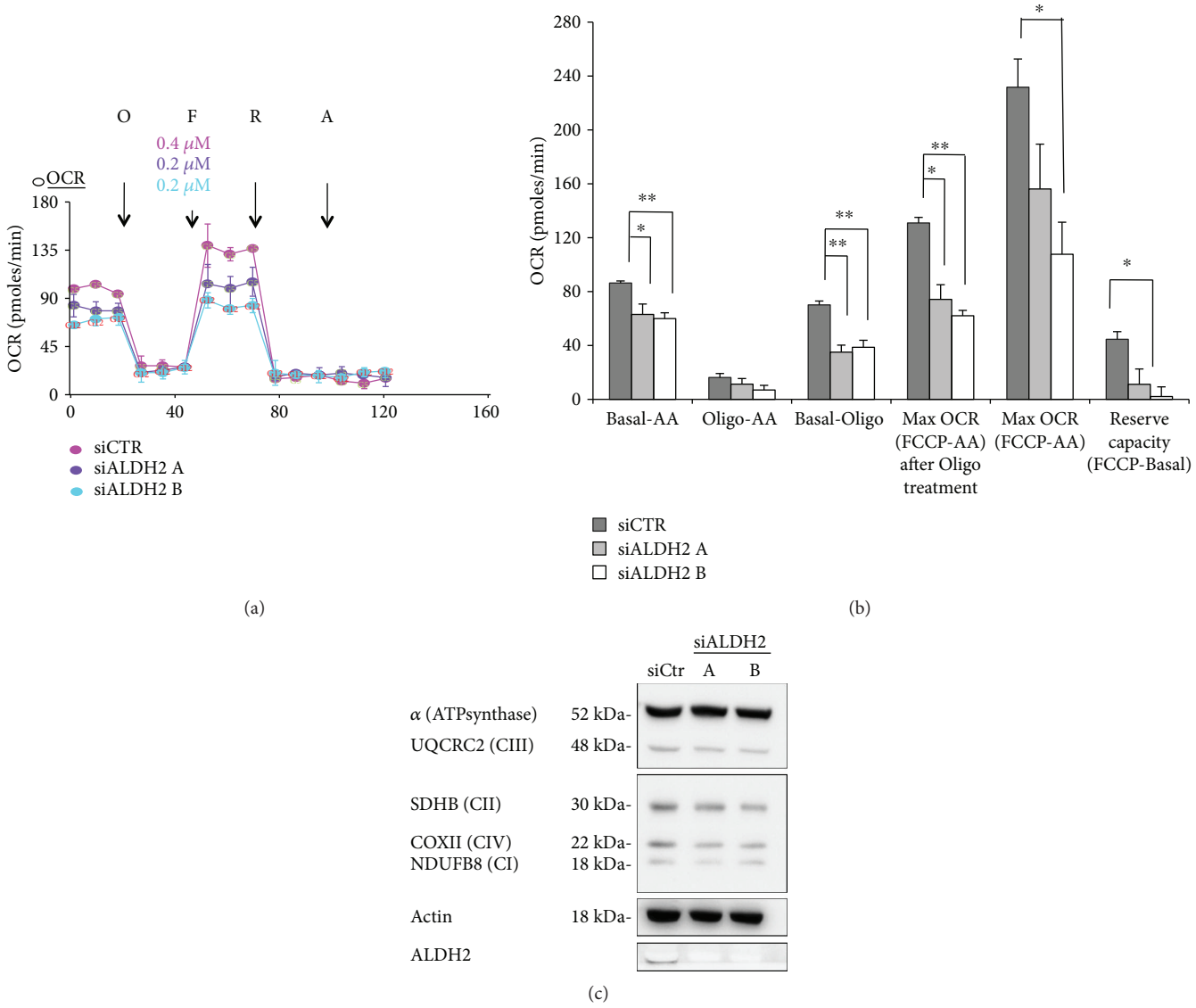

FIGURE 5: ALDH2 silencing is associated with mitochondrial dysfunction. (a) OCR was assessed by a Seahorse XF24 cell culture microplate in siCTR and siALDH2 ECs that were harvested and seeded 24 h posttransfection in XF24 cell culture plates at a density of 3×10^4 cells/well. Where indicated (arrows), oligomycin (O) (1 $\mu g \times ml^{-1}$), FCCP (F) (0.2–0.4 μM), rotenone (R) (1 μM), and antimycin A (AA) (1 μM) were added. Data are representative of three experiments. (b) Basal OCR, proton leak, ATP-linked OCR, maximal OCR, and reserve capacity in siALDH2 ECs exposed to 2% FBS for 24 h. The means ± SEM of each parameter are shown. $^{**}p < 0.01$ and $^{*}p < 0.05$ vs. siCTR. (c) Western blot analysis of OXPHOS representative complexes detected by the OXPHOS antibody cocktail kit in siALDH2 (two clones A and B) or siCTR cultured in 2% FBS for 24 h. Knockdown efficiency was verified with an ALDH2 antibody. Actin was used as a loading control. Blots are representative of 3 with similar results.

characterized by an enlarged and elongated cell shape, in sharp contrast to the polygonal one of wild-type endothelial cells. Functionally, the ALDH2 loss yielded a reduced mobility and augmented permeability, a finding consistent with the marked decline of VE-cadherin and ZO-1 expression at cell-cell contacts and with the changes in cell morphology. We also observed a reduction of cell proliferation that results in a reduction of the cell number. Predictably, ALDH2 silencing produced intracellular accumulation of 4-HNE adducts and ROS production, which appears to be the primary cause of the observed impairment of endothelial cell functions and morphological changes, as corroborated by using the scavenger NAC.

The study of mitochondrial respiration provided further insight into the mechanism underlying endothelial dysfunction, as mitochondria possess a considerable respiratory reserve, which is important in the response to oxidative stress [11, 12]. Indeed, we found that ALDH2 silencing diminished the inherent oxidative metabolism, as indicated by a decline in the oxygen consumption rate. Specifically, siALDH2 cells showed a reduction in basal and maximal respiration measured under basal conditions

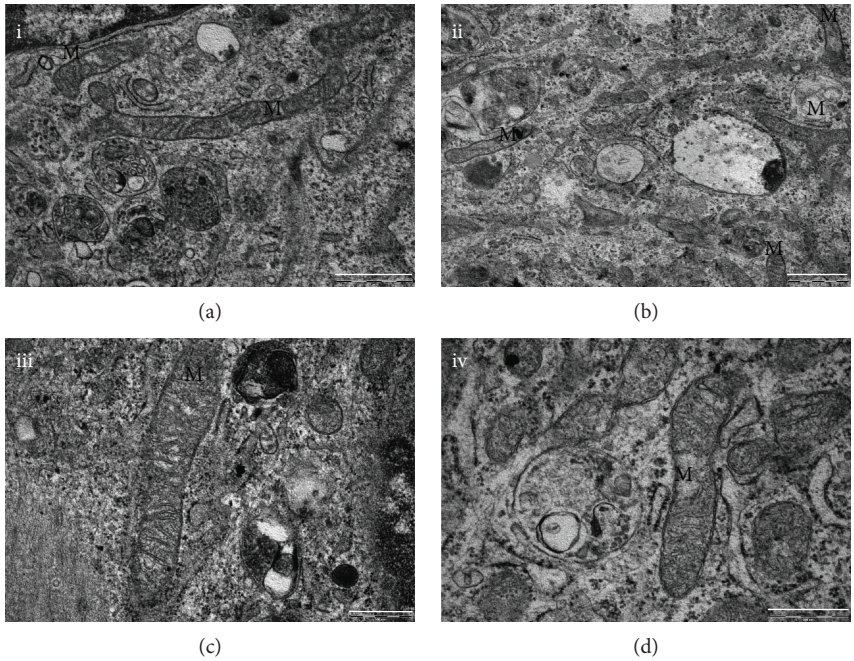

Figure 6: ALDH2 silencing affects the HUVEC mitochondrial ultrastructure. Cells were transfected with siRNA as described above. Then, they were harvested and seeded 24 h posttransfection and treated as described in Materials and Methods. TEM representative images of siCTR or siALDH2: (a, c) siCTR and (b, d) siALDH2. M: mitochondria. Scale bar: (a, b) 1 μm and (c, d) 500 nm. Images are representative of results obtained with siALDH2 B.

and in response to FCCP, with a clear decrease in the reserve capacity. While mitochondrial respiration decreased, the analysis of the expression of all respiratory complexes does not change upon ALDH2 downregulation, indicating that the protein level of all respiratory complexes is not the leading cause of reduced respiration in siALDH2 cells. We therefore suggested that the decrease in basal OCR and spare reserve capacity might be due to some posttranslational modifications.

Furthermore, TEM images suggest alterations in mitochondrial morphology of siALDH2 cells. Thus, the endothelial dysfunction, noted in siALDH2 cells and in ECs exposed to daidzin, may be attributed to the effects of accumulated toxic products and to subtle defects of mitochondrial respiration.

Investigation on endothelial cell senescence was initiated in view of the observed morphological similarities between siALDH2 and those typical of senescent cells, i.e., the flat morphology and enlarged cell size. Evidence sustaining the hypothesis of an incipient senescent state was gleaned from the analysis of SA-β-Gal activity and specific intracellular signals measured in siALDH2 cells and in daidzin-treated cells subjected to stress-induced senescence experiments in which population doublings (PD) were recorded. Indeed, cellular senescence ensued as early as at PD 5 progressing steadily up to PD 21. In fact, increases in signals, e.g., SA-β-Gal, p21/p53, Egr1, and c-Myc, were noted when comparing signalling patterns at PD 5 vs. PD 21. The onset of senescence in siALDH2 cells as well as in ECs exposed to daidzin is considerably faster than what was observed in the earlier work on HUVECs exposed to exogenous amyloid peptides (PD 5 vs. PD 21) [16]. This underscores the protective role of ALDH2 exerted toward the endothelium to an extent not appreciated before.

5. Conclusions

Our results demonstrate that in the vascular endothelium, loss of ALDH2 accelerates the acquisition of a premature senescence phenotype leading to endothelial dysfunction. These events are associated with an increase in ROS levels, accumulation of 4-HNE protein adducts, and impairment of mitochondrial bioenergetic functions. The senescence phenotype of the endothelium, with exhaustion of the regenerative capacity, may represent a defensive response from the damage caused by an accumulation of toxic aldehydes and can lead to the expansion of the senescent cell population further aggravating the loss of function in the vasculature.

Abbreviations

AA: Antimycin A
ALDH2: Aldehyde dehydrogenase 2
DAPI: 4′,6-diamidino-2-phenylindole
EGM-2: Endothelial growth medium
EBM-2: Endothelial basal medium
ECs: Endothelial cells
FCCP: Carbonylcyanide-p-trifluoromethoxyphenyl hydrazone
NAC: N-Acetyl-L-cysteine
PD: Cumulative population doubling
siALDH2: siRNA targeting ALDH2
siCTR: Scrambled control siRNA.

Data Availability

The data used to support the findings of this study are included within the article.

Disclosure

Some results showed in the manuscript have been presented in the 1st Meeting in Translational Pharmacology: Invited Societies SPF-SIF-EEI.

Conflicts of Interest

The authors declare that there is no conflict of interest regarding the publication of this paper.

Acknowledgments

We thank Daria Mochly-Rosen (Stanford University) for stimulating discussions during the course of this work. We are grateful to Eugenio Paccagnini (University of Siena) for the technical support with electron microscopy analysis. This work was supported by Associazione Ricerca sul Cancro (AIRC) (IG 15443) and MIUR-PRIN (20152HKF3Z) through MZ.

References

[1] C. López-Otin, M. Blasco, L. Partridge, M. Serrano, and G. Kroeme, "The hallmarks of aging," *Cell*, vol. 153, no. 6, pp. 1194–1217, 2013.

[2] J. D. Erusalimsky, "Vascular endothelial senescence: from mechanisms to pathophysiology," *J Appl Physiol. 1985.*, vol. 106, no. 1, pp. 326–332, 2009.

[3] X. L. Tian and Y. Li, "Endothelial cell senescence and age-related vascular diseases," *Journal of Genetics and Genomics*, vol. 41, no. 9, pp. 485–495, 2014.

[4] F. Paneni, C. Diaz Cañestro, P. Libby, T. F. Lüscher, and G. G. Camici, "The aging cardiovascular system: understanding it at the cellular and clinical levels," *Journal of the American College of Cardiology*, vol. 69, no. 15, pp. 1952–1967, 2017.

[5] M. Mittal, M. R. Siddiqui, K. Tran, S. P. Reddy, and A. B. Malik, "Reactive oxygen species in inflammation and tissue injury," *Antioxidants & Redox Signaling*, vol. 20, no. 7, pp. 1126–1167, 2014.

[6] A. Quaegebeur, C. Lange, and P. Carmeliet, "The neurovascular link in health and disease: molecular mechanisms and therapeutic implications," *Neuron*, vol. 71, no. 3, pp. 406–424, 2011.

[7] Y. Koga, Y. Akita, N. Junko et al., "Endothelial dysfunction in MELAS improved by l-arginine supplementation," *Neurology*, vol. 66, no. 11, pp. 1766–1769, 2006.

[8] L. H. Rodan, G. D. Wells, L. Banks, S. Thompson, J. E. Schneiderman, and I. Tein, "L-Arginine affects aerobic capacity and muscle metabolism in MELAS (mitochondrial encephalomyopathy, lactic acidosis and stroke-like episodes) syndrome," *PLoS One*, vol. 10, no. 5, article e0127066, 2015.

[9] M. Potente and P. Carmeliet, "The link between angiogenesis and endothelial metabolism," *Annual Review of Physiology*, vol. 79, no. 1, pp. 43–66, 2017.

[10] P. Fraisl, M. Mazzone, T. Schmidt, and P. Carmeliet, "Regulation of angiogenesis by oxygen and metabolism," *Developmental Cell*, vol. 16, no. 2, pp. 167–179, 2009.

[11] M. A. Kluge, J. L. Fetterman, and J. A. Vita, "Mitochondria and endothelial function," *Circulation Research*, vol. 112, no. 8, pp. 1171–1188, 2013.

[12] B. P. Dranka, B. G. Hill, and V. M. Darley-Usmar, "Mitochondrial reserve capacity in endothelial cells: the impact of nitric oxide and reactive oxygen species," *Free Radical Biology & Medicine*, vol. 48, no. 7, pp. 905–914, 2010.

[13] C. H. Chen, L. Sun, and D. Mochly-Rosen, "Mitochondrial aldehyde dehydrogenase and cardiac diseases," *Cardiovascular Research*, vol. 88, no. 1, pp. 51–57, 2010.

[14] C. Chen, C. B. Julio Ferreira, E. Gross, and D. Mochly Rosen, "Targeting aldehyde dehydrogenase 2: new therapeutic opportunities," *Physiological Reviews*, vol. 94, no. 1, pp. 1–34, 2014.

[15] R. Solito, F. Corti, C. Chen et al., "Mitochondrial aldehyde dehydrogenase-2 activation prevents β-amyloid-induced endothelial cell dysfunction and restores angiogenesis," *Journal of Cell Science*, vol. 126, no. 9, pp. 1952–1961, 2013.

[16] S. Donnini, R. Solito, E. Cetti et al., "Aβ peptides accelerate the senescence of endothelial cells in vitro and in vivo, impairing angiogenesis," *The FASEB Journal*, vol. 24, no. 7, pp. 2385–2395, 2010.

[17] M. Monti, I. Hyseni, A. Pacini, E. Monzani, L. Casella, and L. Morbidelli, "Cross-talk between endogenous H_2S and NO accounts for vascular protective activity of the metal-nonoate Zn(PipNONO)Cl," *Biochemical Pharmacology*, vol. 152, pp. 143–152, 2018.

[18] L. Bazzani, S. Donnini, A. Giachetti, G. Christofori, and M. Ziche, "PGE2 mediates EGFR internalization and nuclear translocation," *Oncotarget*, vol. 9, no. 19, pp. 14939–14958, 2018.

[19] E. Terzuoli, G. Nannelli, M. Frosini, A. Giachetti, M. Ziche, and S. Donnini, "Inhibition of cell cycle progression by the hydroxytyrosol-cetuximab combination yields enhanced chemotherapeutic efficacy in colon cancer cells," *Oncotarget*, vol. 8, no. 47, pp. 83207–83224, 2017.

[20] V. Ciccone, M. Monti, G. Antonini et al., "Efficacy of AdipoDren® in reducing interleukin-1-induced lymphatic endothelial hyperpermeability," *Journal of Vascular Research*, vol. 53, no. 5-6, pp. 255–268, 2016.

[21] V. Giorgio, V. Petronilli, A. Ghelli et al., "The effects of idebenone on mitochondrial bioenergetics," *Biochimica et Biophysica Acta*, vol. 1817, no. 2, pp. 363–369, 2012.

[22] M. Schiavone, A. Zulian, S. Menazza et al., "Alisporivir rescues defective mitochondrial respiration in Duchenne muscular dystrophy," *Pharmacological Research*, vol. 125, Part B, pp. 122–131, 2017.

[23] L. Stepanek and G. Pigino, "Millisecond time resolution correlative light and electron microscopy for dynamic cellular processes," *Methods in Cell Biology*, vol. 140, pp. 1–20, 2017.

[24] O. I1, K. Nishimaki, C. Yasuda, K. Kamino, and S. Ohta, "Deficiency in a mitochondrial aldehyde dehydrogenase increases vulnerability to oxidative stress in PC12 cells," *Journal of Neurochemistry*, vol. 84, no. 5, pp. 1110–1117, 2003.

[25] D. Muñoz-Espín and M. Serrano, "Cellular senescence: from physiology to pathology," *Nature Reviews Molecular Cell Biology*, vol. 15, no. 7, pp. 482–496, 2014.

[26] V. Vasiliou and D. W. Nebert, "Analysis and update of the human aldehyde dehydrogenase (ALDH) gene family," *Human Genomics*, vol. 2, no. 2, pp. 138–143, 2005.

[27] C. H. Chen, G. R. Budas, E. N. Churchill, M. H. Disatnik, T. D. Hurley, and D. Mochly-Rosen, "Activation of aldehyde dehydrogenase-2 reduces ischemic damage to the heart," *Science*, vol. 321, no. 5895, pp. 1493–1495, 2008.

Hindawi
Oxidative Medicine and Cellular Longevity
Volume 2018, Article ID 3053704, 9 pages
https://doi.org/10.1155/2018/3053704

Research Article

Exercise-Induced Reductive Stress Is a Protective Mechanism against Oxidative Stress in Peripheral Blood Mononuclear Cells

Ypatios Spanidis,[1] Aristidis S. Veskoukis,[1] Christina Papanikolaou,[1] Dimitrios Stagos,[1] Alexandros Priftis,[1] Chariklia K. Deli,[2] Athanasios Z. Jamurtas,[2] and Demetrios Kouretas[1]

[1]*Laboratory of Animal Physiology, Department of Biochemistry and Biotechnology, University of Thessaly, 41500 Viopolis, Larissa, Greece*
[2]*Laboratory of Exercise Biochemistry, Exercise Physiology and Sports Nutrition (SmArT Lab), Department of Physical Education and Sport Science, University of Thessaly, 42100 Trikala, Greece*

Correspondence should be addressed to Demetrios Kouretas; dkouret@uth.gr

Received 28 June 2018; Accepted 10 September 2018; Published 11 October 2018

Academic Editor: Márcio Carocho

Eccentric exercise is a well-studied modality that induces oxidative stress and muscle damage. Furthermore, it promotes inflammatory response in which peripheral blood mononuclear cells (PBMCs) are the major mediators. Although free radicals are necessary in a specific range of concentrations, yet unknown, it remains unclear whether reductive redox status (i.e., increased antioxidant defenses and impaired free radical generation) is beneficial or not. Thus, the aim of the present investigation was to examine the effects of reductive stress and the impact of reduced glutathione (GSH) baseline values on the ability of PBMCs to counteract oxidative stress induced by a potent oxidative agent. PBMCs were isolated from the blood of subjects who performed eccentric exercise and treated with *t*-BOOH for 24 h. The subjects were clustered in the reductive and the oxidative group on the basis of increased or decreased GSH concentration postexercise compared to preexercise values, respectively. According to our results in PBMCs, lipid peroxidation levels as depicted by thiobarbituric acid reactive substances (TBARS) remained unchanged in the reductive group contrary to the observed enhancement in the oxidative group. In addition, GSH concentration and catalase activity increased in the reductive group, whereas they were not affected in the oxidative group. In conclusion, the effects of an oxidizing agent on the redox status of PBMCs isolated from the blood of athletes after acute eccentric exercise are dependent on the baseline values of GSH in erythrocytes. Otherwise, reductive stress defined by increased GSH levels is a protective mechanism, at least when followed by an oxidative stimulus.

1. Introduction

Exercise has been widely associated with free radical generation and oxidative stress induction in an intensity-dependent manner due to diverse mechanisms [1, 2]. Eccentric exercise is a well-studied type of demanding exercise that alters tissue redox status [3, 4]. It is characterized by active contractions and lengthening of the skeletal muscle being, therefore, a severe tissue-damaging exercise modality followed by decreased muscle force production and, finally, inflammation [5, 6]. It is established that muscle damage postexercise initiates a rapid and sequential migration of inflammatory cells from the circulation into the muscle fibers that typically remain there for days [7]. Moreover, reactive oxygen species (ROS) and cytokines produced by the aforementioned cells, when present in specific concentrations, can act as signaling molecules to mediate muscle repair process after a damaging exercise [8]. As a consequence, inflammation or even low levels of oxidative stress are considered beneficial in terms of exercise recovery and tissue repair [9].

During the last decades, there was a common belief that the action of redox status-altering stimuli, such as eccentric

exercise and antioxidant supplementation, is preferably assessed in the participants without taking into account the redox individuality [4, 10–12]. However, new, scarce experimental evidence suggests that this might not be the case [3, 4, 13, 14]. These well-designed studies have approached a seemingly paradoxical phenomenon that the differential responses of individuals to such treatments depend on their initial/baseline redox values. Specifically, Block et al. have reported that vitamin C and E supplementation reduces biomarkers of oxidative stress only when their initial values are high [13]. Margaritelis et al. have observed that eccentric exercise induces smaller percent increases in oxidative stress biomarkers (i.e., F2-isoprostanes and protein carbonyls) when their initial values are high and vice versa, whereas glutathione is highly decreased when its initial value is also elevated and vice versa [4]. On the other hand, according to Stagos et al., eccentric exercise induces oxidative stress only in the participants with low baseline antioxidant reserves [3]. Finally, Veskoukis et al. have reported that individuals with low baseline (i.e., resting) reduced glutathione (GSH) levels are linked with decreased physical performance, increased oxidative stress, and impaired redox metabolism of erythrocytes [14]. Intriguingly, administration of N-acetylcysteine (NAC) improved redox status only in the individuals with low resting GSH values and not in those with moderate or high resting GSH values providing novel integrative evidence and formulating a new regime regarding antioxidant supplementation [14]. Thus, it is apparent that baseline values of redox biomarkers should be taken into account in order to state whether a redox stimulus induces either oxidative or reductive stress.

Exercise-induced reductive stress is a rather neglected biological outcome that has gained many adherents recently [14]. Indeed, experimental evidence generated from our research group supports this hypothesis [3, 12]. The consensus in the field of redox biology until a decade ago was that oxidative stress and free radicals are damaging for normal tissue function. Nevertheless, we know today that they are a necessary premise for fundamental biological procedures, namely, signal transduction [11]. This is the reason for the proposal of a modern, acceptable definition of oxidative stress by Jones in 2006 as "a disruption in redox signaling and control" [15] which replaced the most influential definition of oxidative stress as "a disturbance in the prooxidant-antioxidant balance in favor of the former" given by Sies in 1985 [16]. On the grounds of this idea, it could probably be deduced that reductive stress seems to be better than oxidative stress since there is a lower free radical concentration available; thus, there is no need for the activation of the antioxidant mechanism. But this seems to be far from reality. On the contrary, there are no convincing findings towards either direction. On the one hand, there is compelling evidence that reductive stress may be harmful for eukaryotic cells with specific reference to GSH and oxidized (GSSG) glutathione ratio (GSH/GSSG) [17]. Specifically, during reductive stress and similarly to oxidative stress, the production of ROS overwhelms the ability of the antioxidant mechanisms to scavenge them. Two antioxidant enzymes, glutathione and thioredoxin reductases, donate electrons to O_2 generating H_2O_2 mostly because of the impaired availability of the natural electron acceptors, that is, GSSG and oxidized thioredoxin. Therefore, the high levels of GSH seem to be noxious triggering mitochondrial oxidation and cytotoxicity. In the same line, a recent study which examined this phenomenon has also claimed that low exercise-induced oxidative stress blunts adaptations in antioxidant status [18]. On the other hand, it has been demonstrated that reductive stress postexercise induces beneficial effects [3, 12, 19]. According to the above findings, GSH is situated at the spotlight as it is considered critical for cell redox status since it is an integral oxidant scavenger and is considered as a major regulator of ROS production by mitochondria and subsequently of the control of cellular redox environment [20]. Collectively, all the aforementioned observations reinforce the "redox-optimized ROS balance" hypothesis proposed by Aon et al. and Cortassa et al. according to which both oxidative stress and reductive stress are extreme biological conditions, since antioxidant defenses of cell populations such as peripheral blood mononuclear cells (PBMCs) are probably overwhelmed [21, 22].

It is widely known that PBMCs are blood cells being in the front line of the human immune system [23]. They are the most essential mediators of stress and inflammation by producing cytokines, chemokines, and growth factors that may lead to beneficial or even pathological effects on tissues. Intense bouts of heavy exercise, like eccentric, may lead to a robust increase in circulating PBMCs [24, 25]. Thus, they are susceptible to agents able to alter redox status and can be considered a proper model for testing the biological impact of reductive stress and redox individuality.

Considering the aspect that a normal concentration of free radicals or reactive species in general is desired or even required for normal tissue function and muscle regeneration (which is desired after damaging exercise), it remains unclear whether a reductive redox status is beneficial or not. Thus, the aim of the present study was to examine the effects of reductive stress as well as the impact of redox individuality on the ability of PBMCs to cope with oxidative stress induced by a widely used prooxidant agent [3, 4, 12, 19]. We have approached reductive stress on terms of high GSH (i.e., the most important nonenzymatic antioxidant) levels postexercise compared to preexercise values (the individuals with this trait will hereafter be considered as the reductive group), whereas the group that hereafter will be considered as the oxidative group includes subjects with low GSH levels postexercise compared to preexercise values.

2. Materials and Methods

2.1. Subjects. Seven male and three female volunteers (age 23.6 ± 0.81 years; age range 21–28 years; height 179.1 ± 1.86 cm; weight 76.86 ± 3.71 kg) participated in the present study. Written consent was provided by all athletes after they were informed about the benefits and risks of the investigation. All subjects confirmed the absence of any history of musculoskeletal injury to their lower limbs. Additionally, smoking, alcohol consumption, and any nutritional supplementation as well as any kind of exercise were prohibited over the last days before and until the experiment

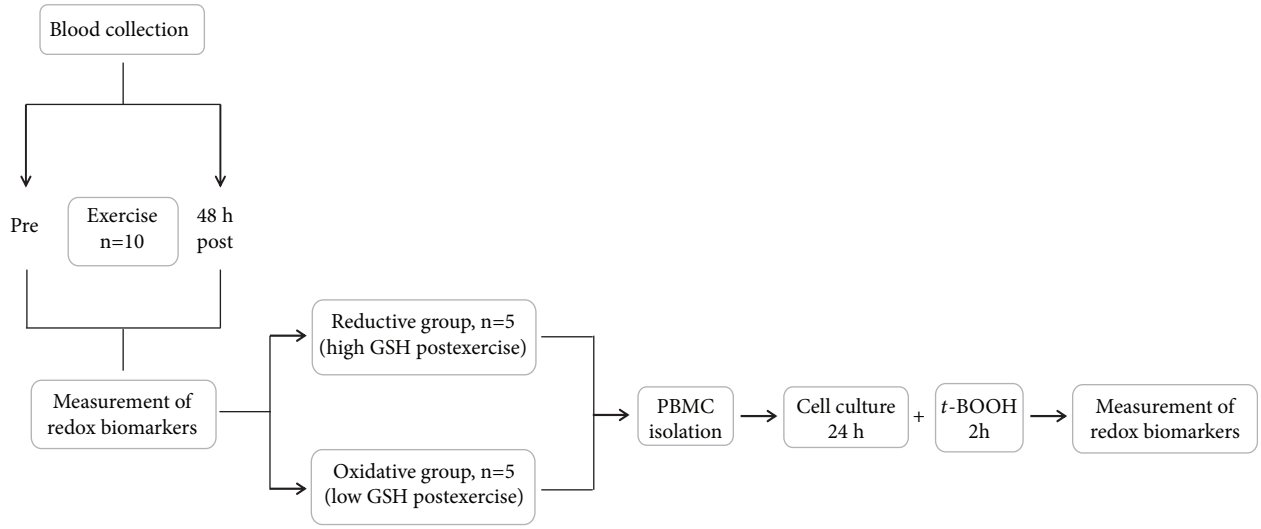

Figure 1: The study design.

was completed. Body mass of the subjects being lightly dressed and barefoot was measured to the nearest 0.5 kg (BeamBalance 710, Seca, United Kingdom). Standing height was also measured to the nearest 0.5 cm (Stadiometer 208, Seca). The procedures were in accordance to the Helsinki declaration of 1964 as revised in 2000 and approval was received by the Human Subjects Committee of the University of Thessaly.

2.2. Study Design. All participants performed an eccentric exercise protocol, and blood samples were collected pre- and 48 h postexercise. The subjects were divided in the reductive and the oxidative groups according to the high or low levels of erythrocyte GSH postexercise compared to preexercise values, respectively. Subsequently, PBMCs were isolated from both groups cultivated, at 37°C for 24 h, treated with the potent oxidizing agent *tert*-butyl hydroperoxide (*t*-BOOH) for 2 h, and redox biomarkers were evaluated in the cell lysate. The experimental design is illustrated in detail in Figure 1.

2.3. Eccentric Exercise Protocol. Eccentric exercise was performed on an isokinetic dynamometer (Cybex Norm, Ronkonkoma, NY), and exercise protocols were undertaken from the seated position (120° hip angle) with the lateral femoral condyle aligned with the axis of rotation of the dynamometer. Participants were coupled to the dynamometer by an ankle cuff, attached proximal to the lateral malleolus and finally stabilized according to the manufacturer's instructions. Participants completed 5 sets of 15 eccentric maximal voluntary contractions (knee range, 0° full extension to 90° flexion) at an angular velocity of 60°/s. A 2 min rest interval was used between sets, and the total workout time was 15 min. Before the exercise session, subjects performed a 10 min warm-up consisting of cycling on a Monark cycle ergometer (Vansbro, Sweden) at 70–80 rpm and 50 W.

2.4. Plasma and Red Blood Cell Lysate (RBCL) Isolation. Ten ml of whole blood was drawn from a forearm vein with subjects in seated position and divided in two ethylenediaminetetraacetic acid (EDTA) tubes. The first one (i.e., 6 ml) was used for PBMC isolation and the second one (i.e., 4 ml) for the determination of redox biomarkers in plasma and erythrocyte lysate. For erythrocyte separation, the tubes were centrifuged (1370 *g*, 10 min, 4°C) and the supernatant (i.e., plasma) was collected. Then, the packed erythrocytes were lysed with 1 : 1 (*v*/*v*) distilled water, inverted vigorously, and centrifuged (4020 *g*, 15 min, 4°C), and the supernatant (i.e., RBCL) was collected. The plasma and RBCL samples were then stored at −80°C prior to biochemical analyses.

2.5. Isolation and Cultivation of PBMCs. PBMCs were isolated by Ficoll-Histopaque 1077 density gradient centrifugation according to the manufacturer's instruction. More specifically, 10 ml of whole blood was carefully added into 10 ml of Ficoll reagent and the samples were centrifuged (400 *g*, 20 min, 20°C). The centrifugation was performed without a brake and acceleration in order to separate the monocytes without mixing with Ficoll, which is a cytotoxic agent for blood cells. The monocytes (i.e., lymphocytes, mononuclear cells, and thrombocytes) are located at the semiwhite layer between the plasma and the erythrocytes and Ficoll. The cell layer was carefully harvested by syringe and added to 10 ml of RPMI-1640 medium. The cells were rinsed twice with the medium by centrifugation (400 *g*, 20 min, 20°C) at normal brake and acceleration. The cell pellet after washing was resuspended in 20 ml of RPMI-1640 medium enriched with 1% L-glutamine, 1% antibiotic/antifungal solution, and 10% fetal bovine serum (FBS). The cells were cultured for 24 h in an incubator at 37°C prior to performing the experiments.

2.6. Treatment of PBMCs with t-BOOH. The cells after isolation and their 24-h incubation were measured using a Neubauer-type cytometer (Hausser Scientific, USA). For the experiments, the cells were plated on a Corning 24-well plate (Sigma-Aldrich, St. Louis, USA). About 1×10^6 PBMCs were added to each position in the 24-well

plate diluted in LM-L-glutamine-supplemented RPMI-1640 medium, 1% antibiotic/antifungal solution, and 0% FBS. After 24 h of incubation, the oxidative agent *t*-BOOH was added to the cells to induce oxidative stress. The cells were incubated for 2 h in the RPMI-1640 medium in the absence of serum FBS. The samples containing the cells in the medium were used as the negative control, while the samples containing the cells and the oxidizing agent (80 μM of *t*-BOOH) were used as the positive control. The selected concentration of the oxidizing agent (i.e., 80 μM) did not exert cytotoxic action during the 2 h of incubation, yet induced oxidative stress. Then, the cells were harvested from the plate and centrifuged (3000 *g*, 5 min, 4°C), the supernatant was removed, and the cell pellet was collected. Subsequently, it was washed with 1 ml of phosphate buffer (PBS, 0.01 M, pH = 7.4) at room temperature (RT) and centrifuged (3000 *g*, 5 min, 4°C). The cell pellet was resuspended in 1 ml of PBS, and, finally, PBMCs were ruptured after sonication for 1 min with 10 sec interruptions on ice. Finally, total protein concentration of each sample was determined using the Bradford reagent and the samples were stored at −80°C until further analysis.

2.7. Protocols for the Measurement of Redox Biomarkers. To evaluate the participant redox status, GSH concentration and catalase (CAT) activity were determined in RBCL and PBMCs, whereas thiobarbituric acid reactive substances (TBARS) and total antioxidant capacity (TAC) were measured in plasma and PBMCs. All the spectrophotometric assays in the plasma and RBCL were performed with slight modifications as previously described by Spanidis et al. [12] and Veskoukis et al. [26], whereas regarding PBMCs, they were carried out as described below. We should note that the protein concentration of each sample required for the measurement of the aforementioned biomarkers is equal to 30 μg/sample.

For GSH in PBMCs, the reaction was performed in 1 ml containing 520 μl of 67 mM sodium phosphate buffer (pH = 8), 150 μl of cytoplasmic suspension, and 330 μl of 1 mM 5,5′-dithiobis (2-nitrobenzoic acid) (DTNB) solution. The samples were mixed and incubated at RT in the dark for 15 min, and the absorbance was monitored at 412 nm. The concentration of GSH was calculated on the basis of the millimolar extinction coefficient of DTNB (13.6 l/mmol/cm) and is expressed as nmol GSH/mg protein.

For the determination of CAT activity in PBMCs, the reaction was performed in 3 ml containing 150 μl of cytoplasmic suspension and 2845 μl of 67 mM potassium phosphate buffer (pH = 7.4). The samples were incubated for 10 min at 37°C. Then, 5 μl of a 30% *w*/*v* H_2O_2 solution was added, and the absorbance was immediately monitored at 240 nm for 1.5 min. The activity of CAT was based on the molar extinction coefficient of H_2O_2 (40 l/mol/cm) and is expressed as U/mg protein.

For TBARS, 400 μl of cell suspension was mixed with 500 μl of 35% trichloroacetic acid (TCA) solution and 500 μl of Tris-HCl solution (200 mM, pH = 7.4), and the samples were incubated for 10 min at RT. Then, 1 ml of 2 M Na_2SO_4 solution with 55 mM of thiobarbituric acid (TBA) were added, and the samples were incubated for 45 min at 95°C in a water bath. Then, the samples were cooled for 5 min on ice followed by the addition of 1 ml of 70% TCA, the samples were centrifuged (15,000 *g*, 3 min), and the absorbance of the supernatant was monitored at 530 nm. TBARS concentration was calculated on the basis of the micromolar extinction coefficient of malondialdehyde (MDA) (0.156 l/μmol/cm) and is expressed as nmol/mg protein.

For TAC, the reaction was performed in 1 ml containing 50 μl of cytoplasmic suspension, 450 μl of 10 mM sodium phosphate buffer (pH = 7.4), and 500 μl of 0.1 mM 2,2-diphenyl-1-picrylhydrazyl ($DPPH^{\cdot}$) radical solution. Samples containing only the radical solution were diluted in the sodium phosphate buffer (pH = 7.4) and were used as the control. The samples were mixed vigorously and incubated for 60 min at RT in the dark. Then, they were centrifuged (20,000 *g*, 3 min, 4°C), and the absorbance was monitored at 517 nm. TAC was expressed as μmol $DPPH^{\cdot}$ reduced to 1,1-diphenyl-2-picryldrazine (DPPH-H) by the antioxidant components of the cytoplasmic suspension per mg of sample protein.

Total protein of the samples was determined using the Bradford assay [27]. Each assay was performed in triplicates. Blood samples were stored in multiple aliquots at −80°C and thawed only once before analysis. All reagents were purchased from Sigma-Aldrich (St. Louis, MO, USA).

2.8. Statistical Analysis. The statistical analysis was based on one-way ANOVA followed by Dunnett's test for multiple pairwise comparisons. The statistical significance level was set at $p < 0.05$. For all statistical analyses, SPSS version 20.0 (SPSS Inc., Chicago, IL, USA) was used. Data are presented as mean ± SEM.

3. Results

The participants were divided on the basis of those who exerted increased GSH concentration in RBCL postexercise by 13.5% (i.e., the reductive group, $n = 5$) and those with decreased GSH concentration in RBCL postexercise by 12.1 (i.e., the oxidative group, $n = 5$) compared with the preexercise values (Figure 2). These GSH values will hereafter be considered as the initial or baseline values. The athletic history of the participants was not considered as a criterion since the reductive group constituted 3 individuals who performed regular resistance training, while 2 individuals had never been in contact with any kind of exercise. The inverse proportion existed in the oxidative group, which constituted 2 well-trained and 3 nontrained individuals. With respect to our results, an expected significant difference was observed in GSH levels between these two groups (i.e., reductive and oxidative). Similarly, a significant difference between the two groups was also observed in TBARS, as they were significantly increased by 20.1% in the oxidative group and they remained unaffected in the reductive group (Figure 2). Therefore, the participants of the reductive group seem to be protected against exercise-induced lipid peroxidation. Moreover, there were no significant changes in TAC and CAT activity between the two groups.

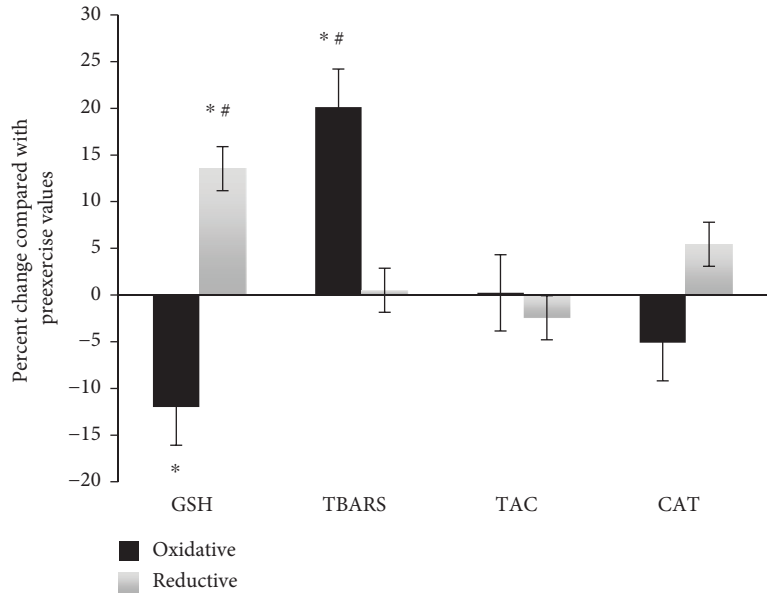

Figure 2: Percent changes of GSH and CAT in RBCL and plasma TBARS and TAC 48 h postexercise compared with preexercise in both oxidative and reductive groups. *Statistically significant compared with the preexercise value ($p < 0.05$) #Statistically significant difference between the two groups in the same time point ($p < 0.05$). GSH: reduced glutathione; CAT: catalase; RBCL: red blood cell lysate; TBARS: thiobarbituric acid reactive substances; TAC: total antioxidant capacity.

The analyses of the redox biomarkers tested in PBMCs were based on the comparison of their levels in PBMCs treated with *t*-BOOH compared with control cells in both the reductive and oxidative groups. The differences between the two groups were expressed as percent change. With respect to the TBARS levels of the oxidative group, a statistically significant increase was observed 48 h postexercise compared with the preexercise value indicating that eccentric exercise induced a high level of lipid peroxidation (Figure 3). There were no significant changes in GSH, TAC, and CAT activity between the two time points. On the contrary, the analyses in the reductive group revealed statistically significant increases in the GSH and CAT levels 48 h postexercise compared with the preexercise values (Figure 4). In the same pattern, a significant decrease in postexercise TBARS levels was also observed indicating that the lipids in the reductive group are protected against exercise-induced oxidative stress. The latter finding is in contrary with the corresponding data from the oxidative group (Figure 3).

4. Discussion

Over the last few years, several studies have made serious efforts to approach "reductive stress," a condition in which cells exhibit a reductive (i.e., increased antioxidant defenses and impaired free radical generation) redox status after a redox-altering stimulus (e.g., exercise, nutritional, and pharmacological interventions) [14]. In this study, we report that the effects of an oxidizing agent (i.e., *t*-BOOH) on the redox status of PBMCs isolated from the blood of athletes after acute eccentric exercise are dependent on the RBCL baseline values of GSH. As GSH is considered the most important and abundant endogenous nonenzymatic antioxidant [28], we divided the participants in two groups according to their initial (the postexercise as we stated in the results) erythrocyte GSH levels. In particular, half of the participants that have their GSH levels increased 48 h postexercise were clustered in the reductive group. The rest 5 individuals were included in the oxidative group because their GSH concentration postexercise (i.e., GSH baseline values) was decreased. According to our results in PBMCs, lipid peroxidation levels as depicted by TBARS concentration remained unchanged after exercise in the reductive group compared to preexercise, contrary to the observed enhancement in the oxidative group. In addition, the GSH concentration and CAT activity were increased in the reductive group, whereas they were not affected in the oxidative group. It seems, therefore, that reactive species production postexercise followed by administration of an oxidizing agent can be successfully buffered by high baseline levels of GSH sufficiently protecting macromolecules against subsequent oxidative modifications.

It is widely established that eccentric exercise, which was used in the present study in order to group our participants, is linked to remarkable muscle damage [5]. Some common outcomes of eccentric exercise include large elevations of oxidative stress biomarkers and increased levels of creatinine kinase and myoglobin in plasma lasting for days [9]. Furthermore, a previous research of our group has reported that eccentric exercise induces severe delayed-onset muscle soreness accompanied by low antioxidant reserves and impaired reducing activity highlighting the direct connection between muscle damage and the degree of exercise-induced oxidative stress [29]. However, even though eccentric exercise is linked to remarkable muscle damage, recent findings indicate that individuals exhibit significant variations regarding their oxidative status postexercise [4]. Given that eccentric exercise

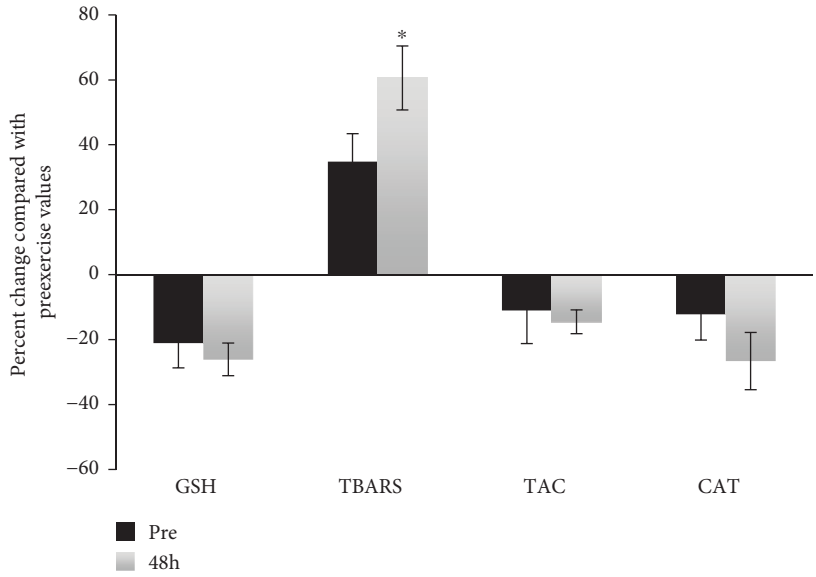

Figure 3: Percent change of the tested redox biomarkers in the *t*-BOOH-treated PBMCs pre- and 48 h postexercise in the oxidative group compared with the control. *Statistically significant compared with the preexercise value ($p < 0.05$). GSH: reduced glutathione; CAT: catalase; RBCL: red blood cell lysate; TBARS: thiobarbituric acid reactive substances; TAC: total antioxidant capacity.

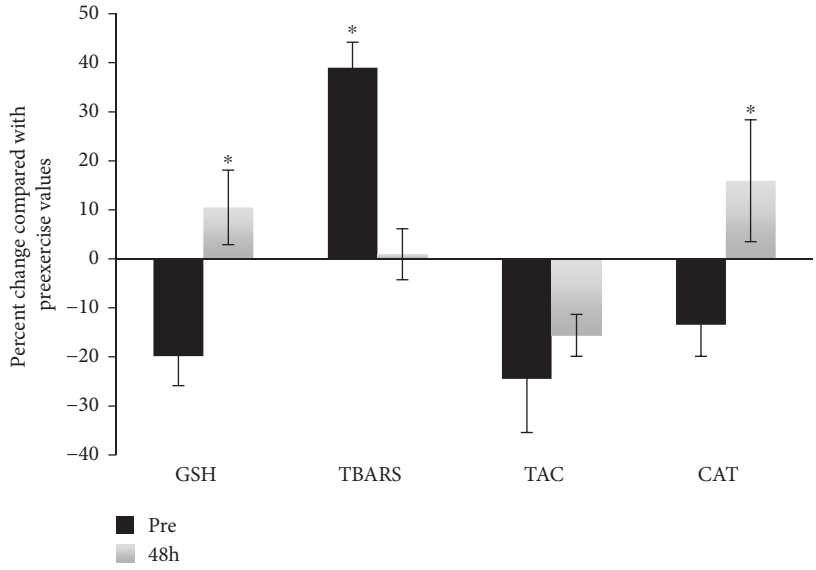

Figure 4: Percent change of the tested redox biomarkers in the *t*-BOOH-treated PBMCs pre- and 48 h postexercise in the reductive group compared with the control. *Statistically significant compared with the preexercise value ($p < 0.05$). GSH: reduced glutathione; CAT: catalase; RBCL: red blood cell lysate; TBARS: thiobarbituric acid reactive substances; TAC: total antioxidant capacity.

generates greater amount of muscle damage compared to other exercise modalities [9], it becomes apparent that it highly affects exercise-induced oxidative stress and, thus, it is an excellent model for clustering individuals according to high or low values of redox biomarkers (GSH in particular).

The major characteristic of this elaborative study is that we take into consideration the initial values of GSH in order to cluster the participants in the reductive and oxidative groups. This approach has been scarcely adopted by other important papers of the field, as well [3, 4, 13, 14]. A novel feature, though, that this article touches upon is that the GSH baseline values, although referred to postexercise GSH values, they are considered as the initial GSH levels for our subsequent cell culture experiment. According to our findings, this approach is quite reasonable. A paper that has been published recently reported that individuals with low resting (i.e., preexercise) GSH levels are more susceptible to oxidative stress and impaired physical performance compared to their counterparts with high resting GSH values [14]. This finding is in line with the results we present here (i.e., high

initial GSH values are linked to protection against oxidative challenge). Although we define initial values differently than Paschalis et al., our results are on the same page. Therefore, we believe that our findings would not be much different if we had grouped our subjects on the basis of resting (i.e., preexercise) values.

It has been reported that strenuous exercise leads to increased circulating levels of proinflammatory mediators, such as PBMCs, and upregulates PBMC growth factor genes like epiregulin and platelet-derived growth factor, which are effective in healing wounds and in stimulating muscle cell regeneration [30, 31]. Moreover, it has been stated that PBMCs could also contribute to tissue growth and repair [30]. Given that reactive species are considered crucial signaling molecules for exercise adaptations [32], we wondered whether the reductive group could be benefited from exercise in the same extent compared to their counterparts of the oxidative group. In order to address this issue, we focused on the response of PBMCs isolated from individuals postexercise after their treatment with a potent and widely used oxidizing agent. PBMCs were selected as they are cells of major importance in the human immune system [33]. We hypothesized that PBMCs isolated from reductive volunteers might more effectively counteract the *t*-BOOH-derived oxidation. The data obtained by our experiment confirmed this notion. Intriguingly, in the reductive group, *t*-BOOH led to an induction of CAT and GSH. The induction of both GSH and CAT seems to represent a protective mechanism against lipid peroxidation as the levels of TBARS remained unchanged after exercise even if *t*-BOOH caused severe oxidative response.

Taking into consideration the mechanism of *t*-BOOH action when administered to PBMCs, our results are very interesting. Typically, *t*-BOOH is an organic hydroperoxide that is commonly used as a toxic, redox-altering agent [34]. It is known that *t*-BOOH is metabolized by glutathione peroxidase generating GSSG via GSH oxidation [35, 36]. As it has been previously shown, increased GSH concentration may become harmful for physiological cells by transferring electrons to O_2 since there are no available natural electron acceptors (e.g., GSSG) as it happens in reductive stress context [17, 37]. Although this could be the case in our study, it seems that the increased baseline values of GSH are not harmful because, due to the presence of a potent oxidizing agent, GSH is oxidized to form GSSG. Thus, reductive stress on the basis of baseline values is perhaps a protective mechanism when followed by a stimulus that induces oxidative stress, such as administration of *t*-BOOH. It has also been proposed that *t*-BOOH interacts with Fe^{+2} leading to the formation of *t*-$BO^{\cdot}$ radicals [36], whereas it can also be converted to peroxyl and alkoxyl radicals by enzymes of cytochrome P450 complex and through free iron-dependent reactions [35]. It is obvious that the production of free radicals can further decrease GSH levels, impair the mechanisms of antioxidant defense, and initiate lipid peroxidation. This decrease in GSH concentration implies that it is a protective mechanism present after the combination of reductive stress with an oxidizing stimulus.

The observed responses could be mainly attributed, at the molecular level, to specific transcription factors, namely, NF-κB, p38 MAPK, members of the FoxO family, and nuclear factor erythroid-derived 2-like 2 (Nrf2) all activated by low ROS levels [38, 39]. Focusing on Nrf2, it has been suggested that it is critical for the regulation of the intracellular redox status [40, 41]. It acts by promoting both constitutive and inducible expressions of the antioxidant response element- (ARE-) regulated genes, which code for numerous antioxidant metabolites and enzymes [42]. Two glutathione-related ARE-regulated enzymes are glutathione reductase (GR) and GSH synthase (GSS) that play significant roles in GSH synthesis and regeneration [28]. Therefore, we can aptly hypothesize that Nrf2 is a key player in the control of exercise and chemically induced shift between oxidative and reductive stress in the examined individuals.

5. Conclusion

In conclusion, it is a fact that there is a debate in the pertinent literature whether reductive stress is beneficial or detrimental. In this study, we report that the effects of an oxidizing agent on redox status of PBMCs isolated from the blood of athletes after acute eccentric exercise are dependent on the baseline values of GSH in erythrocytes. Otherwise, on the basis of our results, reductive stress defined by increased GSH levels in erythrocytes postexercise is a protective mechanism, at least when followed by an oxidizing stimulus. These findings can be considered as a starting point in the effort to examine the relatively new concept of postexercise reductive stress and shed light on its potential beneficial impact on blood redox homeostasis using differential experimental treatments.

Data Availability

All data, tables, and figures in this manuscript are original and are available upon request.

Ethical Approval

All procedures performed in this study involving human participants were in accordance with the ethical standards of the institutional and/or national research committee and with the 1964 Helsinki declaration and its later amendments or comparable ethical standards, and approval was received by the "Human Subjects Committee" of the University of Thessaly (reference number: 1074, date: 10/02/2016).

Conflicts of Interest

The authors had no financial, consultant, or other relations that might lead to bias or a conflict of interest. The results of the present study are presented clearly, honestly, and without fabrication, falsification, or inappropriate data manipulation.

Acknowledgments

The study was funded by the Hellenic General Secretariat for Research and Technology (GSRT) and the Hellenic Foundation for Research and Innovation (HFRI) (grant number 5450).

References

[1] P. Steinbacher and P. Eckl, "Impact of oxidative stress on exercising skeletal muscle," *Biomolecules*, vol. 5, no. 2, pp. 356–377, 2015.

[2] C. E. Cooper, N. B. J. Vollaard, T. Choueiri, and M. T. Wilson, "Exercise, free radicals and oxidative stress," *Biochemical Society Transactions*, vol. 30, no. 2, pp. 280–285, 2002.

[3] D. Stagos, N. Goutzourelas, A.-M. Ntontou et al., "Assessment of eccentric exercise-induced oxidative stress using oxidation-reduction potential markers," *Oxidative Medicine and Cellular Longevity*, vol. 2015, Article ID 204615, 10 pages, 2015.

[4] N. V. Margaritelis, A. Kyparos, V. Paschalis et al., "Reductive stress after exercise: the issue of redox individuality," *Redox Biology*, vol. 2, pp. 520–528, 2014.

[5] D. H. Serravite, A. Perry, K. A. Jacobs, J. A. Adams, K. Harriell, and J. F. Signorile, "Effect of whole-body periodic acceleration on exercise-induced muscle damage after eccentric exercise," *International Journal of Sports Physiology and Performance*, vol. 9, no. 6, pp. 985–992, 2014.

[6] M. A. Brentano and L. F. Martins Kruel, "A review on strength exercise-induced muscle damage: applications, adaptation mechanisms and limitations," *The Journal of Sports Medicine and Physical Fitness*, vol. 51, no. 1, pp. 1–10, 2011.

[7] M. G. Nikolaidis, A. Z. Jamurtas, V. Paschalis, I. G. Fatouros, Y. Koutedakis, and D. Kouretas, "The effect of muscle-damaging exercise on blood and skeletal muscle oxidative stress: magnitude and time-course considerations," *Sports Medicine*, vol. 38, no. 7, pp. 579–606, 2008.

[8] J. G. Tidball, "Inflammatory processes in muscle injury and repair," *American Journal of Physiology-Regulatory, Integrative and Comparative Physiology*, vol. 288, no. 2, pp. R345–R353, 2005.

[9] I. G. Fatouros and D. Kouretas, "Exercise, oxidative stress, and inflammation," *Exercise Physiology: from a Cellular to an Integrative Approach*, vol. 75, p. 245, 2010.

[10] A. S. Veskoukis, M. G. Nikolaidis, A. Kyparos et al., "Effects of xanthine oxidase inhibition on oxidative stress and swimming performance in rats," *Applied Physiology, Nutrition, and Metabolism*, vol. 33, no. 6, pp. 1140–1154, 2008.

[11] Z. Radak, Z. Zhao, E. Koltai, H. Ohno, and M. Atalay, "Oxygen consumption and usage during physical exercise: the balance between oxidative stress and ROS-dependent adaptive signaling," *Antioxidants & Redox Signaling*, vol. 18, no. 10, pp. 1208–1246, 2013.

[12] Y. Spanidis, D. Stagos, M. Orfanou et al., "Variations in oxidative stress levels in 3 days follow-up in ultramarathon mountain race athletes," *Journal of Strength and Conditioning Research*, vol. 31, no. 3, pp. 582–594, 2017.

[13] G. Block, C. D. Jensen, J. D. Morrow et al., "The effect of vitamins C and E on biomarkers of oxidative stress depends on baseline level," *Free Radical Biology & Medicine*, vol. 45, no. 4, pp. 377–384, 2008.

[14] A. S. Veskoukis, A. M. Tsatsakis, and D. Kouretas, "Dietary oxidative stress and antioxidant defense with an emphasis on plant extract administration," *Cell Stress and Chaperones*, vol. 17, no. 1, pp. 11–21, 2012.

[15] D. P. Jones, "Redefining oxidative stress," *Antioxidants & Redox Signaling*, vol. 8, no. 9-10, pp. 1865–1879, 2006.

[16] H. Sies, *1 - Oxidative Stress: Introductory Remarks*, Academic Press, London, UK, 1985.

[17] P. Korge, G. Calmettes, and J. N. Weiss, "Increased reactive oxygen species production during reductive stress: the roles of mitochondrial glutathione and thioredoxin reductases," *Biochimica et Biophysica Acta (BBA) - Bioenergetics*, vol. 1847, no. 6-7, pp. 514–525, 2015.

[18] N. V. Margaritelis, A. A. Theodorou, V. Paschalis et al., "Adaptations to endurance training depend on exercise-induced oxidative stress: exploiting redox interindividual variability," *Acta Physiologica*, vol. 222, no. 2, 2018.

[19] Y. Spanidis, A. Priftis, D. Stagos et al., "Oxidation of human serum albumin exhibits inter-individual variability after an ultra-marathon mountain race," *Experimental and Therapeutic Medicine*, vol. 13, no. 5, pp. 2382–2390, 2017.

[20] D. Shen, T. P. Dalton, D. W. Nebert, and H. G. Shertzer, "Glutathione redox state regulates mitochondrial reactive oxygen production," *Journal of Biological Chemistry*, vol. 280, no. 27, pp. 25305–25312, 2005.

[21] M. A. Aon, S. Cortassa, and B. O'Rourke, "Redox-optimized ROS balance: a unifying hypothesis," *Biochimica et Biophysica Acta (BBA) - Bioenergetics*, vol. 1797, no. 6-7, pp. 865–877, 2010.

[22] S. Cortassa, B. O'Rourke, and M. A. Aon, "Redox-optimized ROS balance and the relationship between mitochondrial respiration and ROS," *Biochimica et Biophysica Acta (BBA) - Bioenergetics*, vol. 1837, no. 2, pp. 287–295, 2014.

[23] J. Pourahmad and A. Salimi, "Isolated human peripheral blood mononuclear cell (PBMC), a cost effective tool for predicting immunosuppressive effects of drugs and xenobiotics," *Iranian Journal of Pharmaceutical Research*, vol. 14, no. 4, p. 979, 2015.

[24] H. B. Nielsen, "Lymphocyte responses to maximal exercise: a physiological perspective," *Sports Medicine*, vol. 33, no. 11, pp. 853–867, 2003.

[25] R. J. Shephard, "Adhesion molecules, catecholamines and leucocyte redistribution during and following exercise," *Sports Medicine*, vol. 33, no. 4, pp. 261–284, 2003.

[26] A. S. Veskoukis, A. Kyparos, V. Paschalis, and M. G. Nikolaidis, "Spectrophotometric assays for measuring redox biomarkers in blood," *Biomarkers*, vol. 21, no. 3, pp. 208–217, 2016.

[27] M. M. Bradford, "A rapid and sensitive method for the quantitation of microgram quantities of protein utilizing the principle of protein-dye binding," *Analytical Biochemistry*, vol. 72, no. 1-2, pp. 248–254, 1976.

[28] C. Espinosa-Diez, V. Miguel, D. Mennerich et al., "Antioxidant responses and cellular adjustments to oxidative stress," *Redox Biology*, vol. 6, pp. 183–197, 2015.

[29] Y. Spanidis, D. Stagos, C. Papanikolaou et al., "Resistance-trained individuals are less susceptible to oxidative damage after eccentric exercise," *Oxidative Medicine and Cellular Longevity*, vol. 2018, Article ID 6857190, 11 pages, 2018.

[30] K. Ostrowski, T. Rohde, S. Asp, P. Schjerling, and B. K. Pedersen, "Pro- and anti-inflammatory cytokine balance in strenuous exercise in humans," *The Journal of Physiology*, vol. 515, no. 1, pp. 287–291, 1999.

[31] B. K. Draper, T. Komurasaki, M. K. Davidson, and L. B. Nanney, "Epiregulin is more potent than EGF or TGFα in promoting in vitro wound closure due to enhanced ERK/MAPK activation," *Journal of Cellular Biochemistry*, vol. 89, no. 6, pp. 1126–1137, 2003.

[32] M. Schieber and N. S. Chandel, "ROS function in redox signaling and oxidative stress," *Current Biology*, vol. 24, no. 10, pp. R453–R462, 2014.

[33] P. Autissier, C. Soulas, T. H. Burdo, and K. C. Williams, "Evaluation of a 12-color flow cytometry panel to study lymphocyte, monocyte, and dendritic cell subsets in humans," *Cytometry Part A*, vol. 77A, no. 5, pp. 410–419, 2010.

[34] M. Alia, S. Ramos, R. Mateos, L. Bravo, and L. Goya, "Response of the antioxidant defense system to *tert*-butyl hydroperoxide and hydrogen peroxide in a human hepatoma cell line (HepG2)," *Journal of Biochemical and Molecular Toxicology*, vol. 19, no. 2, pp. 119–128, 2005.

[35] C. F. Lima, M. Fernandes-Ferreira, and C. Pereira-Wilson, "Phenolic compounds protect HepG2 cells from oxidative damage: relevance of glutathione levels," *Life Sciences*, vol. 79, no. 21, pp. 2056–2068, 2006.

[36] C. Martin, R. Martinez, R. Navarro, J. I. Ruiz-Sanz, M. Lacort, and M. B. Ruiz-Larrea, "*tert*-Butyl hydroperoxide-induced lipid signaling in hepatocytes: involvement of glutathione and free radicals," *Biochemical Pharmacology*, vol. 62, no. 6, pp. 705–712, 2001.

[37] J. Bauersachs and J. D. Widder, "Reductive stress: linking heat shock protein 27, glutathione, and cardiomyopathy?," *Hypertension*, vol. 55, no. 6, pp. 1299-1300, 2010.

[38] S. L. Dodd, B. J. Gagnon, S. M. Senf, B. A. Hain, and A. R. Judge, "Ros-mediated activation of NF-κB and Foxo during muscle disuse," *Muscle & Nerve*, vol. 41, no. 1, pp. 110–113, 2010.

[39] F. Derbre, B. Ferrando, M. C. Gomez-Cabrera et al., "Inhibition of xanthine oxidase by allopurinol prevents skeletal muscle atrophy: role of p38 MAPKinase and E3 ubiquitin ligases," *PLoS One*, vol. 7, no. 10, article e46668, 2012.

[40] E. Kerasioti, D. Stagos, A. Tzimi, and D. Kouretas, "Increase in antioxidant activity by sheep/goat whey protein through nuclear factor-like 2 (Nrf2) is cell type dependent," *Food and Chemical Toxicology*, vol. 97, pp. 47–56, 2016.

[41] A. Priftis, A.-. E. Angeli-Terzidou, A. Veskoukis, D. Spandidos, and D. Kouretas, "Cell-specific and roasting-dependent regulation of the Keap1/Nrf2 pathway by coffee extracts," *Molecular Medicine Reports*, vol. 17, pp. 8325–8331, 2018.

[42] U. Garbin, A. Fratta Pasini, C. Stranieri et al., "Cigarette smoking blocks the protective expression of Nrf2/ARE pathway in peripheral mononuclear cells of young heavy smokers favouring inflammation," *PLoS One*, vol. 4, no. 12, article e8225, 2009.

Hindawi
Oxidative Medicine and Cellular Longevity
Volume 2018, Article ID 3732842, 8 pages
https://doi.org/10.1155/2018/3732842

Research Article

Protective Effect of Increased Zinc Supply against Oxidative Damage of Sublingual Gland in Chronic Exposure to Cadmium: Experimental Study on Rats

Paula Kostecka-Sochoń,[1] Barbara M. Onopiuk,[2] and Ewa Dąbrowska[3]

[1]*Department of Restorative Dentistry, Medical University of Białystok, Białystok, Poland*
[2]*Medical University of Białystok and Private Dental Practice in Białystok, Białystok, Poland*
[3]*Department of Social and Preventive Dentistry, Medical University of Białystok, Białystok, Poland*

Correspondence should be addressed to Barbara M. Onopiuk; barbara.maria.dabrowska@gmail.com

Received 18 April 2018; Accepted 20 June 2018; Published 4 July 2018

Academic Editor: Patricia Morales

Cadmium is one of the main chemical pollutants found in the daily environment of developed countries. Cigarettes are a significant source of that metal, which makes it important in terms of oral cavity health. The aim of this study was to determine if increased supply of zinc in chronic exposure to cadmium might protect the sublingual gland structure against oxidative damage. The experiment took 12 months and was conducted on 72 adult male rats. They were randomized into 9 groups. Eight groups received cadmium in drinking water (as $CdCl_2$) at 5 or 50 mg Cd/dm^3 and/or zinc (as $ZnCl_2$) at 30 or 60 mg Zn/dm^3. The control group received regular water. In the sublingual gland of all animal groups, levels of oxidative parameters were measured. The oxidative stress index was calculated as a TOS/TAS ratio. Cadmium exposure at 5 mg and 50 mg Cd/dm^3 induced oxidative stress in the sublingual glands of the rats. Cadmium reduced the TAS and GSH levels and increased LPO, H_2O_2, TOS, and OSI. In cadmium exposure conditions, increasing the supply of zinc by 79% or 151%, as compared to the standard dietary intake of this microelement, completely prevented the reduction of TAS and GSH levels and accumulation of LPO, H_2O_2, and TOS in the examined gland at both exposure levels to that metal. The outcome data confirm the protective effect of increased zinc intake on the sublingual gland tissue in chronic cadmium exposure.

1. Introduction

Cadmium is one of the main chemical pollutants found in the daily environment of developed countries [1–4]. Cigarettes are a significant source of this metal, which makes it important in terms of oral cavity health [4–6].

Cadmium is accumulated in various tissues and organs and may have serious consequences for the general population health. Chronic exposure to cadmium may damage the kidneys, bones, liver, lungs, and other organs, including sublingual glands [7–12]. An important role in the cadmium activity mechanism is attributed to its strong prooxidative properties [9, 13–15]. Cadmium has the ability to form reactive oxygen species (ROS) through direct impact, that is, by disrupting the electron transport chain, or indirectly by weakening the enzymatic and nonenzymatic antioxidative barrier [8, 9, 13, 15]. Disruptions of the cellular oxidation-reduction balance may cause damage to tissues and organs and impair their functions [8, 12, 16, 17].

The available literature of the subject indicates that many toxic effects of cadmium can be prevented or at least reduced by increasing the supply of zinc [8, 18–21], as zinc exhibits antagonistic activity towards that toxic metal. It has been shown that this bioelement is able to provide efficient protection against damage to the organs in which cadmium accumulates the most, that is, the liver, kidneys, and bones

[10, 19, 20, 22]. It is believed that the protective role of zinc against cadmium toxicity arises from the former's antioxidant properties [21, 23–26].

Thus far, the impact of zinc on the sublingual gland of an organism exposed to cadmium has not been studied. In consideration thereof, this study involved experimental analysis to determine if the increased supply of zinc in chronic exposure to cadmium might protect the sublingual gland structure against oxidative damage. For this purpose, in the sublingual gland of rats which received cadmium and/or zinc and of control animals, the oxidative stress markers were assayed.

2. Materials and Methods

The experiment took 12 months and was conducted on 72 adult male Wistar rats with an initial body weight of 220 g. Throughout the experiment period, the animals were kept in standard conditions (air temperature 18–21°C, relative humidity 50 ± 10%, and 12-hour circadian rhythm) and were provided with unlimited access to balanced granulated LSM fodder (Motycz near Lublin) and drinking water.

The research protocol was approved by the Local Ethics Committee for Animal Experiments in Białystok (Poland) and performed in accordance with the ethical principles and institutional guidelines and International Guide for the Use of Animals in Biomedical Research.

The rats were randomized into 9 groups, and in each group was 8 animals. In research, 2 groups received Zn alone, 2 groups were treated with Cd alone, and 4 groups received Zn supplementation during exposure to Cd. Zn and Cd were administered in drinking water at the concentrations of 30 or 60 mg Zn/L (as $ZnCl_2$; Merck) and 5 or 50 mg Cd/L (as $CdCl_2 \cdot 2\ 1/2H_2O$; POCH; Gliwice, Poland) alone (30 mg Zn/L, 60 mg Zn/L, 5 mg Cd/L, and 50 mg Cd/L groups) and in combination (5 mg Cd/L + 30 mg Zn/L, 5 mg Cd/L + 60 mg Zn/L, 50 mg Cd/L + 30 mg Zn/L, and 50 mg Cd/L + 60 mg Zn/L groups) for up to 12 months. The control group received drinking water without cadmium or zinc. During the experiment, the daily intake of fluids and body weight gain were controlled. Both the fluid intake and body weight gains were similar across all rat groups. Rat exposure to cadmium at 5 mg/dm^3 is an equivalent of environmental exposure of humans to that metal, particularly smokers; at 50 mg of Cd/dm^3, it is equivalent to occupational exposure and exposure arising from high pollution and heavy smoking. Administering zinc at 30 mg or 60 mg/dm^3 to the animals increased the daily intake of this bioelement by 79% and 151%, respectively, in comparison with standard dietary intake. This dose was chosen based on findings of other authors and observations of the Department of Toxicology of the Medical University of Białystok [10, 19].

After ending the exposure, the animals were put under barbiturate anesthesia (Vetbutal 30 mg/kg of body weight i.p.) and various types of biological material were collected for analysis, including sublingual glands which were flushed in PBS, drained on blotting paper, and secured for further analysis by deep freezing at −80°C. After thawing, the dissected glands were weighted and 20% homogenates were prepared using a glass tissue homogenizer (Schuett Homogen, Göttingen, Germany) in a cold 50 mM potassium phosphate buffer with pH = 7.4. In order to prevent automatic oxidation of the analyzed material, 0.5 M BHT acetonitrile was added to the samples (10 μL per 1 cm^3 of homogenate). The homogenates were centrifuged (MPW-350R, Medical Instruments laboratory centrifuge; Warsaw, Poland) 700 ×g for 20 minutes at 4°C. After centrifugation, the supernatant was immediately isolated and the oxidative stress markers and protein levels were assayed [27].

The total antioxidative capacity (TAS) and the total oxidative status (TOS) of the homogenates were determined using ImAnOx (TAS) ELISA kit and PerOx (TOS) ELISA kit by Immundiagnostik AG (Germany). The TAS values assayed in the control samples provided with the kit were 191.88 ± 10.7 and 264.33 ± 15.6 μmol/L (average ± SEM; $n = 2$) and fell within the range of values provided by the manufacturer (170–230 μmol/L and 258–350 μmol/L). The precision of the method expressed as a coefficient of variation (CV) was <6%. The TOS values assayed in the control samples provided with the kit were 156.36 ± 4.27 and 424.85 ± 10.16 μmol/L (average ± SEM; $n = 2$) and fell within the range of values provided by the manufacturer (170–230 μmol/L and 305–509 μmol/L). The precision of the method expressed as CV was <3%.

The glutathione (GSH) levels were assayed using the Glutathione Assay Kit, Cayman Chemical (USA). The precision of the method expressed as CV was <1.5%.

The lipid peroxidation (LPO) levels (Bioxytech® LPO-586™) and hydrogen peroxide (H_2O_2) (Bioxytech® H_2O_2-560™) were assayed using kits supplied by OxisResearch (USA). The precision of the method expressed as CV was <4.5%.

All assays performed using commercial kits were performed as per the manufacturers' instructions, and the measured parameters were adjusted for protein concentration.

The obtained results were analyzed statistically using Statistica 10 software (StatSoft; Tulsa, USA). In order to assess the statistical significance of differences between the study groups, a one-way analysis of variance (ANOVA) was performed using Duncan's post hoc test. The independent and interactive impact of cadmium and zinc on the stress index levels was assessed using a two-way analysis of variance (ANOVA/MANOVA). Also, Spearman's rank correlation test was performed for the assessed parameters in the tissue of the studied gland. The differences between groups and correlations between variables were considered statistically significant at $p < 0.05$.

3. Results

3.1. The Impact of Zinc and/or Cadmium on Glutathione (GSH) Levels in the Rat Sublingual Gland. The GSH levels in the sublingual gland of the rats are provided in Table 1. The animals' exposure to 5 mg or 50 mg Cd/dm^3 resulted in the reduction of GSH levels by 24% ($p < 0.001$) and 29% ($p < 0.01$), respectively, as compared to the control group. In the rat group which, throughout the period of exposure to cadmium at 5 mg/dm^3, received 60 mg Zn/dm^3, the

Table 1: The impact of zinc on GSH, LPO, and H_2O_2 levels in the sublingual gland of rats exposed to cadmium.

	Nonenzymatic antioxidant	Oxidative stress index	
	GSH (nmol/mg of protein)	LPO (nmol/mg of protein)	H_2O_2 (nmol/mg of protein)
Control	1.881 ± 0.800	0.122 ± 0.011	21.320 ± 2.343
30 mg Zn/dm^3	1.926 ± 0.181	0.095 ± 0.008	19.110 ± 0.617
60 mg Zn/dm^3	1.838 ± 0.570	0.093 ± 0.015	$15.740 \pm 1.336^{a*}$
5 mg Cd/dm^3	$1.433 \pm 0.086^{a\ddagger b\ddagger c*}$	$0.263 \pm 0.034^{a\dagger b\ddagger c\dagger}$	$26.930 \pm 1.000^{a* b\ddagger}$
5 mg Cd/dm^3 + 30 mg Zn/dm^3	$1.933 \pm 0.136^{d\dagger}$	$0.113 \pm 0.020^{d\dagger}$	$17.480 \pm 0.720^{d\ddagger}$
5 mg Cd/dm^3 + 60 mg Zn/dm^3	$2.334 \pm 0.144^{a\dagger b* c\dagger d\ddagger e\dagger}$	$0.104 \pm 0.012^{d\dagger}$	$18.020 \pm 1.248^{d\ddagger}$
50 mg Cd/dm^3	$1.340 \pm 0.046^{a\dagger b\ddagger c\dagger e\ddagger f\ddagger}$	$0.376 \pm 0.066^{a\ddagger b\ddagger c\ddagger d* e\ddagger f\ddagger}$	$41.800 \pm 2.877^{a\ddagger b\ddagger d\ddagger f\ddagger}$
50 mg Cd/dm^3 + 30 mg Zn/dm^3	$1.715 \pm 0.067^{f\ddagger g*}$	$0.233 \pm 0.045^{a* b\dagger c\dagger f* g\dagger}$	$21.860 \pm 1.480^{d* g\ddagger}$
50 mg Cd/dm^3 + 60 mg Zn/dm^3	$1.739 \pm 0.052^{f\ddagger g*}$	$0.167 \pm 0.023^{d* e* g\ddagger}$	$17.540 \pm 1.963^{d\ddagger g\ddagger}$

The values are arithmetic means ± SEM. $^*p < 0.05$; $^\dagger p < 0.01$; $^\ddagger p < 0.001$ as compared to [a]control, [b]30 mg Zn/dm^3, [c]60 mg Zn/dm^3, [d]5 mg Cd/dm^3, [e]5 mg Cd/dm^3 + 30 mg Zn/dm^3, [f]5 mg Cd/dm^3 + 60 mg Zn/dm^3, [g]50 mg Cd/dm^3, and [h]50 mg Cd/dm^3 + 30 mg Zn/dm^3.

GSH levels were 24% ($p < 0.01$) higher as compared to the GSH levels in the control group, whereas for zinc received in 30 mg/dm^3 doses, the GSH levels remained unchanged. In the animal groups which, throughout the period of exposure to cadmium at 5 mg/dm^3, received 30 mg or 60 mg Zn/dm^3, the GSH levels were 39% ($p < 0.01$) and 63% ($p < 0.001$) higher, respectively, as compared to the GSH levels in the animals exposed solely to cadmium. Also, in the rat groups which, throughout the period of exposure to cadmium at 50 mg/dm^3, received 30 mg or 60 mg Zn/dm^3, the GSH levels were 28% ($p < 0.05$) and 30% ($p < 0.05$) higher, respectively, as compared to the GSH levels in the animals exposed to cadmium.

3.2. The Impact of Zinc and/or Cadmium on Oxidative Stress Index (Lipid Peroxidation and Hydrogen Peroxide) in the Rat Sublingual Gland. Exposure of rats to 5 mg or 50 mg Cd/dm^3 resulted in the increase of LPO levels 2.2-folds ($p < 0.01$) and 3-folds ($p < 0.001$), respectively, as compared to the control group; the increase was larger at a higher exposure level. In the rat groups which, throughout the period of exposure to cadmium at 5 mg/dm^3, received 30 mg or 60 mg Zn/dm^3, the LPO levels were 2.3- and 2.5-folds lower ($p < 0.01$), respectively, as compared to the LPO levels in the animals exposed to cadmium and did not differ from the values observed in the control group. Also, in the rat groups which, throughout the period of exposure to cadmium at 50 mg/dm^3, received 30 mg or 60 mg Zn/dm^3, the LPO levels were 38% ($p < 0.01$) and 56% ($p < 0.001$) lower, respectively, as compared to the LPO levels in the animals exposed to cadmium. In the animal group which, throughout the period of exposure to cadmium at 50 mg/dm^3, received 30 mg Zn/dm^3, the LPO levels were higher than the LPO levels in the control group but did not differ at a higher level of supplementation of that bioelement (Table 1).

Supplementation of zinc at 30 mg/dm^3 had no impact on the H_2O_2 levels in the analyzed gland, but a higher concentration of that bioelement would reduce it by 26%. Exposure of rats to 5 mg or 50 mg Cd/dm^3 resulted in the increase of H_2O_2 levels by 26% ($p < 0.05$) and 96% ($p < 0.001$), respectively, as compared to the control group; the increase was larger at a higher exposure level. In the rat groups which, throughout the period of exposure to cadmium at 5 mg/dm^3, received 30 mg or 60 mg Zn/dm^3, the H_2O_2 levels were 35% and 33% lower ($p < 0.001$), respectively, as compared to the H_2O_2 levels in the animals exposed to cadmium and did not differ from the values observed in the control group. Also, in the rat groups which, throughout the period of exposure to cadmium at 50 mg/dm^3, received 30 mg or 60 mg Zn/dm^3, the H_2O_2 levels were 48% and 58% lower ($p < 0.001$), respectively, as compared to the H_2O_2 levels in the animals exposed to cadmium and did not differ from the values observed in the control group (Table 1).

3.3. The Impact of Zinc and/or Cadmium on Total Oxidant State and Total Antioxidant Status and the Stress Index in the Rat Sublingual Gland. The TOS levels in the sublingual gland of rats are provided in Table 2. Exposure to cadmium at 5 mg and 50 mg/dm^3 resulted in significant increase of TOS levels in the sublingual gland. The TOS levels in both groups were 1.7- and 2-folds higher ($p < 0.001$) than in the control group. Furthermore, the TOS levels in rats exposed to 50 mg Cd/dm^3 was 1.2-folds higher ($p < 0.05$) than in those exposed to lower cadmium levels. In the animal groups which, throughout the period of exposure to cadmium at 5 mg/dm^3, received 30 mg or 60 mg Zn/dm^3, the TOS levels were 46% and 42% lower ($p < 0.001$), respectively, as compared to the TOS levels in the animals exposed solely to cadmium. Also, in the rat groups which, throughout the period of exposure to cadmium at 50 mg/dm^3, received 30 mg or 60 mg Zn/dm^3, the TOS levels were 52% and 40% lower ($p < 0.001$), respectively, as compared to the TOS levels in the animals exposed to cadmium and did not differ from the values observed in the control group.

The TAS levels in the sublingual gland of rats which, throughout the experiment period, received only zinc at 30 mg or 60 mg/dm^3 were 2.3- and 1.8-folds higher ($p < 0.001$), respectively, than the TAS levels in control animals. Exposure to 5 mg and 50 mg Cd/dm^3 resulted in significant

Table 2: The impact of zinc on TOS and TAS levels, and the TOS/TAS ratio in the sublingual gland of rats exposed to cadmium.

	TOS (nmol/mg of protein)	TAS (nmol/mg of protein)	TOS/TAS
Control	21.846 ± 3.751	3.466 ± 0.468	7.709 ± 1.971
30 mg Zn/dm^3	16.393 ± 1.157	$7.843 \pm 0.590^{a\ddagger}$	$2.181 \pm 0.236^{a\dagger}$
60 mg Zn/dm^3	17.951 ± 0.985	$6.138 \pm 0.839^{a\ddagger b*}$	$3.272 \pm 0.435^{a*}$
5 mg Cd/dm^3	$36.284 \pm 3.438^{a\ddagger b\ddagger c\ddagger}$	$1.770 \pm 0.080^{a* b\ddagger c\ddagger}$	$20.565 \pm 1.796^{a\ddagger b\ddagger c\ddagger}$
5 mg Cd/dm^3 + 30 mg Zn/dm^3	$19.700 \pm 1.557^{d\ddagger}$	$7.879 \pm 0.379^{a\ddagger c* d\ddagger}$	$2.515 \pm 0.519^{a\dagger d\ddagger}$
5 mg Cd/dm^3 + 60 mg Zn/dm^3	$20.974 \pm 1.626^{d\ddagger}$	$12.009 \pm 0.559^{a\ddagger b\ddagger c\ddagger d\ddagger e\ddagger}$	$1.777 \pm 0.157^{a\dagger d\ddagger}$
50 mg Cd/dm^3	$44.153 \pm 3.943^{a\ddagger b\ddagger c\ddagger d* e\ddagger f\ddagger}$	$1.930 \pm 0.213^{a* b\ddagger c\ddagger e\ddagger f\ddagger}$	$24.208 \pm 2.543^{a\ddagger b\ddagger c\ddagger d* e\ddagger f\ddagger}$
50 mg Cd/dm^3 + 30 mg Zn/dm^3	$21.205 \pm 2.054^{d\ddagger g\ddagger}$	$5.382 \pm 0.627^{a* b\dagger d\ddagger e\dagger f\ddagger g\ddagger}$	$4.093 \pm 0.411^{d\ddagger g\ddagger}$
50 mg Cd/dm^3 + 60 mg Zn/dm^3	$26.684 \pm 2.313^{b* c* d\dagger g\ddagger}$	$5.104 \pm 0.454^{a* b\ddagger d\ddagger e\ddagger f\ddagger g\ddagger}$	$5.433 \pm 0.533^{d\ddagger g\ddagger}$

The values are arithmetic means ± SEM. $^*p < 0.05$; $^\dagger p < 0.01$; $^\ddagger p < 0.001$ as compared to [a]control, [b]30 mg Zn/dm^3, [c]60 mg Zn/dm^3, [d]5 mg Cd/dm^3, [e]5 mg Cd/dm^3 + 30 mg Zn/dm^3, [f]5 mg Cd/dm^3 + 60 mg Zn/dm^3, [g]50 mg Cd/dm^3, and [h]50 mg Cd/dm^3 + 30 mg Zn/dm^3.

Table 3: Independent and interactive impact of cadmium and zinc on the levels of selected oxidative stress indices in the rat sublingual gland.

ANOVA/MANOVA	GSH	LPO	H_2O_2	TOS	TAS	TOS/TAS
Independent impact of Cd	6.389^*	$24.84^\ddagger$	$20.38^\ddagger$	$35.05^\ddagger$	0.635	$62.04^\ddagger$
Independent impact of Zn	$9.526^\dagger$	$14.09^\ddagger$	$37.82^\ddagger$	$33.31^\ddagger$	$53.18^\ddagger$	$149.5^\ddagger$
Interaction effect of Cd and Zn	$9.461^\dagger$	$7.091^\dagger$	$13.67^\ddagger$	$11.56^\dagger$	3.049	$50.87^\ddagger$

The values reflect the F coefficient, where $^*p < 0.05$; $^\dagger p < 0.01$; $^\ddagger p < 0.001$.

decrease of TAS levels by 49% and 44% ($p < 0.05$), respectively, as compared to the control group. In the rat groups which, throughout the period of exposure to cadmium at 5 mg/dm^3, received 30 mg or 60 mg Zn/dm^3, the TAS levels were 2.3- and 3.5-folds higher ($p < 0.001$), respectively, than The TAS levels in the control group and 4.5- and 6.8-folds higher ($p < 0.001$) as compared to The TAS levels in the animals not receiving zinc during exposure to cadmium. Also, in the rat groups which, throughout the period of exposure to cadmium at 50 mg/dm^3, received 30 mg or 60 mg Zn/dm^3, the TAS levels were 1.6- and 1.5-folds higher ($p < 0.05$), respectively, than the TAS levels in the control group and 2.8- and 2.6-folds higher ($p < 0.001$) as compared to the TAS levels in the animals not receiving zinc during exposure to cadmium (Table 2).

In the animals which, throughout the experiment, received only zinc at 30 mg and 60 mg/dm^3, the TOS/TAS ratio was 3.5-folds ($p < 0.01$) and 2.4-folds ($p < 0.05$) lower, respectively, than the TOS/TAS ratio in the control groups. Exposure to 5 mg and 50 mg Cd/dm^3 resulted in a significant increase of the TOS/TAS ratio in the sublingual gland. The TOS/TAS ratio in both groups was 2.7- and 3.1-folds higher ($p < 0.001$) than that in the control group. Furthermore, the TOS/TAS ratio in both groups was 9.4- and 6.3-folds, which was significantly higher as compared to that in animals which received only zinc with drinking water at 30 mg and 60 mg/dm^3 ($p < 0.001$), respectively, when exposed to 5 mg Cd/dm^3, and 11.1- and 7.4-folds higher ($p < 0.001$), respectively, when exposed to 50 mg Cd/dm^3. The TOS/TAS ratio was significantly higher in the group of animals receiving cadmium at 50 mg/dm^3 than in the group exposed to 5 mg Cd/dm^3 by 15% ($p < 0.05$). In the rat groups which, throughout the period of exposure to cadmium at 5 mg/dm^3, received 30 mg or 60 mg Zn/dm^3, the TOS/TAS ratio was 67% and 77% lower ($p < 0.01$), respectively, than the TOS/TAS ratio in the control group and 8.2- and 11.6-folds lower ($p < 0.001$), respectively, as compared to the TOS/TAS ratio in the animals receiving only cadmium. The TOS/TAS ratio in the rat groups which, throughout the period of exposure to 50 mg Cd/dm^3, received 30 mg or 60 mg Zn/dm^3 was 5.9- and 4.5-folds lower ($p < 0.001$), respectively, than in the group of animals receiving only cadmium (Table 2).

3.4. Independent and Interactive Impact of Cadmium and Zinc on the Levels of Selected Oxidative Stress Indices in the Rat Sublingual Gland (Table 3). The independent and interactive impact of cadmium and zinc on the levels of selected stress indices was assessed using a two-way analysis of variance (ANOVA/MANOVA).

3.5. Analysis of Spearman's Rank Correlation between the Assessed Parameters in the Sublingual Gland Tissue (Table 4)

4. Discussion

Cadmium is a toxic metal commonly found in the daily environment. Due to the increasing number of reports of the harmful impact of low exposure to those toxic elements published worldwide, the researchers are focused on finding methods to reduce dietary cadmium intake and mitigate its impact on the organism [2, 8, 10]. Particular attention is being paid to using certain nutrients for this purpose, including zinc. Studies on animals revealed that zinc reduces cadmium absorption from the gastrointestinal tract and its accumulation in the liver and the kidneys, and it prevents

Table 4: Analysis of Spearman's rank correlation between the assessed parameters in the sublingual gland tissue.

	TAS	TOS	TOS/TAS	GSH	H_2O_2
TAS	—				
TOS	$-0.485^{\ddagger}$	—			
TOS/TAS	$-0.915^{\ddagger}$	$0.756^{\ddagger}$	—		
GSH	$0.580^{\ddagger}$	$-0.431^{\ddagger}$	$-0.588^{\ddagger}$	—	
H_2O_2	$-0.523^{\ddagger}$	$0.388^{\ddagger}$	$0.510^{\ddagger}$	$-0379^{\dagger}$	—
LPO	$-0.583^{\ddagger}$	$0.416^{\ddagger}$	$0.570^{\ddagger}$	$-0.503^{\ddagger}$	$0.501^{\ddagger}$

The values reflect the rank correlation coefficient r, where $^{\dagger}p < 0.01$; $^{\ddagger}p < 0.001$.

some effects of cadmium, in particular its hepato- and nephrotoxicity and toxicity to the bones [10, 19].

Similar to other heavy metals, cadmium has the ability to accumulate in living organisms. The largest accumulation of cadmium occurs in organs rich in metallothionein (MT), that is, the liver and kidneys [10, 28, 29]. However, in chronic exposure to cadmium, the concentration levels of this metal in various tissues and body fluids increased, including those in which the accumulation is much lower than in shielding organs, for example, in the salivary gland tissue [30, 31].

The oral cavity, serving as the initial section of the gastrointestinal tract, is an integral element of the organism. Its liquid environment is the saliva which hosts a number of biochemical reactions necessary to maintain the oral cavity healthy. Exposure to cadmium also affects its condition. Consequences of chronic exposure to that toxic element were also observed both in hard tissue, such as teeth [5, 22, 32], and in soft tissue of the oral cavity and in the saliva [7, 30, 31, 33, 34].

Fischer et al. [5] assessed the presence of bioelements and toxic metals in milk teeth of children exposed to tobacco smoke from cigarettes smoked by their parents. In the milk teeth of children who had not been exposed to tobacco smoke, a higher content of elements with a confirmed physiological role for the organism (Fe, Zn, K, Na, and Ca) was found, as compared to the content of those metals in the milk teeth of children subjected to passive exposure. On the other hand, the content of toxic metals (Pb and Cd) was higher ($p = 0.05$) in the teeth's tissue of children exposed to passive smoking. The authors suggest that exposure to tobacco smoke causes the toxic metals in the smoke to be integrated with the structure of mineralized tissues, including teeth [5].

Kakei et al. [22] concluded that cadmium disrupted the formation of tooth enamel in rats by inhibiting the crystallization buds in the form of zinc phosphate. The authors suggested that Cd^{2+} ions, by replacing Zn^{2+} ions in carbonic anhydrase, reduce the catalytic activity of the enzyme and impair enamel mineralization.

Smoking is a major source of exposure to cadmium, especially for people living in areas with low environmental levels of that metal, who have no occupational contact with cadmium [35, 36]. In their study on humans, Han et al. [36] have confirmed a relationship between the blood cadmium levels in smokers and the increased oxidative stress in the oral cavity and periodontium diseases. Active smokers were confirmed by quantifying the cotinine level in urine ≥ 164 ng/mL. The average blood cadmium levels in persons with periodontium diseases were 1.10 μ/L in females and 1.24 μg/L in males and were significantly higher by 29% and 32%, respectively, as compared to the average blood cadmium levels in the control population [36].

Thus far, little attention has been paid to the destructive effect of cadmium on salivary glands. The available study outcomes indicate that exposure to that metal may also cause structural and functional changes in those glands, impairing their function and development [7, 34, 37, 38].

Cadmium toxicity derives from its prooxidative properties. Although cadmium is unable to directly generate RFT through Fenton or Haber-Weiss reaction, it does induce stress indirectly through depleting glutathione and other antioxidant in cells, including vitamins, antioxidant enzymes, and bioelement, among those zinc [8, 9, 16, 17, 21], thus impairing the function of numerous tissues and organs, including salivary glands [7, 37, 38]. However, the prooxidative effect of cadmium on salivary glands has not been studied as extensively as its other effects. As a result, it remains insufficiently analyzed and prevents a broader discussion of own research outcomes.

In this study, the long-term exposure to cadmium at both levels induced oxidative stress in the sublingual gland. In the analyzed gland, there was a reduction of the level of nonenzymatic antioxidant (GSH) and of the total antioxidant status (TAS) and an increase of total oxidant status (TOS) and stress indices (LPO, H_2O_2, and TOS/TAS). The TAS level was positively correlated to the GSH level ($r = 0.580$) and negatively correlated to TOS ($r = -0.485$), TOS/TAS ($r = -0.915$), LPO ($r = -0.583$), and H_2O_2 ($r = -0.523$). On the other hand, TOS and the stress index (TOS/TAS) of the analyzed salivary gland were increased, which in turn conformed to the trend exhibited by LPO ($r = 0.416$; $r = 0.570$) and H_2O_2 ($r = 0.388$; $r = 0.510$).

The impact of cadmium on the induction of oxidative stress in the saliva originating from the submandibular gland of rats was studied by Abdollahi et al. [7]. The authors administered i.p. cadmium chloride at 10 mg Cd/kg of body weight and pilocarpine at 8 mg/kg of body weight, as a stimulant of saliva production. Under barbiturate anesthesia, saliva was collected directly from the submandibular gland ducts to microtubes for 30 minutes. In the analyzed material, the TAS level and the complete –SH and LPO groups were assayed. It was determined that exposing rats to cadmium results in a nearly 2-fold reduction of TAS, with simultaneous reduction of the total pool of –SH groups, and 3-fold increase of LPO. In the studies analyzed herein, exposure of rats to 5 mg and 50 mg Cd/dm^3 resulted in significant decrease of TAS levels by 49% and 44%, respectively, as compared to the control group.

LPO is a lipid peroxidation marker [9, 16]. The majority of researchers quantify the level of malondialdehyde (MDA) as the indicator of oxidative damage to lipid compounds. However, in order to accurately assess this process, LPO levels were assayed, that is, the sum of MDA and 4-hydroxynonenal (4-HNE) [9, 16]. In our own research, the

LPO levels were assayed. It increased 2.2-folds at 5 mg Cd/dm^3 and 3-folds at 50 mg Cd/dm^3, as compared to the control group, and was higher at a higher exposure level. The increase of LPO level in the sublingual gland at both cadmium exposure levels, as compared to the control group, indicates not only the intensification of lipid peroxidation but also the significant rise of oxidative stress. This is confirmed by the increased level of hydrogen peroxide in the analyzed salivary glands of those rats.

An important indicator of oxidative cellular damage is also the hydrogen peroxide, which is a natural product of cellular metabolism [9]. Due to its strong oxidation properties, that compound is highly reactive and also toxic to the cell. Under normal physiologic conditions, H_2O_2 is deactivated by CAT and GPx [9]. Those enzymes prevent excessive accumulation of H_2O_2 in cells, thus protecting the organism against the destructive effect of that compound on proteins, lipids, or nucleic acids. It follows from this that the increased H_2O_2 levels in the sublingual gland of rats exposed to cadmium, as observed in this study, arise from the inhibition of GPx activity in the analyzed gland, as previously shown in own research [38].

Aside from LPO and H_2O_2, another indicator of increased oxidative stress in the cells is TOS and the mathematically calculated TOS/TAS ratio [9]. In the present study, the TOS level and TOS/TAS ratio increased 1.7- and 2.7-folds, respectively, at 5 mg Cd/dm^3, and 2- and 3-folds, respectively, at higher exposure levels. The obtained results clearly indicate a significantly increased oxidative stress in the sublingual glands of rats exposed to cadmium.

The available study outcomes suggest that antioxidants such as vitamins and polyphenols may protect the organism exposed to cadmium against oxidative stress. Zinc has also been found to have antioxidant properties and has been confirmed to provide efficient protection against many toxic effects of cadmium on the organism, including the damage of the kidneys, liver, and bones [10, 16, 19, 24].

Thus far, the protective role of this bioelement against the consequences of oxidative damage in the sublingual gland of a rat exposed to cadmium has not been studied. This study is a pioneer venture aimed at answering the question whether the increase of zinc supply by 79% and 151%, as compared to standard dietary intake, has protective effect against accumulation of H_2O_2 and LPO and low-molecular-weight thiol that is GSH in the analyzed salivary gland.

In the previous own research, we have shown that administering 30 mg Zn/dm^3 to animals increases the GPx activity, while increasing the supply of that bioelement by 151% (60 mg Zn/dm^3) increases the activity of both CAT and GPx and reduces the H_2O_2 levels, thus confirming zinc's antioxidant effect [38].

This study has shown that administering zinc to animals in both doses during exposure to 5 mg or 50 mg Cd/dm^3 completely inhibited the cadmium-induced increase of LPO and H_2O_2 levels and the reduction of GSH levels in the sublingual gland tissue, allowing us to conclude that zinc supplementation mitigates the oxidative stress in that gland. Furthermore, two-way analysis of variance (ANOVA/MANOVA) has shown that the beneficial effect of zinc supplementation on GSH, LPO, and H_2O_2 levels arises from zinc's independent activity and its interaction with cadmium, whereby the independent impact of that bioelement is stronger than the interactive activity between zinc and cadmium.

The role of zinc for oral cavity health has not been extensively studied yet [24, 39–42]. The bioelement is necessary for correct growth of teeth [41], and it reinforces enamel [40, 41] and prevents dental decay [39, 40] and periodontium diseases [39].

Zinc is also used as an antibacterial agent in toothpastes and mouthwashes to control the formation of dental plaque, reduce tartar, and eliminate halitosis [40, 41].

Uckardes et al. [42] assessed the impact of zinc supplementation on the incidence of dental decay in children. 68 children were randomized into 2 groups (study group and placebo group). The children in the study group received 15 mg of zinc daily, five days a week, for 10 weeks. The status of dental plaque was assessed before and after zinc supplementation. The study clearly showed (through reducing the formation of dental plaque in 18 patients) that increased zinc supply prevents dental decay development in children.

Hegde et al. [39] assessed the SOD activity and the Cu and Zn levels in the saliva of patients with and without dental decay. 80 patients were divided according to WHO criteria into healthy patients without decay (DMFT = 0; 20 persons) and patients with active dental decay (DMFT > 10; 60 persons). Saliva was collected always at the same time, that is, at noon, 2 hours after meal. The increase of SOD activity and of copper and zinc levels in the group with active dental decay, achieved by the authors, confirmed that the disease had radical origin.

Saliva is a biological fluid playing an important role for the health of the oral cavity and can be used not only in diagnostics but also in monitoring the progress of various diseases, including cancer and periodontitis [33, 43–45].

Wei et al. [45] assessed the TOS and MDA levels and SOD activity in the serum, saliva, and gingival crevicular fluid before and 16 weeks after conventional therapy (maintaining appropriate oral cavity hygiene and cleaning gum surface) of chronic periodontitis. The study involved 83 patients, of which 48 had manifest symptoms. Lipid peroxidation assessed as MDA level was higher before therapy only in the gingival crevicular fluid and was reduced by treatment. The SOD activity and total oxidation status of the analyzed biological fluids were higher before therapy and were reduced by treatment. The outcomes of that study indicate that oxidative stress might play an important role in chronic periodontitis and appropriate therapy may help control the process by modifying SOD activity and MDA and TOS levels.

In other studies, Kurku et al. [44] assessed the oxidative stress indices in smokers' serum and saliva. The MDA, TOS, and TOS/TAS ratio were higher in the smokers' serum, while the total level of the –SH groups decreased. In the smokers' saliva, a decrease of activity of the GPx and total –SH groups was observed, coupled with an increase of MDA levels. The authors suggest that disrupting the oxidation-reduction balance of saliva and serum arises from smoking and has destructive effect on tissues and organs, including the oral cavity.

The key outcome of our own research is the confirmation that administering zinc to animals at both concentration levels during exposure to cadmium significantly increases the TAS and reduces the TOS, as well as the TOS/TAS stress index in the sublingual glands of rats, which suggests a reduction of oxidative stress in that gland. Two-way analysis of variance (ANOVA/MANOVA) has shown that the beneficial effect of zinc supplementation on TAS and TOS levels and TOS/TAS ratio arises from zinc's independent activity and its interaction with cadmium, whereby the independent impact of that bioelement is stronger than the interactive activity between zinc and cadmium.

5. Conclusions

In light of the available literature data on the protective effect of zinc, it should be noted that this study is the first attempt to analyze the impact of that bioelement on the sublingual gland tissue during exposure to cadmium. Summing up the outcomes of our own research, it should be concluded that a confirmed increase, in the applied experimental model for both the moderate environmental exposure of humans to cadmium and the occupational exposure, of the zinc supply by 79% and 151% reduces the oxidative stress in sublingual glands of rats and clearly shows a protective effect of that bioelement on the tissue of the analyzed gland.

The outcome of this study contributes new, important data confirming the protective effect of increased zinc intake on the sublingual gland tissue in chronic exposure to cadmium.

Data Availability

The data of the materials and methods and conclusions to support the findings of this study are included within the article. If any other data may be needed, please contact the corresponding author upon request.

Conflicts of Interest

There is no conflict of interest.

References

[1] A. Åkesson, L. Barregard, I. A. Bergdahl, G. F. Nordberg, M. Nordberg, and S. Skerfving, "Non-renal effects and the risk assessment of environmental cadmium exposure," *Environmental Health Perspectives*, vol. 122, no. 5, pp. 431–438, 2014.

[2] L. Järup and A. Åkesson, "Current status of cadmium as an environmental health problem," *Toxicology and Applied Pharmacology*, vol. 238, no. 3, pp. 201–208, 2009.

[3] T. S. Nawrot, J. A. Staessen, H. A. Roels et al., "Cadmium exposure in the population: from health risks to strategies of prevention," *Biometals*, vol. 23, no. 5, pp. 769–782, 2010.

[4] S. Satarug and M. R. Moore, "Adverse health effects of chronic exposure to low-level cadmium in foodstuffs and cigarette smoke," *Environmental Health Perspectives*, vol. 112, no. 10, pp. 1099–1103, 2004.

[5] A. Fischer, D. Wiechuła, and J. Kwapuliński, "Ocena wpływu biernego palenia na zawartość metali w zębach mlecznych," *Journal of Stomatology*, vol. 64, pp. 620–630, 2011.

[6] H. Milnerowicz, M. Sciskalska, and M. Dul, "Pro-inflammatory effects of metals in persons and animals exposed to tobacco smoke," *Journal of Trace Elements in Medicine and Biology*, vol. 29, pp. 1–10, 2015.

[7] M. Abdollahi, A. Bahreini-Moghadam, B. Emami, F. Fooladian, and K. Zafari, "Increasing intracellular cAMP and cGMP inhibits cadmium-induced oxidative stress in rat submandibular saliva," *Comparative Biochemistry and Physiology Part C: Toxicology & Pharmacology*, vol. 135, no. 3, pp. 331–336, 2003.

[8] M. M. Brzóska, J. Rogalska, and E. Kupraszewicz, "The involvement of oxidative stress in the mechanisms of damaging cadmium action in bone tissue. A study in a rat model of moderate and relatively high human exposure," *Toxicology and Applied Pharmacology*, vol. 250, no. 3, pp. 327–335, 2011.

[9] K. Jomova and M. Valko, "Advances in metal-induced oxidative stress and human disease," *Toxicology*, vol. 283, no. 2-3, pp. 65–87, 2011.

[10] J. Rogalska, B. Piłat-Marcinkiewicz, and M. M. Brzóska, "Protective effect of zinc against cadmium hepatotoxicity depends on this bioelement intake and level of cadmium exposure: a study in a rat model," *Chemico-Biological Interactions*, vol. 193, no. 3, pp. 191–203, 2011.

[11] A. Rani, A. Kumar, A. Lal, and M. Pant, "Cellular mechanisms of cadmium-induced toxicity: a review," *International Journal of Environmental Health Research*, vol. 24, no. 4, pp. 378–399, 2013.

[12] F. Thévenod and W. K. Lee, "Toxicology of cadmium and its damage to mammalian organs," *Metal Ions in Life Sciences*, vol. 11, pp. 415–490, 2013.

[13] A. Cuypers, M. Plusquin, T. Remans et al., "Cadmium stress: an oxidative challenge," *Biometals*, vol. 23, no. 5, pp. 927–940, 2010.

[14] V. Matović, A. Buha, D. Đukić-Ćosić, and Z. Bulat, "Insight into the oxidative stress induced by lead and/or cadmium in blood, liver and kidneys," *Food and Chemical Toxicology*, vol. 78, pp. 130–140, 2015.

[15] R. C. Patra, A. K. Rautray, and D. Swarup, "Oxidative stress in lead and cadmium toxicity and its amelioration," *Veterinary Medicine International*, vol. 2011, Article ID 457327, 9 pages, 2011.

[16] M. Jurczuk, M. M. Brzóska, J. Moniuszko-Jakoniuk, M. Gałażyn-Sidorczuk, and E. Kulikowska-Karpińska, "Antioxidant enzymes activity and lipid peroxidation in liver and kidney of rats exposed to cadmium and ethanol," *Food and Chemical Toxicology*, vol. 42, no. 3, pp. 429–438, 2004.

[17] S. M. Prabu, K. Shagirtha, and J. Renugadevi, "Amelioration of cadmium-induced oxidative stress, impairment in lipids and plasma lipoproteins by the combined treatment with quercetin and α-tocopherol in rats," *Journal of Food Science*, vol. 75, no. 7, pp. T132–T140, 2010.

[18] M. M. Brzóska and J. Moniuszko-Jakoniuk, "Interactions between cadmium and zinc in the organism," *Food and Chemical Toxicology*, vol. 39, no. 10, pp. 967–980, 2001.

[19] M. M. Brzóska, J. Rogalska, M. Galażyn-Sidorczuk et al., "Effect of zinc supplementation on bone metabolism in male rats chronically exposed to cadmium," *Toxicology*, vol. 237, no. 1-3, pp. 89–103, 2007.

[20] S. A. Ismail and R. I. Rizk, "Protective effect of zinc, selenium, vitamin C, E and epicatechine on cadmium-induced toxicity and disturbances in the kidney, liver, bone, lipid metabolism and oxidative stress in rats," *Research Journal of Pharmaceutical Biological and Chemical Sciences*, vol. 7, pp. 647–655, 2016.

[21] V. Matović, A. Buha, Z. Bulat, and D. Dukić-Ćosić, "Cadmium toxicity revisited: focus on oxidative stress induction and interactions with zinc and magnesium," *Archives of Industrial Hygiene and Toxicology*, vol. 62, no. 1, pp. 65–76, 2011.

[22] M. Kakei, T. Sakae, and M. Yoshikawa, "Mechanism of cadmium induced crystal defects in developing rat tooth enamel," *Proceedings of the Japan Academy, Series B*, vol. 85, no. 10, pp. 500–507, 2009.

[23] N. Bagherani, M. Omidian, and R. Yaghoobi, "Hypothesis: zinc can be effective in treatment of vitiligo," *Indian Journal of Dermatology*, vol. 56, no. 5, pp. 480–484, 2011.

[24] C. T. Chasapis, A. C. Loutsidou, C. A. Spiliopoulou, and M. E. Stefanidou, "Zinc and human health: an update," *Archives of Toxicology*, vol. 86, no. 4, pp. 521–534, 2012.

[25] C. Livingstone, "Zinc: physiology, deficiency, and parenteral nutrition," *Nutrition in Clinical Practice*, vol. 30, no. 3, pp. 371–382, 2015.

[26] P. I. Oteiza, "Zinc and the modulation of redox homeostasis," *Free Radical Biology & Medicine*, vol. 53, no. 9, pp. 1748–1759, 2012.

[27] E. Şahin and S. Gümüşlü, "Immobilization stress in rat tissues: alterations in protein oxidation, lipid peroxidation and antioxidant defense system," *Comparative Biochemistry and Physiology Part C: Toxicology & Pharmacology*, vol. 144, no. 4, pp. 342–347, 2007.

[28] M. Banni, I. Messaoudi, L. Said, J. El Heni, A. Kerkeni, and K. Said, "Metallothionein gene expression in liver of rats exposed to cadmium and supplemented with zinc and selenium," *Archives of Environmental Contamination and Toxicology*, vol. 59, no. 3, pp. 513–519, 2010.

[29] G. F. Nordberg, T. Jin, X. Wu et al., "Prevalence of kidney dysfunction in humans – relationship to cadmium dose, metallothionein, immunological and metabolic factors," *Biochimie*, vol. 91, no. 10, pp. 1282–1285, 2009.

[30] E. Czykier, J. Dzięcioł, M. Gałażyn-Sidorczuk, and J. Moniuszko-Jakoniuk, "A preliminary study of the submandibular gland of the rat after one-year cadmium intoxication. Part I. Cadmium concentration," *Roczniki Akademii Medycznej w Bialymstoku*, vol. 49, pp. 178-179, 2004.

[31] E. Dąbrowska, M. Szmitowski, E. Kulikowska-Karpińska, J. Łapińska, and R. Letko, "Cadmium content in the rat submandibular salivary gland depending on Cd dose and exposure time," *Polish Journal of Environmental Studies*, vol. 18, pp. 169–172, 2009.

[32] P. Malara, J. Kwapuliński, and B. Malara, "Do the levels of selected metals differ significantly between the roots of carious and non-carious teeth?," *Science of The Total Environment*, vol. 369, no. 1-3, pp. 59–68, 2006.

[33] K. Błochowiak and H. Witmanowski, "Ocena stężenia produktów peroksydacji lipidów w ślinie i w surowicy krwi u pacjentów ze złamaniami żuchwy," *Czasopismo Stomatologiczne*, vol. 63, pp. 250–258, 2010.

[34] C. Friedrichi, R. A. Lopes, M. A. Sala et al., "Effects of cadmium on the rat salivary glands, during lactation," *International Journal of Morphology*, vol. 27, pp. 1129–1137, 2009.

[35] E. Golusińska-Kardach, M. Napierała, J. Sokalski, H. Kardachi, and E. Florek, "Periodonta disease in smokers, and the parameters of oxidative stress," *Przeglad Lekarski*, vol. 72, no. 10, pp. 584–587, 2015.

[36] D. H. Han, H. J. Lee, and S. Lim, "Smoking induced heavy metals and periodontitis: findings from the Korea National Health and Nutrition Examination Surveys 2008-2010," *Journal of Clinical Periodontology*, vol. 40, no. 9, pp. 850–858, 2013.

[37] E. Dąbrowska, B. Szynaka, and E. Kulikowska-Karpińska, "Ultrastructural study of the submandibular gland of the rat after 6-month exposure to cadmium and zinc in drinking water," *Advances in Medical Sciences*, vol. 51, pp. 245–249, 2006.

[38] P. Kostecka-Sochoń and E. Dąbrowska, "Wpływ kadmu i/lub cynku na wybrane enzymatyczne parametry bariery antyoksydacyjnej w śliniance podjęzykowej szczura," *Dental and Medical Problems*, vol. 50, pp. 282–290, 2013.

[39] M. N. Hegde, N. D. Hegde, A. Ashok, and S. Shetty, "Biochemical indicators of dental caries in saliva: an in vivo study," *Caries Research*, vol. 48, no. 2, pp. 170–173, 2014.

[40] R. J. M. Lynch, "Zinc in the mouth, its interactions with dental enamel and possible effects on caries; a review of the literature," *International Dental Journal*, vol. 61, pp. 46–54, 2011.

[41] P. T. Bhattacharya, S. R. Misra, and M. Hussain, "Nutritional aspects of essential trace elements in oral health and disease: an extensive review," *Scientifica*, vol. 2016, Article ID 5464373, 12 pages, 2016.

[42] Y. Uckardes, M. Tekcicek, E. N. Ozmert, and K. Yurdakok, "The effect of systemic zinc supplementation on oral health in low socioeconomic level children," *The Turkish Journal of Pediatrics*, vol. 51, no. 5, pp. 424–428, 2009.

[43] M. Greabu, M. Battino, M. Mohora et al., "Saliva a diagnostic window to the body, both in health and in disease," *Journal of Medicine and Life*, vol. 2, no. 2, pp. 124–132, 2009.

[44] H. Kurku, M. Kacmaz, U. Kisa, O. Dogan, and O. Caglayan, "Acute and chronic impact of smoking on salivary and serum total antioxidant capacity," *The Journal of the Pakistan Medical Association*, vol. 65, no. 2, pp. 164–169, 2015.

[45] D. Wei, X. L. Zhang, Y. Z. Wang, C. X. Yang, and G. Chen, "Lipid peroxidation levels, total oxidant status and superoxide dismutase in serum, saliva and gingival crevicular fluid in chronic periodontitis patients before and after periodontal therapy," *Australian Dental Journal*, vol. 55, no. 1, pp. 70–78, 2010.